COMPUTER SIMULATION OF MICROVASCULAR EXCHANGE AFTER THERMAL INJURY

by

XIAOZHENG GU

A THESIS SUBMITTED IN PARTIAL FULFILMENT OF

THE REQUIREMENTS FOR THE DEGREE OF

MASTER OF APPLIED SCIENCE

in

THE FACULTY OF GRADUATE STUDIES

DEPARTMENT OF CHEMICAL ENGINEERING

We accept this thesis as conforming

to the required standard

THE UNIVERSITY OF BRITISH COLUMBIA

July 1987

46

Abstract

A computer model is developed to study the fluid and protein redistribution after thermal injuries in rats. This model is derived by including the burned skin as a fourth compartment in the microvascular exchange model developed by Bert et al. [6].

The pathological changes that occur after thermal injuries are introduced into the burn model as perturbations. The simulations of short-term and long-term responses were then made in this four compartment (burn) model for two cases: 10% and 40% percent surface area burns. Appropriate ranges of the perturbations were estimated based on the available information in the literature. The perturbations for the 10% burn include: the plasma leak coefficient in the injured skin, the tissue pressure in the injured skin, the fluid exchange coefficients in the injured skin, the arterial capillary pressure in the injured skin and the lymph flow characteristics in the injured skin. The perturbations for the 40% burn include the perturbations for the 10% burn plus the plasma leak coefficients in the intact tissues, the fluid exchange coefficients in the intact tissues and the lymph flow characteristics in the intact tissues. The dynamic responses of the system using these perturbations were plotted. Comparisons between the simulation predictions and the experimental data were

characterized in terms of sum-of-squares of differences between simulation results and experimental data.

Compared to the limited amount of data available in the literature, the burn model describes microvascular exchange after thermal injuries reasonably well. The work in this thesis could easily be extended to account for fluid resuscitation following a thermal injury in rats and, it is hoped that this approach might eventually be applied to the resuscitation management of burn patients.

Table of Contents

List of Tables

List of Figures

Chapter 1

INTRODUCTION

1.1 GENERAL INFORMATION ABOUT BURNS

Burns represent a major surgical trauma worldwide. Each year, thousands of people suffer from burn injuries. To indicate the magnitude of the problem, a summary of such injuries and some consequences are listed in Table 1.1. Note that, in the developing countries of the Third World (e.g. Algeria) the mortality rate is much higher, with about 140 deaths in hospital alone per million population per year [1], compared to Western Nations.

Burns may result from any one of the following sources [2]:

1. thermal (flame,steam, hot liquid, hot metal),
2. electrical (alternating current, direct current, lightning),
3. chemical (acid, alkali, vesicant agents) or,
4. radiation (nuclear, solar).

Thermal injury accounts for 95% of hospital burn admissions and electrical injury for 3% [2].

Table 1.1 Incidence, Morbidity and Mortality of Burns Per Million People [1]

Countries	Burn Injuries	Hospitalization Burn Injuries	Deaths Due to Burn Injuries
United States	8333	292	38
Denmark	4140	325	10
England		250	
Wales		420	
Scotland			30
Algeria			140

1.2 THE TREATMENT OF BURN PATIENTS

Burns can severely damage or destroy tissue components, as well as effect a large fluid shift from the blood to the surrounding tissues. The resulting imbalance in fluid distribution causes the tissue to swell, while blood volume is reduced. This loss of blood volume can lead to shock and death. Fluid resuscitation following a burn injury is often the critical consideration with respect to saving the injured person's life.

Mankind has searched for soothing and healing burn medicines throughout history [3]. In the first century AD, Celsus prescribed the application of honey and bran, then cork and ashes for the treatment of burns. Pliny the Elder proposed allowing burns to remain exposed to air rather than covering them with grease. In the second century AD, Galen prescribed vinegar and wine dressings [3].

The current therapy for burn victims seeks restoration of health with minimal impairment and disfigurement. The main clinical treatment of burns involves fluid replacement (resuscitation), which is accomplished by injecting fluids intravascularly to replace fluid lost from the circulation. Several empirical formulas have been proposed to estimate the amount of fluid to be replaced, based on past clinical experience. Some examples of such formulas are listed in

Table 1.2.

The patient's response to the burn and to resuscitation must be monitored continuously. In particular, urinary output provides a generally reliable guide to the adequacy of resuscitation. Resuscitation fluids are given to maintain a urinary output rate of 30 to 50 ml/h for adults [4].

Since the specific needs of individual burn patients vary, the resuscitation formulas can only serve as general guidelines. For example, burn patients with electrical injury or inhalation injury usually need more fluids than for other types of burns [4]. Fluid replacement formulas risk partial or total failure due to both the variability amongst patients and the approximate nature of the formulas.

1.3 THE POTENTIAL USE OF COMPUTER SIMULATIONS

In the 1980's, the potential has arisen for the use of computer simulations in the management and treatment of burn patients. Mathematical relationships describing microvascular exchange in the human for normal and some pathological conditions now appear in the literature [5].

Table 1.2 Resuscitation Formulas to Prevent Burn Shock [13]

	Evans formula	Brooke formula	Modified Brooke formula	Artz formula	Parkland formula	Hypertonic formula
First 24 hours:						
Electrolyte solution	Normal saline	Ringer's lactate	Ringer's lactate	Ringer's lactate	Ringer's lactate	Hypertonic lactated saline (sodium, 250 mEq/liter)
ml/kg/% burned	1.0	1.5	2.0	3.0	4.0	Rate based on urine output of 70 ml/hour in adults
Colloid	1 ml whole blood plasma, or plasma expanders/kg/% burn	0.5 ml/kg/% burn	None	None	None	None
Free water (D_5W)	2,000 ml	2,000 ml	None	None	None	None
Second 24 hours:						
	One-half first 24-hour dose; same amount D_5W	One-half first 24-hour dose; same amount D_5W	D_5W and colloid	D_5W and colloid	Only D_5W to maintain urine output; colloid, 0.5 to 2 liters	Continued at rate to maintain urine output >30 ml

The physiological changes that occur after a thermal injury can also be incorporated into mathematical models so that the results of a thermal injury can be predicted. The effectiveness of the different fluid resuscitation schemes can then be assessed. The computer simulation, if valid, can therefore be used as an aid in managing resuscitation for this type of injury.

As an example of the use of computer simulations in the assessment of burn injuries, consider the model by Arturson et al. [5]. In this model, the microcirculation is divided into three compartments: plasma, burned tissue and normal tissue. Within each compartment, mass balances for the important constituents (e.g., fluid and albumin) can be written. The dynamic behavior of the system, i.e. the time-dependent movement of these substances into and out of the system and amongst the compartments, is then described by the solution of a set of ordinary differential equations.

Arturson's model has been used to describe postburn edema formation [5]. The model predicted the formation, distribution and composition of two different kinds of edema following thermal injuries: a local edema which is protein-rich, and a general edema which is protein-poor [5].

1.4 OBJECTIVES OF THE PRESENT WORK

Despite its achievements, the model by Arturson et al. provides only a limited amount of information about fluid and protein exchange. Its major weakness is that it combines intact skin and muscle together as a single compartment whereas it is well-known that the properties of these two tissues are quite different. Additionally, other information inputs into his model are questionable. Thus, the primary objective of the present work is to develop a four compartment (plasma, injured skin, intact skin and muscle) simulation model which will adequately describe the dynamic exchanges of fluid and protein which take place these compartments following burn injuries. Because of the limited amount of experimental information available for humans, the present work will use the rat as the animal model. This approach has several advantages including:

1. the existence of a validated model of microvascular exchange for the normal (uninjured) rat developed by Bert et al. [6],
2. a large amount of experimental information available in the literature for this animal under normal conditions, and
3. the availability in the literature of both qualitative and quantitative experimental information about the systemic changes which take place in the rat following a burn.

In addition, experimental data for both normal and thermally injured rats is being provided to us by a group of researchers (notably R. Reed and T. Lund) from the Department of Physiology, School of Medicine, University of Bergen in Norway. The computer simulation presented here represents a part of the collaborative effort between UBC and the University of Bergen.

The general steps leading to the development of a non-resuscitative burn simulation for rats were as follows:

1. The three compartment (plasma, skin and muscle) model of Bert et al. [6] for normal rats was extended to four compartments by dividing the skin compartment into two separate portions; injured and intact skin. Fluid and protein mass balances were written for each compartment yielding a set of eight ordinary differential equations which, along with appropriate constants as well as auxiliary and constitutive relationships, defined the burn model.
2. Assuming that normal steady-state conditions prevailed at zero time, the system was than perturbed by altering one or more of the characteristic parameters used in the model of Bert et al [6]. to describe microvascular exchange in the noninjured rat. Reasonable changes to both the coefficients governing fluid and protein exchange as well as the hydrostatic pressures within the system were considered. All such parametric changes

were permitted to decay with time to allow the system to return to normal (recuperate) after a sufficiently long period.

3. The resulting set of initial-value ordinary differential equations was solved numerically using the Runge-Kutta-Fehlberg method to predict the changes in all compartmental variables (hydrostatic and osmotic pressures, fluid and protein fluxes, fluid volume and protein content) which occurred as a function of time following a 10% or 40% surface area burn.
4. By comparing the model predictions with the quantitative experimental results of Lund and Reed [45] for 10% and 40% burns in rats as well as with other, more qualitative results recorded in the literature for rats and other animals, a so-called "best-fit" model was determined for both the 10% and 40% burn cases. The "best fit" simulation was considered to be that which was able to provide an adequate interpretation of the experimental results while requiring the simplest and most reasonable parametric changes to the original model.

Obvious extensions to the present model which were not considered here include:

1. development of a burn resuscitation model for rats by adding fluid and protein sources and sinks such as intravascular injection, wound exudation and urine

production to the mass balances,

2. development of a burn resuscitation model for humans along similar lines.

However, such developments will have to wait until sufficient experimental data become available to allow estimates of all the transport parameters and constitutive relationships needed to adequately describe the extended models.

Chapter 2

PHYSIOLOGICAL BACKGROUND

In order to understand the fluid and plasma protein exchanges resulting from thermal injuries, a review of the physiology relevant to microvascular exchange system, such as the normal function of the blood circulation, the blood plasma composition, the tissue properties and lymph flow behaviour, is required. These will be discussed in the following sections.

2.1 CIRCULATORY SYSTEM

2.1.1 DESCRIPTION OF THE CIRCULATORY SYSTEM

Simplistically, the circulatory system can be considered as a closed system, consisting of the heart and various kinds of blood vessels. It is a very complex, self-regulating, feedback control system which keeps the systemic variables, such as arterial blood pressure, within a narrow range. Except for severe upsets, adequate blood flow through all organs and tissues is maintained. The driving force for this flow is the arterial blood pressure, produced by ventricular contraction [7].

From the left ventricle of the heart, blood is injected into the aorta and into the coronary blood vessels which supply the heart muscle with nutrients. The aorta branches into arteries, arterioles and then capillaries. The capillary walls allow the necessary exchange of O_2, CO_2 and other substances between the blood and the tissues. Following this exchange process, the blood, now depleted of O_2 and enriched in CO_2, is returned to the right ventricle by way of the venous blood vessels. From the right ventricle, blood is injected into the pulmonary circulatory system where the exchange of O_2 and CO_2 takes place in the lung, such that blood returning to the left atrium and the left ventricle is oxygen-rich [7]. This circuit is illustrated in Figure 2.1.

The total cross-sectional area of all capillaries, the smallest diameter elements in the circulatory system, is 500 to 600 times that of the aorta. Since the volume flow rate of blood through the aorta must be identical to that in the capillary bed, the average flow velocity through the capillaries is much lower than that in the aorta. The area and velocity variations throughout this system are shown in Figure 2.2.

Figure 2.1 The Circulation [14]

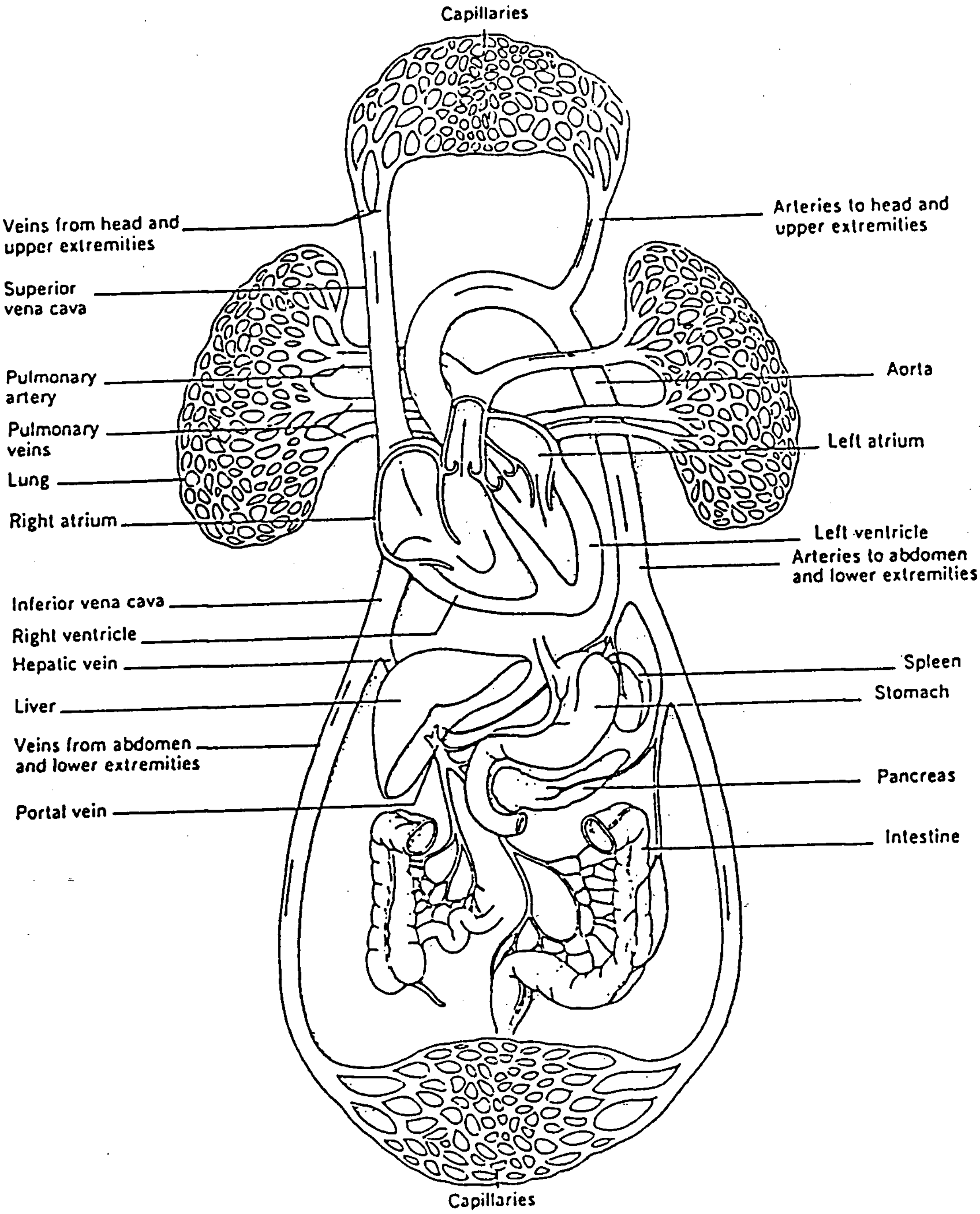

Figure 2.2 Cross Sectional Area and Velocity Variations in the Human Circulation [15]

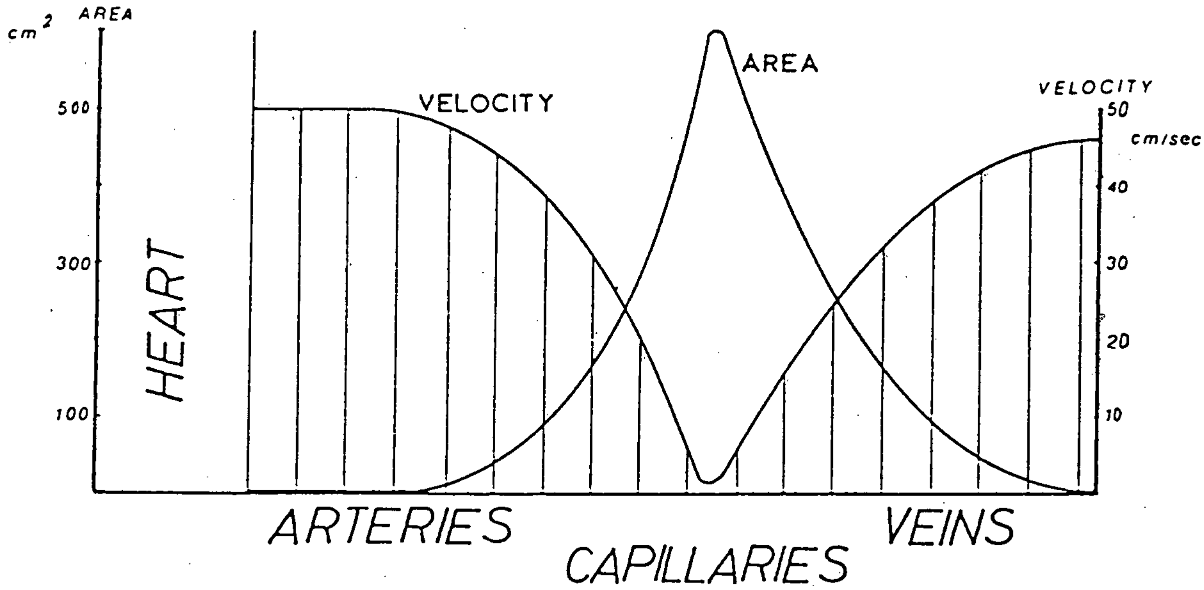

2.1.2 THE CLASSIFICATION OF THE BLOOD VESSELS

The circulatory system contains a number of different types of blood vessels including Windkessel vessels, precapillary resistance vessels, followed by precapillary sphincters, capillary exchange vessels, and venous vessels. Differences in the microstructure of the various blood vessels reflect their particular function (see Figure 2.3).

Windkessel vessels, such as the aorta and the large arteries, offer little resistance to flow. Their elastic walls serve as energy-storing reservoirs which enact a damping effect on the pulsatile output of the ventricles. Therefore, the pressure drop in the windkessel vessels is very small [7].

Precapillary resistance vessels are responsible for most of the total resistance to flow. Compared to Windkessel vessels, the elastic components of the wall are replaced by muscle fibres which function as variable resistors. The diameter of these vessels depends primarily on local physical and chemical factors; this dependence is particularly acute in the resistance vessels of the heart and the brain [7].

Figure 2.3 Schematic of the Vascular System [15]

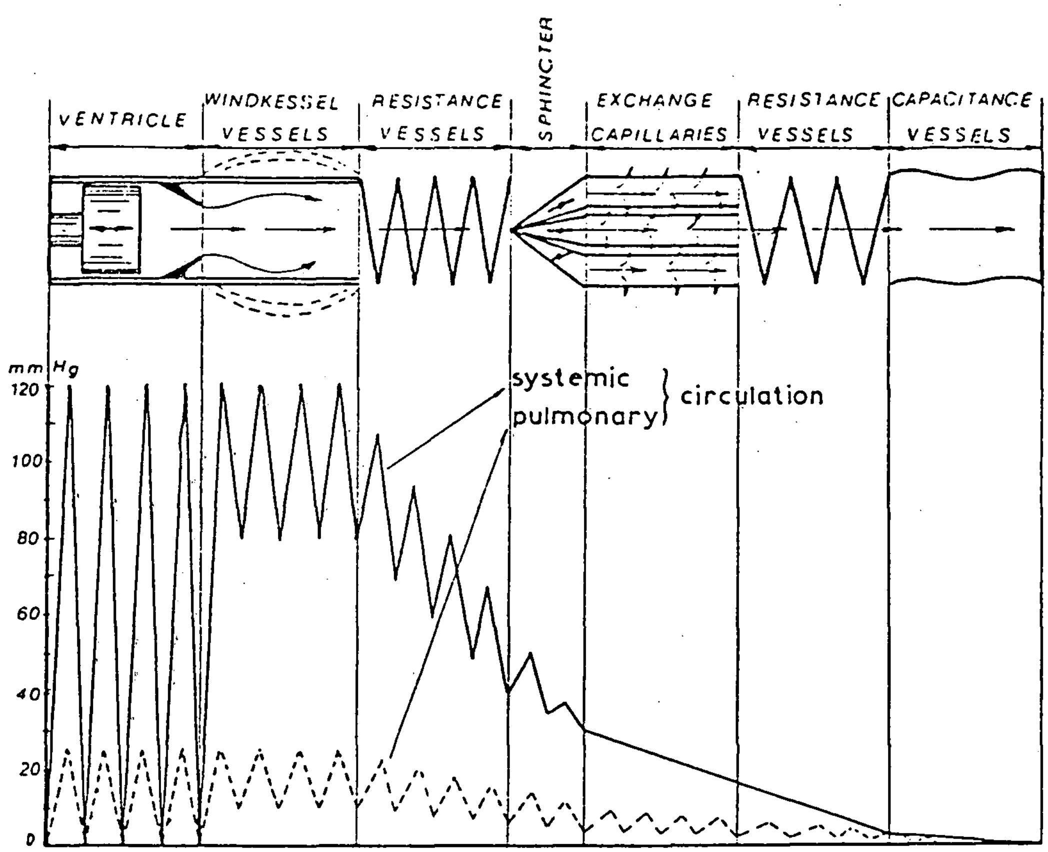

Precapillary sphincters consist of rings of smooth muscle. They are typically located near the arterial entrance to the microvascular bed, surrounding arterial blood vessels. Contraction of the sphincters determines the size of the capillary exchange area by modifying the number of capillaries perfused at any one moment [8].

The capillary exchange vessels form the most important region of the vascular system with respect to the exchange of fluid and other material between the blood and tissues (microvascular exchange). The capillary wall acts as a selective membrane, influencing the transfer of life-sustaining chemical compounds between the blood and tissue cells [8]. This delicately balanced system is obviously highly susceptible to burn injuries in tissues such as skin.

2.1.3 MICROVASCULAR EXCHANGE

The microvascular exchange system is essential for the maintenance of the health and well-being of the individual. Since it is the subject of our model, a more detailed description of its physiology will be given.

2.1.3.1 General Description

The microvascular system can be divided into six parts (see Figure 2.4) based on their different location and function:

1. precapillary sphincters,
2. arterial capillaries,
3. true capillaries,
4. venous capillaries,
5. the surrounding tissue and
6. the lymphatics.

As previously mentioned, the precapillary sphincters form the connection between arterioles and the capillaries. The capillaries of the network nearest to the arterioles are called arterial capillaries, and those nearest to the venules are called venous capillaries. The capillary network between arterioles and venules often contains a thoroughfare channel called the central channel, where the blood flow is continuous, in contrast to the branches of the capillary network, where the flow tends to be intermittent. The surrounding tissues include muscle and skin or other tissues. The drained substances of the surrounding tissues return to the circulation via lymphatic channels (see Figure 2.5).

Figure 2.4 The Microvascular System [9]

a) Branching Network of Circulation

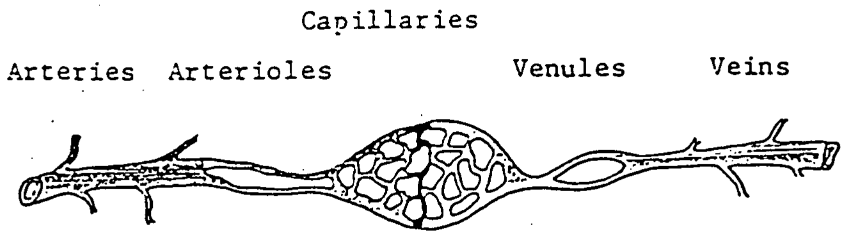

b) A Typical Microvasular Pattern

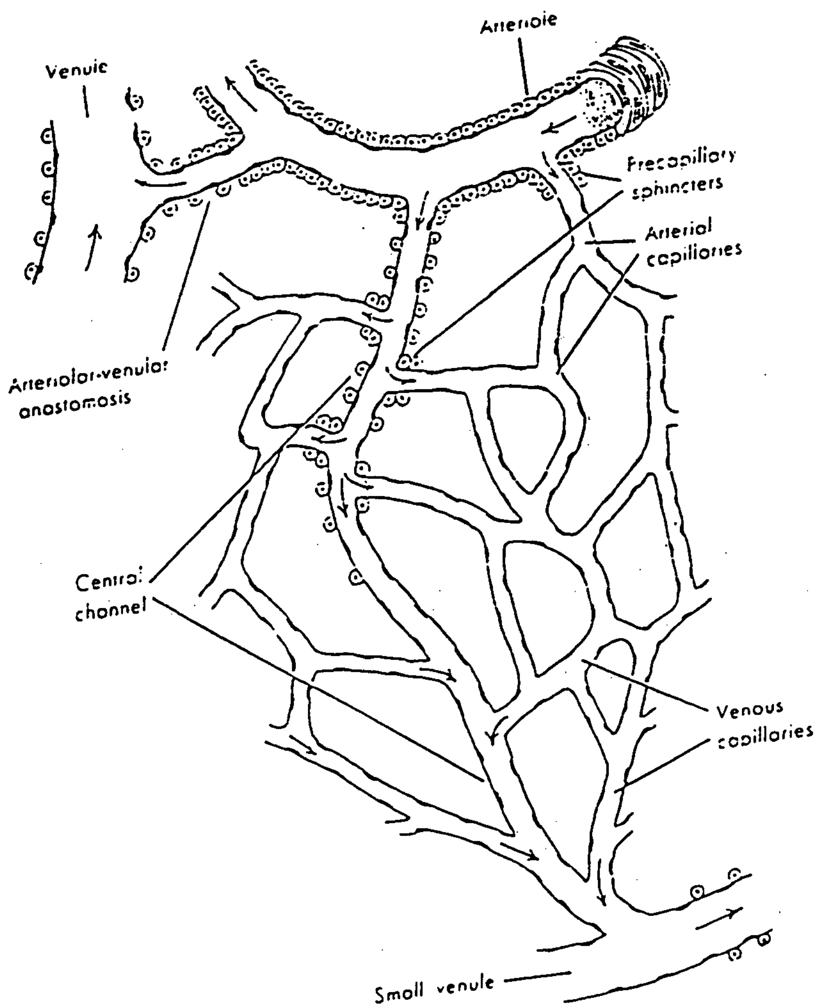

Figure 2.5 Relationship of Capillaries, Tissues and Lymphatics [9]

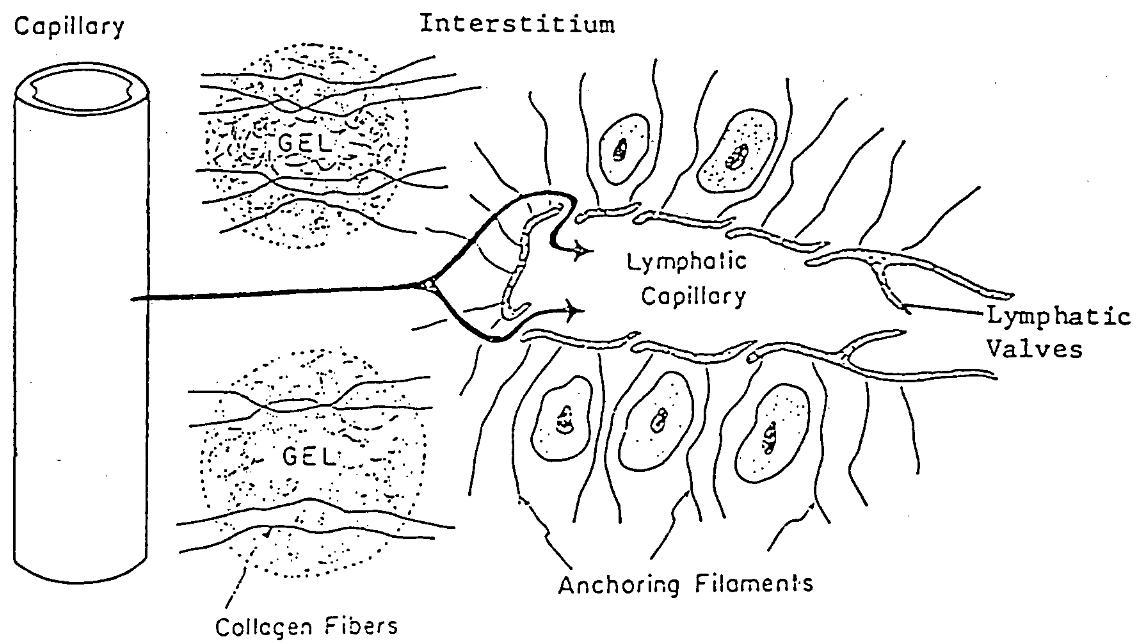

The capillary walls consist of a single endothelial cell layer which separates the blood from the interstitium. Ordinarily, adjacent endothelial cells are separated by a narrow cleft (see Figure 2.6) [8].

The capillaries branch extensively without much change in calibre. The density and pattern of the capillary networks vary in the different tissues and organs. The tissues with the highest metabolic activity have more elaborate branches and closely packed capillaries than low metabolic activity tissues. In skin, for example, the branches are numerous [8].

Normally, a capillary is closed to blood flow about 60% to 95% of the time. Apparently being perfused 5% of the time is adequate under resting circumstances. Therefore, only about 5% of capillaries may be open at any one time but this 5% is constantly changing so that all capillaries are perfused in turn. This may be compared to a farmer opening and closing irrigation head gates so as to insure that each row of crops is irrigated in turn. Increased metabolic activity increases the percentage of capillaries open (Figure 2.7) [8].

Figure 2.6 Clefts in the Capillary Membrane [16]

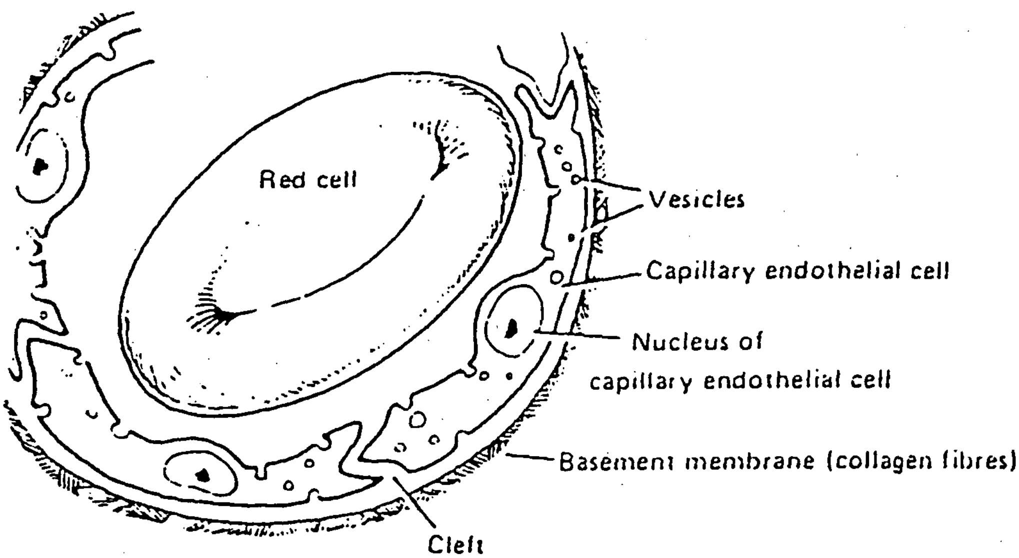

Figure 2.7 Farmer Irrigating Crops - an Analog to Capillary Perfusion [16]

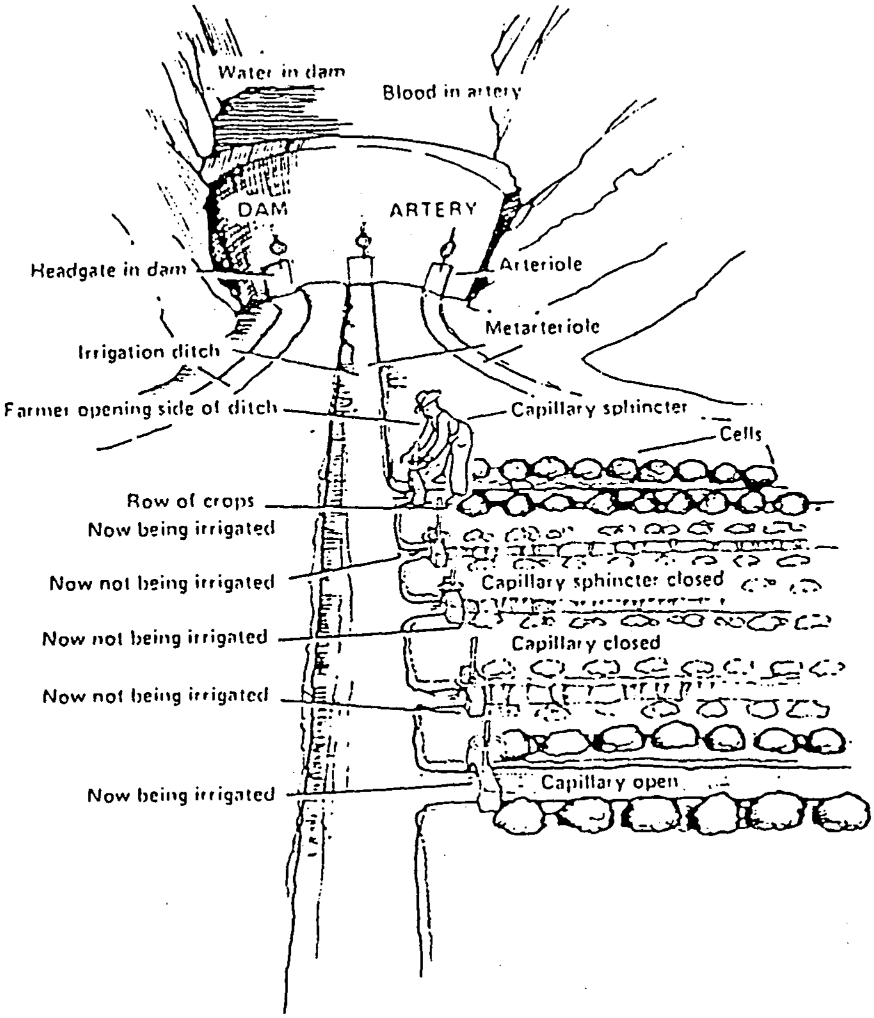

2.1.3.2 The Driving Force for Microvascular Exchange

The passage of fluid across the capillary wall is dependent on the following driving forces:

1. the blood pressure within the capillaries,
2. the colloid osmotic pressure in the interstitium,
3. the colloid osmotic pressure in the blood and
4. the hydrostatic pressure in the interstitium.

According to Starling's Hypothesis, the first two factors promote passage of fluid from the vessels to the tissues, while the last two factors favor reabsorption into the blood.

The blood pressure in the arterial capillaries is normally higher than in the venous capillaries, and the blood pressure on the arterial side also normally exceeds the colloid osmotic pressure of the blood plasma. Based on these pressure relationships, fluids normally pass from the vessels to the tissues in the arterial part of the capillary bed and return to the vessels via the venous capillaries, small venules, and lymphatic channels [8]. Pressure within the capillaries can be modified at the local level by vasoconstriction and vasodilation through contraction and relaxation of smooth muscle cells in the walls of arterioles, metarterioles and precapillary sphincters. Arterial blood pressure also influences capillary flow. Elevation in pressure caused by an increase in cardiac output will increase capillary flow. Elevation in blood pressure caused by arteriolar constriction decreases capillary flow. Actually, changes in arterial pressure usually involve elements of both, so that capillary flow may be increased, decreased or unchanged [8].

2.2 PHYSICOCHEMICAL CHARACTERISTICS OF BLOOD

Blood, which is composed of cells and plasma medium, is circulated through the vascular system. Almost all the blood cells are red cells. Their main function is to transport the oxygen from the lungs to the tissues and organs. White and red cells exist in a ratio of 1:500 in the blood. White cells protect against invasion by disease organisms [9].

The plasma medium of blood is composed of primarily of water containing proteins and small dissolved ions. The plasma proteins can be classed as albumins, globulins and fibrinogen based on their molecular weight and function. Both in blood and in interstitial fluid, the albumin content is dominant (see Table 2.1). Albumin is normally the principle determinant of colloid osmotic pressure [10].

Table 2.1 The Protein Composition of the Blood and Interstitial Fluid for Humans Under Normal Conditions [11]

Protein	Blood (g/ml)	Interstitial Fluid (g/ml)
Albumin	0.042	0.025
Globulins	0.027	0.011
Fibrinogen	0.003	N.A.
Total Protein	0.073	N.A.

N.A. - not available

2.3 TISSUE AND PARTITION PROPERTIES

"The interstitium is the connective tissue space outside the vascular and lymphatic systems and the cells" [12]. There is a certain amount of water, its dissolved constituents, plasma proteins and glycosaminoglycans in the interstitial space [12]. The basic structure of the interstitium involves collagenous fibers which are made up of bundles of smaller units of collagen [12]. "The main functional effects of the collagenous fibers are that they resist changes in tissue configuration and volume, they exclude proteins, and they immobilize the glycosaminoglycans" [12]. Other than collagenous fibers, some tissues contain elastic fibers which have a rubberlike consistency, hyaluronate which is composed of unbranched high molecular weight polysaccharide, proteoglycans and cells [12].

Due to the geometric shapes of the interstitium components, the extravascular space accessible to a plasma protein or other macromolecules is limited [12]. Therefore, the effective volume available to proteins is reduced, and the effective protein concentration is increased.

This exclusion phenomenon can be described by the model of a sphere in a random network of rods. The protein is assumed to be in the shape of a sphere and the collagenous fibers are assumed to be cylindrical rods (see Figure 2.8). The volume into which the protein cannot enter (shaded area) due to the steric hindrance of the rods is termed the excluded volume [12]. The volume accessible to the spheres can be calculated by substracting the excluded volume from the total fluid content of this system. The colloid osmotic pressure in a given compartment (be it blood or tissue) is a function of the effective protein concentration in that compartment; which is obtained from the protein content and the nonexcluded volume of that compartment.

Another important property of the interstitium involves the relationship between interstitial fluid volume and tissue pressure. These are related through a compliance relationship often expressed as tissue pressure as a function of interstitial volume (see Figure A.1). In this figure note that as interstitial fluid volume becomes very large, only slight changes in tissue hydrostatic pressure result. At moderate values of interstitial fluid volume, the change in tissue pressure due to a change in fluid volume is substantially greater.

Figure 2.8 Model of Volume Exclusion [12]

Sphere in a Random Network of Rods

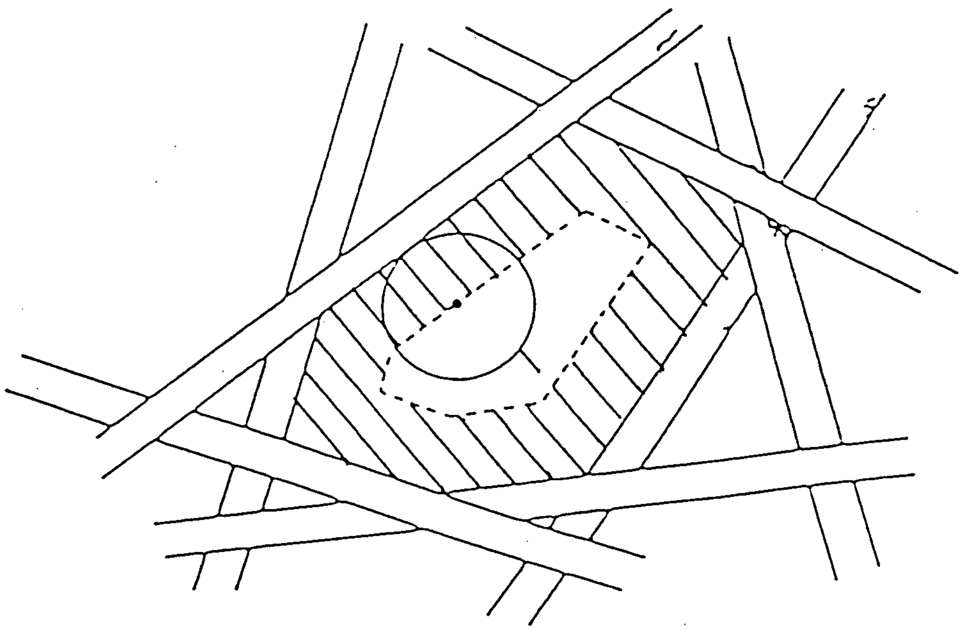

2.4 THE LYMPHATICS

The lymphatic system is a closed vascular system [13]. It is composed of endothelial-lined channels, which run parallel to the arterial and venous system. Interstitial fluid containing plasma protein normally drains from the interstitium and is returned to the blood circulation via the lymphatics (see Figure 2.5).

The mechanism of lymph flow is very complex but may be controlled by tissue hydrostatic pressure [13]. As the interstitial fluid volume increases, the tissue hydrostatic pressure increases according to the tissue compliance relationship. This in turn causes a marked increase in local lymph flow (Figure 2.9), hence preventing tissue overloading (edema) [13]. It is hypothesized [13] that when interstitial fluid pressure rises to a certain level, the relative lymph flow does not increase. If that is true, the lymphatic system protects against edema formation only up to limiting tissue pressure.

Figure 2.9 Relationship Between Tissue Pressure and Lymph Flow [13]

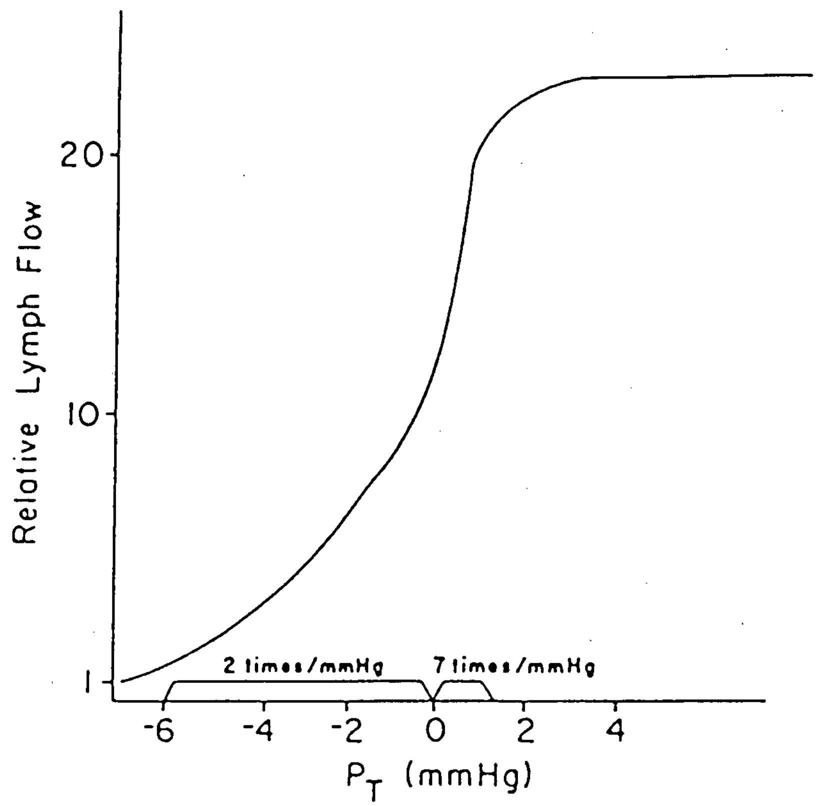

Chapter 3

PHYSIOLOGICAL CHANGES AFTER BURNS

The experimental information in the literature concerning the characteristic changes of the microvascular exchange system after a burn injury will be reviewed. These changes may be grouped into the following three categories:

1. changes in capillary permeability and effective surface area,
2. changes within the blood circulation, and
3. changes within the interstitium.

The results of the above physiological changes are also reviewed with respect to the following:

1. plasma volume loss,
2. edema and increased protein content in the tissues, and
3. increased lymph flow.

The literature contains a number of experimental burn studies using different animal species. The live animal subjects were exposed to varying extents of thermal injury. Most of the experiments were conducted without fluid resuscitation. Due to differences between protocols, these experiments will be compared only in very general terms.

3.1 CHANGES IN CAPILLARY PERMEABILITY

Following a burn, the transfer of fluid and plasma proteins from the blood to the tissue increases. This was first demonstrated in 1943 by Netsky and Leiter [18], who measured the rate of serum protein crossing the capillary endothelium of dogs. The finding of an increase in transcapillary macromolecular transport was confirmed later using radioactive dyes and Evans blue as test substances [18]. In fact, molecules as large as 125,000 MW, which do not normally cross the endothelial barrier, have been exchanged following a burn [19], implying an increase in entholelial permeability.

The investigation of change in capillary permeability surface area product as a result of a thermal injury has been the subject of many studies [18,20,21,22,23,24]. The results of some of these experiments are listed Table 3.1. It is difficult to compare these works directly due to differences in the animal model, degree and area of burn as well as the time interval under investigation. At best we can hope to identify trends in the behaviour of this system resultant to a thermal injury. One example of these experiments is the work of Arturson and Mellander in 1964. In his work, cats were subjected to a second degree burn. The capillary filtration coefficient in the injured tissue was then measured. It was found that, following an acute

TABLE 3.1 PERMEABILITY CHANGE [18, 20, 21, 22, 23, 24]

					PARAMETERS MEASURED IN INJURED SKIN			PARAMETER MEASURED IN INTACT TISSUES		
	ANIMAL	BURN DEGREE	PERCENT BURN AREA	EXPT. TIME	PARAMETERS	PERCENT CHANGE	DURATION OF THE CHANGE	PARAMETER	PERCENT CHANGE	DURATION OF THE CHANGE
Arturson et al. 1964	cat	2nd	one paw	0-60 minutes	Capillary Filtration Coefficient	Increases ~ 300% maximum	~ 60 minutes			
Carvajal et al. 1975	guinea pig	2nd	$6 cm^2$	The 3rd hour after burn	Protein Extravasation	Increases ~ 8.4 times maximum				
Brouhard et al. 1977	rat	2nd	0.2%	0-48 hour	Protein Extravasation	Increases ~ 16 times maximum	12 hours			
Brouhard et al. 1978	rat	2nd	0.2%	1/2 hour post burn 3 hour post burn 6 hour post burn	Protein Extravasation	Increases ~14 times maximum Increases ~2.3 times maximum Increases~1.14 times maximum				
Carvajal* et al. 1978	rat	deep 2nd	10% 20% 30% 40%	0-24 hours	Protein Extravasation	Increases ~14 times maximum Increases ~12 times maximum Increases ~19 times maximum Increases ~12 times maximum	12 hours	Protein Extravasation	Remain normal Increases ~70% maximum Increases ~ 6 times maximum Increases ~ 2 times maximum	12 hours
Lund et al. 1986	rat	3rd	10% 40%	0-3 hours	Protein Extravasation	Increases ~54 times maximum Increases ~7 times maximum				

* Injured animals are resuscitated in these experiments
C/min/GDW: counts/minutes/gram of dry weight

burn, there was a very rapid transfer of fluid from the intravascular to the extravascular space of the injured tissue, and that the capillary filtration coefficient increased by 100 to 300 percent of its control value [18].

The increased capillary fluid conductivity may reflect two distinct changes in the microvascular bed:

1. Due to the application of heat, intercellular junctions in the capillary membrane become wider [18]. Fluid and proteins exude rapidly from the capillary to the interstitial space through these gaps in the endothelial wall. In severe cases, direct damage to the endothelial cell may disrupt the capillary wall, increasing its conductivity [25].
2. Following thermal injury to the microvascular bed there is an associated release of histamine-like mediators. These mediators increase the metabolic level in the capillaries, which in turn increases the number of relaxed precapillary sphincters. Hence more capillaries are perfused. The effective capillary surface area for exchange is therefore increased [21]. However, the blood flow to the tissues may decrease which effectively decreases the capillary perfusion rate and the surface area for exchange. This will be discussed further in Section 2.2.5.

In any burn, increased capillary leakage occurs in the injured skin. However, in the case of thermal injury involving over 25% of the total body surface, this increased leakage has been observed in nonburned tissues as well [26,27].

The information in Table 3.1 indicates that the protein exchange rate in the injured skin typically increases to more than ten times its normal value after a burn. For rats, this permeability increase lasts for approximately 12 hours. For the noninjured tissues, protein exchange rate remains normal for 10% burns, and increases for burns larger than 20%. However, the protein exchange rate increase in the noninjured tissues is not as much as in the injured skin, only 1 to 5 times its normal value. The permeability changes in the intact tissues tend to last about 12 hours as well. Unforturnately, there is not enough information available in the literature to allow a distinction to be made between the fraction of the capillary permeability surface area product change which is due to changes in conduction across the endothelial membrane and the fraction which is due to changes in capillary perfusion.

3.2 CHANGES WITHIN THE BLOOD CIRCULATION

Associated with the profound changes in the capillary permeability after thermal injuries, are acute effects on the circulation. In particular the following aspects of the blood circulation as reported in the literature have been investigated:

1. the cardiac output,
2. the main arterial pressure,
3. the central venous pressure,
4. total peripheral resistance, and
5. the blood perfusion.

The results are summarized in Table 3.2 and briefly discussed in the following sections.

3.2.1 THE CARDIAC OUTPUT

There is a marked fall in cardiac output soon after injury in experimental animals with extensive burns [28,29,30,31,32,33] (see Table 3.2). This large decrease in cardiac output is due to reduced stroke volume and reduced heart rate [33]. For example, Figure 3.1 illustrates the changes in the heart rate, the stroke volume, and the cardiac output following thermal injury in guinea pigs [31].

TABLE 3.2 HEMODYNAMIC CHANGE [28, 29, 30, 31, 32, 33]

					PRESSURE CHANGE		PERFUSION				
										BLOOD FLOW	
	ANIMAL	BURN DEGREE	PERCENT BURN AREA	EXPT. TIME	MAIN ARTERIAL PRESSURE	CENTRE VENOUS PRESSURE	CARDIAC OUTPUT	STROKE VOLUME	TOTAL RESISTANCE	INJURED TISSUE	NON INJURED TISSUES
Wolfe et al. 1976	guinea pig	Between 2nd and 3rd.	55%	0-24 hours	Decreases ~ 35% maximum		Decreases ~ 60% maximum	Decreases ~ 50% maximum	Increases ~2.0 times maximum		
		Between 2nd and 3rd	70%	0-24 hours	Decreases ~ 10% maximum		Decreases ~ 85% maximum	Decreases ~ 60% maximum	Increases ~5.5 times maximum		
Ferguson et al. 1977	guinea pig	3rd	70%	0-75 minutes			Decreases ~ 60% maximum	Decreases ~ 50% maximum		Decreases ~ 95% maximum	Muscle: decreases ~30-60% maximum Intact Skin: decreases 80% maximum
Delming* et al. 1978	sheep	3rd	40%	0-69 hours		remains normal	Decreases ~ 15% maximum				
Ferguson et al. 1980	guinea pig	3rd	over 70%	0-8 hours	Decreases ~ 25% maximum		Decreases ~ 57% maximum	Decreases ~ 45% maximum	Increases ~ 2 times maximum		
Harms* et al. 1981	sheep	3rd	25%	0-72 hours	Increases ~ 13% maximum	Decreases ~ 67% maximum					
Lund et al. 1986	rat	3rd	10%	0-3 hours	Decreases ~ 20% maximum	remains normal	Decreases ~ 10% maximum	Decreases ~ 8% maximum			
			40%	0-3 hours	Decreases ~ 35% maximum	remains normal	Decreases ~ 40% maximum	Decreases ~ 25% maximum			

* Injured animals are resuscitated in these experiments

Figure 3.1 Cardiac Output, Stroke Volume and Heart Rate for Guinea Pigs After a 70% Burn [31]

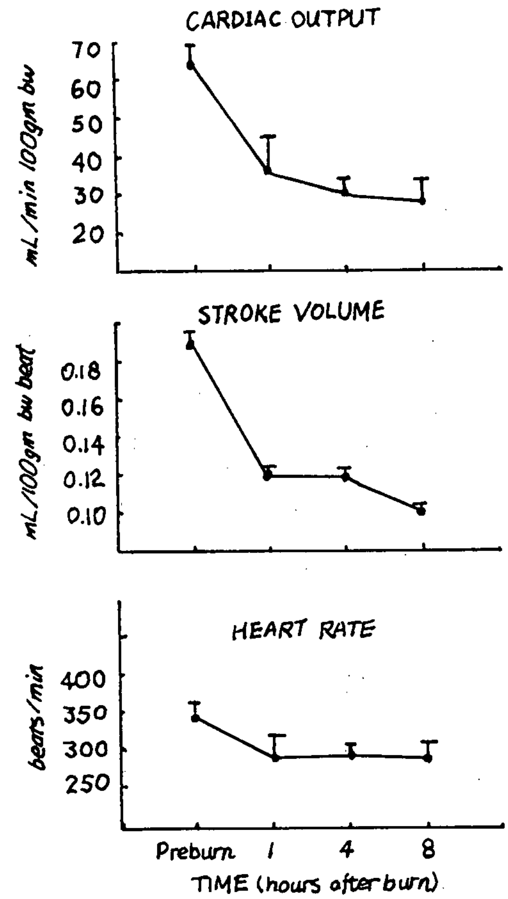

3.2.2 THE MAIN ARTERIAL PRESSURE

The main arterial pressure (MAP) is reported to decrease following a burn [28,31,33] (see Table 3.2). The degree of reduction is dependent in part on the fraction of total surface area burned [33]. For example, in the experiments of Lund and Reed [33], the fall in the MAP following a 40% burn is greater than that following a 10% burn. The MAP in the 10% burn group decreased from 110 mmHg to 97 mmHg after 15 minutes postburn, and remained at around 86-94 mmHg up to 3 hours afterwards. The maximum fall of the MAP in the 10% burn group was 20% of the control value. However, in the 40% burn group, MAP fell from 110 mmHg to 80 mmHg in the first 15 minutes after the burn was induced and remained at a 70-80 mmHg level after 30 minutes postburn up to three hours. The maximum fall in the 40% burn group is 30% of the control value [19].

3.2.3 THE CENTRAL VENOUS PRESSURE

Experimentally, the central venous pressure (CVP) did not appear to change significantly following a burn injury [24,30] (see Table 3.2). In some experiments, no change was observed [24,31]. In one experiment, the CVP decreased slightly [32]. The experiment of Lund and Reed [33] on rats subjected to 10% and 40% burns showed that the CVP did not change significantly [33].

3.2.4 TOTAL PERIPHERAL RESISTANCE

While the cardiac output and mean arterial pressure decreased following a burn, the total peripheral resistance increased (see Table 3.2). This finding has been supported by a number of investigators, including Wolf et al. [28] and Ferguson et al. [31]. Unlike other investigators, Arturson measured a decrease in the regional resistance of the venous capillary following a thermal injury [18].

3.2.5 THE BLOOD FLOW

As a consequence of the depressed cardiac output, the decrease of the mean arterial pressure and the assumed increase of the total peripheral resistance, a reduced capillary blood flow occurs both throughout the general systemic circulation and in the injured tissue [29]. In some cases, the high resistance may even halt the capillary flow [29]. These factors therefore tend to decrease the perfusion rate both in the injured skin and the non-injured tissues. For example, the experiments of Ferguson et al. on guinea pigs [29] showed that blood flow in different organs and tissues was depressed tremendously. Following a third degree burn over 70% of the surface area, the blood flow decreased by 95% in the injured skin, 30% to 60% in the muscle, and 80% in the intact skin (see Table 3.2). Very little additional quantitative information is available concerning the blood flow in tissues following a thermal injury. Personal communications with A. Haugan of The Department of Physiology, University of Bergen, Norway corroborate these findings.

With respect to fluid exchange between the circulation and the tissue space, the tendency towards decreased perfusion opposes the effect of the histamine-like mediators discussed earlier (see Section 3.1).

3.3 CHANGES WITHIN THE INTERSTITIUM

In 1964, Arturson noticed that after a second degree burn to cats, there was a very rapid increase of interstitial volume, but only a moderate increase of the capillary filtration coefficient [18]. He suggested that some mechanism, other than the increase of capillary permeability, also contributed to edema formation. He suggested that the early edema may be due primarily to a temporary change in the transcapillary osmotic pressure difference. However, this has not been proved experimentally.

Lund et al. [34] investigated the importance of the tissue pressure (P_b) in injured skin with respect to edema formation following a burn. P_b in rats was measured both in 10% and 40% body surface area burns up to three hours after the burn. A rapid decrease in P_b, uncharacteristic of the normal tissue compliance behaviour was noted. The injured tissue hydrostatic pressure following a burn as a function of time is shown Figure 3.2 and Figure 3.3 for 10% and 40% burns, respectively. Though the experimental errors associated with measurement of tissue pressure in the injured skin (one standard error is shown) are large, clearly some dramatic changes are occurring within the interstitium.

Following a 10% burn, the intradermal P_b decreased rapidly from its control value of -1.21 mmHg. At around 40 minutes postburn, it reached a minimum value of -20 mmHg. In the 40% burn, P_b dropped more dramaticlly to a minimum of -24 to -30 mmHg at 30 to 40 minutes postburn [34]. In both cases, P_b rose to slightly above its normal value within 180 minutes postburn [34].

Whether this strongly negative pressure drop is related to the transcapillary osmotic pressure gradient advocated by Arturson is not clear, but is is believed to be a major driving force in interstitial edema formation at least in the early stage of the burn injury.

Figure 3.2 The Tissue Hydrostatic Pressure of Injured Skin for Rats Subjected to a 10% Burn [34]

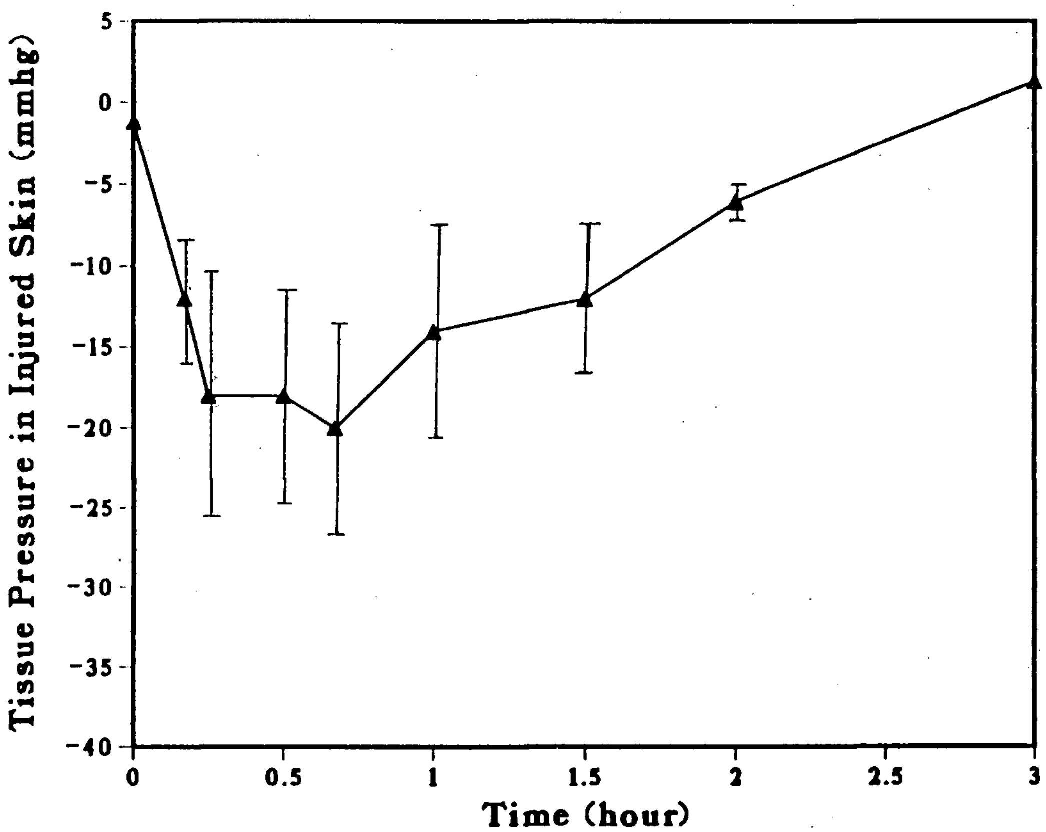

Figure 3.3 The Tissue Pressure Hydrostatic Pressure of Injured Skin for Rats Subjected to a 40% Burn [34]

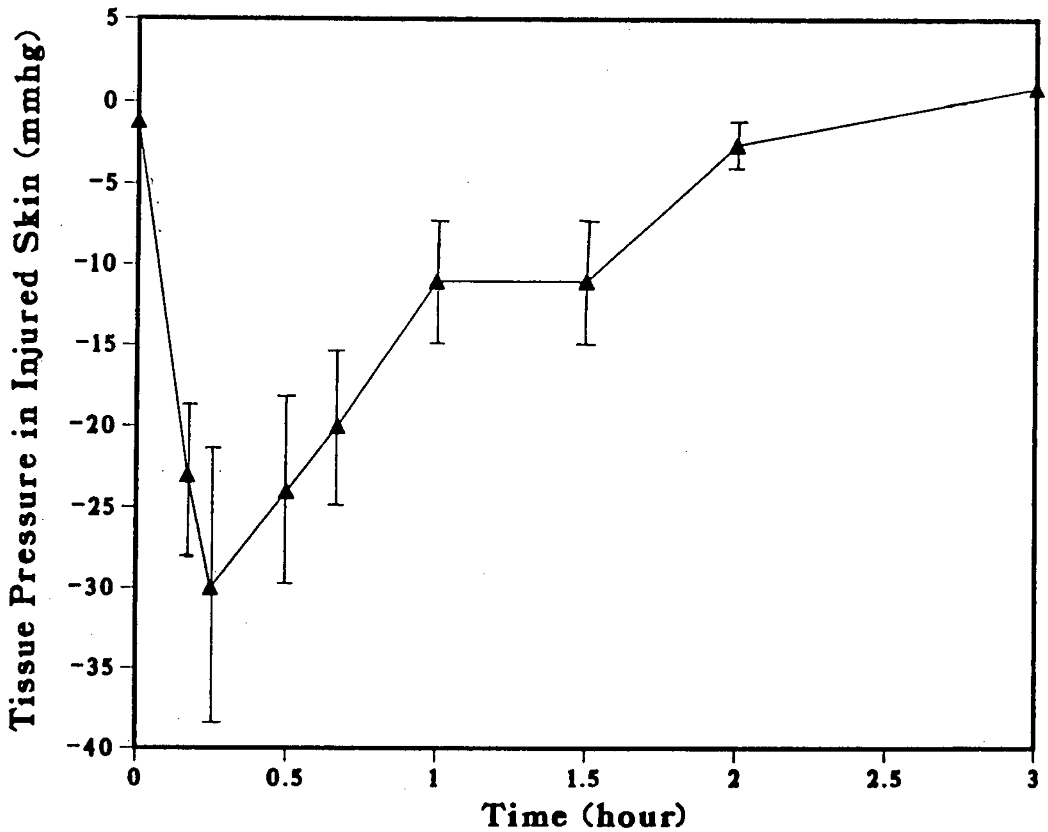

3.4 SYMPTOMS OF BURN INJURIES

The permeability, hemodynamic and tissue pressure changes described above cause a number of physiological responses in experimental animals following a burn injury. The available experimental data concerning these responses is summarized in Table 3.3 and discussed briefly in the sections which follow.

3.4.1 PLASMA VOLUME LOSS (HYPOVOLEMIA)

Owing to the postburn physiological changes mentioned in Sections 3.1 to 3.3, fluid and proteins from the circulation leak rapidly to the burned tissue and, in more severe cases, even to the nonburned tissues [1]. This causes a large loss of plasma volume (hypovolemia) and a decreased protein content in the circulation. These results are confirmed by many investigators including Leap [37] and Reed et al. [45] (see Table 3.3).

For example, Leap measured the hematocrit change in monkeys following a 50% burn [37]. The estimated plasma volume from the hematocrit data showed a maximal plasma volume decrease of 30% to 40% in 4 hours. He also demonstrated a decrease in plasma albumin concentration of 10% to 20%.

Table 3.3 CHARACTERISTIC EFFECTS OF EXPERIMENTAL BURN INJURIES

[18, 35, 36, 37, 38, 39, 40, 41, 42, 43, 44, 45]

	ANIMAL	BURN DEGREE	PERCENT BURN AREA	EXPT. TIME	VOLUME OF PLASMA	COP OF PLASMA	COP OF INJURED SKIN	FLUID CONTENT OF INJURED SKIN	FLUID CONTENT OF INTACT SKIN OR MUSCLE	PROTEIN CONTENT OF INJURED SKIN	PROTEIN CONTENT OF INTACT SKIN OR MUSCLE	LYMPH FLOW IN INJURED SKIN	DURATION OF EDEMA
Arturson et al. 1964	cat	2nd	one paw	0 1 60 min.				Increases ~170ml/100g tissue maximum					
Arturson et al. 1967	dog	2nd		0 1 14 days				Increases 40-50% maximum				Increases 4-6 times maximum	Injured tissue: longer than 14 days
Leape 1968	rat	3rd	50%	0 1 4 hours				Increases ~ 63% maximum		Increases ~ 90% maximum			
Leape 1970	Rheeus monkey	3rd	50%	0 1 4 hours	Decreases 30-40% maximum	Plasma conc. decreases 10-20% maximum		Increases 70-80% maximum	remains constant	Increases ~ 5 times maximum	Intact skin: remain constant muscle: decreases 10%-20% maximum		
K.L. Green 1977	mouse		one paw	0 1 40 min.				Increases		Increases			
Brouhard et al. 1978	rat	2nd	0.2%	0 1 48 hours				Increases ~ 72% maximum	remains constant	Increases			24 hours
Carvajal* et al. 1979	rat	deep 2nd	10% 20% 30% 40%	0 1 24 hours				Increases ~ 94% maximum	intact skin: increases 20% maximum muscle: remains ~ constant				longer than 24 hours
Demling* et al. 1981	sheep	3rd	25%	0 1 72 hours								Increases 4.5 times maximum	
Demling* et al. 1983	sheep	3rd	30%	0 1 2 hours		decreases ~ 20% maximum							
Demling* et al. 1984	sheep	2nd		0 1 168 hours				Increases 100% maximum				Increases 10 times maximum	168 hours
Arturson* et al. 1984	patients	2nd	26% 1 58%										
Reed et al. 1986	rat	3rd	10% 40%	0 1 3 hours	decreases ~ 20% maximum decreases ~ 30% maximum	decreases ~ 20% maximum decreases ~ 30% maximum	Increases ~ 40% maximum Increases ~ 20% maximum	Increases ~80% maximum Increases ~20% maximum	Increases 8% maximum Increases 11% maximum	Increases 2-5-3 times Increases ~2 times	Increases 50% maximum Increases 50% maximum		

* Injured animals are resuscitated in these experiments

Lund and Reed [45] recently measured the volume and colloid osmotic pressure (COP) of plasma in rats with third degree, 10% and 40% surface area burns. Their results showed that the volume of plasma decreased by 20% to 30% within three hours postburn. Over the same time period, the plasma COP also decreased by 20-30%.

3.4.2 EDEMA FORMATION AND TISSUE PLASMA PROTEIN CONTENT

In all the experiments listed in Table 3.3, the fluid and the protein content of the injured tissue increased after burns. For example, Leap measured the fluid and protein content in the injured skin of rats subjected to third degree, 50% burns. His results showed that the fluid content of the injured skin increased by 70% of its normal value and the protein content by 90% [36]. Among the investigators listed in Table 3.3, Reed et al. [45] are the only ones who measured the COP of the injured skin. Their results revealed that the burned skin COP increased by 40% after a 10% burn, and by 20% after a 40% burn.

The responses of fluid and protein content in the intact tissues from Table 3.3 are not consistent. Some investigators found that the fluid content in the intact tissues remained approximately normal after burns [37,39]. Others measured an increased fluid content in the intact tissues [40,45]. Thus the protein content in the intact tissue could increase, decrease or remain constant according to Table 3.3.

The duration of the edema also varies considerably from one investigation to the next. For example, Carvajal et al. [24] used rats as animal models. They reported that the water content of burned tissues increases rapidly, is maximal at about 3 hours, and disappears by 24 hours postinjury. Others use different animals in their experiments and claim that the edema is present for several days to two weeks [35,43].

3.4.3 LYMPH FLOW

The lymph flow draining the various tissues has frequently been used to assess microvascular fluid filtration rate and protein permeability characteristics for the particular tissues involved. The composition of lymph is often assumed to reflect interstitial fluid volume and the flow rate to reflect the quantity of edema [46].

The increase of lymph flow in the injured skin postburn was reported by many investigators including Arturson et al. [35] and Demling et al. [41,43] (see Table 3.3). Both have estimated the lymph flow change in the injured skin. Arturson measured lymph flow in dogs after a second degree burn, and found an increase in lymph flow of 4 to 6 times the control value within 6 hours postinjury [35]. Demling noticed a marked increase in lymph flow in the sheep which lasted more than four days after the burn [41,43]. However, it is questionable whether the lymph flow measured by either group represented only that from injured skin.

Chapter 4

BRIEF SURVEY OF COMPUTER SIMULATIONS OF MICROVASCULAR EXCHANGE

Computer simulations have provided an additional method by which physiological systems may be studied. Models of microvascular exchange have been developed to describe the distribution and transport of fluid and plasma proteins between the circulation, interstitial space and the lymphatic system. The most pertinent of these models will be reviewed here.

4.1 MODELS OF MICROVASCULAR EXCHANGE IN NORMAL TISSUES

Models of microvascular exchange fall into two categories, distributed and compartmental models. The compartmental models divide the microvascular exchange system into several well-mixed but separate compartments. The overall mass balances, which account for fluid and protein transport between each compartment, are written as a set of ordinary differential equations. The distributed or position-dependent models eliminate the well-mixed assumption. Hence, a more complex description of the fluid and protein transport in the microvascular system is required. The fluid and protein balances must now be written around a differential volume element in each part of the system yielding a set of partial differential equations which are more difficult to solve. The distributed models are not sufficiently well-developed at present and have yet to be extensively applied to existing experimental or clinical data. Compartmental models, on the other hand, have been used reasonably successfully in describing the behaviour of the microvascular exchange system resultant to perturbed states.

One of the most successful compartmental models of microvascular exchange for humans is the model of Wiederhielm [47]. In this two-compartment model, the dynamics of fluid and plasma protein transport between the circulation and the interstitium were studied. The interstitial compartment included muscle, skin and all the other tissues. To account for exclusion effects, the interstitium was assumed to have two phases: a gel phase composed of mucopolysaccharides which is accessible to fluid but not to proteins and a free fluid phase containing the plasma proteins. At any time, this two-phase system is in osmotic equilibrium. The model was used to analyse the behaviour of the microvascular exchange system following a variety of perturbations, such as changes in plasma colloid osmotic pressure, arterial and venous pressures, interstitial mucopolysaccharide content and lymphatic obstruction [47]. This model has been shown to some extent to predict the redistribution of fluid and proteins which take place during pathological conditions.

Studies of fluid and protein transport have been furthered in the model by Bert and Pinder [48]. This model was developed from Wiederhielm's compartmental model, but an interstitial "excluded volume" was used in place of the gel phase of Wiederhielm's model. The model of Wiederhielm was modified by Bert and Pinder based on the assumption and experimental observations that the volume exclusion in a given tissue is a function of its collagenous fiber content and remains constant even if the tissue swells. Using the same input parameters as Wiederhielm, the "volume exclusion" model of Bert and Pinder predicted results for both normal and perturbed conditions which were in good agreement with those of the earlier model. The introduction of constant volume exclusion eliminated several uncertain assumptions required by the two-phase model of Wiederhielm and, as a consequence, resulted in a significant simplification to the overall model.

Based on the model of Wiederhielm [47] and the model of Bert and Pinder [48], a dynamic model for interstitial fluid exchange in rats, the Plasma Leak model, has been developed by Bert et al. [6]. This model divided the interstitium into two separate compartments: muscle and skin. The reason for subdividing the interstitium was that the colloid osmotic pressure relationship, the compliance curve and the normal steady-state conditions for muscle and skin are very different. The Plasma Leak model was able to provide a much more elaborate description of the fluid and protein exchanges taking place between the circulation, the interstitial space of skin and muscle and the lymphatics. The model was used to predict the behaviour of all microvascular exchange parameters in rats for several perturbations, such as for changes in venous pressure and plasma colloid osmotic pressure as well as for over- and dehydration. The predictions of the model compare well with the large amount of experimental data available in the literature for this experimental animal.

4.2 MODELS OF MICROVASCULAR EXCHANGE FOLLOWING A THERMAL INJURY

Recently, compartmental models have been applied to study the fluid and protein redistribution that occurs following a thermal injury. For example, Arturson [6] has recently modified the model of Wiederhielm to make it applicable to thermal injuries in humans. In his burn model, Arturson divided the microvascular exchange system into three compartments: the plasma, the nonburned tissues (including both muscle and intact skin) and the burned tissue (assumed to be skin). It was also assumed that each compartment was well-mixed, that there was no exchange of protein or fluid between the burned and nonburned tissues and that the fluid and protein were lost from the system only by exudation and evaporation in the injured skin [5].

Arturson's mathematical model parallels that of Wielderhielm, except for the additional equations required to account for the existence of the burned tissue and the additional input/output. The total protein loss from the wound, was taken to be the product of fluid loss by exudation and the protein concentration in the injured skin [5]. The model was used to describe the rate of local and general edema formation. Its potential use would be in the evaluation of the fluid resuscitation requirements for patients who suffer from thermal injuries. This simplistic model predicted the distribution of overall edema and the rate of the edema formation. Arturson's model which considers only overall "tissue" fails to distinguish between muscle and skin and their different effects on microvascular exchange. The model needs to be improved in order to estimate fluid resuscitation requirements more realistically.

Another model which describes the fluid shifts which take place throughout the whole body during a burn is the model of Wachtel et al. [49]. This model does not consider microvascular exchange. Here, the plasma water input, urinary output, burn water loss, and insensible water losses via the unburned skin, lung, and gastrointestinal tract were simulated. This model can be applied to acute burn patients. Given the patient's body size and percentage of surface area burned, the model can be used to anticipate the loss of water from the wound, and calculate appropriate levels and time of resuscitation treatment. However, the model does not include the interstitial space which is an important location for fluid and protein exchange. Hence the structure of the model did not contain several necessary components. This gave rise to many clinically unrealistic features.

Thus, in order to find application in a clinical setting, present day burn models need to simulate more accurately not only the systems involved but also the changes which occur as a result of thermal injury.

Chapter 5

THE BURN MODEL

5.1 FORMULATION OF THE BURN MODEL

The burn model described here is an extension of the compartment model developed by Bert et al. [6] for microvascular exchange. The major difference between the present model and the previous model is that the former has an extra compartment. As was discussed in Chapter 3, the pathological responses in burned and nonburned skin immediately after a thermal injury can be very different. It is therefore necessary to divide the skin compartment into two parts: the burned and nonburned skin. As a consequence, the new model consists of four compartments: blood, muscle, injured skin and noninjured skin.

The primary objective of the simulation is to determine how fluid and plasma proteins are redistributed amongst the four compartments following a burn injury. For simplicity, it is assumed that the behaviour of all plasma proteins can be referenced to a single protein species, albumin. A schematic drawing of the four compartment model showing the various exchange paths for fluid (solid lines) and albumin (dashed lines) is given in Figure 5.1. As in the model of Bert et al., complete mixing is assumed to exist in each compartment except for the plasma compartment where a

Figure 5.1 Schematic Diagram of Burn Model

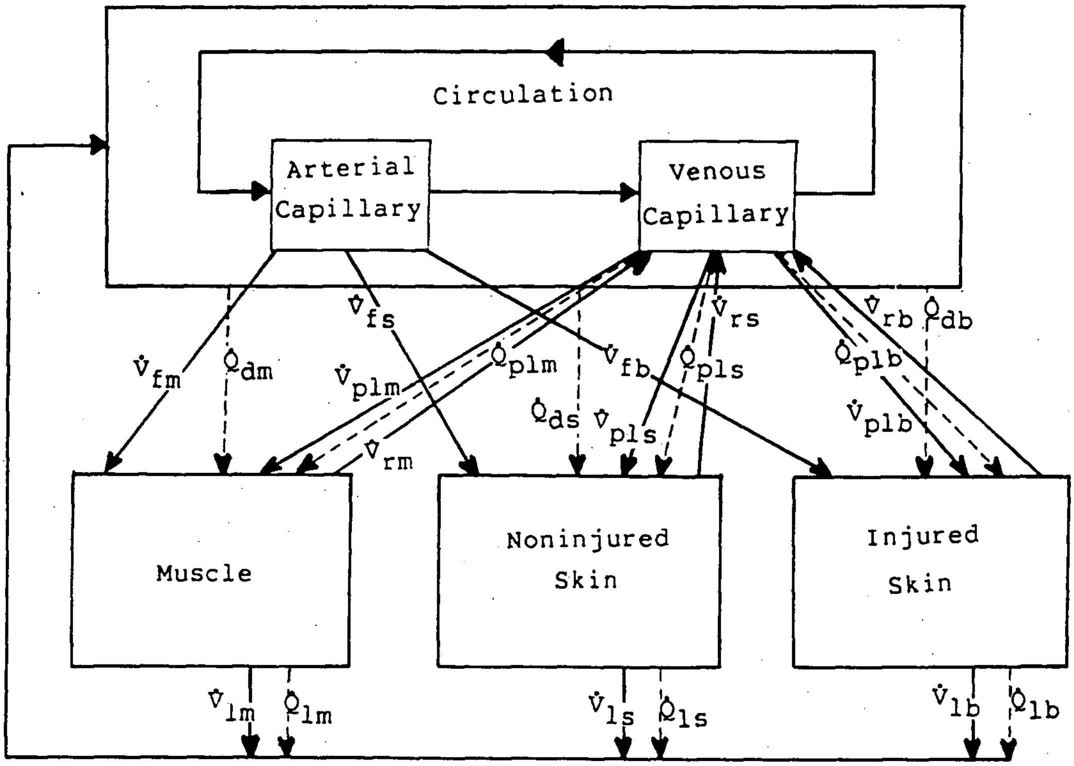

hydrostatic pressure difference is maintained between the arterial and venous ends of each capillary. Furthermore, in some numerical fitting experiments, the arterial and venous capillary pressures are allowed to have different values for injured skin than for noninjured skin and muscle. It is also assumed that there is no direct interchange of fluid or proteins between the tissue compartments; direct exchanges occur only between the circulation and each tissue separately.

At the capillary level, mass exchange is hypothesized to take place through a variety of mechanisms. Fluid is transfered by filtration ($\dot{V}_f$) from plasma to tissue at the arterial end of the capillary, by plasma leak ($\dot{V}_{pl}$) in the same direction but at the venous end of the capillary and by reabsorption ($\dot{V}_r$) which normally takes place from tissue to plasma also at the venous end. Filtration and reabsorption occur through small completely-sieving pores which are assumed to exist at both ends of the capillary, while plasma leak takes place through large non-sieving channels in the venous capillary only. Fluid in the tissue is drained by a unidirectional lymph flow ($\dot{V}_l$) and returned to the circulation. Albumin is exchanged between the capillary and the tissue space either by convection with the plasma leak ($\dot{Q}_{pl}$) or by diffusion across the capillary membrane ($\dot{Q}_d$). Plasma Proteins can only leave the tissue with the lymph ($\dot{Q}_l$).

It should also be noted that in our model, attention is focussed only on the transport of fluid and plasma proteins (albumin) in the microvascular exchange system. The transport of small ions between compartments and between the tissues and their cells is ignored. It is assumed therefore that the small ions in the blood, interstitium and lymphatics are always in equilibrium with one another and that there is no change to the cells before, during and after burns.

5.2 MATHEMATICAL RELATIONSHIPS

5.2.1 FLUID AND PROTEIN MASS BALANCES

The equations used in the burn model to describe the various fluid exchanges between the plasma and each tissue compartment are based on a Starling's type equation [46]. In these equations, the volumetric rate ($\dot{V}$) of fluid movement across the vascular endothelium is assumed to be proportional to the hydrostatic pressure (P) and the protein colloid osmotic pressure (Π) differences on either side of the membrane:

$$\dot{V} = K[(P_p - P_i) - \sigma(\Pi_p - \Pi_i)] \qquad 5.1$$

In Equation 5.1, K is a transport coefficient which depends on the fluid exchange area and the size of the fluid exchange channels within the endothelial barrier [46]. The second parameter σ is the protein reflection coefficient which usually has a value between zero and unity. If the vascular membrane is impermeable to protein, σ is 1. If the protein can pass through the membrane freely, σ is 0. The subscripts "p" and "i" denote the plasma and interstitial compartments, respectively. Fluid moves into the interstitium when the net driving pressure difference is positive (e.g. normal filtration); but moves out of the interstitium when the net pressure difference is negative (e.g. normal reabsorption).

The equations which describe the redistribution of fluid and proteins in a compartment following a burn are similar to those derived previously by Bert et al. for their "Plasma Leak Model" (submitted to the American Journal of Physiology). They are obtained by carrying out a mass balance of fluid or albumin around each compartment. For example, consider the fluid balance around a general tissue compartment. At any instant in time, the rate of accumulation of fluid within the compartment must be equal to the net rate of transfer of fluid to that compartment, or:

$$dV_i/dt = \dot{V}_f+\dot{V}_{pl}-\dot{V}_r-\dot{V}_l \qquad 5.2$$

where V_i is the volume of fluid in the tissue compartment and t is the time.

Since fluid filtration and reabsorption occur through pores which are impermeable to protein, the reflection coefficient in both cases is equal to unity. Thus when Equation 5.1 is applied,

$$\dot{V}_f = K_f[P_a-P_i-(\Pi_p-\Pi_i)] \qquad 5.3$$

and

$$\dot{V}_r = K_r[P_i-P_v-(\Pi_i-\Pi_p)] \qquad 5.4$$

where K_f and K_r are referred to as the filtration and reabsorption coefficients, respectively, and the subscripts "a" and "v" differentiate the arterial and venous ends, respectively, of the plasma capillary. Note that filtration is considered to be positive when it results in a net transfer of fluid into the tissue. The reverse is true for reabsorption.

In the case of the plasma leak, the large pores in the venous capillary allow the free passage of proteins and the reflection coefficient is zero. Thus, the plasma leak, $\dot{V}_{pl}$, is proportional to the hydrostatic pressure difference only, and Equation 5.1 becomes

$$\dot{V}_{pl} = K_{pl}(P_v - P_i) \qquad 5.5$$

where K_{pl} is the plasma leak coefficient.

For overhydration of the tissue, the lymph flow, $\dot{V}_l$, is assumed to be linearly-related to the change in interstitial fluid pressure, i.e.

$$\dot{V}_l = \dot{V}_{lo} + SL(P_i - P_{io}), \qquad P_i > P_{io} \qquad 5.6a$$

where $\dot{V}_{lo}$ and P_{io} are the lymph flow and tissue pressure, respectively, at normal steady-state conditions. The slope of the lymph flow relationship, SL, is termed the "lymph flow sensitivity". For underhydration, a linear lymph flow relationship is also assumed, but in this case the lymph flow is taken to be zero at the tissue hydrostatic pressure, P_{ie}, corresponding to its excluded volume (see Section 2.3), i.e.,

$$\dot{V}_l = \dot{V}_{lo}(P_i - P_{ie})/(P_{io} - P_{ie}), \qquad P_i < P_{io} \qquad 5.6b$$

Furthermore, if the lymph flow calculated from Equation 5.6b is less than zero, the lymph flow is set equal to zero. It is therefore assumed the lymph flow can only occur in one direction; from the tissues to the lymphatics.

Similarly, a mass balance of albumin around the same general tissue compartment yields:

$$dQ_i/dt = \dot{Q}_{pl} + \dot{Q}_d - \dot{Q}_l \qquad 5.7$$

where Q_i represents the total mass of protein in the interstitial compartment at any given time. The mass flow rate of protein transported into the tissue along with the plasma leak, $\dot{Q}_{pl}$, is given as the product of the plasma leak rate, $\dot{V}_{pl}$, and the plasma protein concentration, C_p, or:

$$\dot{Q}_{pl} = \dot{V}_p \cdot C_p \qquad 5.8$$

The plasma protein (albumin) concentration in blood plasma is defined as:

$$C_p = Q_p/V_p \tag{5.9}$$

where Q_p and V_p are the mass of protein and the total volume, respectively, of the plasma compartment. Similarly, the protein flow in lymph, $\dot{Q}_l$, is the product of the lymph flow rate, $\dot{V}_l$, and the tissue concentration, C_i, i.e.

$$\dot{Q}_l = \dot{V}_l \cdot C_i \tag{5.10}$$

where

$$C_i = Q_i/V_i \tag{5.11}$$

The mass rate of protein diffusion across the capillary wall, $\dot{Q}_d$, is assumed to be proportional to a concentration difference between the plasma and the tissue. In this case, it is more appropriate to use a tissue concentration based on the available fraction of the tissue volume. Thus,

$$\dot{Q}_d = PS(C_p - CA_i) \tag{5.12}$$

where PS is another transport coefficient which represents the product of the protein permeability and the surface area of the capillary wall. CA_i is the effective tissue protein concentration based on the available volume, which is given by:

$$CA_i = Q_i/(V_i-VE_i) \qquad 5.13$$

In the last equation, VE_i is the excluded volume of the tissue, i.e., the fluid volume which cannot be penetrated by the protein (see Section 2.3).

Equations having the form of 5.2 - 5.13 have been derived for all three tissue compartments and are compiled in Table 5.1. Differential equations describing the fluid and protein behaviour in the plasma could be obtained by carrying out similar mass balances around the plasma compartment. However, since we assume there are no fluid or protein losses, no cellular changes and no fluid resuscitation in the present model, the amounts of fluid and protein in the system are constants and it is easy to show that:

$$dV_p/dt = -(dV_m/dt+dV_s/dt+dV_b/dt) \qquad 5.14$$

Table 5.1 Summary of Burn Model Equations

Muscle	Intact Skin	Injured Skin	Plasma
$C_m=Q_m/V_m$	$C_s=Q_s/V_s$	$C_b=Q_b/V_b$	$C_p=Q_p/V_p$
$CA_m=Q_m/(V_m-VE_m)$	$CA_s=Q_s/(V_s-VE_s)$	$CA_b=Q_b/(V_b-VE_b)$	
$\Pi_m=F^n(CA_m)$	$\Pi_s=F^n(CA_s)$	$\Pi_b=F^n(CA_b)$	$\Pi_p=F^n(C_p)$
$P_m=F^n(V_m)$	$P_s=F^n(V_s)$	$P_b=F^n(V_b)$	$P_a=F^n(V_p), P_v=F^n(V_p)$
$\dot{V}_{fm}=K_{fm}[P_{am}-P_m-(\Pi_p-\Pi_m)]$	$\dot{V}_{fs}=K_{fs}[P_{as}-P_s-(\Pi_p-\Pi_s)]$	$\dot{V}_{fb}=K_{fb}[P_{ab}-P_b-(\Pi_p-\Pi_b)]$	
$\dot{V}_{rm}=K_{rm}[P_m-P_{vm}-(\Pi_m-\Pi_p)]$	$\dot{V}_{rs}=K_{rs}[P_s-P_{vs}-(\Pi_s-\Pi_p)]$	$\dot{V}_{rb}=K_{rb}[P_b-P_{vb}-(\Pi_b-\Pi_p)]$	
$\dot{V}_{plm}=K_{plm}(P_{vm}-P_m)$	$\dot{V}_{pls}=K_{pls}(P_{vs}-P_s)$	$\dot{V}_{plb}=K_{plb}(P_{vb}-P_b)$	
$\dot{V}_{lm}=\dot{V}_{lmo}+SL_m(P_m-P_{mo})$	$\dot{V}_{ls}=\dot{V}_{lso}+SL_s(P_s-P_{so})$	$\dot{V}_{lb}=\dot{V}_{lbo}+SL_b(P_b-P_{bo})$	
$\dot{Q}_{plm}=\dot{V}_{plm}\cdot C_p$	$\dot{Q}_{pls}=\dot{V}_{pls}\cdot C_p$	$\dot{Q}_{plb}=\dot{V}_{plb}\cdot C_p$	
$\dot{Q}_{dm}=PS_m(C_p-CA_m)$	$\dot{Q}_{ds}=PS_s(C_p-CA_s)$	$\dot{Q}_{db}=PS_b(C_p-CA_b)$	
$\dot{Q}_{lm}=\dot{V}_{lm}\cdot C_m$	$\dot{Q}_{ls}=\dot{V}_{ls}\cdot C_s$	$\dot{Q}_{lb}=\dot{V}_{lb}\cdot C_b$	
$dV_m/dt=\dot{V}_{fm}+\dot{V}_{plm}-\dot{V}_{rm}-\dot{V}_{lm}$	$dV_s/dt=\dot{V}_{fs}+\dot{V}_{pls}-\dot{V}_{rs}-\dot{V}_{ls}$	$dV_b/dt=\dot{V}_{fb}+\dot{V}_{plb}-\dot{V}_{rb}-\dot{V}_{lb}$	$dV_p/dt=-d(V_m+V_s+V_b)/dt$
$dQ_m/dt=\dot{Q}_{plm}+\dot{Q}_{dm}-\dot{Q}_{lm}$	$dQ_s/dt=\dot{Q}_{pls}+\dot{Q}_{ds}-\dot{Q}_{ls}$	$dQ_b/dt=\dot{Q}_{plb}+\dot{Q}_{db}-\dot{Q}_{lb}$	$dQ_p/dt=-d(Q_m+Q_s+Q_b)/dt$

and

$$dQ_p/dt = -(dQ_m/dt+dQ_s/dt+dQ_b/dt) \tag{5.15}$$

where the subscripts p,m,s and b denote the plasma, muscle, noninjured skin and injured skin compartments, respectively. The necessary equations for the plasma compartment are also shown in Table 5.1. The table also lists other relationships needed to complete the description of the burn model including the compliance and the colloid osmotic pressure relationships which will be discussed in the next section.

5.2.2 CONSTITUTIVE RELATIONSHIPS

5.2.2.1 Compliance Relationships

The compliance relationships between the hydrostatic pressure and the fluid volume for the muscle, intact skin and plasma compartments are taken to be the same as those used in the earlier model of Bert et al. [6]. For skeletal muscle and normal skin, the compliance curves are based on the experimental data of Reed and Wiig [50] and Wiig and Reed [51], respectively, and are tabulated and plotted in Appendix A. To allow interpolation in the computer program, the tabulated curves were divided into three segments and fitted with linear relationships at the extremes of high and low fluid volume and with a set of cubic spline equations [52] over the central portion. Note that in order to use this compliance relationship correctly for intact skin when the fraction of total skin area which is burned (BSA) exceeds zero, the intact skin fluid volume must be divided by (1-BSA).

The compliance relationships for the plasma compartment were obtained by Bert et al. [6] by using their microvascular exchange model to fit the dehydration and overhydration experimental results of Reed and Wiig [53]. Note that separate relationships are required for the arterial and venous ends of the capillary. For convenience, Bert et al. [6] assumed simple linear compliance relationships of the form

$$P_a = P_{ao} + A_1(V_p - V_{po}) \qquad 5.16$$

and

$$P_v = P_{vo} + A_2(V_p - V_{po}) \qquad 5.17$$

where the "o" subscripts indicate normal steady-state values and A_1 and A_2 are constants whose "best fit" values were found to be 0.00 and 5.12 mmHg/ml, respectively. In some of the burn simulations described in the next Chapter, P_{ao} and P_{vo} are assumed to be different for capillaries replenishing the injured tissue compared to those interacting with intact skin or muscle. However, in all cases, A_1 and A_2 were taken to be constant at the values given above.

There is no measured compliance curve available for burned tissue. However, it is clear from the large negative pressure measured by Lund and Reed [34] (See Section 3.3, Figure 3.2 and Figure 3.3) that during the period immediately following a burn, the injured skin compliance is very different from that of intact skin. Thus, for the first three hours postburn, the hydrostatic pressure of the injured skin compartment was unlinked from the fluid volume and was assumed to follow the data plotted in Figure 3.2 for 10% burn and Figure 3.3 for 40% burn. For computational purposes, the pressures at intermediate times were obtained by linearly interpolating the discrete values. Since the measured tissue pressures returned approximately to the intact skin compliance values after three hours, the normal skin compliance relationship was followed for all times subsequent to three hours. Once again, in order to use the latter relationship successfully, the fluid volume in the injured skin compartment must be normalized by dividing its value by BSA.

5.2.2.2 Colloid Osmotic Pressure Relationships

The colloid osmotic pressure associated with the presence of proteins in the fluid is related to the protein concentration. Bert et al. [6] obtained expressions for the colloid osmotic pressure in the plasma, muscle and intact skin compartments by fitting experimental data for rats available in the literature. In all three cases, the data were fit to cubic relationships having the general form:

$$\Pi = B_1C + B_2C^2 + B_3C^3 \qquad 5.18$$

where C is CA for muscle and skin and B_1, B_2 and B_3 are constants whose best-fit values are tabulated in Table 5.2. Note that since C and CA are intensive properties of the compartments, the equations can be used without correction when BSA exceeds zero. For lack of better information, the colloid osmotic pressure relationship for injured skin was assumed to be identical to that of intact skin.

Table 5.2 Coefficients in Osmotic Pressure Relationships

Tissue	B_1	B_2	B_3
Plasma	0.39723	-0.00516	0.00027
Intact Skin	0.42894	-0.00929	0.00038
Muscle	0.40891	-0.00024	0.00040

When these coefficients are used in Equation 5.18, the units of colloid osmotic pressure must be mmHg and the units of concentration, mg/ml.

5.3 CONSTANTS

5.3.1 NORMAL STEADY-STATE CONDITIONS

The normal steady-state conditions are those that are assumed to exist just prior to a burn injury. The normal conditions descriptive of the plasma, muscle and intact skin compartments of a 225g "standard" rat are the same as those used by Bert et al. [6] and are listed in Table 5.3. The excluded volumes of both tissue compartments were estimated by assuming that albumin is restricted from entering one-quarter of the normal fluid volume of skin or muscle. When these excluded volumes are substituted into appropriate compliance relationship (see Appendix A), it is found that the excluded volume tissue pressures needed for Equation 5.6b are P_{me}= -6.78 mmHg and P_{se} = -7.84 mmHg.

The initial normal arterial and venous capillary pressures were calculated using the relationships:

$$P_{ao} = P_{vv}+R_a(P_{aa}-P_{vv}) \qquad 5.19$$

and

$$P_{vo} = P_{vv}+R_v(P_{aa}-P_{vv}) \qquad 5.20$$

respectively, where P_{aa} and P_{vv} are the pressures in the

Table 5.3 Normal Conditions: 225 g rat [6]

	Circulation	Muscle	Skin
V (ml)	6.12	10.41	16.88
VE (ml)	0.00	2.60	4.22
CA or C (mg/ml)	35.9	17.2	22.0
Q (mg)	219.71	134.30	278.50
P_a (mmHg)	24.54	-	-
P_v (mmHg)	5.92	-	-
P (mmHg)	-	-0.51	-1.21
Π (mmHg)	20.0	9.0	9.0
Weight (g)	12.38	102.2	40.5

large arteries and large veins, respectively, while R_a and R_v are constants representing the fractional pressure drop from the arterial capillary and the venous capillary, respectively, to the large veins. In rats under normal conditions the assumption is made that P_{aa}=100 mmHg and P_{vv}=2 mmHg [6]. The fractional resistances are taken to be the same as those for humans [6] and hence, R_a=0.23 and R_v=0.04.

It is assumed that the conditions specified in Table 5.3 are the initial conditions which exist at the start of each burn simulation with the exception of the following modifications. Firstly, the initial intensive properties C, CA, P and Π of the injured skin compartment are presumed to be identical to the corresponding normal properties of the intact skin. Secondly, the initial extensive properties for the burned skin compartment are obtained by multiplying the values of V_s, VE_s and Q_s listed in Table 5.3 by BSA. Similarly, the initial intact skin values are obtained by multiplying V_s, VE_s and Q_s by (1-BSA). Finally, because the main arterial pressure falls after a burn (see Section 3.2.2) and because the distribution of flow resistance may also change (see Section 3.2.4), the initial values for the arterial and venous capillary pressures also depend on BSA and in fact, may differ from one tissue to another. To accommodate these changes, the values of P_{aa} and in some cases, R_a appearing in Equations 5.18 and 5.19 were altered.

These modifications to P_{ao} and P_{vo} are discussed in more detail in Chapter 6.

5.3.2 NORMAL TRANSPORT COEFFICIENTS

An examination of the burn model equations in Table 5.1 reveals that there are six transport coefficients for each tissue compartment which must be specified before the simulation can get underway. For any general tissue compartment, these six coefficients are the filtration coefficient K_f, the reabsorption coefficient K_r, the plasma leak coefficient K_{pl}, the protein diffusion coefficient PS, the initial lymph flow $\dot{V}_{lo}$ and the lymph flow sensitivity SL.

Following a burn injury, many or perhaps all of these coefficients change. In some cases, these changes occur in a time-dependent way. The major emphasis in the next chapter is to try to determine what alterations to the normal transport coefficients are reasonable in order to simulate the burn situation. As a basis for making these alterations, a set of normal transport coefficients must be defined for each of the muscle, intact skin and injured skin compartments.

These normal values were derived from the transport coefficients established by Bert et al. [6] for noninjured rats. These values are listed in Table 5.4 for the two tissue compartments, intact skin and muscle, considered by those authors. The tabulated values were estimated independently for the two tissues by statistically fitting the simulation predictions to experimentally measured interstitial fluid volume and colloid osmotic pressure data as a function of venous pressure for muscle [54] and colloid osmotic pressure versus venous pressure for skin [55] for a series of perturbed states and also for normal conditions. Note that for both tissues, the fitting results predict that diffusion plays a negligible role in protein transport.

The normal transport coefficients used for muscle in the burn model are those given in Table 5.4. Because all of the coefficients are proportional to the fractional surface area burned, BSA, the normal values for injured and intact skin were determined by multiplying the skin values shown in Table 5.4 by BSA and (1-BSA), respectively. The various alterations imposed on this set of normal coefficients are discussed further in Chapter 6.

Table 5.4 Transport Coefficients Determined for Normal Skin and Muscle [6]

Coefficients	Muscle	Skin
K_f(ml/mmHg·h)	0.0634	0.0927
K_r(ml/mmHg·h)	0.1585	0.2943
K_{pl}(ml/mmHg·h)	0.0145	0.0272
PS(ml/h)	0.0	0.0
$\dot{V}_{lo}$(ml/h)	0.2603	0.4220
SL(ml/mmHg·h)	1.2065	1.2651

5.4 COMPUTER PROGRAM

5.4.1 NUMERICAL METHODS

As can be seen in Table 5.1, the burn simulation consists essentially of a set of eight first-order ordinary differential equations obtained by carrying out fluid and protein (albumin) balances around the four separate compartments which make up the model. This set of eight differential equations (along with their corresponding auxiliary and constitutive relationships) must be solved simultaneously subject to a set of imposed initial conditions. Because of the nonlinear nature of some of the auxiliary and constitutive relationships, the differential equations cannot be solved analytically. The numerical method chosen to carry out this solution is the Runge-Kutta-Fehlberg method with error control [56].

Like all Runge-Kutta solvers, Fehlberg's technique uses only first-order derivative evalutions (i.e. evalutions of the right-hand-side functions of the differential equations) in order to obtain the simultaneous solutions of all dependent variables from one time step to the next. However, it produces results which are equivalent in accuracy to a fourth-order Taylor's series and hence, permits the use of fairly liberal time increments. Furthermore, Fehlberg's method includes estimates of each dependent variable which are fifth-order accurate. Thus, by taking the difference between the fourth- and fifth-order estimates, it becomes possible to predict the error corresponding to the chosen time interval or conversly, to adjust that interval to achieve a specified local and global error. In the present simulations, the maximum possible absolute error allowed for any of the eight dependent variables (V_p, V_m, V_s, V_b, Q_p,Q_m, Q_s or Q_b) was 10^{-3} ml of fluid or 10^{-2} mg of protein.

As mentioned earlier, the discrete compliance data available for skin and muscle was interpolated in the program (at least over the middle range of fluid volume) by using the method of cubic splines [56]. The cubic splines are a set of cubic polynomials, one such equation for each pair of pressure-volume points, whose coefficients are determined by forcing each polynomial to pass through its associated data points and making the first and second derivatives of neighbouring splines match at each point. The spline-fitting procedure requires, at one stage, the solution of a tridiagonal set of linear algebraic equations. The latter solution is accomplished by using the tridiagonal matrix algorithm developed by Thomas [56].

5.4.2 PROGRAM

A complete listing of the FORTRAN program used to carry out the burn model simulations is given in Appendix B. The program consists of a main or driver subprogram which directs the overall computation plus a myriad of function and subroutine subprograms which handle the more subordinate tasks. The main subprogram initializes the dependent variables, increments time and calls the Runge-Kutta-Fehlberg subroutine to obtain a solution to the differential equations at each time step. It also outputs all of the dependent and supplemental variables in tabular form for each compartment and calls plotting subroutines which compare predicted responses to experimental data for selected variables. The main subprogram also calculates and outputs the sum-of-squares of differences between the simulation and experimental results for these selected variables. Separate subroutines and function subprograms control the different numerical procedures required, evaluate right-hand-side functions, auxiliary relationships and constitutive relationships, and perform all of the plotting duties. A BLOCK DATA subprogram is used to specify the starting data as well as the discrete data needed by some of the constitutive relationships. The purpose and main features of each subprogram are documented within the program listing contained in Appendix B.

In general, the program is used to predict how the proteins and fluid redistribute themselves with time because of the transient alterations of transport coefficients and/or fluid pressures that occur after a burn injury having an area fraction BSA. Because of the availability of experimental results, only the cases of BSA = 10% and BSA = 40% were studied extensively.

Chapter 6

RESULTS AND DISCUSSION

6.1 INTRODUCTION

It is well-known that the physiological response of any living organism to thermal injuries is very complex. Furthermore, only a limited amount of experimental information is available on the pathological changes to the microvascular exchange system which occur after burns in rats or in other experimental animals. As a consequence, the approach followed in this work is to hypothesize a list of reasonable pathological changes which could be associated with burn injuries in rats and input these as perturbations into the burn model for this animal. Predictions based on the model are then compared with the available experimental information. In this chapter, the perturbations and their resultant short- and long-term responses for 10% and 40% burns are simulated and discussed. The primary objective of this investigation is to identify those changes which not only give a reasonable fit when compared with all of the available experimental data but also have a reasonable physiological basis. These "best" parametric changes for the two types of burns are considered to be the basis of a "satisfactory" burn model whose predictions will then be examined in detail to understand better the underlying mechanisms of the physiological changes that take place following a burn.

The experimental information used as the primary comparison with the model predictions in this work is the rat data of Lund and Reed [45]. The reasons for selecting their results are the following:

1. Their experimental data for the rat are far more complete and wide-ranging than those available from any other experiments. These data include measured changes in fluid content, protein content and colloid osmotic pressure in various compartments after 10% and 40% surface area burns.
2. Their experimental information contains necessary auxiliary information such as burn-induced changes in main arterial and injured tissue hydrostatic pressures.
3. The normal steady-state conditions for the rat are well-characterized by the earlier microvascular exchange model of Bert et al. [6].

From the data of Lund and Reed, six variables were chosen as a basis of comparison between the model predictions and the experimental results. These variables were selected not only because they are important physiological variables in the tissue and plasma compartments but also because the experimental information concerning their behaviour is reasonably complete and accurate. The six variables are the volume of plasma, the interstitial fluid content of injured skin, the interstitial fluid content of intact skin, the colloid osmotic pressure in plasma, the colloid osmotic pressure in the injured skin and the albumin content of the injured skin.

It should be pointed out that these data, considered to be the most complete, also have limitations. Firstly, the time interval between each pair of experimental points is one hour which is quite large, and the total measurement time is restricted to 3 hours postburn. Secondly, in the case of some experimental points, the estimated errors are fairly significant.

The average normal values for some model variables used by Bert et al. were different than those measured by Lund and Reed prior to the initiation of burns. For example, in the case of the 10% burn, the normal value of COP in the plasma is 20.0 mmHg in our simulation, while the average normal value of the same parameter in their burn experiments is 16.5 mmHg (see Tables C.1 and C.2 in Appendix C). Thus, some of the experimental data used to compare with the model required normalization which was carried out by multiplying the original measured result by the ratio of the normal value of the model to that of the experiment. Sample calculations illustrating this normalization procedure are given in Appendix C.

It should be noted that in the experiments of Lund and Reed, the total water in the tissue was measured, including both the water inside the cells as well as the extracellular water. However, only extracellular water was used to represent tissue fluid volumes in our model. Thus, a more accurate normalization procedure was required to estimate the true tissue volume for intact and injured skin. To calculate the extracellular volume, it is necessary to know what fraction of the total tissue water is intracellular and, in the case of injured skin, what fraction of the cells are destroyed during a burn. Since neither fraction is well-known, sample calculations were carried out for the extreme assumptions that 20% of skin fluid is intracellular and, for burned skin, 0% or 100% of the cells are destroyed following a thermal injury. The results of these calculations are also shown in Appendix C. In some cases, the tissue volumes calculated in these alternate ways are substantially larger than those obtained from the simple normalization procedure described above. However, because these estimates require additional assumptions and because the calculated differences for the extreme cases assumed are still small compared to the experimental error, it was concluded that fluid volumes obtained by ignoring the correction for intracellular water were acceptable as a basis of comparison with the model simulations.

In addition to the six selected variables, the model can predict the transient behaviour of all the variables in each compartment including the fluid and plasma protein transfer rates, the fluid and colloid osmotic pressures, and so on. The implications of these other variables in helping form a mechanistic understanding of the various physiological events that take place following a burn will be discussed in later sections. First it is necessary to determine the most reasonable set of parametric changes required to explain the 10% and 40% surface area burns.

6.2 THE 10% BURN

6.2.1 INTRODUCTION

Based on the information presented in Chapter 3, the characteristic perturbations that seem likely to influence the microvascular exchange system after a 10% burn injury are the following:

1. an increase in the plasma leak coefficient in the injured skin (K_{plb}),
2. an alteration in the hydrostatic pressure in the injured skin (P_b),
3. changes in the filtration and reabsorption coefficients in the injured skin (K_{fb} and K_{rb}),
4. a locally induced change which results in a decrease in the arterial capillary pressure in the injured skin

(P_{ab}), and

5. an alteration of the lymph flow in the injured skin ($\dot{V}_{lb}$).

These are listed in what is assumed to be the approximate order of importance with respect to the available information in the literature. The simulations employing the above listed perturbations were examined in phases. Phase One of the simulations started with the first and the second perturbations together, then in each subsequent phase, the remaining perturbations were added and examined one at time.

Following a 10% burn, the main arterial pressure has been measured [33] to decrease to 80% of its normal value. Substituting this new value of P_{aa} into equation 5.19 and 5.20 yields an arterial capillary pressure of P_a = 19.94 mmHg and a venous capillary pressure of P_v = 5.12 mmHg for the entire plasma compartment. It is these altered values of P_a and P_v which were used (at least during the first three hours) for all simulations in the case of the 10% burn.

6.2.2 TRANSIENT RESPONSE TO CHANGES IN THE PLASMA LEAK COEFFICIENT AND THE HYDROSTATIC PRESSURE CHARACTERISTCS OF THE INJURED SKIN (PHASE ONE)

The plasma leak coefficient in the injured skin, K_{plb}, is the product of the capillary permeability and the available exchange surface area in that tissue. Burns cause an increased capillary permeability but the effective surface area for exchange of fluid and protein might decrease due to a lower perfusion rate [29] (personal communication with A.Haugan, Bergen, 1987). According to Table 3.1, K_{plb} increases after a burn, but it appears to return to its normal value within about 12 hours postburn.

Based on the work of Arturson et al. [5], it will be assumed that the transient behaviour of K_{plb} can be expressed as an exponential function having the form

$$K_{plb} = (Ae^{-at}+1)k_{plb} \tag{6.1}$$

In the above equation, the italicized k_{plb} indicates the normal plasma leak coefficient in the injured skin (see Section 5.3). "A" is the magnitude of the K_{plb} change due to the burn injury. Several values of A ranging from 15 to 40 were tested in the 10% burn model. These A values were chosen because they are in the same range as values estimated experimentally (see Table 3.3). The constant a determines the time needed for the coefficient to return to its normal value. The value of a was chosen to be 0.231 h^{-1}

so that K_{plb} falls to half of its maximum value after three hours postburn, and it returns approximately to its initial value after about 12 hours.

The changes in injured tissue hydrostatic pressure P_b which occur within the first three hours following a burn were discussed in Chapter 3. Lund and Reed [34] measured P_b experimentally in rats subjected to 10% and 40% surface area burns. The measured tissue pressures, as shown in Figures 3.2 and 3.3, are characterized by "mean" values and standard errors. Through personal communication with T.Lund, it was suggested that both the "mean" and the "mean+standard error" tissue pressure values should be tried in the simulations due to the large error in the measurements. The tissue pressure variation with time (up to 3 hours) given by Lund and Reed's "mean" values is referred to hereafter as the "middle" pressure curve. The distribution obtained by adding the standard errors to the "mean" value for each point is called the "upper" pressure curve.

An example simulation showing the time-dependent behaviour of the six important variables obtained by perturbing only K_{plb} and P_b is plotted in Figure 6.1. The various input perturbations attempted along with a measure of the overall fit in each case are given in Table 6.1.

Figure 6.1 Simulation for Changing K_{plb} and P_b in 10% Burn ($A=35.0$, Upper Pressure Curve for P_b)

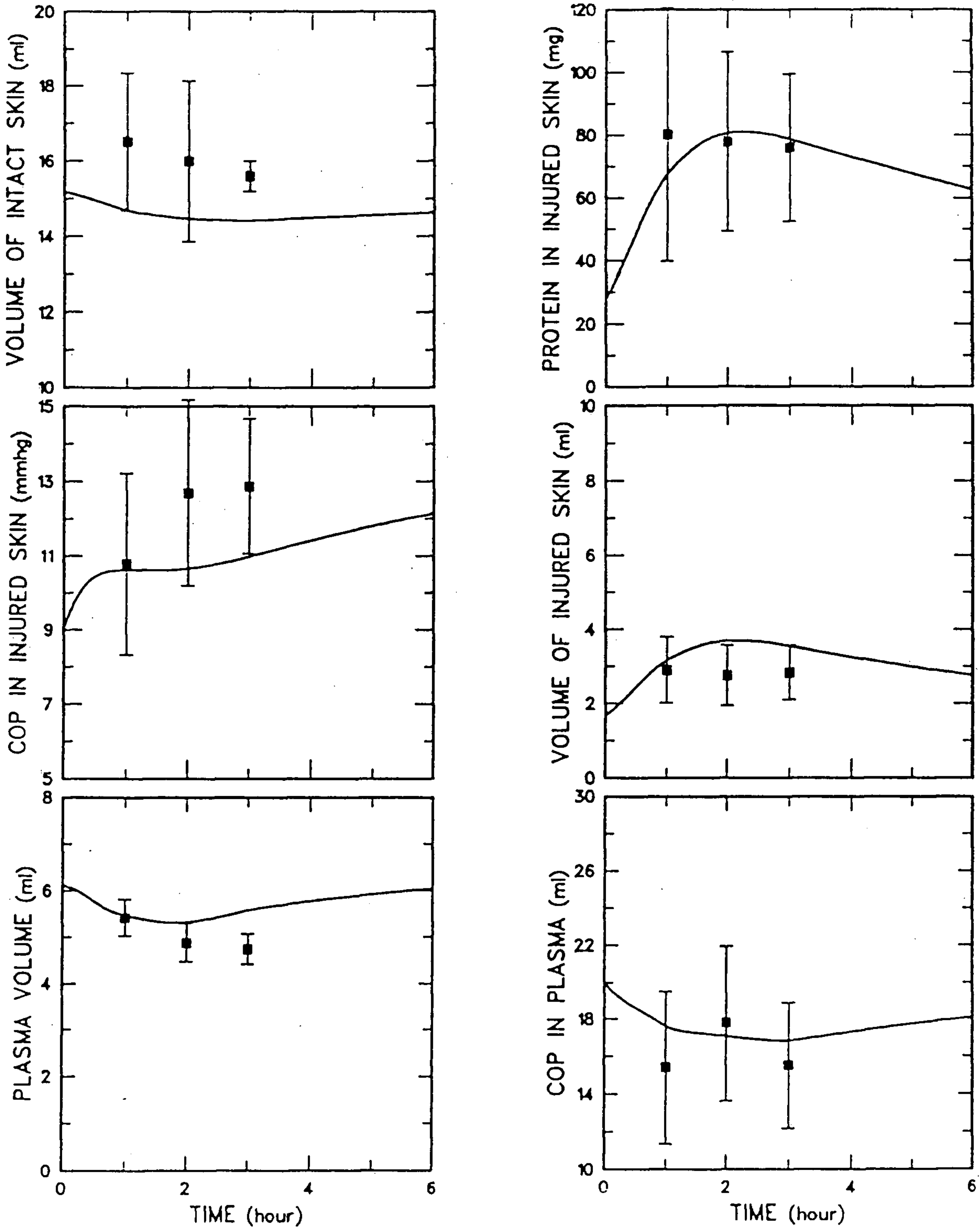

Table 6.1 SS as a Function of K_{plb} and P_b for 10% Burn (Phase One)

P_b \ A (SS)	15.0	20.0	25.0	30.0	35.0	40.0
Upper Curve	—	1.91	—	0.94	0.90	1.03
Middle Curve	2.12	1.99	2.52	3.51	—	—

In Table 6.1 as well as in the remaining tables in this chapter, SS represents the total sum-of-squares of the normalized vertical differences between the experimental points and the simulation for all six variables. The data were normalized by dividing each difference by the initial value of that variable so that all the differences had equal weight. SS therefore represents how close the simulation predicts the experimental data, i.e., the smaller the value of SS, the smaller the overall differences between the experimental and simulation results. For example, in Table 6.1, when A is changed from 20 to 30 using the upper pressure curve, SS falls from 1.91 to 0.94 indicating a significant improvement in the overall fit. The plots shown in the Figure 6.1 are those obtained for the "best" fit of the various possibilities attempted, i.e., using the upper pressure curve with A=35.

Since the injured tissue pressure is very negative following a burn, both filtration and reabsorption act in the same direction causing a greatly increased input of fluid to the injured tissue over the first few hours. The changes made in both K_{plb} and P_b also magnify the plasma leak rate to the injured skin. Thus both the fluid and the protein content of the injured skin compartment increase dramatically. Since most of the fluid transported to the injured skin comes from the plasma compartment, the plasma volume tends to decrease. Also, because the relative increase in the plasma leak rate is many times that of the filtration and reabsorption rates and because the protein concentration in the plasma is initially about twice that in the injured skin, the protein concentration and consequently the colloid osmotic pressure (COP) of the latter tissue increase. Conversely, since the plasma now loses protein at a relatively faster rate than fluid, both the plasma concentration and the COP of the plasma decrease. The massive fluid and protein exchanges between the plasma and the injured skin have only an indirect effect on the fluid content of the noninjured tissues. Consequently, as shown in Figure 6.1, the volume of intact skin tends to decrease only slightly.

When the upper curve is used to represent P_b, the fit of the model predictions to the experimental data improves as A is increased from 15, passes through a minimum at about A = 35 and then begins to deteriorate with further increases in A. Therefore, A = 35 is assumed to be the best fit at this stage. The magnitude A has a direct effect on the fluid and protein contents of the injured skin and also on the plasma volume. Raising the value of A in the simulation increases the amount of the fluid and protein in the injured skin and decreases the plasma volume. When a low value of A is employed, e.g., A = 15, the predicted injured skin fluid and protein contents are too low and the plasma volume is too high compared to the experimental data. When a high value of A is used, such as A=40, the fluid and protein contents are higher and the plasma volume lower than the experimental data. Primarily because of these factors, SS goes through a minimum at the intermediate value of A=35.

For all values of A, the upper pressure curve always yields a better fit than does the middle curve. This is because firstly, the middle pressure curve tends to cause substantial increases in filtration, reabsorption and plasma leak leading to a gross overprediction of the injured skin fluid volume. Secondly, because the filtration and (negative) reabsorption rates are so much higher, the protein content does not increase as rapidly as the fluid content of the injured skin. Hence, the injured skin COP tends to decrease with time while the experimental data shows that it should increase. As a consequence, in the simulations which follow, only the upper curve will be used to estimate the injured tissue pressure P_b for the first three hours postburn.

The predicted results obtained by varying only K_{plb} and P_b are generally representative of those measured experimentally except for one variable, the volume of intact skin. The experimental data show that this volume should increase slightly after a 10% burn, while the simulation results predict a small decrease (see Figure 6.1). Other investigators [37,39] found there was no change in intact skin volume after burns (see Table 3.3). Additionally, the predicted injured skin volume for the best case in Phase One is somewhat too high and the protein content somewhat too low. As Figure 6.1 shows, this yields low values of COP in this compartment.

6.2.3 TRANSIENT RESPONSE INCLUDING CHANGES TO THE FILTRATION AND REABSORPTION COEFFICIENTS IN THE INJURED SKIN (PHASE TWO)

The filtration and reabsorption mechanisms are important causes of fluid interchange between the plasma and each tissue. The magnitudes of the changes in both the filtration and reabsorption coefficients are subject to two competing phenomena. These coefficients could increase due to an rise in the permeability of vessel wall or they could decrease due to a reduction in blood flow (or perfusion rate) following a burn injury. Both types of changes have been suggested in the literature (see Chapter 3). Thus, both increases and decreases in K_{fb} and K_{rb} were examined in the model. K_{fb} and K_{rb} are assumed to undergo a step change at zero time (onset of burn) and to return to normal according to the following exponential relationships:

$$K_{fb} = (Be^{-at}+1)k_{fb} \qquad 6.2$$

and

$$K_{rb} = (Be^{-at}+1)k_{rb} \tag{6.3}$$

Here, the italicized k_{fb} and k_{rb} denote the normal values (see Section 5.3), B reflects the magnitude of the change (assumed to be identical for both K_{fb} and K_{rb}) and a is the time constant. B could be positive (indicating an increase in K_{fb} and K_{rb}), negative (indicating a decrease in K_{fb} and K_{rb}) or zero (indicating that K_{fb} and K_{rb} remain at their normal values). For reasons of simplicity, it is assumed in Equation 6.2 and 6.3 that the changes in these parameters occur synchronically with K_{plb}, (i.e. a=0.231 h^{-1}).

Simulations using different values of K_{plb}, K_{fb} and K_{rb} were generated using the upper pressure curve. The input perturbations and the sum-of-squares of differences, SS, are listed in Table 6.2. Examples of the Phase Two simulations are shown in Figures 6.3 and 6.4 for K_{fb} and K_{rb} decreased by 90% and 50% of their normal values, respectively. In both cases, K_{plb} is assumed to increase initially by 36 times its normal value.

As can be seen in Table 6.2, when K_{fb} and K_{rb} are given larger than normal values (B > 0), the agreement between the model predictions and the experimental data degenerates.

Table 6.2 SS as a Function of K_{plb}, K_{fb}, and K_{rb} for 10% Burn (Upper Curve for P_b, Phase Two)

B \ A (SS)	20.0	30.0	35.0	40.0
2.0	2.43	1.64	1.61	1.74
0.0	1.91	0.94	0.90	1.03
-0.9	1.70	0.62	0.56	0.68
-0.5	1.77	0.75	0.69	0.82

B = 0.0 corresponds to the simulations in Phase One

Figure 6.2 Simulation for Changing K_{plb}, K_{fb} and K_{rb} in 10% Burn (A=35.0, B=-0.9, Upper Curve for P_b)

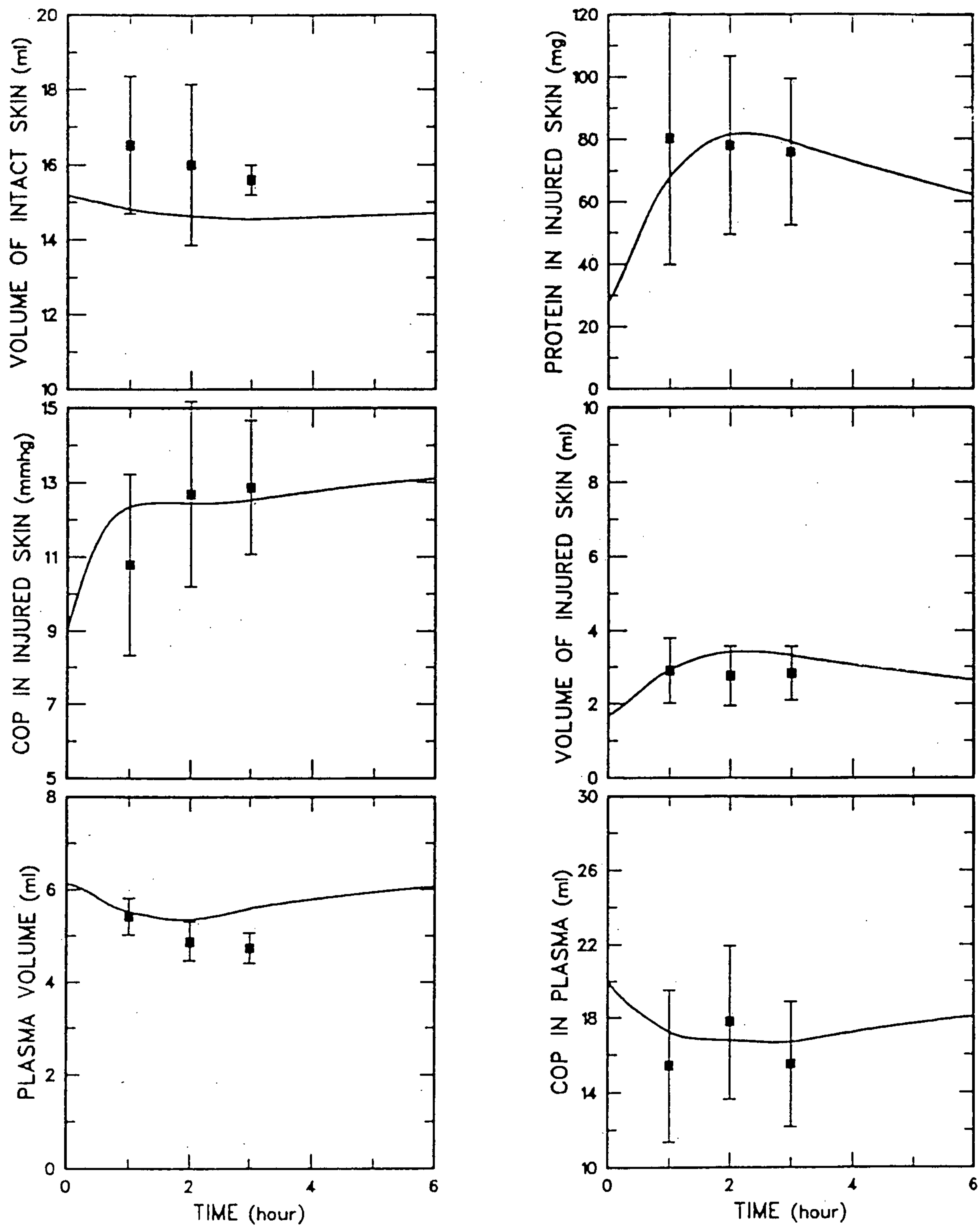

Figure 6.3 Simulation for Changing K_{plb}, K_{fb} and K_{rb} in 10% Burn (A=35.0, B=-0.5, Upper Curve for P_b)

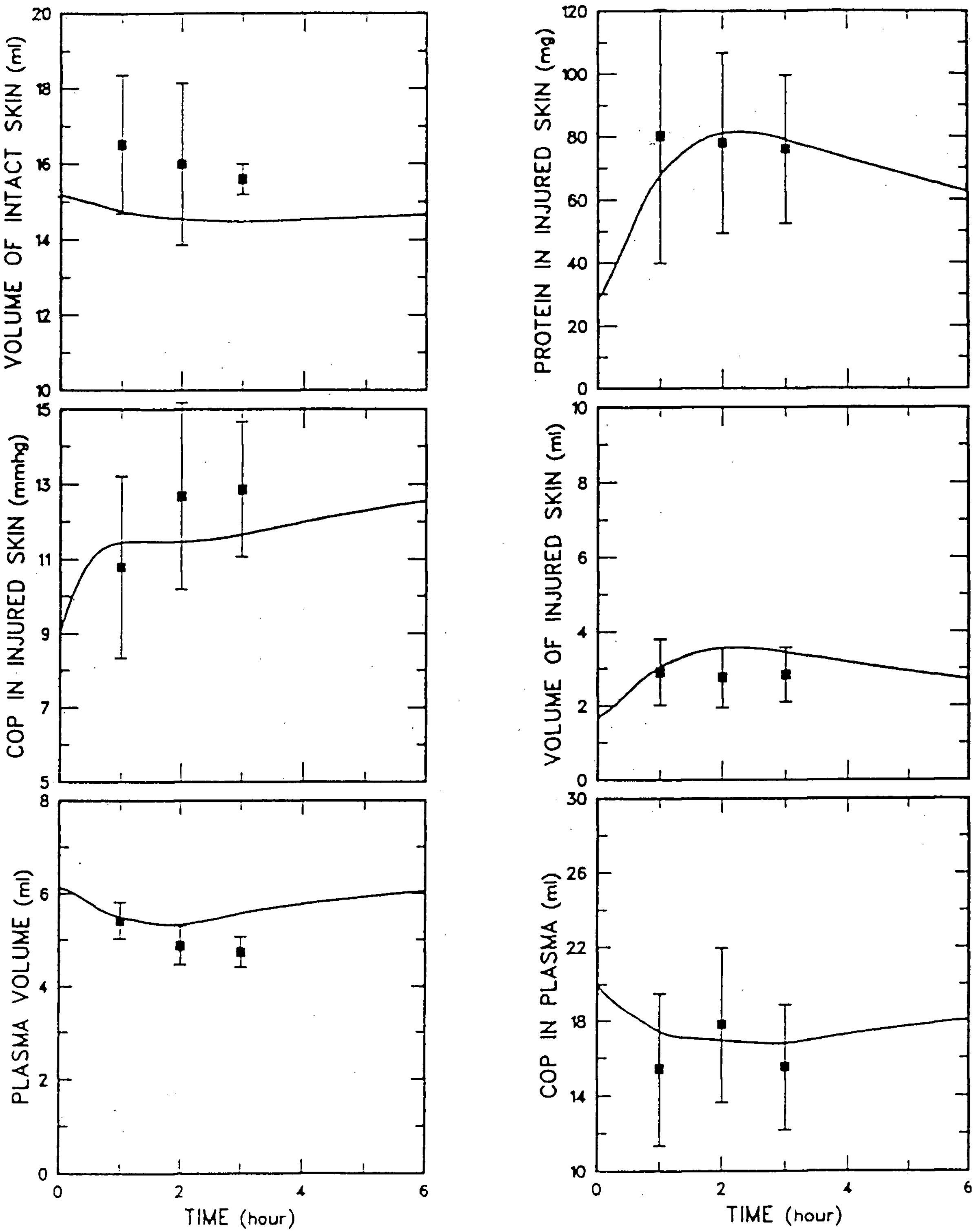

However, if it is assumed that a reduction in injured tissue perfusion dominates the permeability increase for filtration and reabsorption such that $B < 0$, then the results show a significant improvement. No dramatic differences were found in the plotted results obtained by setting $B = -0.5$ and -0.9 although the latter yields a somewhat better overall fit. However there is not enough experimental information available to clearly justify adopting one value of B over the other. The reductions in K_{fb} and K_{rb} are reasonable compared to Ferguson's [29] estimate that in a 70% burn, the blood flow is reduced to only 5% of its normal value (see Table 3.2). The manner by which each of K_{plb}, K_{fb} and K_{rb} change in response to a burn injury is complex and requires further experimental investigation.

The trends predicted in Phase Two are similar to those of Phase One. However, as might be expected, the Phase Two parameter changes result in better fits of the experimental data for COP in injured skin (compare Figures 6.1 and 6.2). One way of gaining separate control over the fluid and protein influx to the injured skin is allow for changes in the filtration and reabsorption coefficients. As mentioned before, the filtration and reabsorption have the same direction in the first few hours postburn, i.e., from plasma to injured skin. Thus changing K_{fb} and K_{rb} together causes a much greater change in the fluid exchange than just changing one of these coefficients. Because of the decreases in filtration and reabsorption rates, the amount of fluid entering the injured tissue is reduced, while the amount of protein, which depends only on the plasma leak rate, is the about same as in Phase One. The net result of these changes is that the protein concentration in the injured tissue rises and hence its COP increases to values which are in better accord with the experimental results.

6.2.4 TRANSIENT RESPONSE INCLUDING CHANGES TO THE ARTERIAL CAPILLARY PRESSURE IN THE INJURED SKIN (PHASE THREE)

As was mentioned earlier, the arterial capillary pressure for all tissues was reduced from its normal value of 25.54 mmHg to 19.94 mmHg because the main arterial pressure is known to drop by about 20% after a 10% burn. The arterial capillary pressure in the burned skin, P_{ab}, may be even lower due to an increase in the local peripheral resistance (see discussion in Chapter 3). Since there is no experimental information about how much P_{ab} might decrease after a 10% burn, two additional values of P_{ab}, 10 mmHg and 15 mmHg, were examined in the simulation.

Figure 6.4 and Figure 6.5 show the simulation results for the Phase Three predictions using several of the better fitting parameter changes from Phase Two as a starting point. Table 6.3 reveals how the sum-of-squares of differences is affected by these two alterations in P_{ab}.

Figure 6.4 Simulation for Changing K_{plb}, K_{fb}, K_{rb} and P_{ab} in 10% Burn (A=35.0, B=-0.9, P_{ab}=10 mmHg, Upper Curve for P_b)

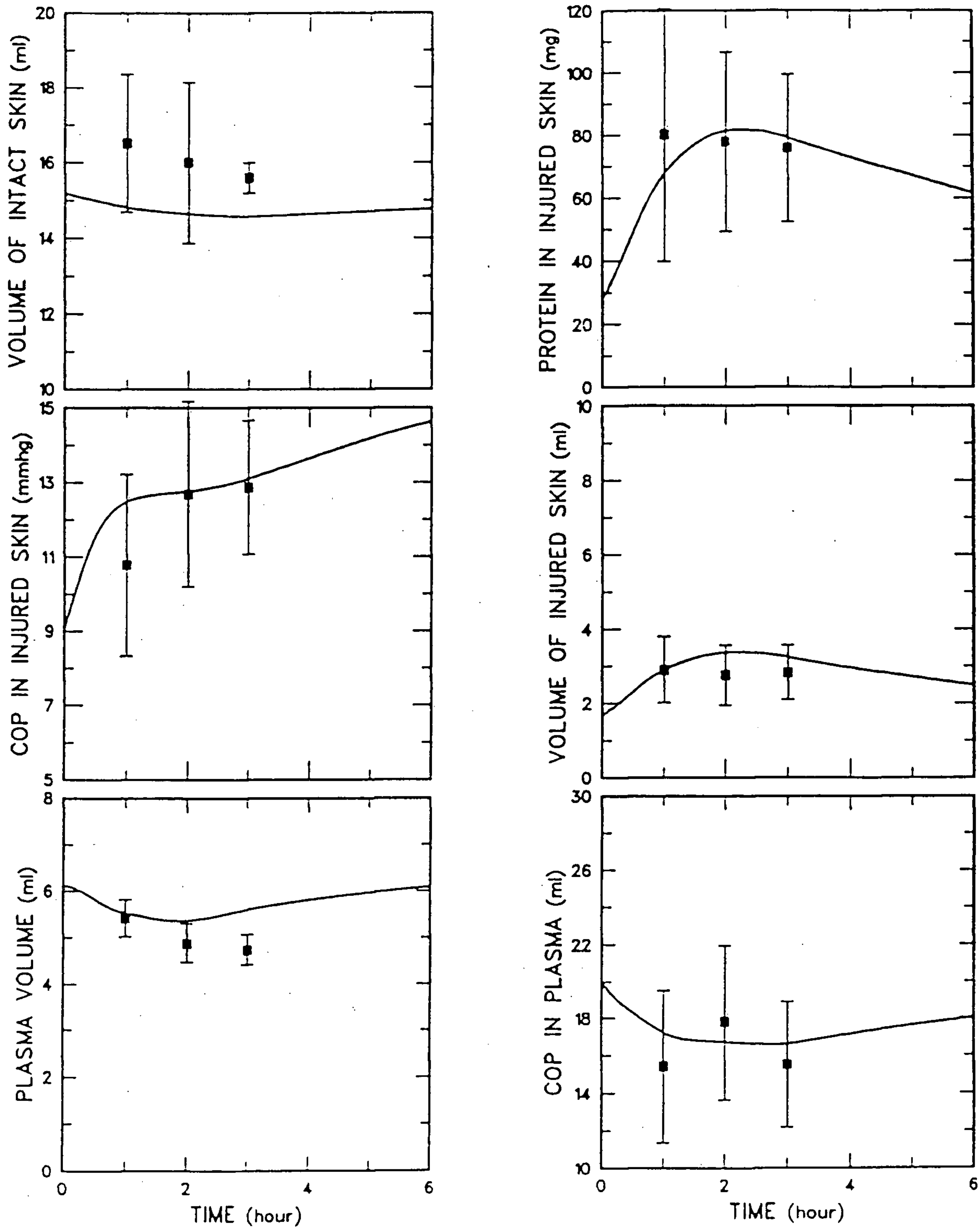

Figure 6.5 Simulation for Changing K_{plb}, K_{fb}, K_{rb} and P_{ab} in 10% Burn (A=35.0, B=-0.9, P_{ab}=15 mmHg, Upper Curve for P_b)

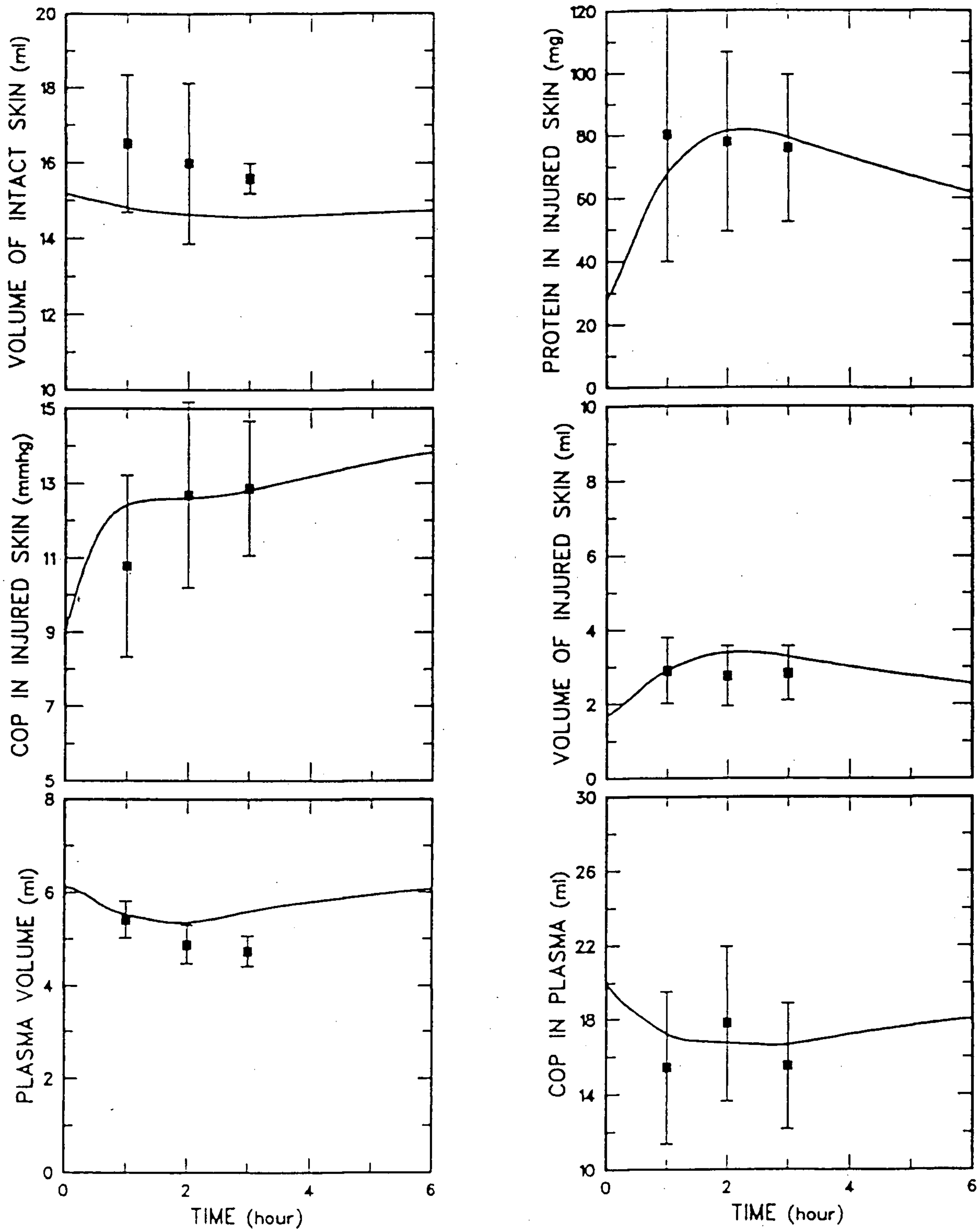

Table 6.3 SS as a function of K_{plb}, K_{fb}, K_{rf} and P_{ab} (mmHg) for 10% Burn (Upper curve for P_b, Phase Three)

P_{ab} \ A,B (SS)	30.0,-0.5	35.0,-0.5	40.0,-0.5	30.0,-0.9	35.0,-0.9	40.0,-0.9
19.9	0.75	0.69	0.82	0.62	0.56	0.68
15.0	0.69	0.63	0.75	0.60	0.54	0.66
10.0	0.64	0.58	0.70	0.59	0.52	0.64

P_{aa} = 19.9 mmHg corresponds to the simulations in Phase Two

Although the lower values of P_{ab} appear to improve the overall fit slightly (Table 6.3), the effects on the plotted results shown in Figures 6.4 and 6.5 are almost indiscernable from the P_{ab} = 19.94 mmHg results in Figure 6.3. Thus, it appears that the predictions are much less sensitive to P_{ab} changes than to the parameter alterations investigated in the previous phases.

6.2.5 TRANSIENT RESPONSE INCLUDING CHANGES TO THE LYMPH FLOW CHARACTERISTICS IN THE INJURED SKIN (PHASE FOUR)

If the normal lymph flow relationship is used (see Equations 5.6a and 5.6b) for burned tissue, lymph flow in the injured skin is predicted to be less than zero in the first hour postburn because of the strongly negative tissue pressure P_b. Since there has never been a reported measurement of a lymph flow reversal, the simulation program takes $\dot{V}_{lb}$ to be zero during this period. From one to two hours after the burn, the injured skin lymph flow is positive but still significantly less than the normal lymph flow, again as a consequence of the low values of P_b. As revealed in Table 3.3, some investigators have measured lymph flow subsequent to a burn injury and found that it consistently increased. However, it is unclear if the lymph flow they obtained represents only that of the injured tissue. More likely it represents fluid from intact tissues as well. In the Phase Four perturbations, the lymph flow in the injured skin for the first three hours postburn is hypothesized to be twice its normal value if the $\dot{V}_{lb}$ calculated from Equation 5.6a or 5.6b is less than $2 \cdot \dot{V}_{lbo}$. After three hours, it's assumed to once again follow the normal relationship, Equation 5.6a or 5.6b.

The model predictions for this altered lymph flow behaviour were generated based on several of the better fitting cases from Phase Three. Table 6.4 shows the sum-of-squares fitting results and Figure 6.6, the plot of the best fit to the experimental data for Phase Four.

The results listed in Table 6.4 indicate that the overall fit between simulations and experimental data is only slightly improved by raising the lymph flow to double its normal value during the first three hours postburn. However, there is once again no discernable difference in the plotted results shown in Figure 6.6 compared to those of Phases Two and Three. Thus, there is no clear indication from the model that lymph flow actually increases following a burn injury and it appears that it is unnecessary to include alterations in the lymph flow characteristics in order to explain the results measured for a 10% burn.

Table 6.4 SS as a Function of K_{fb}, K_{rb}, P_{ab} (mmHg) and $\dot{V}_{1b}$ for 10% Burn (A=35, Upper Curve for P_b, Phase Four)

$\dot{V}_{1b}$ \ SS \ B, P_{ab}	-0.9, 10.0	-0.9, 15.0	-0.5, 10.0	-0.5, 15.0
Normal	0.52	0.54	0.58	0.63
$2\cdot\dot{V}_{1bo}$ (When t<3.0 hours and $\dot{V}_{1b}<\dot{V}_{1bo}$)	0.49	0.50	0.53	0.58

$\dot{V}_{1b}$ = Normal corresponds to the simulations in Phases Two and Three

Figure 6.6 Simulation for Changing K_{fb}, K_{rb}, P_{ab} and $\dot{V}_{lb}$ in 10% Burn (A=35.0, B=-0.9, P_{ab}=10.0 mmHg, Upper Curve for P_b, Altered Lymph Flow Characteristics)

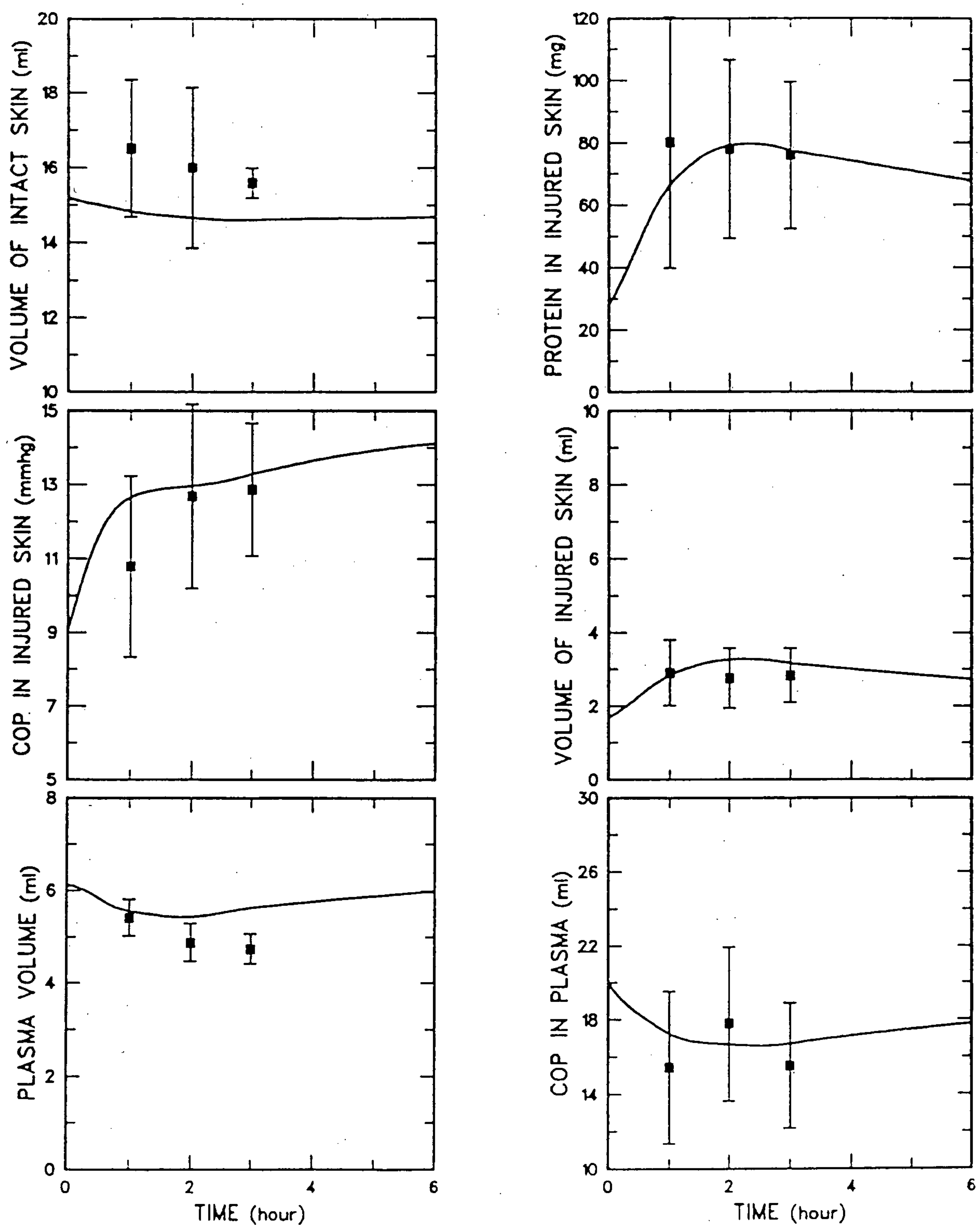

6.2.6 MOST REASONABLE FIT FOR A 10% BURN

Based on the four phases of fitting described above, the influential parameter changes which lead to the most reasonable results can be summarized as follows:

1. The plasma leak coefficient in the injured skin increases, and the magnitude of the change (A in Equation 6.1) is 35. K_{plb} decays to its normal value in about 12 hours following an exponential relationship with time.
2. The tissue pressure in the injured skin falls to very negative values for a limited period postburn. The use of the "mean plus one standard error" pressure curve of Lund and Reed (shown in Figure 3.2) results in a better statistical fit than does the "mean" curve alone.
3. The perfusion rate in the injured skin decreases leading to a reduction of the initial filtration and reabsorption coefficients in the injured skin by at least 50% of their normal values.

A perfusion rate decrease of 50% implies an increase in the protein permeability due to plasma leakage of about 70. The latter increase is in line with the increased protein permeability of about 54 observed in the extravasation experiments of Lund and Reed [25] (see Table 3.1). The other perturbations examined, changes to P_{ab} and $\dot{V}_{lb}$, have only a negligible effect on the sum-of-squares fit and on the predicted results and hence, were not included as the most reasonable changes associated with the 10% burn.

6.2.7 LONG-TERM TRANSIENT RESPONSE

There is a small amount of information in the literature concerning the time required for the 10% burned rat to return to its normal state (see Table 3.3). In the simulation, the arterial and venous capillary pressures were altered from their normal values because of changes to the large artery pressure following a 10% burn. All of the transport coefficient changes were specified in such a way that they returned to their normal values within about 12 hours (the compliance relationship and the lymph flow characteristics in the injured skin returned to normal at three hours postburn). In order to allow the entire microvascular system to eventually recuperate, both the arterial and venous capillary pressures were arbitrarily set to their normal values (P_a=24.54 mmHg and P_v=5.92 mmHg) after either 3, 6 or 9 hours postburn. The steady-state results obtained for these three cases using one of the most reasonable sets of parameter changes are shown in Figures 6.7 - 6.9. In these figures, the dashed lines indicate the normal values for each variable.

Figures 6.7, 6.8 and 6.9 are not significantly different aside from the location of the discontinuity

Figure 6.7 Steady State Result for 10% Burn (A=35.0, B=-0.5, P_{ab}=15.0 mmHg, Upper curve for P_b, $\dot{V}_{lb}=2\cdot\dot{V}_{lbo}$ when t<3 hours and $\dot{V}_{lb}<2\cdot\dot{V}_{lbo}$, Arterial and Venous Capillary Pressure Return to Normal After Three Hours)

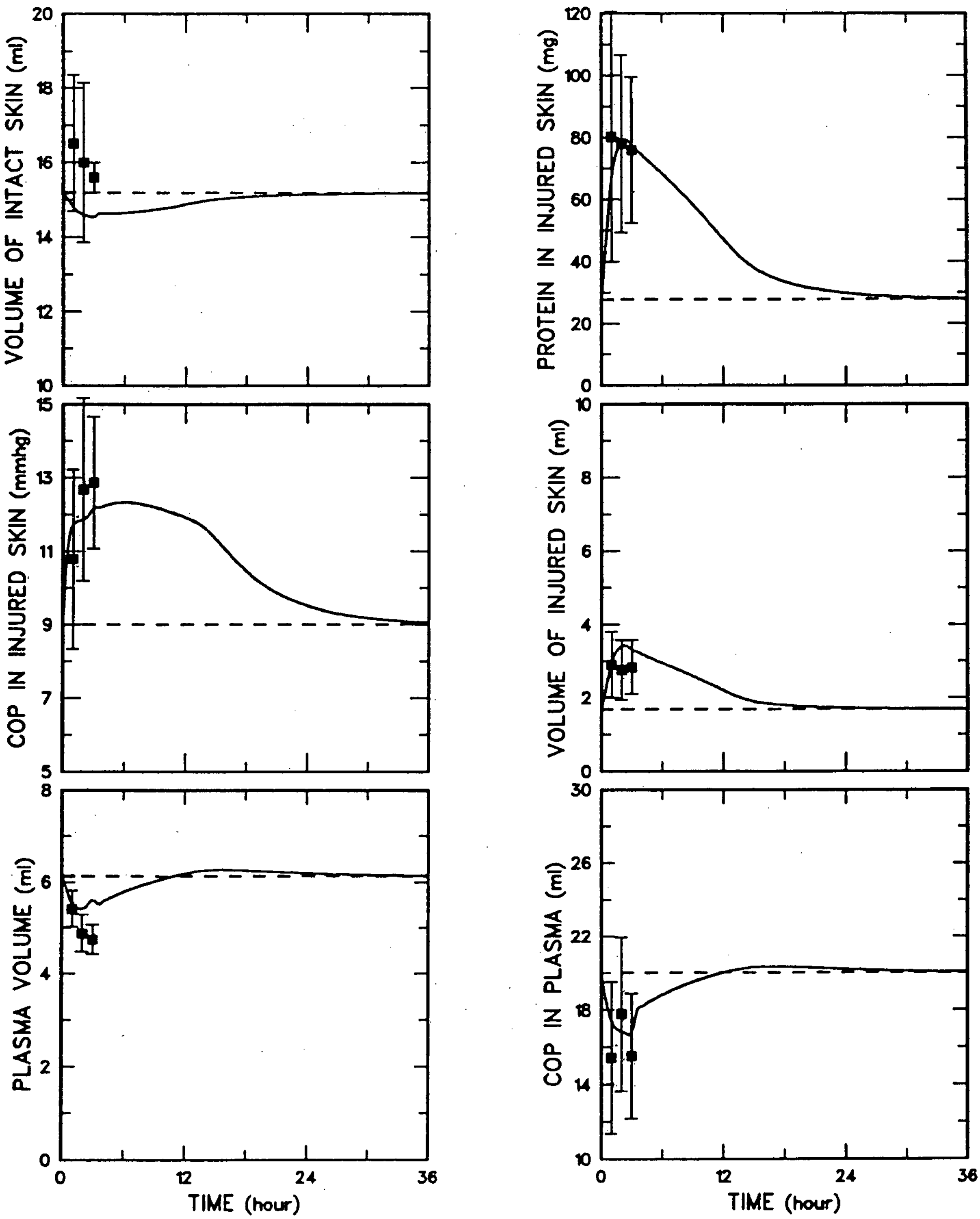

Figure 6.8 Steady State Result for 10% Burn (A=35.0, B=-0.5, P_{ab}=15.0 mmHg, Upper Curve for P_b, $\dot{V}_{lb}=2\cdot\dot{V}_{lbo}$ when t<3 hours and $\dot{V}_{lb}<2\cdot\dot{V}_{lbo}$, Arterial and Venous Capillary Pressure Return to Normal After Six Hours)

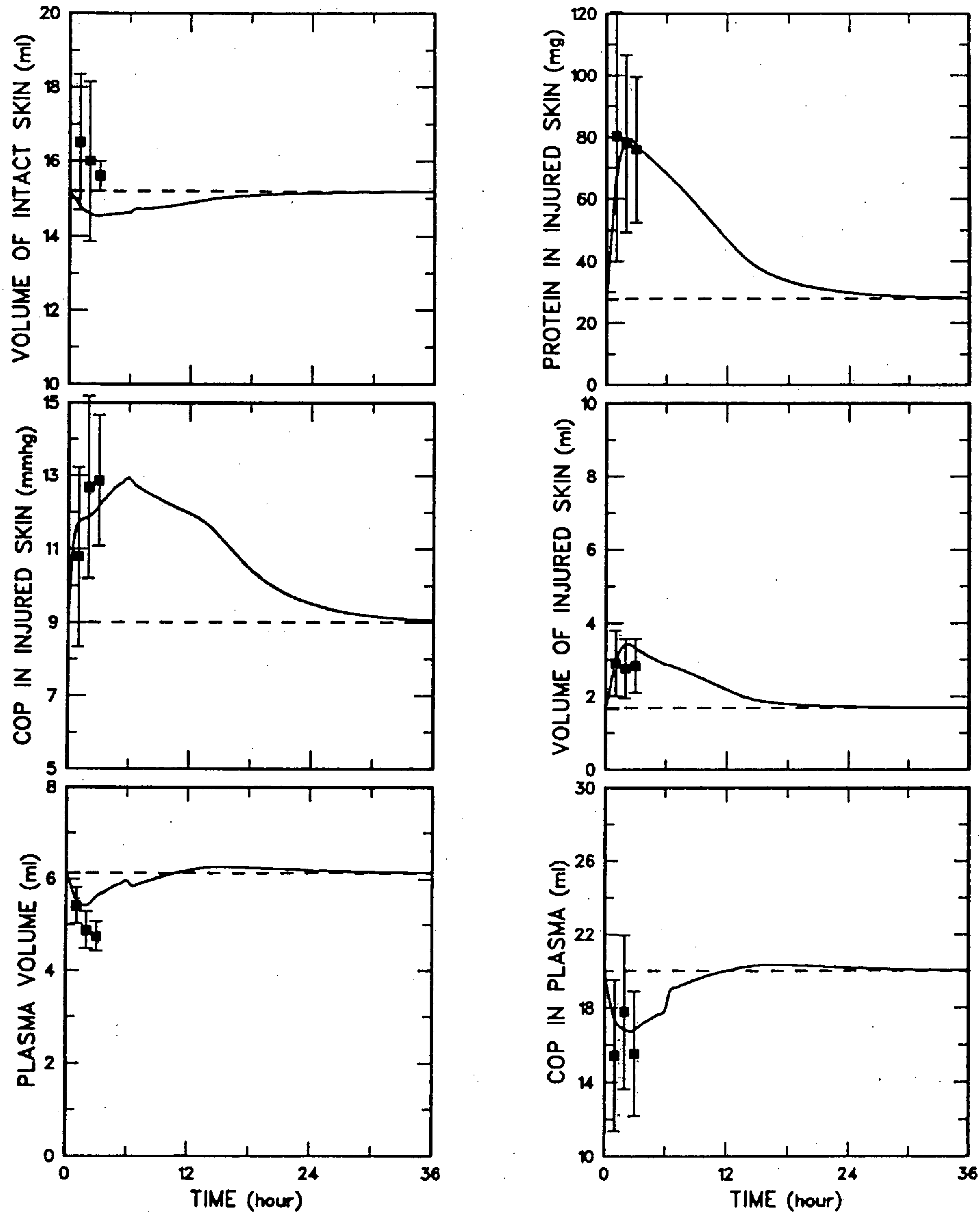

Figure 6.9 Steady State Result for 10% Burn (A=35.0, B=-0.5, P_{ab}=15.0, Upper Curve for P_b, $\dot{V}_{lb}=2\cdot\dot{V}_{lbo}$ when t<3 hours and $\dot{V}_{lb}<2\cdot\dot{V}_{lbo}$, Arterial and Venous Capillary Pressure Return to Normal After Nine Hours)

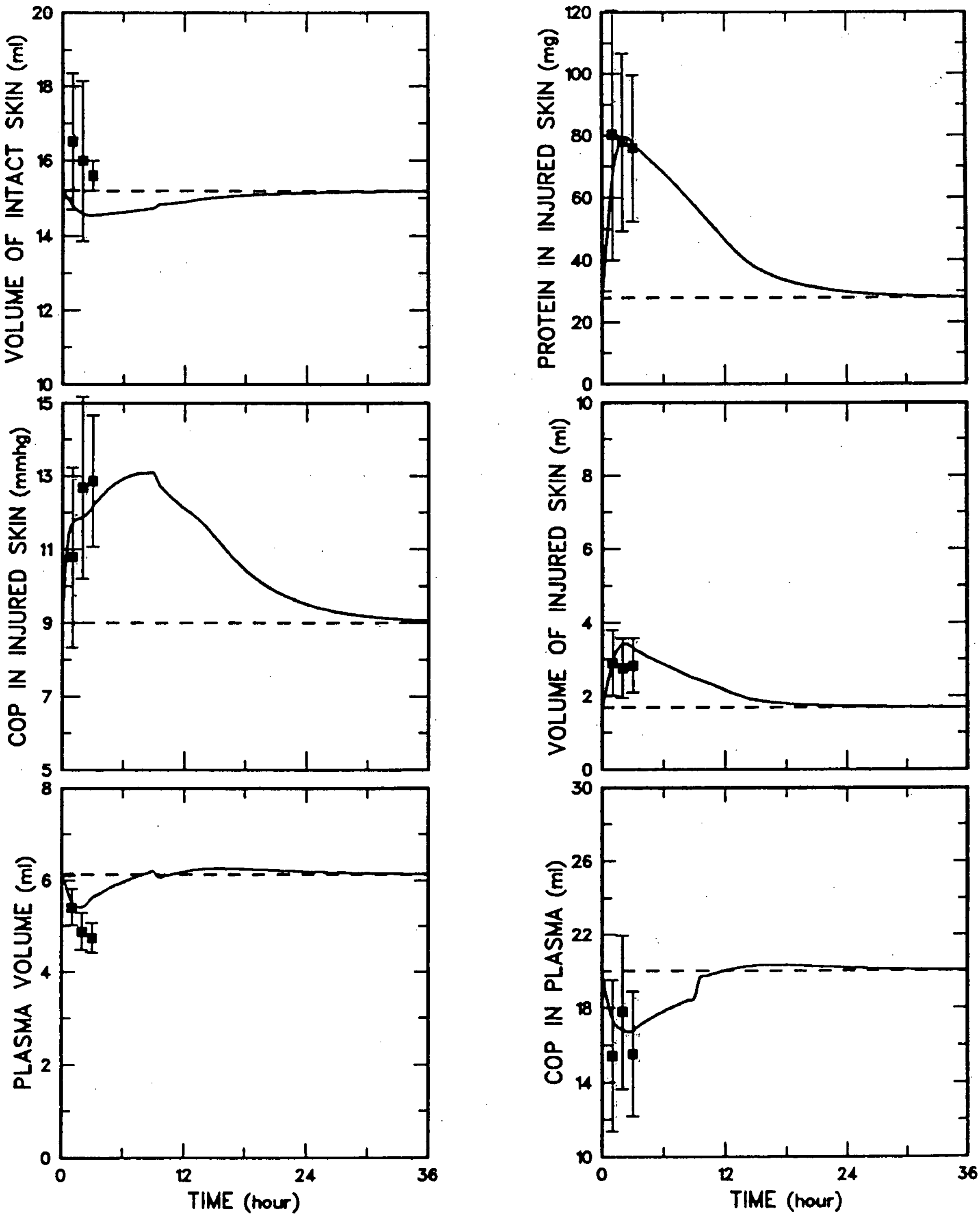

caused by the shift in arterial and venous capillary pressures. The long-term responses, recognized to be very speculative, show that it takes approximately 24 to 36 hours for the various parts of the system to return to normal. This prediction will be discussed in greater detail in the section following.

6.2.8 IMPLICATIONS OF THE 10% BURN MODEL

In this section, the model simulations are used to obtain a more mechanistic understanding of the various events which take place following a 10% surface area burn. The simulations were obtained by using the most "reasonable" set of parameter changes summarized in Section 6.2.6 and by allowing the capillary pressures to return to their normal values after 9 hours. A complete listing of the transient responses of all variables in all four compartments due a 10% burn perturbation is given in Appendix D. The time-dependent behaviour of some of the more important variables is plotted in Figures 6.10-6.14.

Figures 6.10 and 6.11 show how the fluid volumes and protein contents, respectively, of the plasma, muscle, intact skin and injured skin compartments change as a function of time following a 10% burn. As is indicated by the plots, immediately after the burn is initiated, there is a very large transfer of both fluid and protein to the

Figure 6.10 The Changes of Compartmental Fluid Volumes Following a 10% Burn

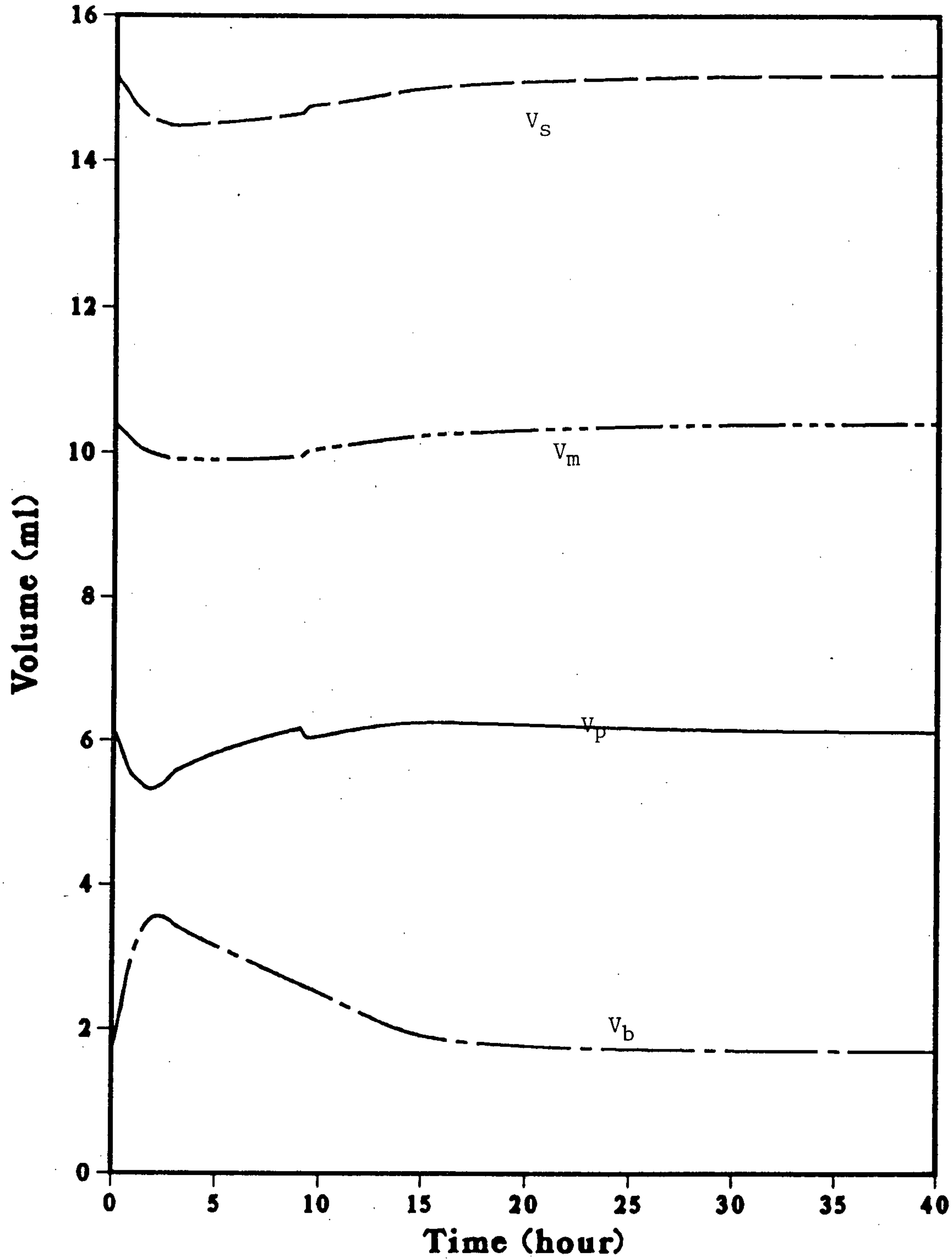

Figure 6.11 The Changes of Compartmental Protein Contents Following a 10% Burn

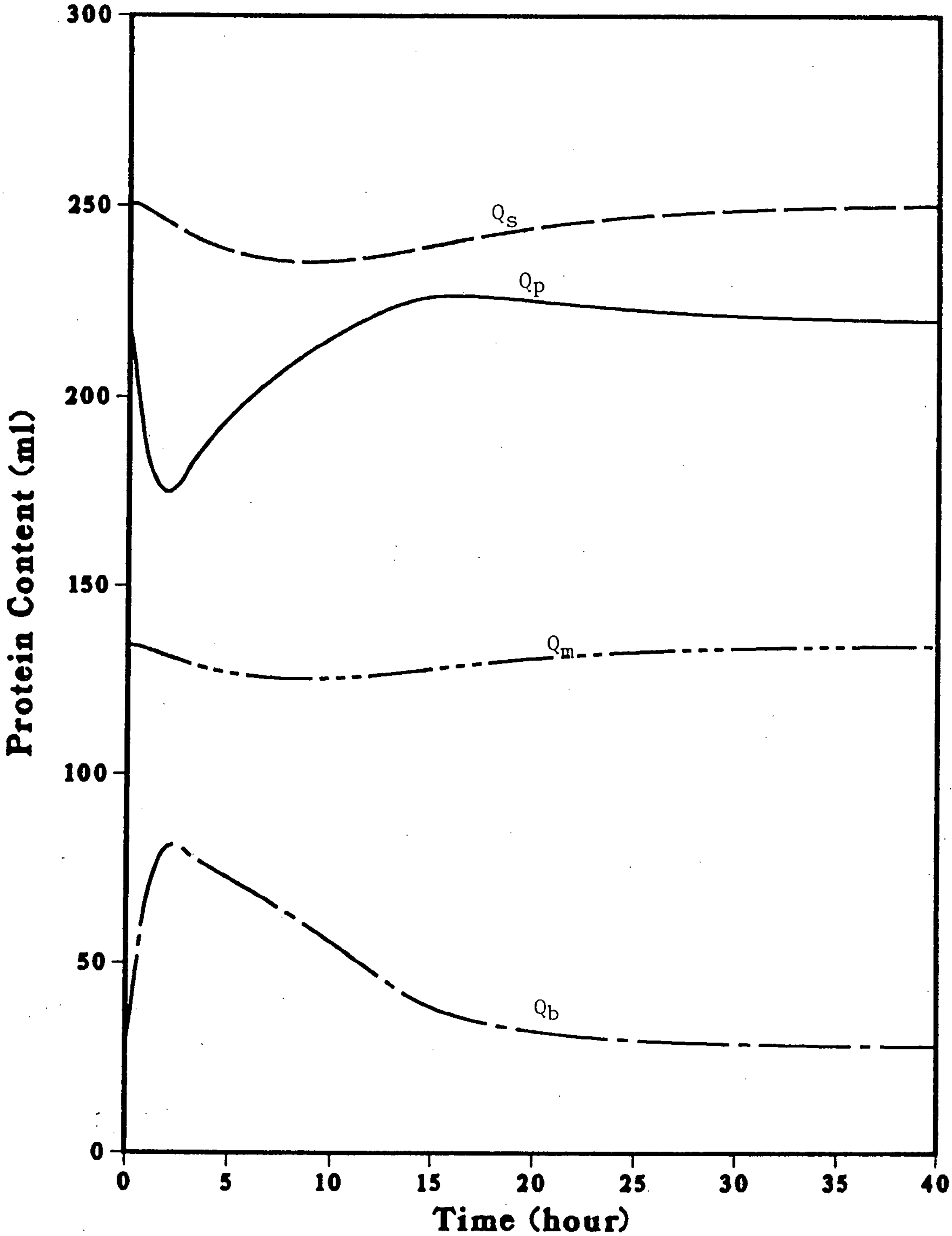

Figure 6.12 The Changes of Fluid Flow Rates in Injured Skin Following a 10% Burn

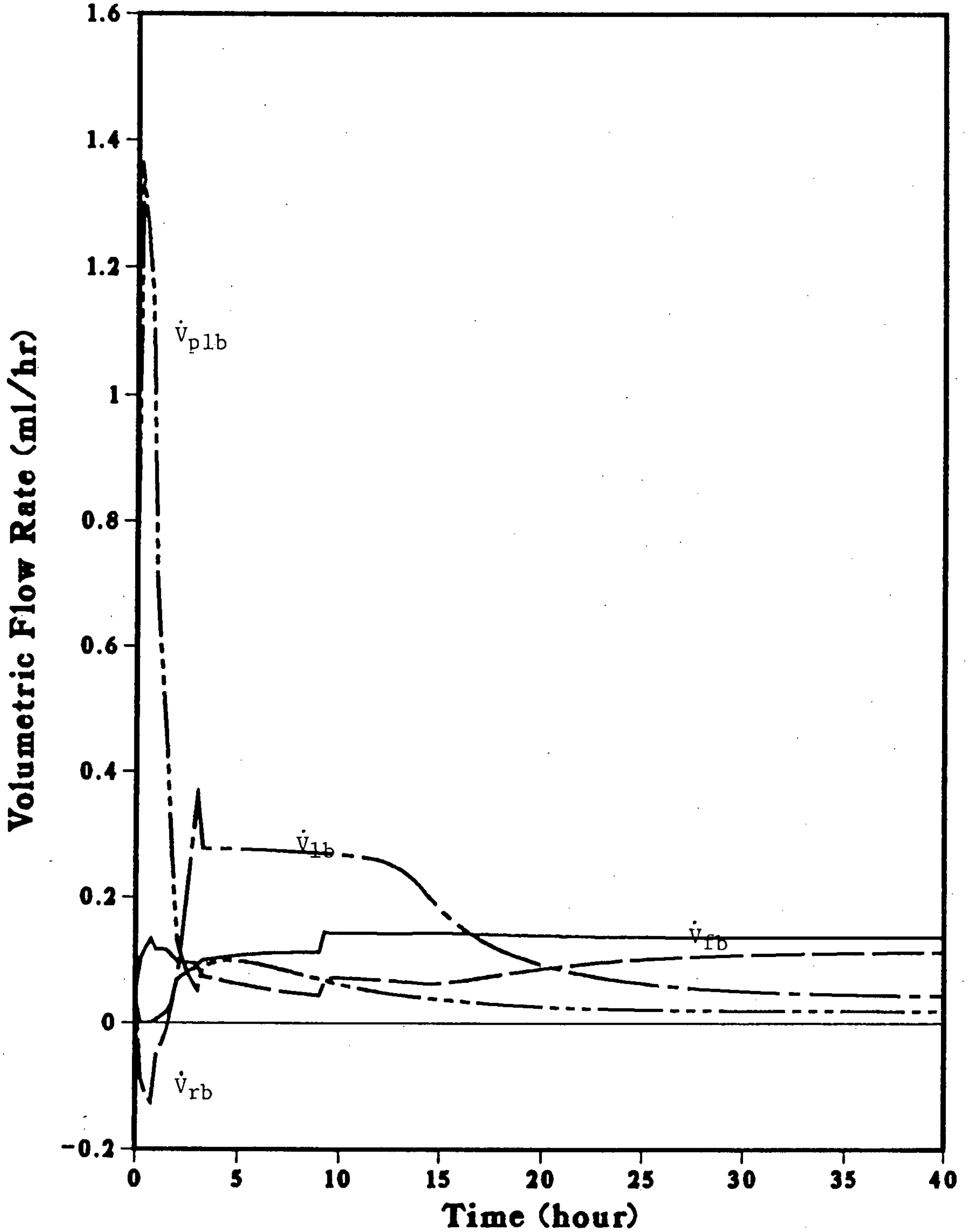

Figure 6.13 The Changes of Albumin Transport Rates in Injured Skin Following a 10% Burn

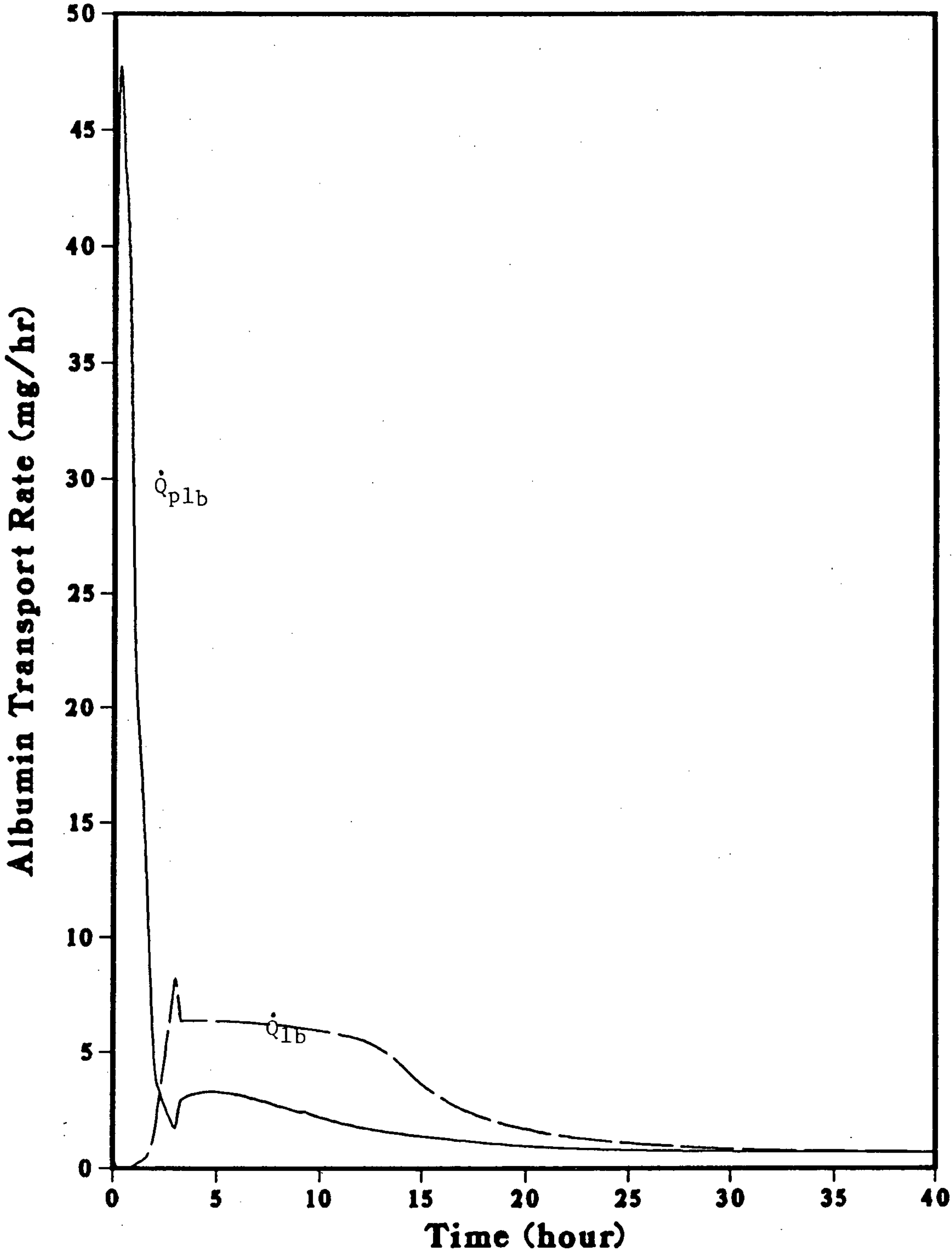

Figure 6.14 The Changes of Capillary and Injured Skin Pressures Following a 10% Burn

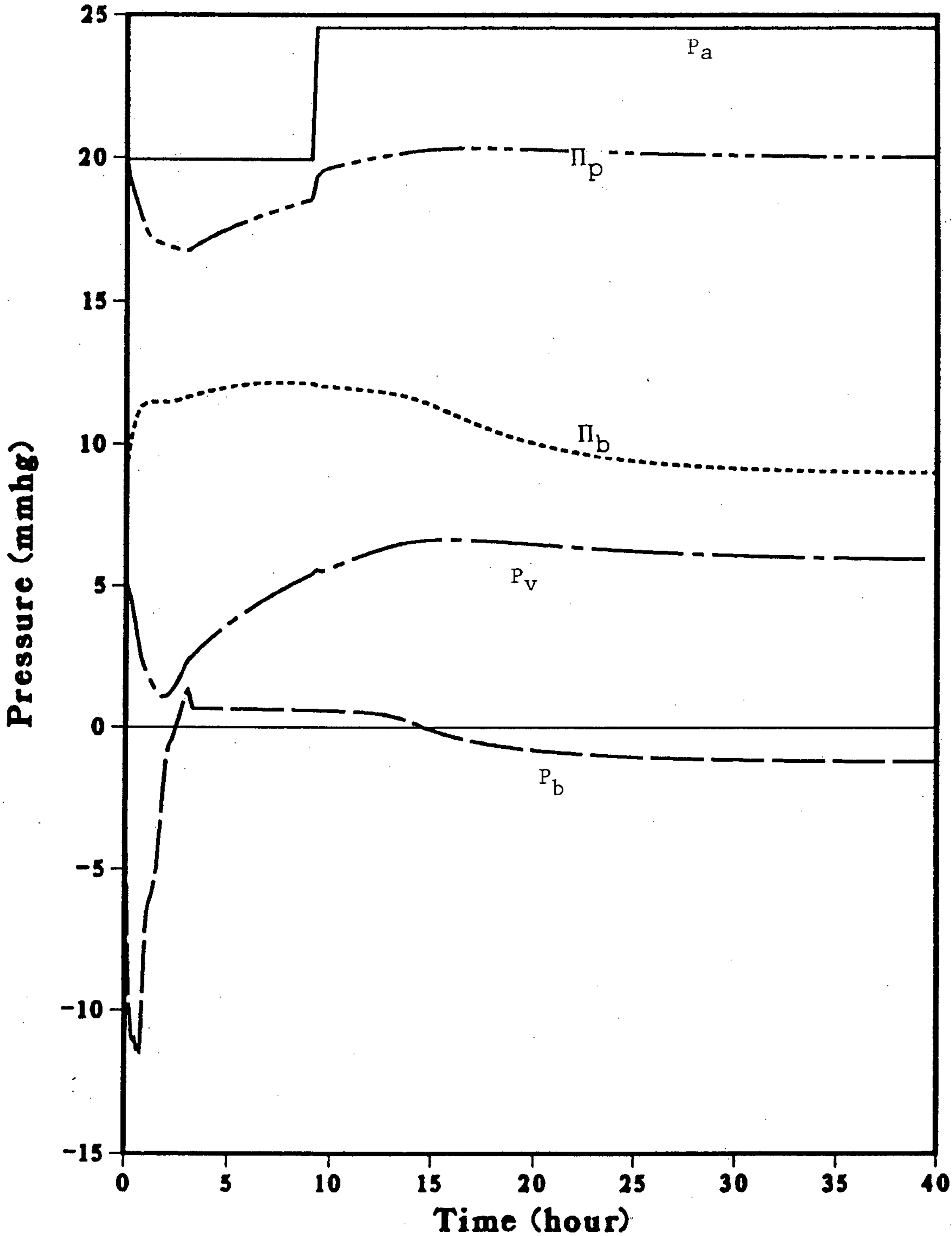

injured tissue. The injured skin becomes edematous, with its volume approximately doubling while its protein content increases by an even greater extent. Although the intact tissue compartments contribute somewhat to this large exchange of fluid and protein, it is the plasma compartment, which is the only compartment in direct communication with the injured skin compartment, that undergoes the severest losses. In order to understand the mechanisms behind these fluid and protein shifts, an analysis of the fluid and protein fluxes into and out of the injured skin compartment is necessary. Figures 6.12 and 6.13 illustrate the transient behaviour of the relevant fluid and protein fluxes, respectively. The driving forces behind the fluid and protein exchanges are functions of the hydrostatic and colloid osmotic pressures that exist in that compartment and in the circulation at any given time. These are shown for the plasma and injured tissue compartments in Figure 6.14.

The most important parameter changes affecting the flow of fluid and protein to the injured skin are the strongly-negative tissue pressure, P_b, which occurs in the first few hours postburn (see Figure 6.14) and the initial large increase in the plasma leak coefficient, K_{plb}. The combined effect of these two changes causes a very large increase in the plasma leak rate and its associated protein flux. Despite the fact that the filtration and reabsorption coefficients are initially reduced to half of their normal values, the negative tissue pressure results in a substantial increase in the magnitudes of both of these flows. Furthermore, because of the initial large change in $P_b - P_v$, the reabsorption flow is actually negative (i.e., into the tissue) for the first two hours postburn. Matters are further exascerbated by the fact that during much of this same period, the lymph flow is shut down entirely due to the low values of P_b.

Thus, because there are only inflows of fluid and protein to the injured skin and no outflows, both the volume and plasm protein content of this compartment rise dramatically during this period. Furthermore, as was explained earlier (see Section 6.2.2), because the plasma leak rate far exceeds the combined filtration and reabsorption rates and because the protein concentration is greater in plasma than that of the tissue, protein enters the injured skin relatively more quickly than does fluid. As a consequence, CA_b and Π_b increase while C_p and Π_p fall. In addition, since the volume of the plasma compartment declines, the compliance relationship for this compartment requires that the venous capillary pressure, P_v, must decrease.

Between 2 and 3 hours postburn, the injured tissue pressure approaches values much closer to normal (-0.51 mmHg) and the plasma leak coefficient falls to about half of its initial value. As a result, the plasma leak fluid and protein fluxes fall rapidly from their maximum values. The plasma leakage is further reduced by the drop in P_v. The increase in P_b causes a decline in the filtration rate which is somewhat offset by the reduction in $\Pi_p-\Pi_b$. More importantly, the very small difference between P_v and P_b which occurs during this period reverses the sign of the reabsorption rate. Furthermore, because P_b rises above its excluded volume limit of -7.84 mmHg, the lymph flow is turned on again. Thus, because both the reabsorption and lymph flows are positive, there are now two mechanisms for relieving the fluid buildup in the injured skin and both V_b and Q_b begin to fall. The extrema in both curves occur when the input and output fluxes are exactly equal, e.g., at 2.3 hours in the case of Q_b. Interestingly, because there are now two paths for fluid return and only one for protein, the protein concentration in the injured tissue continues to rise slightly as exhibited by the further small increase in Π_b. Note also how the lymph flow begins to increase rapidly after about 2 hours when P_b rises above -0.51 mmHg and there is a switchover from Equations 5.6b to 5.6a.

At 3 hours, P_b is returned to its compliance relationship producing the discontinuities apparent in Figure 6.14 and manifested in all of the fluxes shown in Figures 6.12 and 6.13. A second set of noticeable discontinuities occurs at 9 hours when the capillary pressures, P_a and P_v are restored to normal. Here, the larger increase in P_a causes an increased filtration to all tissues, reducing the plasma volume and consequently, raising both C_p and Π_p. The maximum in Q_p at about 16 hours (Figure 6.11) is also probably associated with this change.

Even though all of the coefficient perturbations have died out after approximately 12 hours and the imposed hydrostatic pressure changes have been relaxed at even earlier times, it is of interest to note that all of the fluid volumes and protein contents only return to normal after an elapsed time of 24-36 hours postburn. It is suspected that the main cause of this lag is the inability of the lymph flow to relieve the excessive fluid and plasma protein accumulation in the injured tissue quickly enough. Figure 6.12 demonstrates that $\dot{V}_{lb}$ remains at a relatively constant, but high value (approximately 6 times greater than its normal value) from about 3 to 13 hours postburn. Despite the fact that the tissue volume is abnormally elevated during much of this period, the lymph flow is severely limited by compliance considerations. The volume (when divided through by BSA) places the operating condition far out on the flat portion of the compliance relationship where P_b is almost independent of V_b. It's not until the volume is lowered sufficiently (after about 13 hours) that the tissue pressure begins to follow the more strongly curved part of the relationship, and P_b (Figure 6.14) and

$\dot{V}_{lb}$ (Figure 6.12) fall slowly back to their normal values. Because $\dot{V}_{lb}$ only gradually alleviates the protein buildup in the injured skin, Π_b remains unusually high until after about 15 hours. Beyond this time, the increase in $\Pi_p-\Pi_b$ results in a corresponding rise in the reabsorption rate which further extends the time taken to reach normal. These results are in excellent agreement with the experimental measurements of Carvajal et al. [40] who found that, even though the permeability of thermally injured rat skin returned to normal within 12 hours, the resulting edema lasted longer than 24 hours.

Figures 6.10 and 6.11 indicate that the water and protein contents of the intact skin and muscle compartments decrease only slightly following a 10% burn injury. The initial cause of the fluid volume decrease can be associated with the imposed drop in P_a which decreases the filtration flow to the intact tissues. The decline in the plasma protein content is explained by the large reduction in the plasma leak to muscle and intact skin due to the initial rapid drop in P_v observed in Figure 6.14. The minima in V_m, V_s, Q_m and Q_s occur at times which lag considerably behind the extrema noted earlier for V_p, V_b, Q_p and Q_b. This is because the most important perturbations to the system (K_{plb} and P_b) changes only indirectly affect the intact skin and muscle compartments; these changes made to the injured tissue are eventually communicated to the intact tissues through the intervening plasma compartment. In essence, for the 10% burn, the intact tissue compartments act as aditional fluid and protein reservoirs which mediate the changes which take place in the plasma.

6.3 THE 40% BURN

6.3.1 INTRODUCTION

A similar simulation procedure was applied to rats with 40% surface area burns. As mentioned previously (see Chapter 3), the capillary permeability increases not only in the injured skin, but also in the intact skin and muscle for burns exceeding 25% of the surface area. It is therefore anticipated that the simulation of a 40% burn will be more complex than that of a 10% burn.

The following list includes the parameter perturbations which would likely occur in a 40% burn:

1. an increase in the plasma leak coefficient in the injured skin (K_{plb}),
2. an alteration in the hydrostatic pressure in the injured skin (P_b),
3. an increase in the plasma leak coefficients in the intact tissues (K_{pls} and K_{plm}),
4. a change in the filtration and reabsorption coefficients in the injured skin (K_{fb} and K_{rb}),

in the injured skin (K_{fb} and K_{rb}),

5. a change in the filtration and reabsorption coefficients in the intact tissues (K_{fs}, K_{fm}, K_{rs} and K_{rm}),
6. a decrease in the arterial capillary pressure in the injured skin (P_{ab}), and
7. an alteration the lymph flow in all tissues ($\dot{V}_{lb}$, $\dot{V}_{lm}$ and $\dot{V}_{ls}$).

These perturbations are listed in what is assumed to be their order of importance with respect to causing changes in the microvascular exchange system.

According to Lund and Reed [33], the main arterial pressure, P_{aa}, dropped to an average of 70% of its normal value following a 40% burn. If this P_{aa} is used to recalculate the arterial and venous capillary pressure from Equations 5.18 and 5.19, it is found that P_a=17.64 mmHg and P_v=4.72 mmHg, respectively. These P_a and P_v values are used in all of the simulations for the 40% burn which follow.

6.3.2 TRANSIENT RESPONSE FOR CHANGES TO THE PLASMA LEAKAGE COEFFICIENT AND THE TISSUE PRESSURE CHARACTERISTICS OF THE INJURED SKIN (PHASE ONE)

An increased K_{plb} is known to occur in 40% surface area burns (see Table 3.1). As in the 10% burn, a time-dependent exponential function of the form:

$$K_{plb} = (Ae^{-at}+1)k_{plb} \qquad 6.4$$

is assumed. In Equation 6.4, italicized k_{plb} is the normal plasma leak coefficient of the injured skin for a 40% burn and the time constant a has the same value as for a 10% burn.

P_b follows the experimentally measured relationship shown in Figure 4.3. Again, both the "mean" (middle) and the "mean+standard error" (upper) pressure curves are used in the simulation. The sum-of-squares of differences between the simulation predictions and the experimental data obtained by Lund and Reed for a 40% burn were calculated as before and the same six dependent variables were normalized with respect to their initial values. The SS predictions obtained in Phase One of the 40% burn simulation can be seen in Table 6.5 for a range of changes in K_{plb} and for the two P_b versus time curves. The best fit (i.e., lowest SS) results are shown in graphical form as Figure 6.15.

As was the case for the 10% burn, the use of the middle pressure curve gave poorer fits for all A values tested. Thus, it was decided that only the upper pressure curve would be employed in all of the subsequent simulations.

Table 6.5 SS as a function of K_{plb} and P_b for 40% Burn (Phase One)

P_b \ A (SS)	2.0	3.0	4.0	5.0	6.0	8.0
Upper Curve	—	1.02	0.98	0.99	1.03	1.26
Middle Curve	1.30	—	1.38	—	1.82	—

Figure 6.15 Simulation for Changing K_{plb} and P_b in 40% Burn (A=4.0, Upper Curve for P_b)

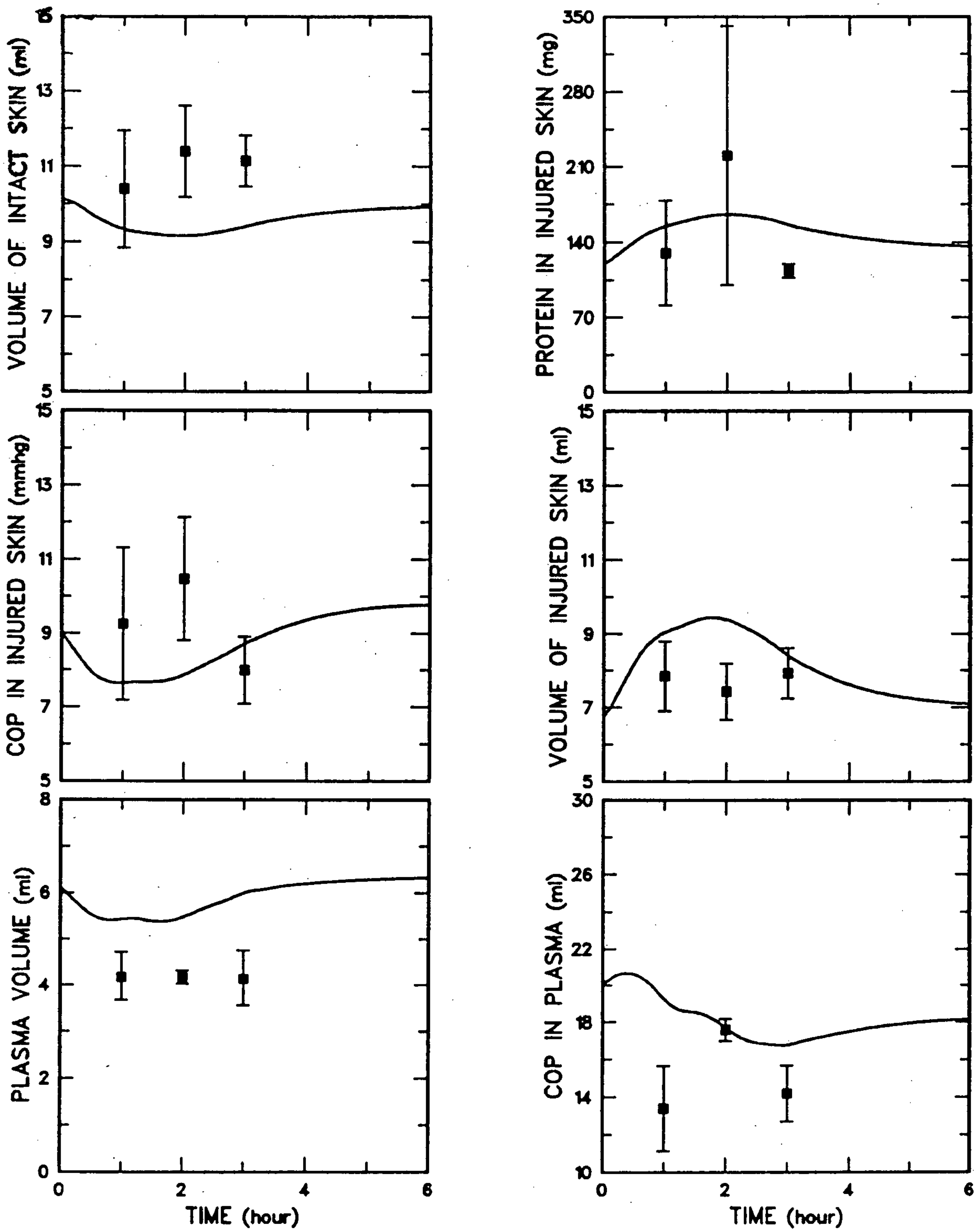

When the upper curve for P_b was used, the SS value went through a minimum at about A = 4 although very little difference in the fits was noted for the range of $3 \leq A \leq 6$. The optimum value of A for a 10% burn was found to be 35, i.e., an order-of-magnitude greater than that determined for a 40% burn. This apparent discrepancy can be rationalized if it is recalled that K_{plb}, like all transport coefficients, is the product of the vascular surface area and the capillary permeability. Thus, if the perfusion of the injured tissue in a 40% burn is substantially less than for a 10% burn, then the actual permeability could be of the same order in both cases. As will be discussed in a later section (Section 6.3.4), there is other corroborating evidence for this hypothesis.

As can be seen from Figure 6.15, predicted results are not in close quantitative agreement with the experimental measurements. However, even though some of the experimental trends are not particularly obvious, five out of the six predicted trends appear to be in the right direction. As was the case for the 10% burn, the only variable for which the trends do not match closely is the volume of intact skin. The model predicts a slight decrease in V_s, while the experimental data show an increase.

The reasons why an increase in K_{plb} and a reduction in P_b lead to the predicted responses illustrated in Figure

6.15 are similar to those already discussed in the Phase One simulations for the 10% burn. The predicted edema in the injured skin is too high compared to the experimental data leading to COP values for this tissue which are somewhat too low. Also, the plasma output is insufficient and, as a consequence, the volume of plasma in the model prediction is far too large. To compensate for these problems of not having enough fluid in the intact skin and too much in the plasma, the Phase Two simulations were introduced.

6.3.3 TRANSIENT RESPONSE INCLUDING CHANGES IN THE PLASMA LEAK COEFFICIENTS IN THE INTACT TISSUES (PHASE TWO)

The justification for increasing the plasma leak coefficients in the noninjured tissues for the 40% burn case has already been discussed. The perturbed plasma leak coefficients for the intact skin and muscle (K_{pls} and K_{plm}) are assumed to behave as time-dependent exponential functions having the following form:

$$K_{pls} = (Be^{-at}+1)\,k_{pls} \qquad 6.5$$

and

$$K_{plm} = (Be^{-at}+1)\,k_{plm} \qquad 6.6$$

where the italicized k_{pls} *and* k_{plm} denote normal values, B reflects the magnitude of the change (assumed equal for both skin and muscle), and a is the time constant (again equal to 0.231 h^{-1}).

Several combinations of different K_{plb}, K_{pls} and K_{plm} were investigated. The input perturbations and the SS values obtained in each trial are listed in Table 6.6. The best fit results for all six measured variables are shown in Figure 6.16.

The SS values reported in Table 6.6 are not dramatically different from, but all represent a slight improvement over the Phase One results given in Table 6.5, In other words, when K_{pls} and K_{plm} are increased, the model provides better predictions than if K_{pls} and K_{plm} remain at their normal values. Since the changes in the intact tissue permeabilities after burns are expected to be significantly less than those of injured skin, only values of $B \leq 10.0$ were examined in this investigation. According to Table 6.6, the best results are obtained when K_{pls} and K_{plm} are allowed to increase to about 8 - 10 times normal. Although the optimum value of B is about twice that of A, it is expected that the actual permeability increase in the injured skin should be considerably greater than in the intact tissues.

Table 6.6 SS as a K_{plb}, K_{pls} and K_{plm} for 40% Burn (Upper Curve for P_b, Phase Two)

B / A / SS	1.0	3.0	5.0	8.0	10.0
2.0	—	—	0.89	—	0.77
3.0	0.97	0.89	0.81	0.75	—
4.0	0.94	0.85	0.79	0.74	—
6.0	—	—	0.89	0.87	—

Figure 6.16 Simulation for Changing K_{plb}, K_{pls}, K_{plm} and P_b in 40% Burn (A=4.0, B=8.0, Upper Curve for P_b)

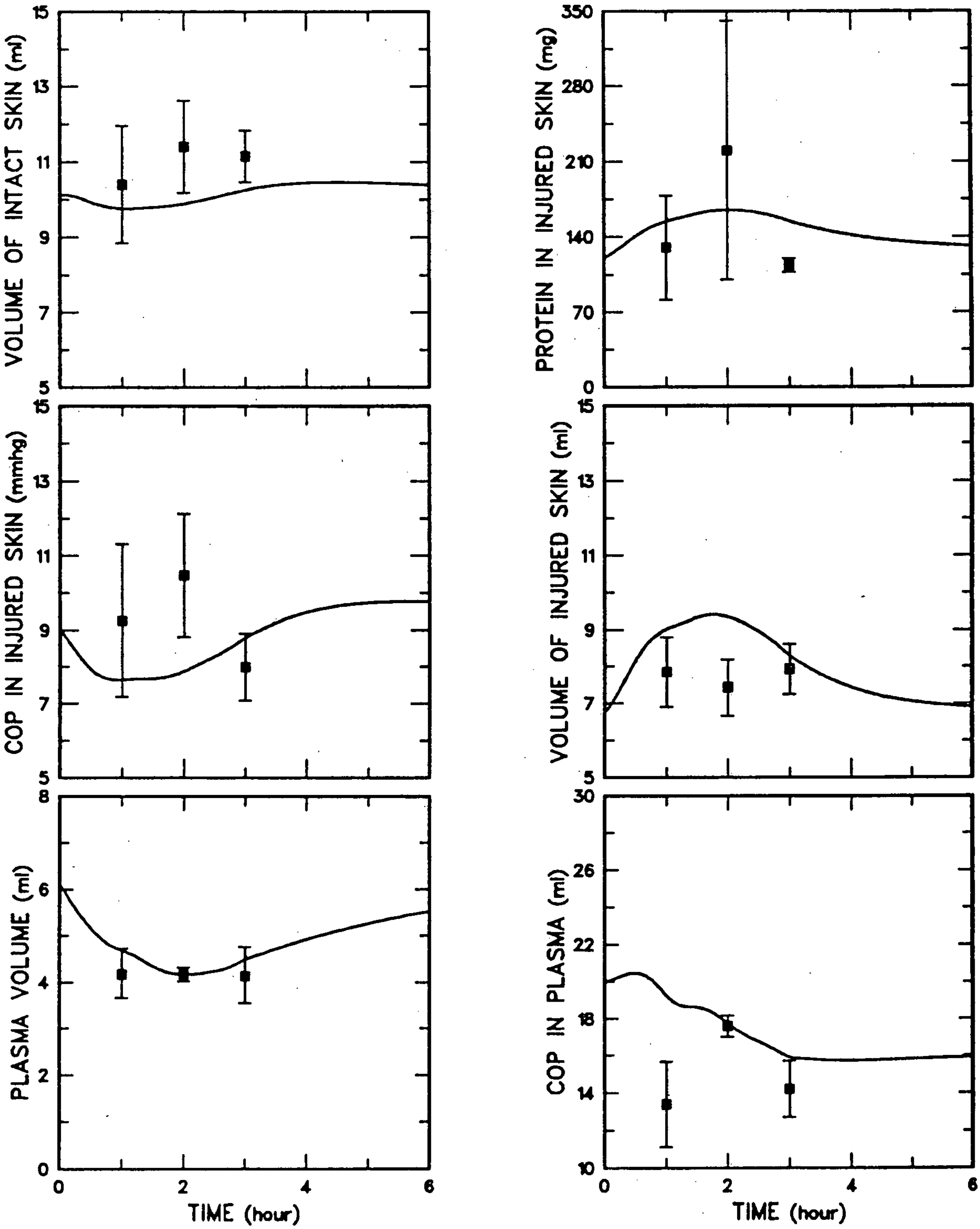

Again, the fitted results can be rationalized if it is assumed that there is a strong depression of the perfusion rate in the injured tissue following a large surface area burn.

When the results of Figure 6.16 are compared to those of Figure 6.15, the two most apparent differences are that the intact skin volume falls less drastically and the plasma volume more drastically than before. Both trends are in better agreement with the experimental data. The changes are consistent with increases in K_{pls} and K_{plm}, which allow for a greater fluid transfer from the plasma to the intact tissues. However, the Phase Two perturbations have no direct effect on the fluid and protein contents of the injured skin. As a consequence, in this tissue, the edema remains overpredicted and the COP underpredicted.

6.3.4 TRANSIENT RESPONSE INCLUDING CHANGES IN THE FILTRATION AND REABSORPTION COEFFICIENTS IN THE INJURED SKIN (PHASE THREE)

The filtration and the reabsorption coeffieints in the injured skin (K_{fb} and K_{rb}) are products of capillary permeability and surface area for transport. Thus, K_{fb} and K_{rb} could increase due to an augmentation of the permeability or decrease due to a drop in the perfusion rate. It is assumed that the coefficient perturbations follow the relationships:

$$K_{fb} = (Ce^{-at}+1)k_{fb} \qquad 6.7$$

and

$$K_{rb} = (Ce^{-at}+1)k_{rb} \qquad 6.8$$

where italicized k_{fb} and k_{rb} are the normal values, C reflects the magnitude of the change (which could be positive or negative) and the time constant a has the same value as before (i.e., a=0.231 h^{-1}).

Table 6.7 lists the sum-of-squares results for the Phase Three simulations obtained by using some of the better combinations of A and B from Phase Two. Figures 6.17 and 6.18 compare predicted and experimental values for the two "best-fit" cases where A=4.0, B=10.0, and C=-0.80 or C=-0.95, respectively.

For the 40% burn, increasing K_{fb} and K_{rb} above their normal values results in a poorer fit of the data. This induces an even higher edema in the injured skin compare to the results of Phase Two. If K_{fb} and K_{rb} are decreased by 50%, the SS results are improved moderately. However, if

Table 6.7 SS as a Function of K_{plb}, K_{pls}, K_{plm}, K_{fb} and K_{rb} for 40% Burn (Upper Curve for P_b, Phase Three)

C \ SS \ A,B	2.0,8.0	3.0,1.0	3.0,8.0	3.0,10.0	4.0,3.0	4.0,5.0	4.0,10.0
2.0	1.03	—	0.99	—	—	—	—
0.0	—	0.97	0.75	—	0.85	0.79	—
-0.50	—	0.86	—	—	0.74	—	—
-0.80	—	0.79	0.58	0.56	0.68	—	0.53
-0.95	—	0.77	0.58	0.55	0.66	0.67	0.52

C = 0.0 corresponds to the simulations in Phase Two

Figure 6.17 Simulation for Changing K_{plb}, K_{pls}, K_{plm}, K_{fb} and K_{rb} in 40% Burn (A=4.0, B=10.0, C=-0.80, Upper Curve for P_b)

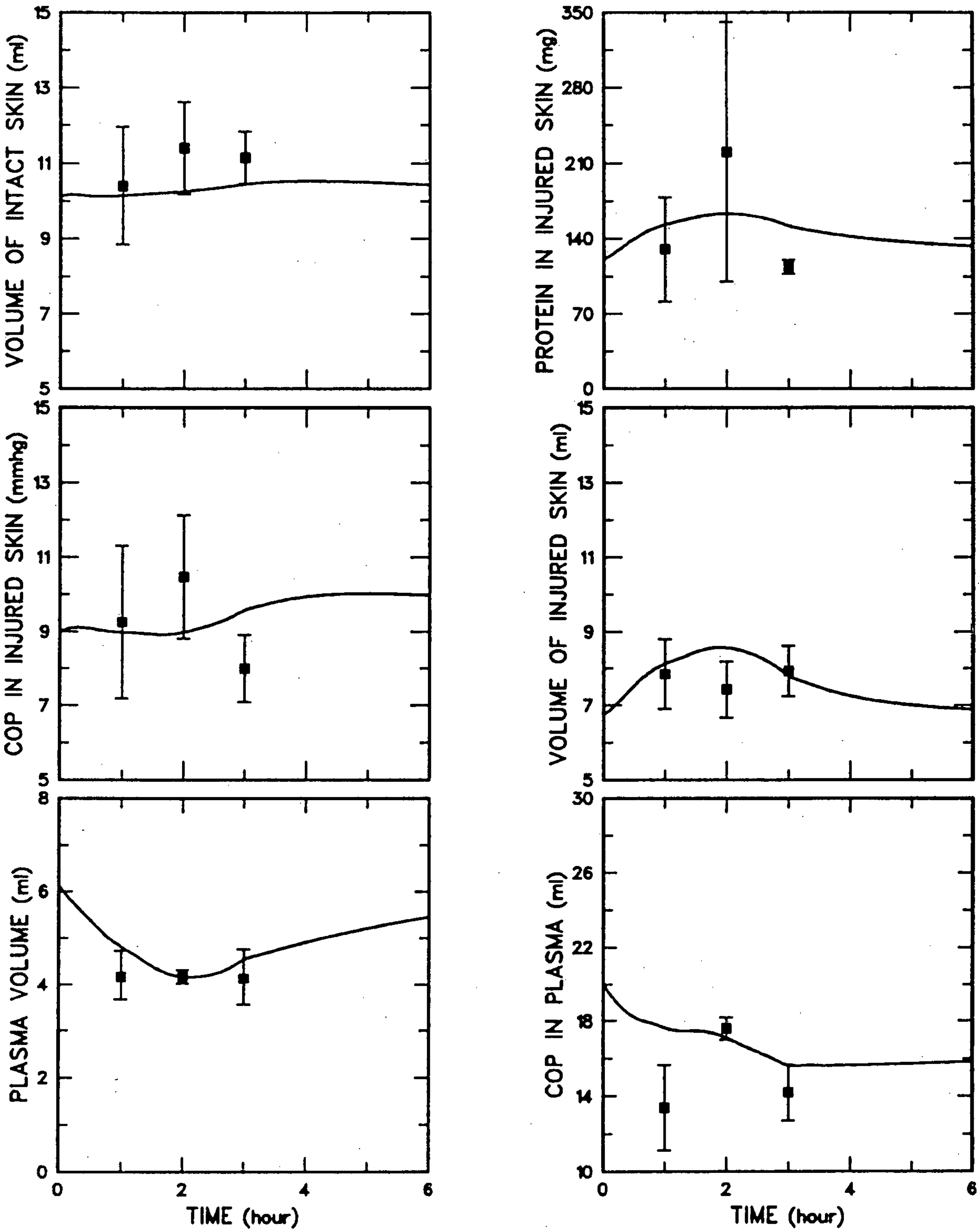

Figure 6.18 Simulation for Changing K_{plb}, K_{pls}, K_{plm}, K_{fb} and K_{rb} in 40% Burn (A=4.0, B=10.0, C=-0.95, Upper Curve for P_b)

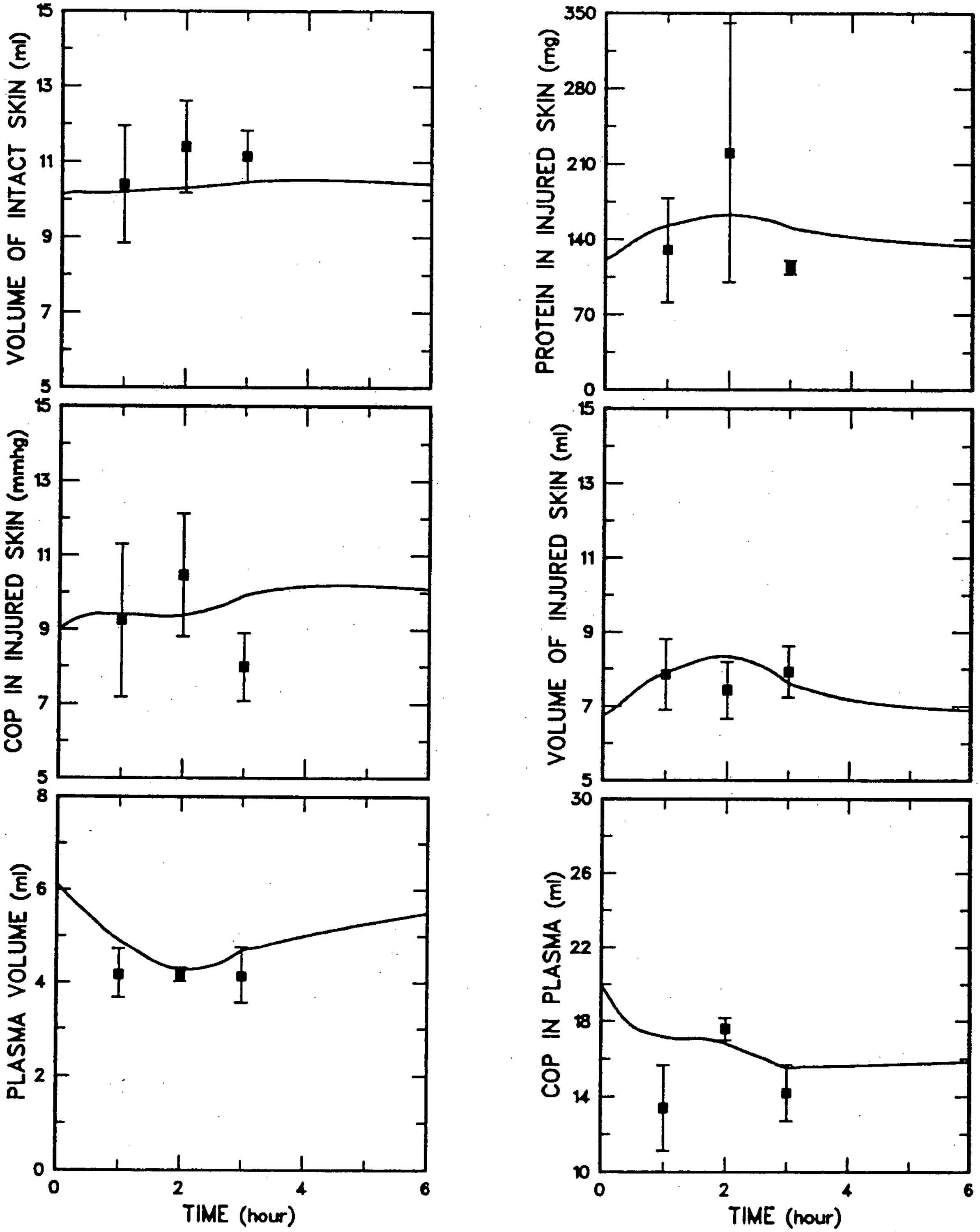

these coefficients are decreased by 80% or even 95%, the SS results show a significant improvement (see Table 6.7). This required reduction in K_{fb} and K_{rb} is additional confirmation that there may be much lower perfusion in the injured skin following a 40% burn than after a 10% burn. There is no discernable differences between the two cases plotted in Figures 6.17 and 6.18. Thus, it appears that the filtration and reabsorption coefficients in injured skin may decline to about 5-20% of their normal values. Since it is expected that the permeability towards fluid transfer through the capillary wall will actually increase after a burn, the inescapable conclusion is that the perfusion rate in a 40% injury must fall to very low values. This prediction is consistent with the published measurements of Ferguson et al. [24] (see Table 3.2) and with the recent experimental observations of A. Haugan in Bergen, Norway (personal communication).

The Phase Three model predictions represent a significant improvement in the fit of the experimental data as compared to the Phase Two perturbations. Additionally, all six predicted variables in Figures 6.17 and 6.18 now have the same trends as the experimental data. The main effect of the Phase Three perturbations is to reduce the edema in the injured skin, making it more consistent with the experimental data. By decreasing K_{fb} and K_{rb} the magnitudes of both the filtration and reabsorption rates are decreased. Since reabsorption is actually reversed during the initial stages of the burn (see Section 6.3.10), these changes lead to a lower input of fluid into the injured skin which tends to adjust conditions in the proper direction. However these changes do not influence the protein content in the injured skin, which remains approximately the same as in Phase Two. As a consequence, the albumin concentration is higher and the COP results are in better correspondence with the measured data.

6.3.5 TRANSIENT RESPONSE INCLUDING CHANGES IN THE FILTRATION AND THE REABSORPTION COEFFICIENTS IN THE INTACT TISSUES (PHASE FOUR)

An increased capillary permeability and decreased perfusion rate could occur in the intact tissues as well as in injured tissue in the case of a 40% burn (see Chapter 3). These changes could increase or reduce the values of K_{fs}, K_{rs}, K_{fm} and K_{rm}, which are assumed to follow time-dependent exponential functions of the form

$$K_{fs} = (De^{-at}+1)k_{fs} \qquad 6.9$$

$$K_{rs} = (De^{-at}+1)k_{rs} \qquad 6.10$$

$$K_{fm} = (De^{-at}+1)k_{fm} \qquad 6.11$$

and

$$K_{rm} = (De^{-at}+1)k_{rm} \qquad 6.12$$

In the above equations, italicized k_{fs}, k_{rs}, k_{fm} and k_{rm} represent normal values, D reflects the magnitude of the initial changes (assumed equal for all four coefficients) and the time constant a remains 0.231 h^{-1}.

Based on several of the better fitting cases from Phase Three, several model predictions for this phase were generated and the sum-of-squares values are given in Table 6.8. The plotted results for the best fit to the experimental data in this phase are shown in Figure 6.19.

Changing K_{fs}, K_{rs}, K_{fm} and K_{rm} for a given set of A,B, and C magnitudes yields the same SS values as the Phase Three predictions (compare Table 6.8 with Table 6.7). This is primarily because reabsorption and filtration in the intact tissues transfer fluid in opposing directions. Thus, if both fluid fluxes change by the same magnitude, their effects tend to cancel one another. However, changing K_{fb} and K_{rb} in injured skin has a much stronger influence. Because reabsorption is actually reversed (due to the very negative tissue pressures in burned skin) during the first few hours postburn, $\dot{V}_{fb}$ and $\dot{V}_{rb}$ are in the same direction. Hence, increases or decreases in the value of K_{fb} and K_{rb} during this time has twice the effect of just increasing one of the coefficients.

Table 6.8 SS as a Function of K_{pl}, K_f, K_r for 40% Burn (Upper Curve for P_b, Phase Four)

D \ C	-0.50			-0.80			-0.95		
A,B / SS	3.0,1.0	3.0,5.0	3.0,10.0	3.0,1.0	3.0,5.0	3.0,10.0	3.0,1.0	3.0,5.0	3.0,10.0
Normal	0.86	—	—	0.79	—	0.56	0.77	—	0.55
-0.30	0.86	0.71	0.61	0.79	0.66	0.56	0.78	0.65	0.55
-0.5	0.86	0.71	0.61	0.80	0.66	0.56	0.78	0.65	0.56

D = Normal corresponds to the simulations in Phase Three

Figure 6.19 Simulation for Changing K_{plb}, K_{pls}, K_{plm}, K_{fb}, K_{rb}, K_{fs}, K_{fm}, K_{rs} and K_{rm} in 40% Burn (A=3.0, B=10.0, C=-0.80, D=-0.30, Upper Curve for P_b)

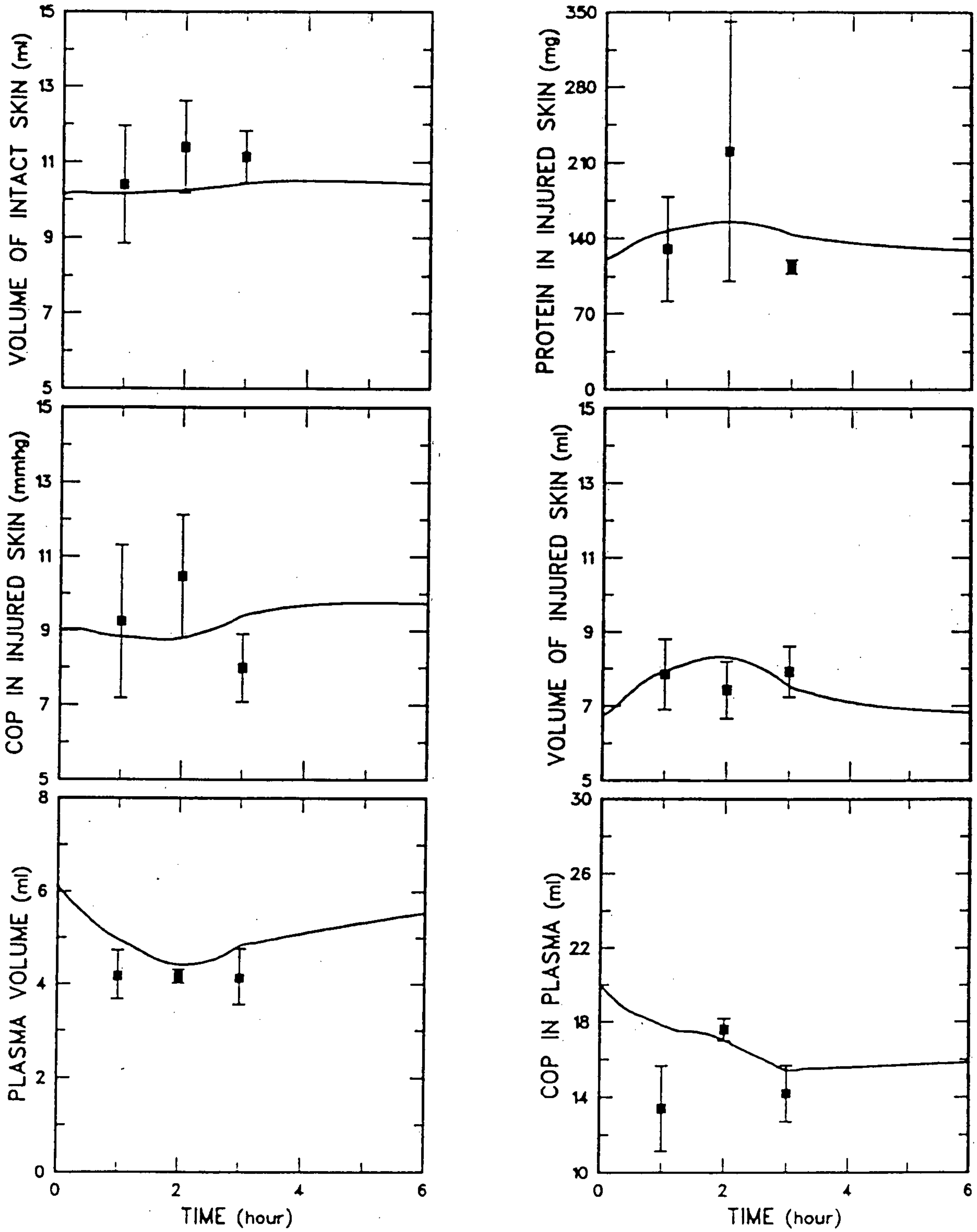

Since the trends predicted in Phase Four are virtually indistinguishable from those obtained in Phase Three, it is concluded that changing the filtration and reabsorption coefficients in the intact tissues does not improve the fitting results and hence, can be left out of all subsequent model predictions.

6.3.6 TRANSIENT RESPONSE INCLUDING CHANGES IN THE ARTERIAL CAPILLARY PRESSURE IN THE INJURED SKIN (PHASE FIVE)

The main arterial pressure in the 40% burn is depressed more than in the 10% burn [33] (see Table 3.2). This factor was assumed to decrease the arterial and venous capillary pressures for all tissues (see Section 6.3.1). It is also expected that, because of a local increase in peripheral resistance in thermally injured tissue, P_{ab} may be even lower than the value estimated in Section 6.3.1. Thus, Phase Five involved the examination of the effect of two lower values of P_{ab}; namely, 10 mmHg and 15 mmHg.

Based on several of the better fitting cases from Phase Three (since Phase Four does not have much influence on SS), the model predictions for these decreased P_{ab} values were generated. Table 6.9 compares the sum-of-squares fitting values for the resultant simulations.

Table 6.9 SS as a Function of K_{pl}, K_f, K_r and P_{ab} (mmHg) for 40% Burn (Upper Curve for P_b, Phase Five)

C	-0.8			-0.95		
A,B	3.0,1.0	3.0,8.0	4.0,10.0	3.0,1.0	3.0,8.0	4.0,10.0
P_{ab} \ SS						
10.0	0.80	0.60	0.54	—	0.60	0.54
15.0	0.79	0.59	0.54	—	0.58	0.53
17.6	0.79	0.58	0.53	0.77	0.58	0.52

P_{ab} = 17.6 mmHg corresponds to the simulations in Phase Three

No dramatic differences can been seen in Table 6.9 as P_{ab} is decreased from 17.6mmHg to 15mmHg or to 10mmHg. In fact, if anything, the fit becomes slightly worse as P_{ab} is lowered. Thus, as was the case for the 10% burn, P_{ab} changes do not seem to have a significant effect on the behaviour of the system and hence do not need to be consided in future simulations. The transient results predicted in this phase were so similar to those obtained in Phase Three and Phase Four that no plots will be presented.

6.3.7 TRANSIENT RESPONSE INCLUDING CHANGES IN THE LYMPH FLOW CHARACTERISTICS (PHASE SIX)

Not much information about lymph flow after burns is available in the literature. Unlike the 10% burn, the lymph flow of intact tissues in the 40% burn might change as well. Four different cases of lymph flow change were simulated. These cases are:

1. $\dot{V}_{lb} = 2 \cdot \dot{V}_{lbo}$, when $t<3$ hours and $\dot{V}_{lb} < 2 \cdot \dot{V}_{lbo}$

2. $\dot{V}_{lb} = 5 \cdot \dot{V}_{lbo}$, when $t<3$ hours and $\dot{V}_{lb} < 5 \cdot \dot{V}_{lbo}$

3. $\dot{V}_{lb} = 2 \cdot \dot{V}_{lbo}$, When $t < 3$ hours and $\dot{V}_{lb} < 2 \cdot \dot{V}_{lbo}$

$\dot{V}_{ls} = (0.5e^{-at}+1) \cdot \dot{V}_{lso}$

$\dot{V}_{lm} = (0.5e^{-at}+1) \cdot \dot{V}_{lmo}$

4. $\dot{V}_{lb} = 5 \cdot \dot{V}_{lbo}$, When $t < 3$ hours and $\dot{V}_{lb} < 5 \cdot \dot{V}_{lbo}$

$\dot{V}_{ls} = (2.5e^{-at}+1) \cdot \dot{V}_{lso}$

$\dot{V}_{lm} = (2.5e^{-at}+1) \cdot \dot{V}_{lmo}$

Here, $\dot{V}_{lbo}$, $\dot{V}_{lmo}$ and $\dot{V}_{lso}$ are the initial lymph flows in the injured skin, muscle and intact skin, respectively. The parameter a is a time constant which determines how long it takes for the intact tissue lymph flows to return to normal. It is assumed to be the same (i.e., a=0.231 h^{-1}) as the time constant used to relax the transport coefficient changes. After three hours, the lymph flow characteristics in the injured skin are assumed to return to the normal relationship given by Equations 5.6a or 5.6b.

The input perturbations and sum-of-squares values for the fits are listed in the Table 6.10. Two plots illustrating the consequences of lymph flow changes 2 and 3 above are shown in Figures 6.20 and 6.21, respectively.

Table 6.10 SS as a Function of K_{pl}, K_f, K_r and Lymph Flow Characteristics for 40% Burn (Upper Curve for P_b, P_{ab} = 17.6 mmHg, Phase Six)

$\dot{V}_L$ / SS	Normal	First case	Second case	Third case	Fourth case
A = 4.0 B = 10.0 C = -0.95 D = 0.0	0.52	0.60	0.96	0.62	0.97
A = 3.0 B = 8.0 C = -0.80 D = 0.0	0.58	0.69	1.05	0.72	1.05

$\dot{V}_L$ = Normal corresponds the simulations in Phase Three

Figure 6.21 Simulation for Changing K_{plb}, K_{pls}, K_{plm}, K_{fb}, K_{rb}, K_{fs}, K_{fm}, K_{rs}, K_{rm}, $\dot{V}_{lb}$, $\dot{V}_{ls}$ and $\dot{V}_{lm}$ in 40% Burn (A=4.0, B=10.0, C=-0.95, D=0.0, Upper Curve for P_b, Second Condition for Lymph Flow Characteristic)

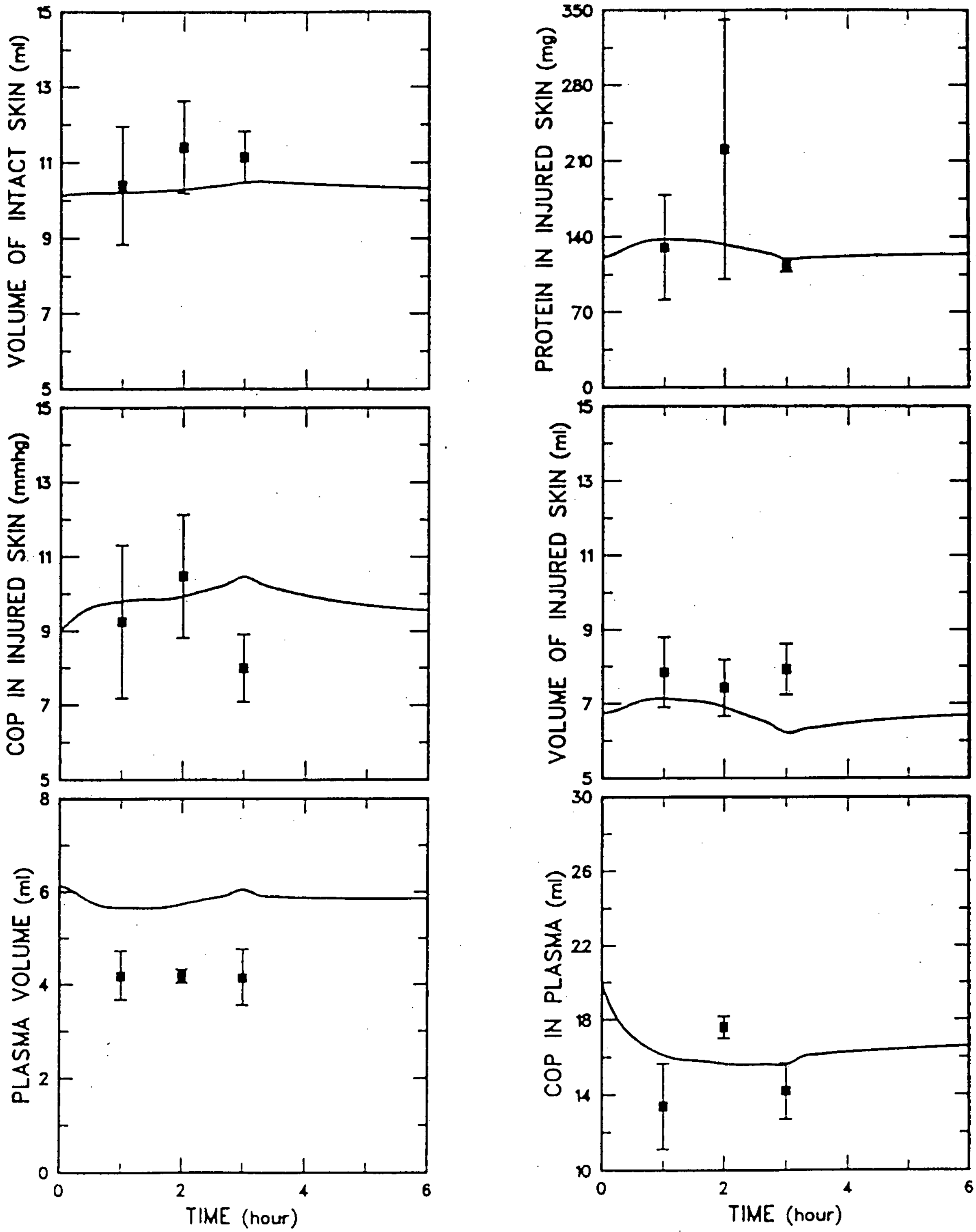

Figure 6.20 Simulation for Changing K_{plb}, K_{pls}, K_{plm}, K_{fb}, K_{rb}, K_{fs}, K_{fm}, K_{rs}, K_{rm}, $\dot{V}_{lb}$, $\dot{V}_{ls}$ and $\dot{V}_{lm}$ in 40% Burn (A=4.0, B=10.0, C=-0.95, D=0.0, Upper Curve for P_b, Third Condition for Lymph Flow Characteristic)

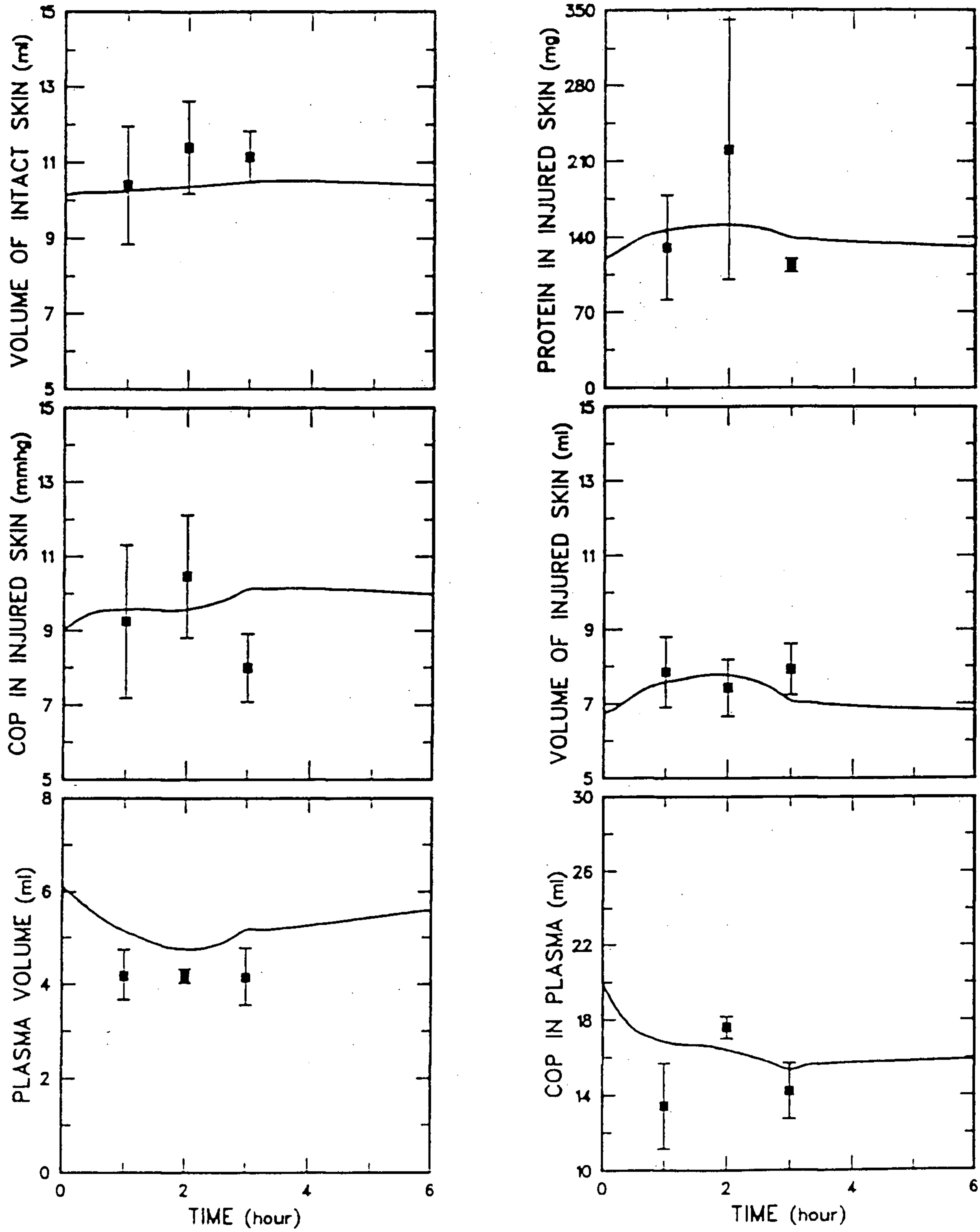

According to Table 6.10, the more the lymph flow in the injured skin increases, the worse is the fit of the predicted versus experimental results. For example, Figure 6.20 shows that, when the lymph flow in the injured skin is 5 times its normal value in the first three hours postburn, the plasma and injured skin volumes predicted both change much less significantly from their initial values. This is because the rate of return of the fluid from the injured skin to the plasma through the lymphatics is too rapid such that neither the volume of the injured skin or the volume of plasma demonstrate the expected changes. Table 6.10 also indicates that changing the lymph flow rate in the intact tissue has little effect on the overall fits. For example, the SS results for the second case (where only $\dot{V}_{lb}$ changes) are almost identical to the fourth case (where $\dot{V}_{lb}$, $\dot{V}_{ls}$ and $\dot{V}_{lm}$ all change). It therefore seems reasonable to continue using the original lymph flow characteristics for the 40% burn.

6.3.8 MOST REASONABLE FIT FOR A 40% BURN

The parameter changes which appear to yield the most reasonable results for a 40% surface area burn are the following:

1. The plasma leak coefficient in the injured skin increases. The initial magnitude of the change A = 4.0 leads to the "best" fit.

2. The tissue pressure in the injured skin declines dramatically for 3 hours postburn. The upper curve yields a more reasonable fit than does the middle curve.
3. The plasma leak coefficient in the two intact tissues increases to an even greater extent than in the injured skin. The magnitude of the change for both intact tissues is taken to be B = 10.0.
4. The filtration and reabsorption coefficients in the injured skin are reduced to 5% of their normal values (C = -0.95).

6.3.9 LONG TERM TRANSIENT RESPONSE

In the simulations of the 40% burn discussed thus far, the arterial and venous capillary pressures have been changed from their normal values. All of the other changes have been designed so that they will return to normal within about 12 hours postburn. In order to find the time required for the system to restore itself, P_a and P_v were set to their normal values after either 3, 6 or 9 hours postburn. The long term transient responses based on one of the best sets of conditions from Phase Three was then obtained. Figures 6.22 - 6.24 show how the injured system returns to normal after a 40% burn using these reasonable parameter changes from the earlier investigation and capillary pressure changes at 3, 6 and 9 hours, respectively. In

Figure 6.22 Steady State Result for 40% Burn (A=4.0, B=10.0, C=-0.95, D=0.0, Upper Curve for P_b, Arterial and Venous Capillary Pressure Return to Normal After Three Hours)

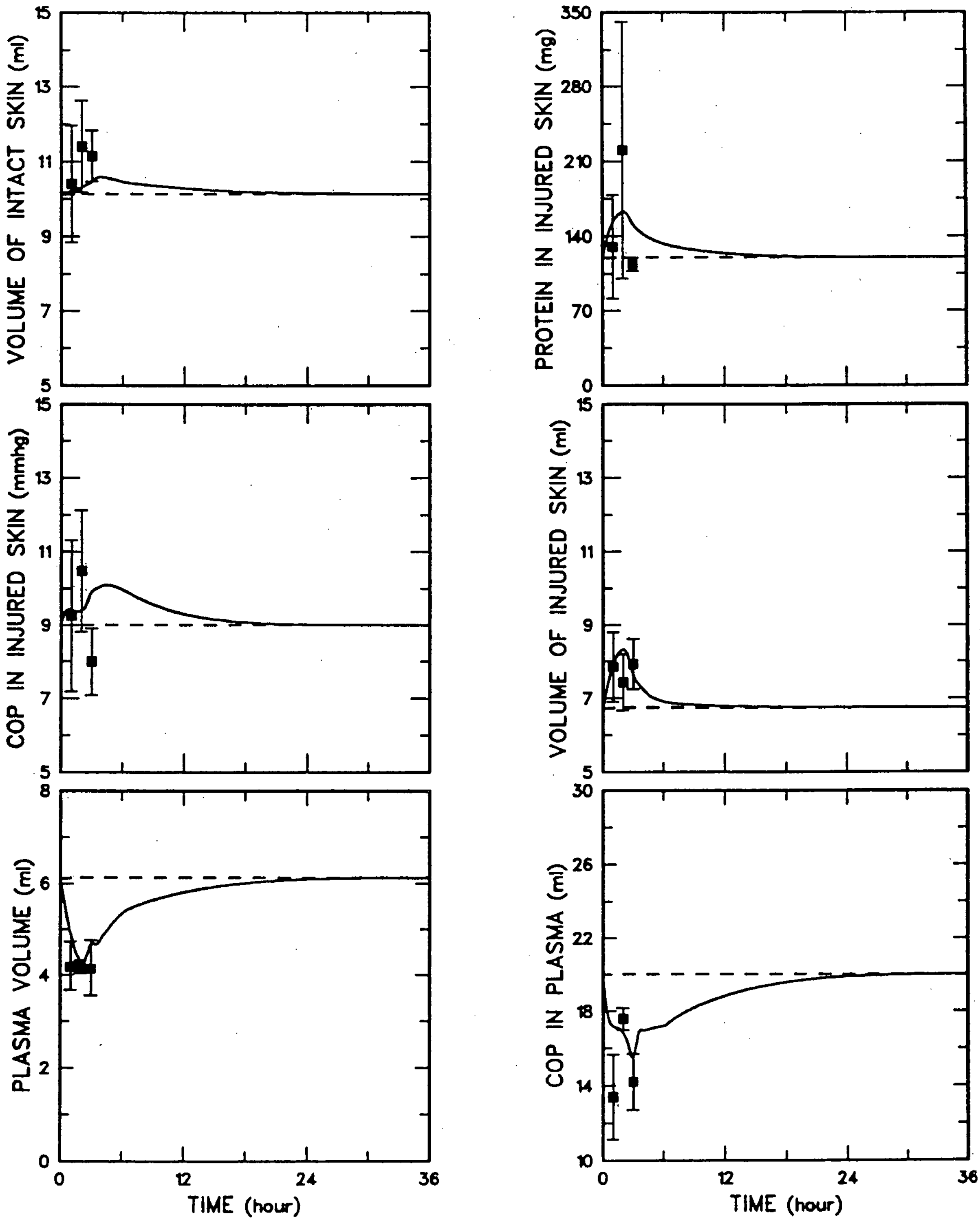

Figure 6.23 Steady State Result for 40% Burn (A=4.0, B=10.0, C=-0.95, D=0.0, Upper Curve for P_b, Arterial and Venous Capillary Pressure Return to Normal After Six Hours)

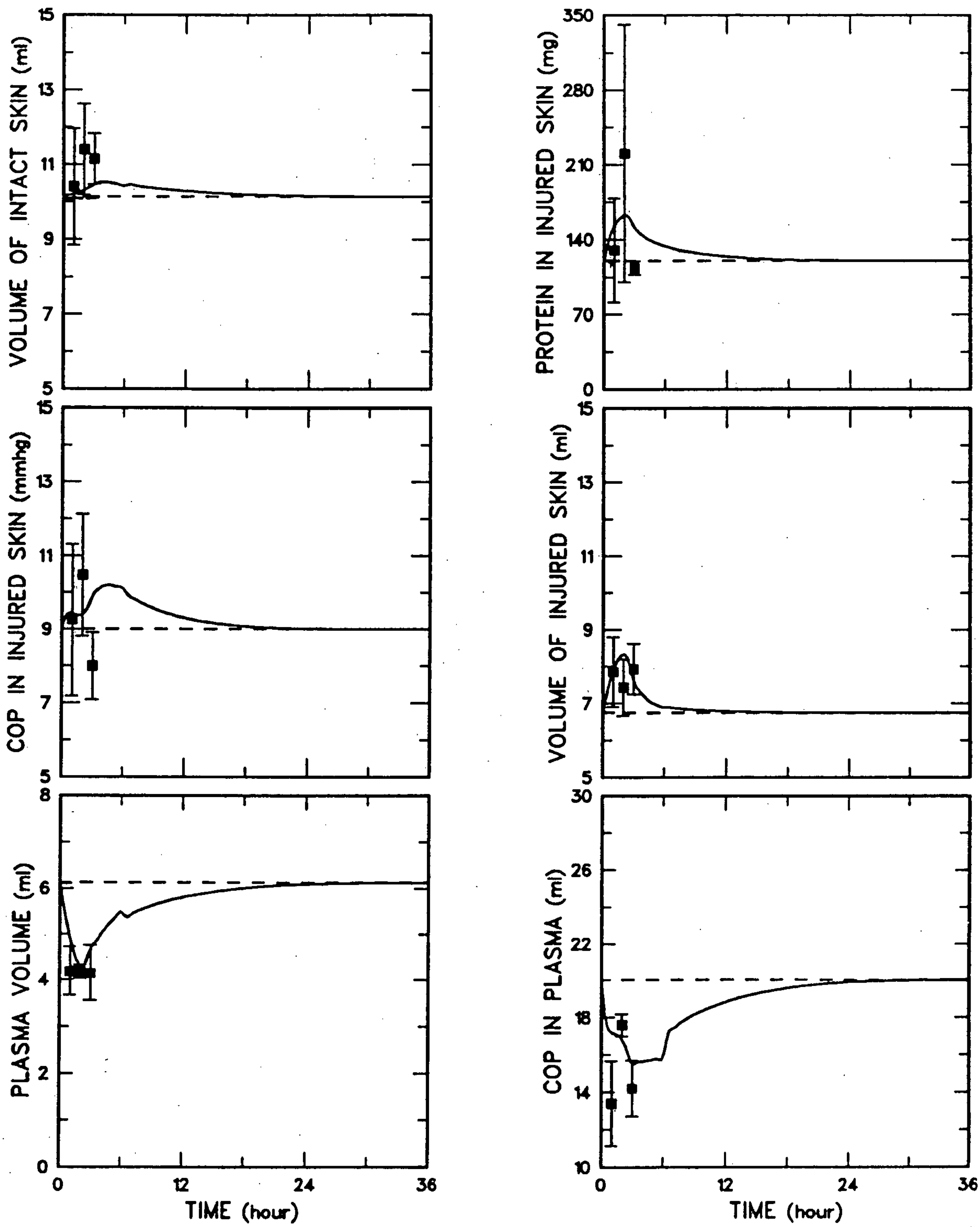

Figure 6.24 Steady State Result for 40% Burn (A=4.0, B=10.0, C=-0.95, D=0.0, Upper Curve for P_b, Arterial and Venous Capillary Pressure Return to Normal After Nine Hours)

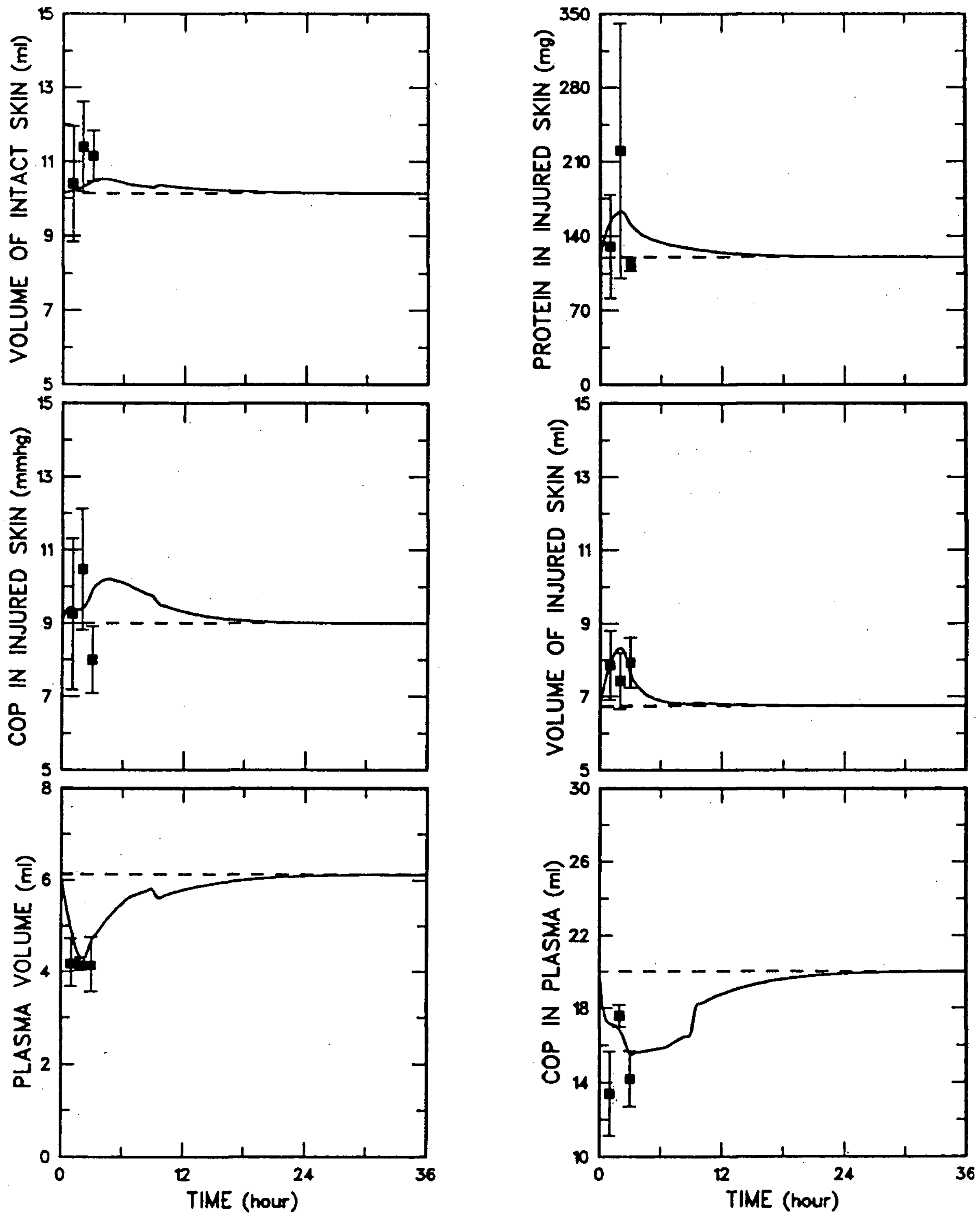

these figures, the dashed lines indicate the normal values for each parameter.

In burn experiments such as those by Lund and Reed [45], rats subjected to a 40% injury are not expected to survive beyond 4-6 hours without fluid resuscitation. In the simulations shown in Figures 6.22 - 6.24, since no resuscitation is provided, it is recognized that the longer-term results are not only very speculative but also highly unrealistic. Nonetheless, these longer-term transients can be used to better understand the workings of the model. For example, perhaps the most interesting feature of these figures when compared to the corresponding 10% burn results, is that most of the system variables return to normal in a shorter period, from 12 - 24 hours postburn. These results are consistent with the explanation given earlier for the the 24 - 36 hour recovery times predicted for the 10% burn. In the present case, because the injured skin edema is significantly less, the tissue compliance is able to increase the lymph flow sufficiently to more rapidly relieve the fluid and protein buildup.

6.3.10 IMPLICATIONS OF THE 40% BURN MODEL

Based on the most reasonable fit for the 40% burn summarized in Section 6.3.8, the simulation results obtained for all dependent parameters are listed in Appendix D for a period of 0-6 hours postburn. The transient responses of several of the more important model variables are plotted in Figures 6.25-6.32. Only the short-term behaviour of rats subjected to 40% burns is discussed in detail since, without resuscitation, all such animals are known to succumb at longer times.

Figures 6.25 and 6.26 reveal how fluid and plasma proteins, respectively, redistribute themselves amongst the four compartments immediately following a 40% burn injury. The two figures indicate that all of the tissue compartments initially accumulate both fluid and proteins. This behaviour is quite different than for a 10% burn where only the injured skin compartment acts as a sink for both fluid and plasma proteins, while the two intact tissue compartments act as sources to make up for the losses from the plasma compartment. Consequently, in the 40% burn, the plasma volume and protein content are far more depressed than in the 10% case. However, the fluid and protein accumulation in the injured skin is still much more prevalent than in the intact tissues. Also, as was the case for the 10% burn, the changes in muscle and intact skin occur in parallel. Thus, only the behaviour of one of these intact tissue compartments, the noninjured skin, will be examined in detail.

Figure 6.25 The Changes of Compartmental Fluid Volumes Following a 40% Burn

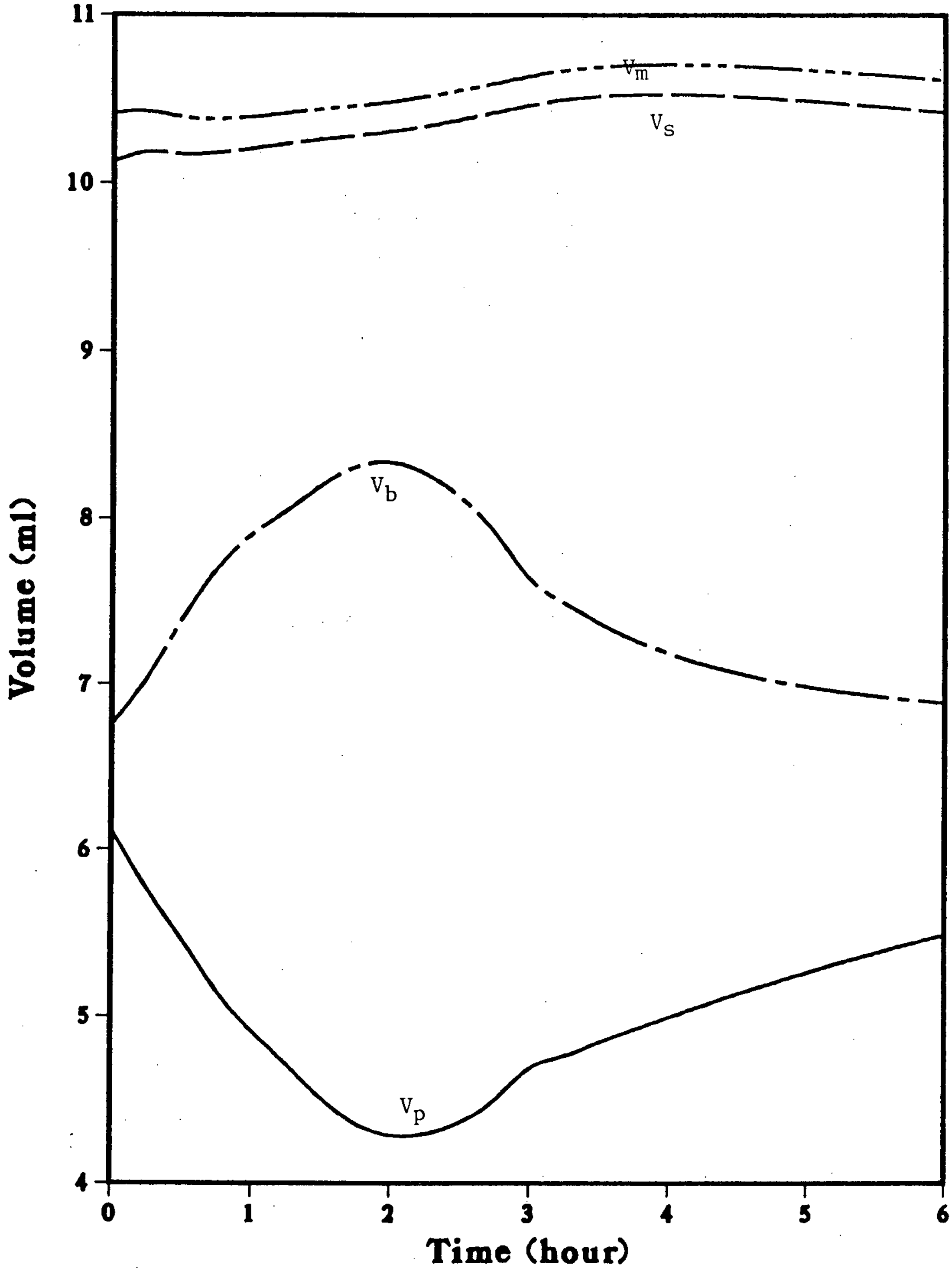

Figure 6.26 The Changes of Compartmental protein Contents Following a 40% Burn

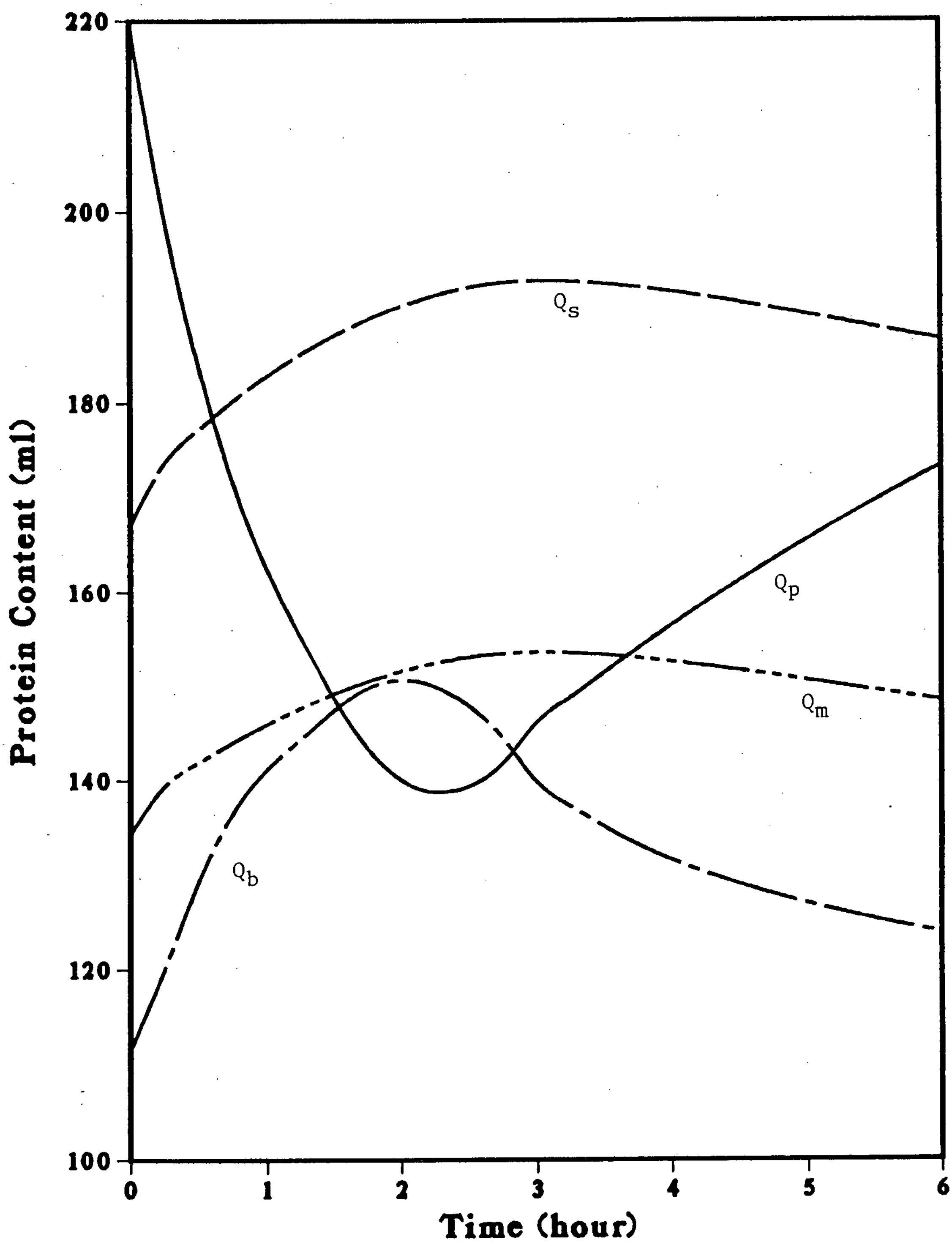

Figure 6.27 The Changes of Fluid Flow Rates in Intact Skin Following a 40% Burn

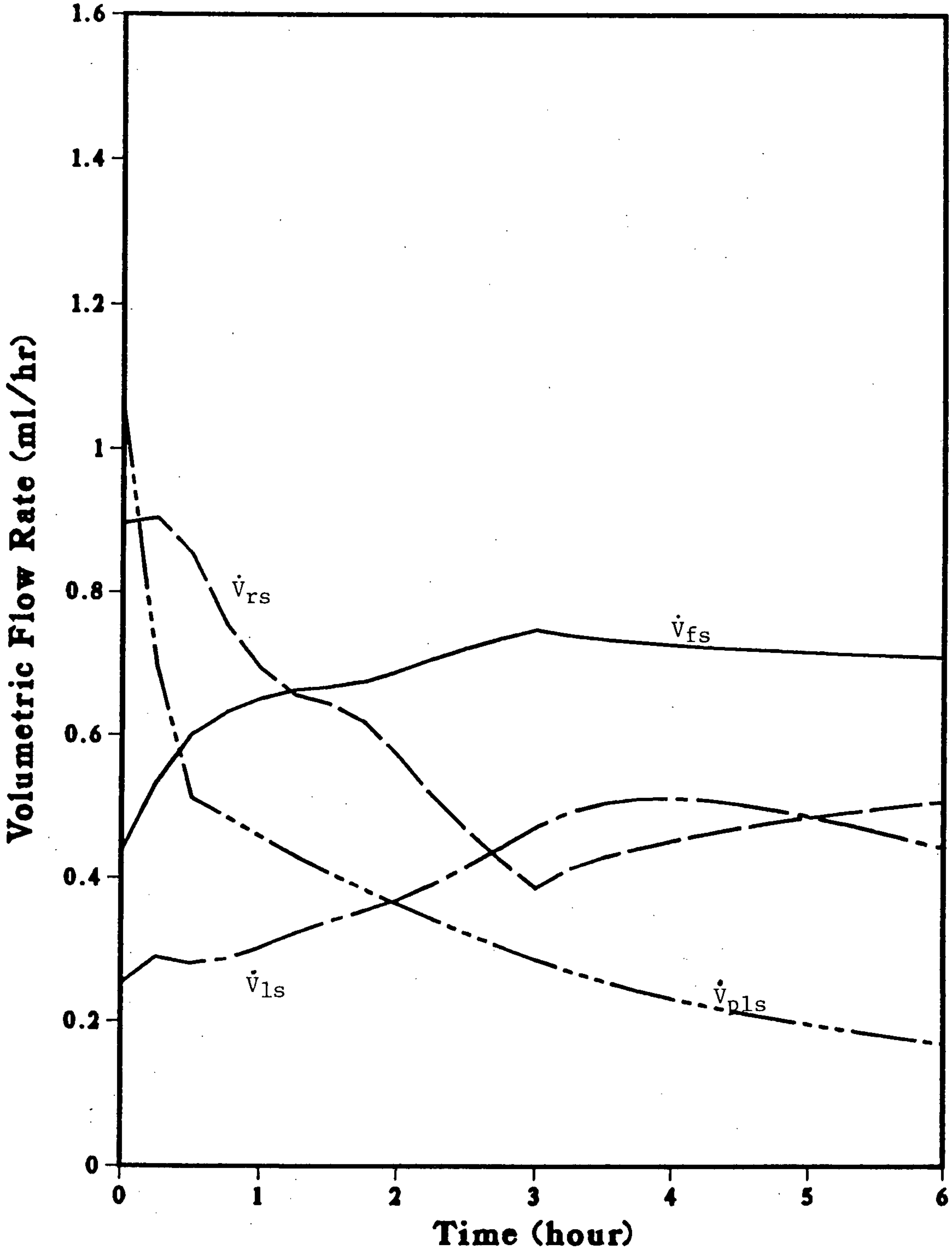

Figure 6.28 The Changes of Albumin Transport Rates in Intact Skin Following a 40% Burn

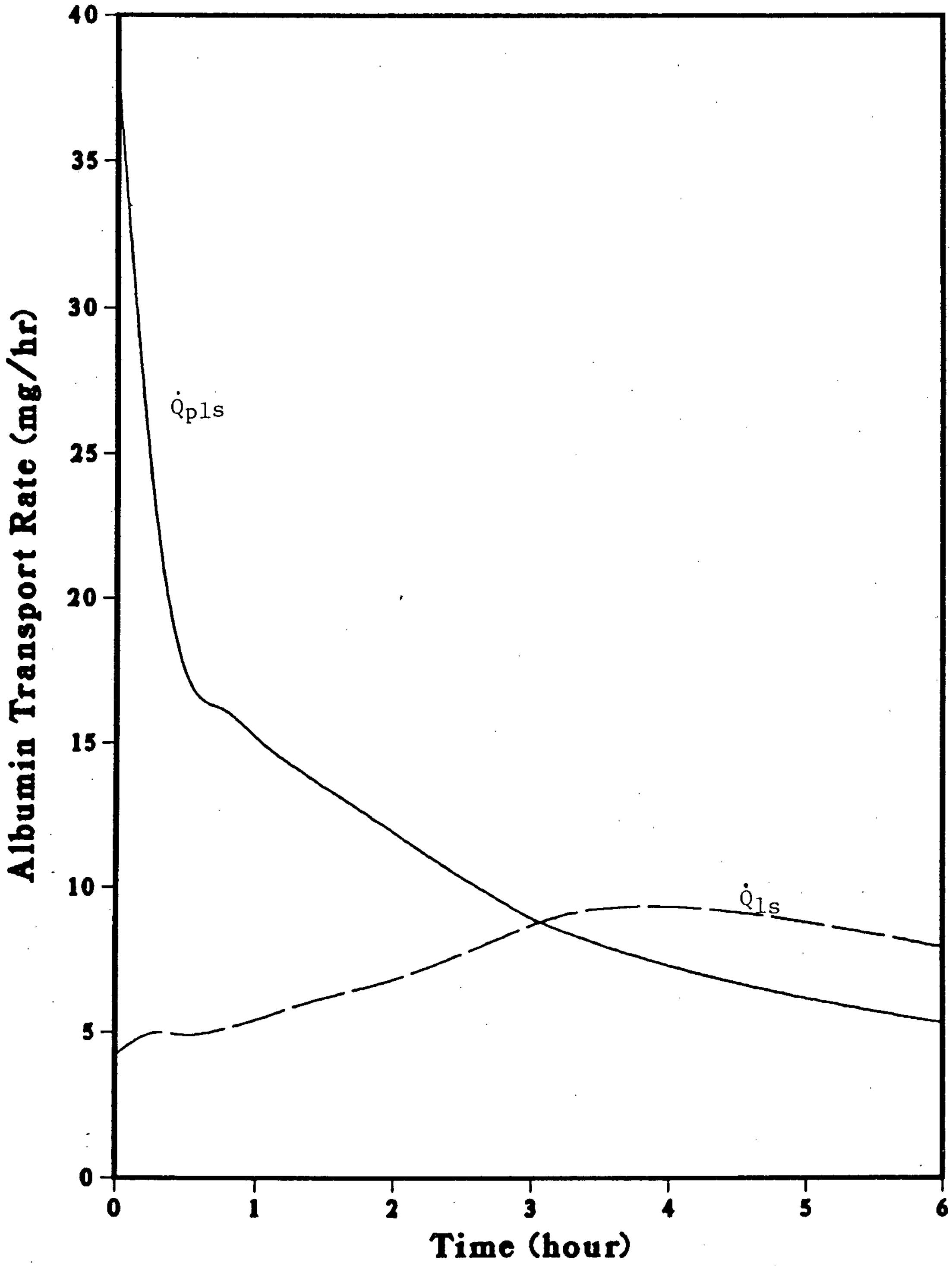

Figure 6.29 The Changes of Capillary and Intact Skin Pressures Following a 40% Burn

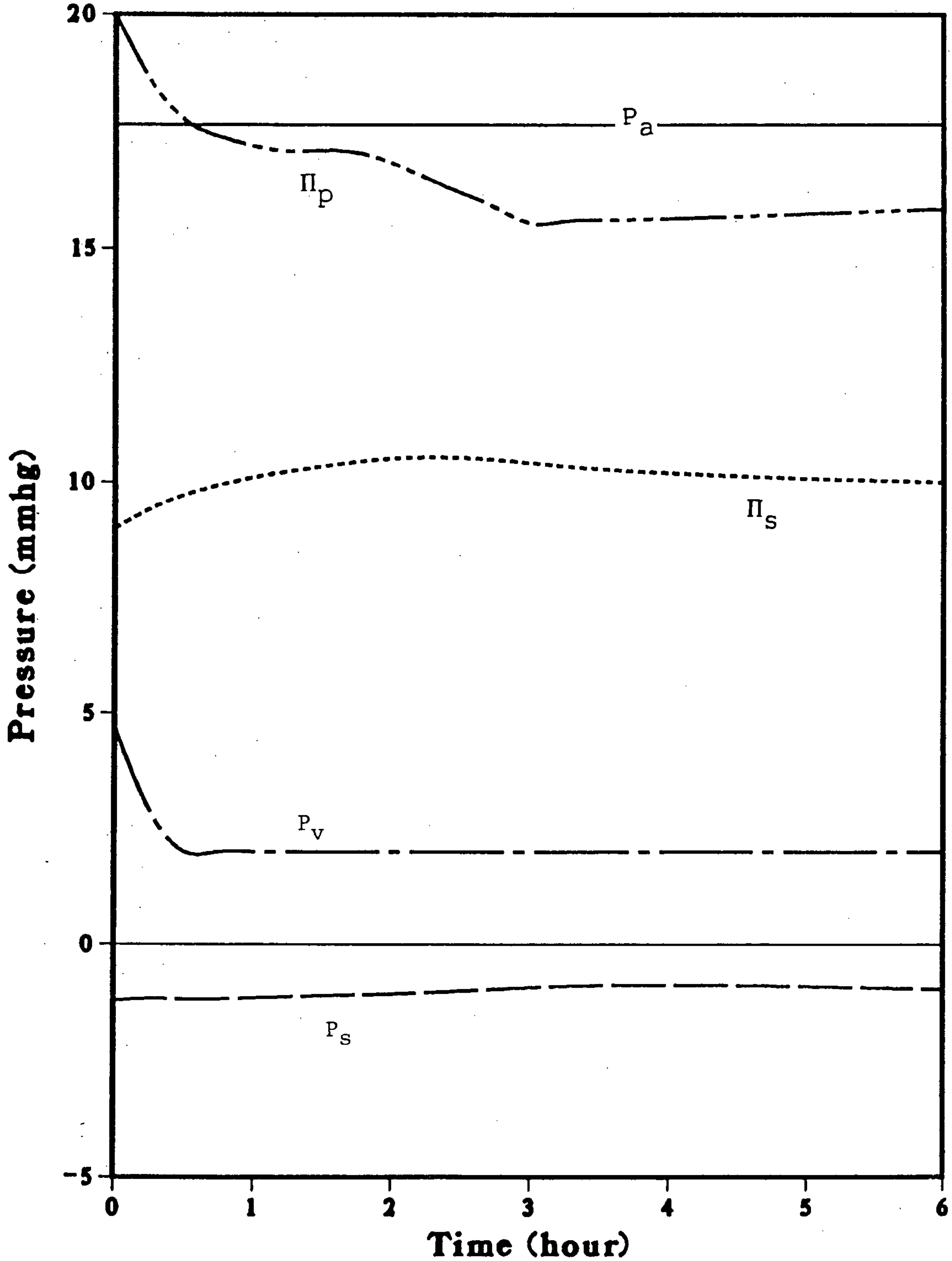

Figure 6.30 The Changes of Fluid Flow Rates in Injured Skin Following a 40% Burn

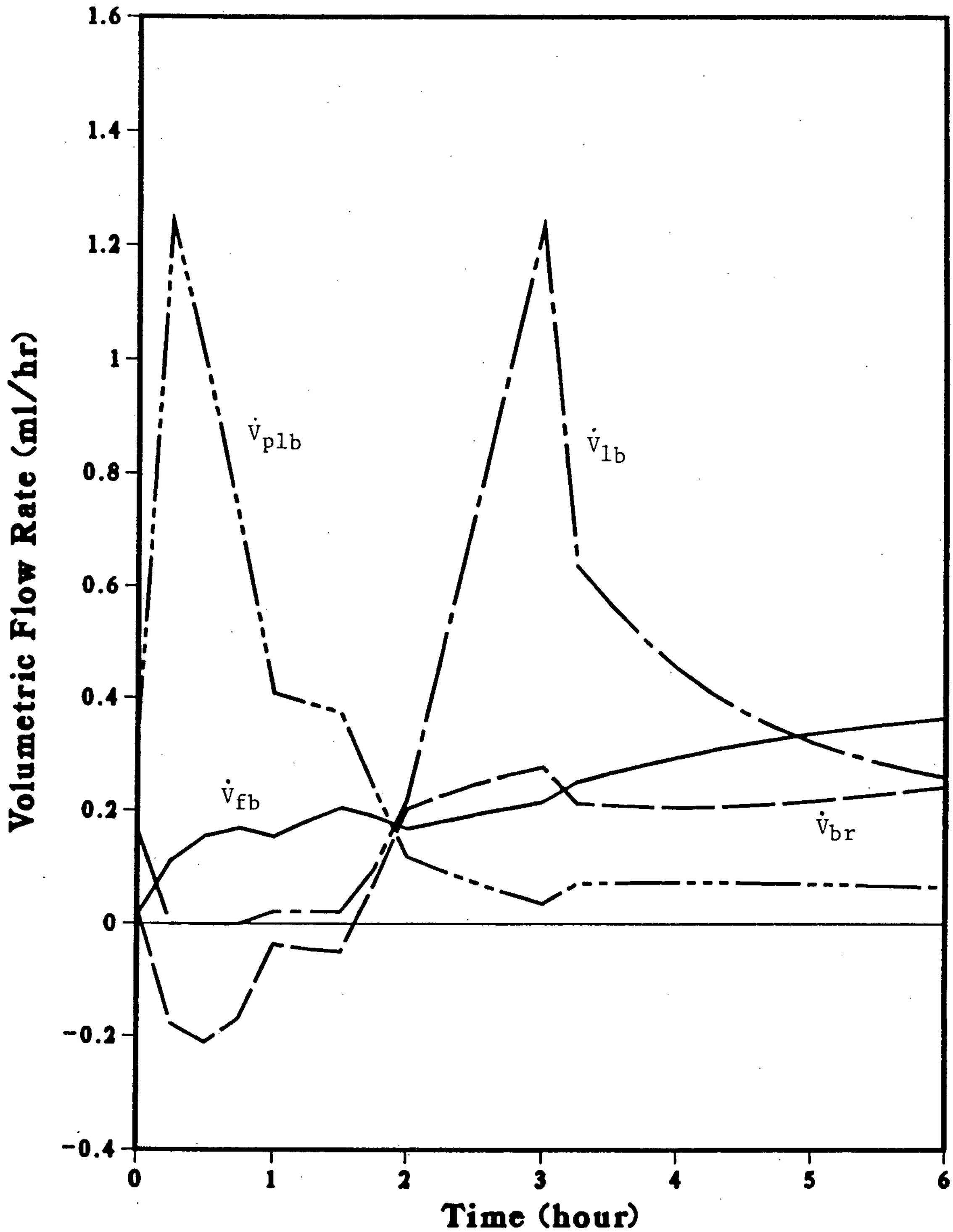

Figure 6.31 The Changes of Albumin Transport Rates in Injured Skin Following a 40% Burn

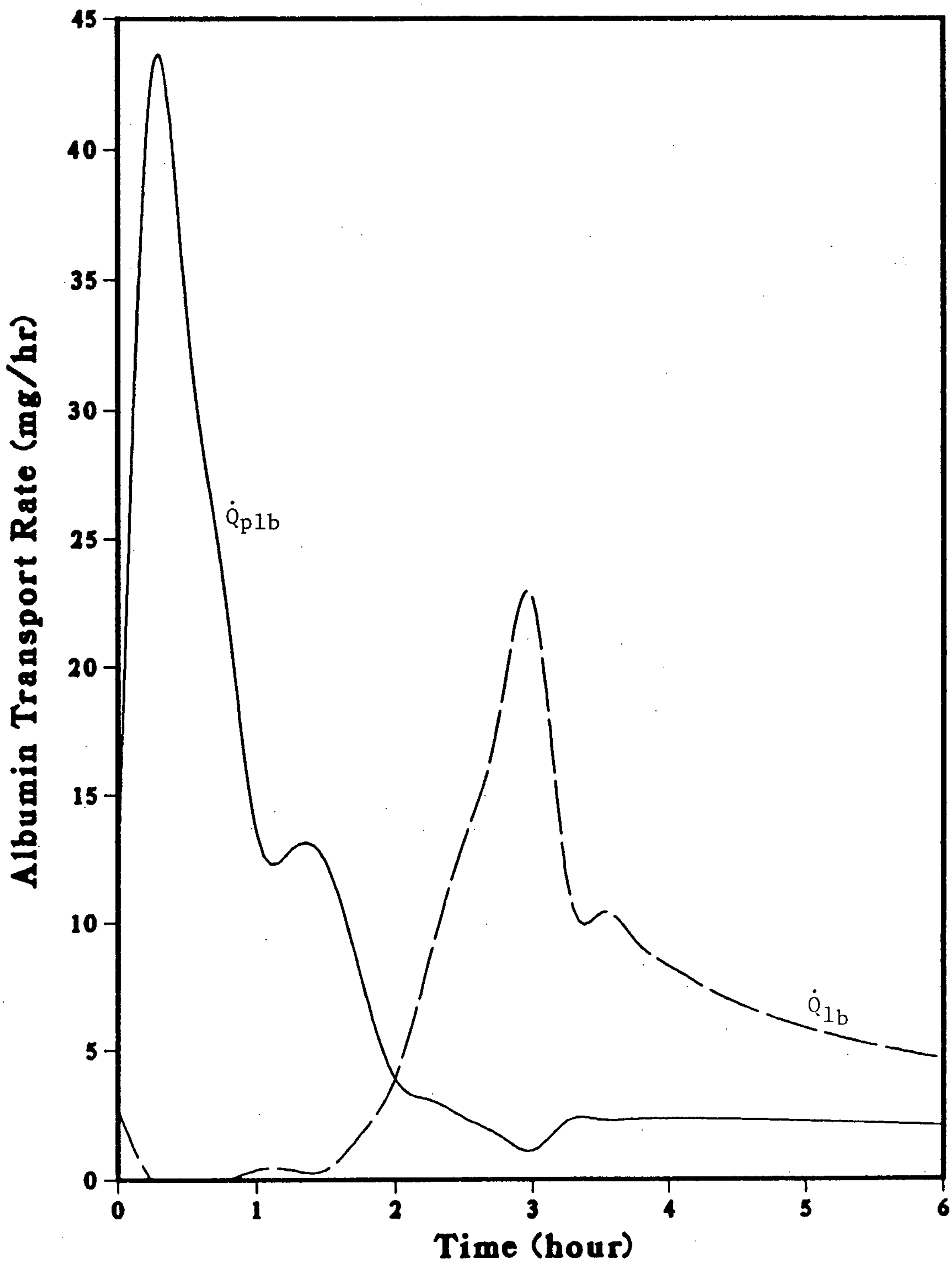

Figure 6.32 The Changes of Capillary and Injured Skin Pressures Following a 40% Burn

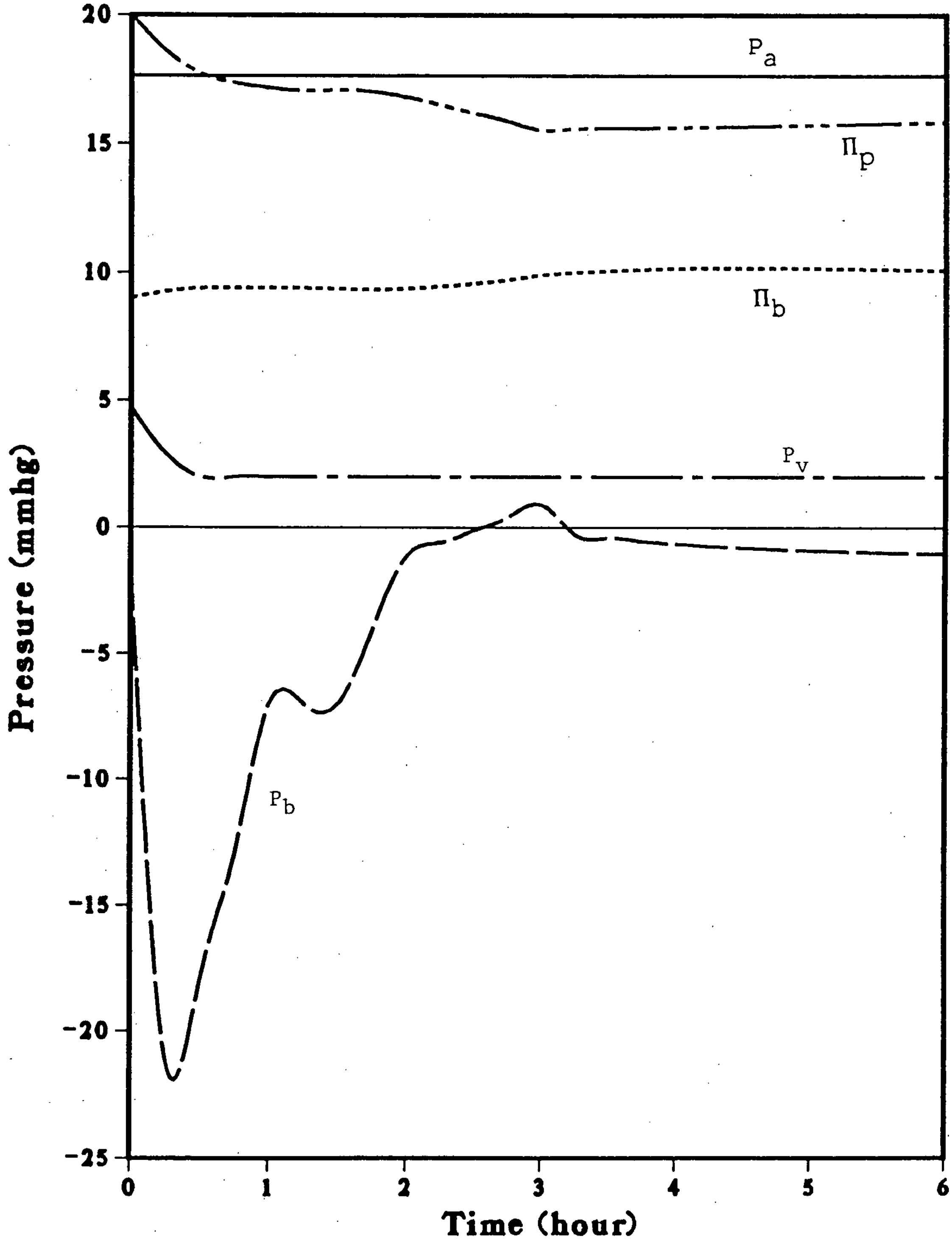

Figure 6.27 and 6.28 portray the time-dependent changes in the intact skin fluid and protein fluxes, respectively, which occur after the initiation of a 40% burn. Figure 6.29 shows the behaviour of the capillary and intact skin hydrostatic and colloid osmotic pressures during the same period. The initial changes to the intact skin are due to the large increase of the plasma leak coefficient, K_{pls}, which is 11 times its normal value at t=0. As a consequence of this increase, both the fluid and protein fluxes associated with the plasma leak rise sharply. The increased protein influx raises the protein content of the intact skin. However, the plasma leak fluid flux is tempered to some extent by an initial drop in the filtration rate due to the step decline in P_a. Partly because of the latter effect and partly because the protein concentration in plasma is much higher than that of any tissue, C_s and Π_s also begin to rise. Similar changes occur in muscle (where K_{plm} is also raised by a factor of 11) and in injured skin (where K_{plb} increases 5 times). Consequently, the plasma loses significant amounts of fluid and proteins (the latter more quickly than the former) and both C_p and Π_p decline. The rapid loss of plasma fluid also causes a precipitous fall in P_v.

Largely because of the behaviour of P_v, the plasma leak fluid and protein fluxes in intact skin decrease rapidly for the first 30 minutes. After this time, since P_v is not allowed to descend below 2 mmHg (the large vein pressure), the plasma leak fluxes fall off more slowly due to the exponential decrease in K_{pls}. Simultaneously, the filtration rate rises from an initially depressed value and the reabsorption rate, after a short initial increase, begins to fall. Both of these changes can be attributed to a decrease in the colloid osmotic pressure difference, $\Pi_p - \Pi_s$. The initial rise in $\dot{V}_{rs}$ is associated with the initial rapid fall in P_v. Over the first half hour, because $\dot{V}_{pls}$ falls more rapidly than the changes in $\dot{V}_{fs}$ and $\dot{V}_{rs}$ can compensate for, the intact skin fluid volume actually goes through a maximum and then decreases slightly. However, after 30 minutes, when $\dot{V}_{pls}$ decreases at a slower rate, the rise in $\dot{V}_{fs}$ and the fall in $\dot{V}_{rs}$ begin to dominate, and the volume of the tissue begins to increase once again.

As the fluid content of the intact tissue compartment becomes large, the interstitial pressure P_s begins to rise causing a corresponding increase in the lymph flow fluid and protein fluxes. Similar lymph flow changes in the other two tissues causes a restoration of proteins in the plasma compartment which, after about 3 hours has elapsed postburn, begins to raise its concentration and consequently its colloid osmotic pressure. It is clear from Figure 6.26, that the protein return flow from the injured skin compartment is primarily responsible for this phenomenon. Once Π_p begins to increase, $\dot{V}_{fs}$ declines and $\dot{V}_{rs}$ rises and, since both changes reduce fluid input to the intact tissue, the compartmental volume begins to fall. Similarly, because the protein outflux due to the lymph flow overwhelms the protein influx due to the plasma leak at just over 3 hours, the compartmental protein content also begins to decline. If the intact skin transients were obtained for a longer period of time, the latter changes would eventually return the tissue to its normal conditions.

Figures 6.30, 6.31 and 6.32 show the volumetric flow rates, albumin transport rates and hydrostatic and colloid osmotic pressures, respectively, associated with the injured tissue compartment following a 40% burn. The explanation for the events which take place after this more extensive injury is very similar to that already described in detail for the 10% burn (see Section 6.2.8). In essence, the combination of the augmented plasma leak coefficient and the initially lowered tissue hydrostatic pressure increases the plasma leak and filtration rates, reverses the reabsorption rate and shuts down the returning lymph flow. Because there are essentially only inflows of fluid and proteins during the first two hours postburn, the fluid volume and protein content of the injured skin build up much more rapidly than either of the two intact tissues, accounting for the major losses from the plasma. However, once the reduced tissue pressure is relieved and the alterations in the transport coefficients decay, the plasma leak falls, reabsorption again becomes positive, lymph flow rises steadily (because of the increase in the tissue volume) and the injured tissue begins to return to normal.

The major differences in the behaviour of the injured skin after a 40% burn as compared to its responses to a 10% burn are the following:

1. In order to adjust the protein concentration in the injured tissue to suit the experimental data, the initial filtration and reabsorption coefficients, K_{fb} and K_{rb}, were depressed even more strongly in the present case. As a consequence, the filtration and reabsorption rates were affected less by the very low tissue pressures which occurred over the first 2 hours postburn and these two mechanisms therefore played a much less important role in potential edema formation.
2. Primarily because the magnitude of the plasma leak coefficient change was much smaller than in the 10% case, the maximum percentage increase in the injured skin volume and protein content was considerably less than before.
3. Much larger changes in the plasma volume and protein content occurred over the first 3 hours postburn. These responses were primarily due to the fact that the injured skin compartment is 4 times larger in the present case and hence, is able to absorb greater

quantities of both fluid and protein. The losses from the plasma compartment were aggravated further because, during the first few hours of the simulation, there was a net transfer of both materials to the two intact tissue compartments as well as to the injured tissue compartment. These large decreases in plasma volume and protein concentration produced large changes in the plasma hydrostatic and colloid osmotic pressures, both in directions which helped restore the microvascular exchange system more quickly to normal.

4. For the various reasons described above, the injured skin does not become as edematous as in the 10% burn case. As a consequence, the fluid volume in this compartment is always sufficiently low that the lymph flow can react through tissue compliance to quickly relieve the accumulation of fluid. Thus, as was discussed in Section 6.3.9, the entire system takes less time to return to normal than in the 10% burn case.

Chapter 7

CONCLUSIONS

Based on a statistical fitting of the model simulations to the experimental data on thermally injured rats by Lund and Reed [45], the model predictions can be summarized as follows for 10% and 40% burns, respectively.

1. For the 10% burn, the two most important perturbations to the system are an increase in the plasma leak coefficient and a reduction in the tissue pressure of the injured skin compartment. By changing only these two parameters, the model predicts reasonable short-term and long-term transient results compared to the available experimental data. A decrease in the injured skin filtration and reabsorption coefficients (attributed to a decrease in the tissue perfusion rate) allows for an adjustment of the protein concentration but otherwise has only a moderate effect on the results. The other parameters investigated such as the the arterial capillary pressure and the lymph flow in the burned tissue, do not appear to have an important influence on the simulations. All the changes and predictions made in Phase One to Phase Four of the 10% burn simulation are in reasonable agreement with the experimental data presented in Tables 3.1, 3.2 and 3.3. The best results from Phase Two, Three and Four not only

produce very good fits to the experimental data of Lund and Reed [45], but also yield the correct trends as compared to the measurements of other investigators compiled in Table 3.3.

The simulation results reveal that following a 10% burn, the large negative tissue pressure causes a reversal in reabsorption and a zero lymph flow during first few hours postburn. Because of this lack of drainage and also because of a very large increase in plasma leakage during this period, there is an initial massive influx of fluid (causing edema) and proteins to the injured tissue. Due to compliance considerations, the tissue edema tends to limit the longer-term lymph flow. As a consequence, it takes a relatively long time (24-36 hours) to relieve the fluid buildup and restore the system to normal.

2. For the 40% burn, the experimental results indicate that the system is more complex. Hence, to adequately describe its behaviour, more changes had to be made to the model. The four important perturbations required to obtain a reasonable fit of the data were: an increase in K_{plb}, an increase in K_{pls} and K_{plm}, a decrease in K_{fb} and K_{rb} and an alteration in injured tissue hydrostatic pressure. When these four parameters were changed, the model yielded a reasonable fit of the short-term

experimental data of Lund and Reed [45] for a 40% burn. The other parameter changes, including the arterial capillary pressure, the intact tissue filtration and reabsorption coefficients and the lymph flow in all three tissues did not significantly influence the fit. As was the case for 10% burn, the changes made and the results simulated are also in general agreement with the trends indicated by other investigators and summarized in Tables 3.1 - 3.3.

Compared to the 10% burn, the plasma and intact tissue compartments no longer act as inexhaustable sources of fluid and protein in this case. In fact, the plasma loses material to muscle and intact skin as well as injured skin. As a consequence of the limited volume of the plasma compartment and the large changes it is forced to undergo, there is considerably less accumulation of fluid and protein (on a relative basis) in the injured skin compartment. Because of this lower volume (and its location on the compliance curve), lymph flow more easily alleviates the fluid accumulation leading to a much faster speculated return to normal.

It is recognized that the experimental data with which the simulation results were compared are very sparse and have large associated errors. Thus, the present model for 10% and 40% burns in rats should be considered as being very preliminary. When more experimental information, particularly about the effects of burns on tissue properties, become available, the model can be more extensively tested and fine-tuned. In the meantime, it is believed that the present model provides a more rigorous representation of the microvascular changes following a burn injury than does any simulation model previously reported in the literature.

Chapter 8

RECOMMENDATIONS

1. In order to better quantify the specific perturbations needed for the burn model, verify the model predictions and analyze the pathological changes that occur after burns, the following additional experimental data are required:
   a. more complete and longer-term data on the fluid, albumin content and colloid osmotic pressure in each compartment after thermal injuries,
   b. independent measurements of the changes in transport coefficients which take place after burns,
   c. more accurate measurement of the injured tissue hydrostatic pressure distribution,
   d. measurement of the plasma perfusion rate to each tissue compartment before and after burns, and
   e. determination of the lymph flow changes in each tissue due to burn injuries.
2. The simulation for postburn fluid resuscitation could be easily incorporated into the present model by adding appropriate sink and source terms to each compartment. Experimental information for resuscitation in thermally injured rats is anticipated in the near future (personal communication with R. Reed, 1987).
3. One future development of the model would be to subdivide the injured skin compartment in the present

model into two compartments: a central and an outer burn compartment. The central burn compartment incorporates the area of actual tissue necrosis whose size would depend on the severity of the injury. This compartment would receive no direct perfusion of blood but would communicate with the rest of the system through the outer burn compartment. The latter compartment surrounds the central compartment and consists of less extensively-injured skin which receives some direct perfusion. It is expected that such a model could provide a more realistic representation of the true nature of injured tissue.

4. Another potentially fruitful development of model would be to include a description of the small ion transport in all four compartments. There exists hypothetical evidence that large amount of ionic material is released from the damaged cells after thermal injuries [18]. If this is true, the assumption of small ion equilibrium in our model no longer holds and there may be a large osmotic pressure gradients caused by non-equilibrium differences in small ion concentrations between compartments. Inclusion of ionic transport in the present model requires four additional mass balances (one for each compartment) for each ionic species.
5. Since cellular water makes up a significant fraction of rat skin, another possible extension to the model would be to include a cellular subcompartment in the injured

and intact skin compartments and allow for fluid, protein and small ion exchange between this subcompartment and the interstitium.

NOMENCLATURE

A	constant in Equations 6.1 and 6.4
B	constant in Equations 6.2, 6.3, 6.5 and 6.6
BSA	fractional burn area
C	constant in Equations 6.7 and 6.8
C	concentration of albumin (mg/ml)
CA	available concentration of albumin (mg/ml)
COP	colloid osmotic pressure (mmHg)
CVP	central venous pressure (mmHg)
D	constant in Equations 6.9, 6.10, 6.11 and 6.12
F^n	function of
K	transport coefficient (ml/mmHg·h)
MAP	main arterial pressure (mmHg)
P	hydrostatic pressure (mmHg)
PS	permeability times surface area (ml/h)
Q	albumin content (mg)
$\dot{Q}$	albumin transport rate (mg/h)
R	fractional pressure drop of the blood vessel
SL	lymph flow sensitivity (ml/mmHg·h)
SS	sum-of-squares of differences between predicted and normalized experimental results
V	volume
$\dot{V}$	volumetric flow rate of fluid (ml/hr)
VE	volume exclusion (ml)
α	time constant in Equations 6.1 to 6.12 (h^{-1})
Π	colloid osmotic pressure (mmHg)
σ	protein reflection coefficient

SUBSCRIPTS

a	arterial capillary
aa	artery
b	injured skin
d	diffusive
e	excluded volume
f	filtration
i	interstitium
l	lymph
m	muscle
o	normal steady-state value
p	plasma
pl	plasma leak
r	reabsorption
s	intact skin
v	venous capillary
vv	large vein

REFERENCES

1. Davies, J.W.L., Physiological Responses to Burning Injury, Academic Press, London (1982).

2. Harvey, J.S., Watkin, G.M. & Sherman, R.T., "Emergent Burn Care", Southern Medical Journal 77(2): 204-214, 1984.

3. Robinson, D.W., "The Care of Burns: Early History to Present", The Journal of the Arkansas Medical Society 80(11): 517-525, 1984.

4. Antz, C.P., Moncrief, J.A. & Pruitt B.A., Burns: a Term Approach, W.B. Saunders Company, Philadelphia (1979).

5. Arturson, G., Groth, T., Hedlund, A. & Zaar, B., "Potential Use of Computer Simulation in Treatment of Burns with Special Regard to Edema Formation", Scandinavian Journal of Plastic Reconstruction Surgery 18: 39-48, 1984.

6. Bert, J.L., Bowen, B.D. & Reed, R.K., "Microvascular Exchange and Interstitial Volume Regulation in the Rat: Model Validation", Submitted to American Journal of Physiology, 1987.

7. Folkow, B. & Neil, E., Circulation, Oxford University Press (1971).

8. Rushmer, R., Cardiovascular Dynamics, W.B. Saunders Company (1970).

9. Guyton, A.C., Function of the Human Body, Fourth Edition, W.B. Saunders Company, Philadelphia (1974).

10. Guyton, A.C., Human Physiology and Mechanisms of Disease, Third Edition, W.B. Saunders Company, Toronto (1982).

11. Bert, J.L. & Pinder, K.L., "Pulmonary Microvascular Exchange: An Analog Computer Simulation", Microvascular Research 27: 51-70, 1984.

12. Bert, J.L., Mathieson, J.M. & Pearce R.H., "The Exclusion of Human Serum Albumin by Human Dermal Collagenous Fibers and Within Human Dermis", Biochemical Jounal 201: 395-403, 1982.

13. Staub, N.C. & Taylor A.E., Edema, Raven Press, New York (1984).

14. Copley, A.L., Hemorheology, Pergamon Press, New York (1968).

15. Vander, A., Sherman, J. & Luciano, S., Human Physiology, McGraw-Hill (1970).

16. Hardaway, R.M., Capillary Perfusion in Health and Disease, Futura Publishing Company, Inc., New York (1981).

17. Netsky, M.G. & Leiter, S.S., "Capillary Permeability to Horse Proteins in Burn Shock", American Journal of Phsiology 140: 1-5, 1943.

18. Arturson, G. & Jonsson C.E., "Transcapillary Transport after Thermal Injury", Scandinavian Journal of Plastic Reconstruction Surgery 13: 29-38, 1979.

19. Cope, O. & Moore, F.D., "A Study of Capillary Permeability in Experimental Burns and Burn Shock Using Radioactive Dyes in Blood and Lymph", Journal of Clinical Investigation 23: 241-257, 1944.

20. Carvajal, H.F., Brouhard B.H. & Linares, H.A., "Effect of Antihistamin-Antiserotonin and Ganglionic Blocking Agents Upon Increased Capillary Permeability Following Burn Trauma", The Jounal of Trauma 15(11): 969-975, 1975.

21. Brouhard, B.H., Carvajal, H.F. & Linares, H.A., "Burn Edema and Protein Leakage in the Rat", Microvascular Research 15: 221-228, 1978.

22. Brouhard, B.H., Carvajal, H.F. & Miller, T.H., "Effect of Nicotinic Acid on Vascular Permeability after Thermal Trauma in the Rat", The Journal of Trauma 18(11): 774-776, 1978.

23. Carvajal, H.F., Lineares, H.A. & Brouhard B.H., "Relationship of Burn Size to Vascular Permeability Changes in Rats", Surgery, Gynecology & Obstetrics 149: 193-202, 1979.

24. Lund, T. & Reed, R.K., "Microvascular Fluid Exchange Following Thermal Skin Injury in the Rat: Changes in Extravascular Colloid Osmotic Pressure, Albumin Mass, and Water Content", Circulatory Shock 20: 91-104, 1986.

25. Arturson, G. & Mellander S., "Acute Changes in Capillary Filtration and Diffusion in Experimental Burn Injury", Acta Physiology Scandinavian 62: 457-463, 1964.

26. Pruitt, B.A. & Colonel, F.A.C.S., "Advances in Fluid Therapy and the Early Care of the Burn Patient", World Journal of Surgery 2(2): 139-148, 1978.

27. Demling, R.H., "Burns", in Staub, N.C. & Taylor, A.E. (eds): "Edema", pp 579-599, Raven Press, New York (1984).

28. Wolfe, R.R. & Miller, H.I., "Cardiovascular and Metabolic Responses During Burn Shock in the Guinea Pig", Americal Journal of Physiology 231(3): 892-897, 1976.

29. Ferguson, J.L., Merrill, G.F., Miller, H.I. & Spitzer, J.J., "Regional Blood Flow Redistribution During Early Burn Shock in the Guinea Pig", Circulatory Shock 4: 317-326, 1977.

30. Delming, R.H., Will, J.A. & Belzer, F.O., "Effect of Major Thermal Injury on the Pulmonary Microcirculation", Surgery 83(6): 746-751, 1978.

31. Ferguson, J.L., Hikawyi-Yevich, I. & Miller, H.I., "Body Fluid Compartment Changes During Burn Shock in the Guinea Pig", Circulatory Shock 7: 457-466, 1980.

32. Harms, B.A., Bodai, B.I., Kramer, G.C. & Delming, R.H., "Microvascular Fluid and Protein Flux in Pulmonary and Systemic Circulations after Thermal Injury", Microvascular Research 14: 11-25, 1977.

33. Lund, T. & Reed, R.K., "Acute Hemodynamic Effects of Thermal Skin Injury in the Rat", Circulatory Shock 20: 105-114, 1986.

34. Lund, T. & Reed, R.K., "A 'New' Mechanism for Edema Generation: Strongly Negative Interstitial Fluid Pressure Causes Rapid Fluid Flow into Thermally Injured Skin", will appear in Acta Physiologica Scandinavica, 1987.

35. Arturson, G. & Soeda, S., "Changes in Transcapillary Leakage During Healing of Experimental Burns", Acta Chiropody Scandinavian 133: 609-614, 1967.

36. Leape. L.L., "Early Burn Wound Changes", Journal of Pediatric Surgery 3(2): 292-299, 1968.

37. Leape, L.L., "Initial Changes in Burns; Tissue Changes in Burned and Unburned Skin of Rhesus Monkeys", The Journal of Trauma 10: 488-492, 1970.

38. Green, K.L., "Quantitative Studies on the Accumulation of Serum Albumin and Erythrocytes in Mouse Paw Edema Induced by Bradykinin or Thermal Injury", British Journal of experimental Pathology 59: 38-47, 1978.

39. Brouhard, B.H., Carvajal, H.F. & Linares, H.A., "Burn Edema and Protein Leakage in the Rat", Microvascular Research 15: 221-228, 1978.

40. Carvajal, H.F., Linares, H.A. & Brouhard B.H., "Relationship of Burn Size to Vascular Permeability Changes in Rats", Surgery, Gynecology & Obstetrics 149: 193-202, 1979.

41. Delming, R.H., Mazess, R.B. & Wolberg, W., "The Effect of Immediate and Delayed Cold Immersion on Burn Edema Formation and Resorption", The Journal of Trauma 19(1): 56-60, 1979.

42. Delming, R.H., Trunkey, D. & Way, L., "Burns and Other Thermal Injuries", in Way, L. (ed): Current Surgical Diagnosis and Treatment, p 233, Lange Medical Publications, Los Altos, California (1983).

43. Demling, R.H., Kramer, G. & Harms, B., "Role of Thermal Injury-Induced Hypoproteinemia on Fluid Flux and Protein Permeability in Burned and Nonburned Tissue", Surgery 95(2): 136-144, 1984.

44. Arturson, G. & Jakobsson, O.P., "Edema Measurements in a Standard Burn Model", Burns 12: 1-7, 1985.

45. Lund, T. & Reed, R.K., "Microvascular Fluid Exchange Following Thermal Skin Injury in the Rat: Changes in Extravascular Colloid Osmotic Pressure, Albumin Mass, and Water Content", Circulatory Shock 20: 91-104, 1986.

46. Gabel, J.C. & Drake, R.E., "Plasma Proteins and Protein Osmotic Pressure", in Staub, N.C. & Taylor, A.E. (ed): Edema, pp 371-382, Raven Press, New York (1984).

47. Wielderhielm, C.A., "Dynamics of Capillary Fluid Exchange: A Nonlinear Computer Simulation", Microvascular Research 18: 48-82, 1979.

48. Bert, J.L. & Pinder, K.L., "An Anolog Computer Simulation Showing the Effect of Volume Exclusion on Capillary Fluid Exchange", Microvascular Research 24: 94-103, 1982.

49. Bush, J.W., Schneider, A.M., Wachtel, T.L. & Brimm J.E., "A Simulation Analysis of Plasma Water Dynamics and Treatment in Acute Burn Resuscitation", The Journal of Burn Care 7(2): 86-94, 1986.

50. Reed, R.K. & Wiig, H., "Compliance of the Interstitial Space in Rats: Studies on Hindlimb Skeletal Muscle", Acta Physiology Scandinavian 113: 307-315, 1981.

51. Wiig, H. & Reed, R.K., "Compliance of the Interstitial Space in Rats: Studies on Skin", Acta Physiology Scaninavian 307: 315, 1981.

52. Bowen, B.D., U.B.C., Department of Chemical Engineering' Internal Report, 1986.

53. Reed, R.K. & Wiig, H., "Compliance of the Interstitial Space in Rats: Contribution of Skin and Skeletal Muscle Interstitial Fluid Volume to Changes in Total Extracellular Fluid Volume", Acta Physiology Scandinavian 121: 57-63, 1984.

54. Reed, R.K., "Interstitial Fluid Volume, Colloid Osmotic and Hydrostatic Pressures in Rat Skeletal Muscle: Effect of Venous Stasis and Muscle Activity", Acta Physiology Scandinavian 112: 7-17, 1981.

55. Fadnes, H.O, "Effect of Increased Venous Pressure on the Hydrostatic and Colloid Osmotic Pressure in Subcutaneous Interstitial Fluid in Rats: Edema-Preventing Mechanisms", Scandinavian Journal of Clinical Laboratory Investigation 36: 371-377, 1976.

56. Carnahan, B., Luther, H.A. & Wilkes J.O., Applied Numerical Methods, John Wiley & Sons Inc. (1969).

APPENDIX A:

COMPLIANCE CURVES FOR RAT MUSCLE AND SKIN

1. Table A.1 Compliance Relationship for Skin [6]

V_S(ml)	P_S(mmHg)
5.92	-6.95
8.88	-5.40
11.85	-3.85
14.81	-2.30
16.88	-1.21
17.77	-0.75
18.51	-0.38
19.25	-0.07
19.99	0.19
20.73	0.35
21.47	0.44
22.21	0.50
22.95	0.53
23.69	0.55
26.65	0.60
29.61	0.63
32.58	0.65
51.82	0.69
81.44	0.73
106.62	0.77

2. Table A.2 Compliance Relationship for Muscle [6]

V_m(ml)	P_m(mmHg)
2.60	-6.78
5.21	-4.69
7.81	-2.60
10.41	-0.51
11.06	-0.13
11.71	0.07
12.36	0.18
13.01	0.26
13.66	0.33
14.31	0.38
14.96	0.42
15.62	0.45
16.92	0.49
18.22	0.50
20.82	0.51
26.03	0.54
31.23	0.57
36.44	0.60
46.82	0.65

3. Figure A.1 Compliance Curves for Muscle and Skin of Rats [6]

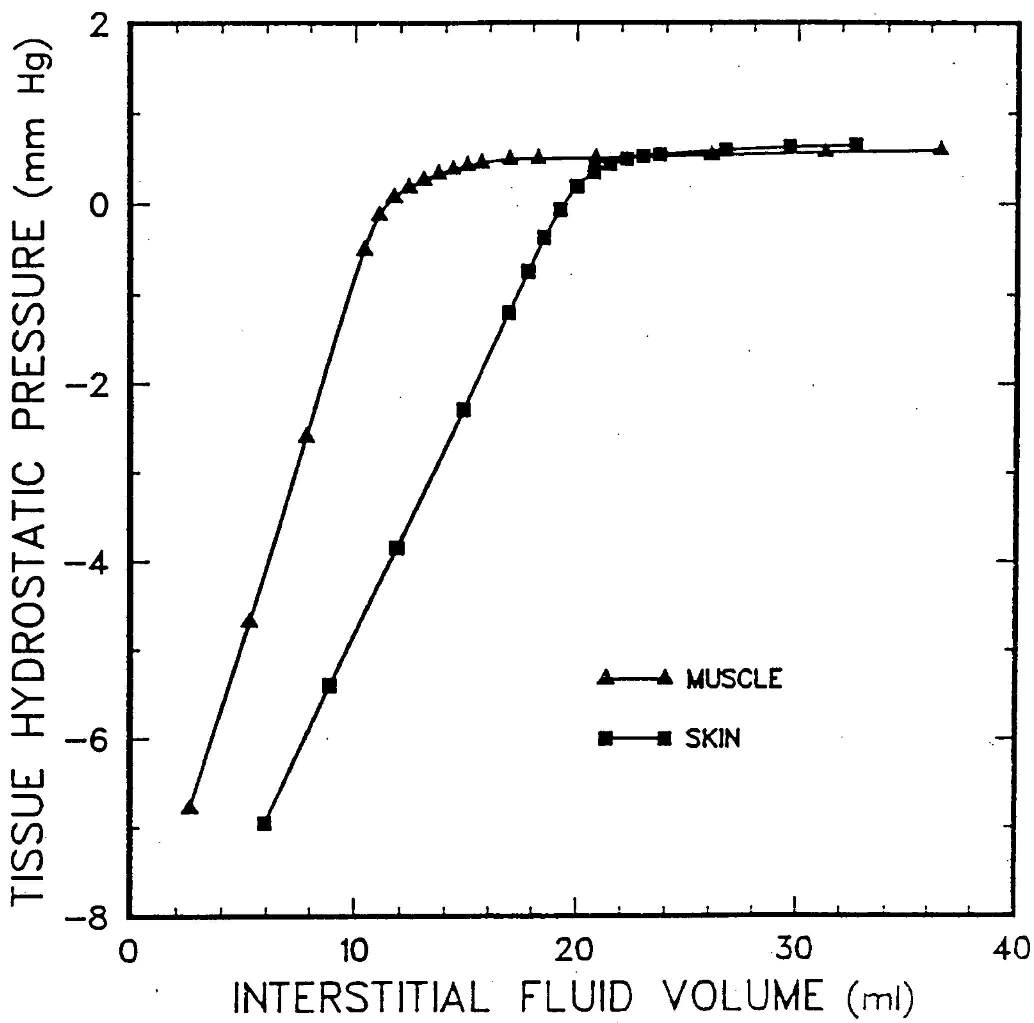

APPENDIX B:

COMPUTER PROGRAM

The computer program used to predict the transient responses of the four compartment microvascular exchange system after various burn perturbations is listed on the following pages. Documentation about the purpose of and procedures used in each routine are presented throughout the program listing in the form of comment statments.

```
C       The main program:
C       This program is used to predict how the protein
C       and fluid redistribute themselves with time following
C       a burn having an area fraction BSA.
C
      IMPLICIT REAL*8(A-H,K,L,O-Z)
      REAL*4 RK1,RK2,RK3,RK4,RK5,RK6,RK7
      INTEGER FLAG
      COMMON/BLKA/PAO,PVO,VES,VEM,VESI
      COMMON/BLKB/VPLO,QPLO,VSO,VSOI,QSO,QSOI,VMO,QMO
      COMMON/BLKC/APL1,APL2,APL3,AS1,AS2,AS3,AS1I,AS2I,AS3I,AM1,AM2,
     1       AM3
      COMMON/BLKL/KFSI,KPLSI,KRSI,LSOI,SLSI,PSOI,PSSI
      COMMON/BLKM/FSI,VPLSI,RSI,LSI,QPLSI,QDSI,QLSI
      COMMON/BLKG/FS,VPLS,RS,LS,QPLS,QDS,QLS
      COMMON/BLKH/FM,VPLM,RM,LM,QPLM,QDM,QLM
      COMMON/BLKI/KFS,KPLS,KRS,LSO,SLS,PSO,PSS
      COMMON/BLKJ/KFM,KPLM,KRM,LMO,SLM,PMO,PSM
      COMMON/BLKK/PA,PV,CPL,PIPL,CS,CAVS,PS,PIS,CM,CAVM,PM,PIM,
     1            CSI,CAVSI,PSI,PISI
      COMMON/BLKZ/DEGREE
      COMMON/BLKS/AA,BB
      COMMON/BLKW/K1,K2,K3,K4,K5,K6,K7
      DIMENSION YOLD(8),YNEW(8),VT(501),VPL(501),VS(501),VM(501),
     1 QPL(501),QS(501),QM(501),T(501),VSI(501),QSI(501)
      DIMENSION SOLN(50,501),SOL(50),DIS(3,6),DIST(6)
      EXTERNAL RHSF
      DATA NV,NP,DT,EPS,EPSR,ALPHA/8,51,0.25D0,1.D-5,1.D-7,.5D0/
      DATA RDLS,RFRS,SLPS/.0D0,.3149D0,1.2651D0/
      DATA RDLM,RFRM,SLPM/.0D0,.4001D0,1.2065D0/
      DATA RDLSI,RFRSI,SLPSI/.0D0,.3149D0,1.2651D0/
      DATA TKFM,TKRM,TKPLM,TSLM,TLMO,TKFS,TKRS,TKPLS,TSLS,TLSO/
     1 0.0634D0,0.1585D0,0.0145D0,1.2065D0,0.2603D0,
     2 0.0927D0,0.2943D0,0.0272D0,1.2651D0,0.422D0/

      TSTART=1.D-1*DT
      TMIN=1.D-4*DT
      TMAX=DT
      NPM=NP-1
C
C       Determination of the initial values of volume, excluded volume
C       protein content in the skin compartments
C
      VSOI=DEGREE*VSO
      VSO=(1.D0-DEGREE)*VSO
      QSOI=DEGREE*QSO
      QSO=(1.D0-DEGREE)*QSO
      VESI=DEGREE*VES
      VES=(1.D0-DEGREE)*VES
C
      CALL SPLINS
      CALL SPLINM
C
C       Estimation of the transport coefficients in each tissue
C       compartment
C
C       1) intact skin compartment
C
      CPLO=QPLO/VPLO
      PIPLO=CPLO*(APL1+CPLO*(APL2+CPLO*APL3))
```

```
      CSO=QSO/VSO
      CAVSO=QSO/(VSO-VES)
      PSO=FCOMPS(VSO/(1.DO-DEGREE))
      PISO=CAVSO*(AS1+CAVSO*(AS2+CAVSO*AS3))
      LSO=(0.025DO*VSO*(CPLO-CAVSO))/(RDLS*CSO+CPLO-CAVSO)
      PSS=0.025DO*VSO-LSO
      VPLSO=LSO*CSO*(1.DO-RDLS)/CPLO
      KPLS=VPLSO/(PVO-PSO)
      KRS=(LSO-VPLSO)/(RFRS*(PAO-PSO-PIPLO+PISO)-(PSO-PVO-PISO+
     1 PIPLO))
      KFS=RFRS*KRS
      SLS=(1-DEGREE)*SLPS
C
C       2) injured skin compartment
C
      CPLOI=QPLO/VPLO
      PIPLO=CPLOI*(APL1+CPLOI*(APL2+CPLOI*APL3))
      CSOI=QSOI/VSOI
      CAVSOI=QSOI/(VSOI-VESI)
      PSOI=FCOMPS(VSOI/DEGREE)
      PISOI=CAVSOI*(AS1I+CAVSOI*(AS2I+CAVSOI*AS3I))
      LSOI=(0.025DO*VSOI*(CPLOI-CAVSOI))/(RDLSI*CSOI+CPLOI-CAVSOI)
      PSSI=0.025DO*VSOI-LSOI
      VPLSOI=LSOI*CSOI*(1.DO-RDLSI)/CPLOI
      KPLSI=VPLSOI/(PVO-PSOI)
      KRSI=(LSOI-VPLSOI)/(RFRSI*(PAO-PSOI-PIPLO+PISOI)-
     1 (PSOI-PVO-PISOI+PIPLO))
      KFSI=RFRSI*KRSI
      SLSI=DEGREE*SLPSI
C
C       3) muscle compartment
C
      CMO=QMO/VMO
      CAVMO=QMO/(VMO-VEM)
      PMO=FCOMPM(VMO)
      PIMO=CAVMO*(AM1+CAVMO*(AM2+CAVMO*AM3))
      LMO=(0.025DO*VMO*(CPLO-CAVMO))/(RDLM*CMO+CPLO-CAVMO)
      PSM=0.025DO*VMO-LMO
      VPLMO=LMO*CMO*(1.DO-RDLM)/CPLO
      KPLM=VPLMO/(PVO-PMO)
      KRM=(LMO-VPLMO)/(RFRM*(PAO-PMO-PIPLO+PIMO)-(PMO-PVO-PIMO+
     1 PIPLO))
      KFM=RFRM*KRM
      SLM=SLPM
C
C       Input the initial values of dependent varaiables for the eight
C       differential equations
C
      YNEW(1)=VPLO
      YNEW(2)=QPLO
      YNEW(3)=VSO
      YNEW(4)=QSO
      YNEW(5)=VMO
      YNEW(6)=QMO
      YNEW(7)=VSOI
      YNEW(8)=QSOI
C
C       Solve the differential equations using
C       Runge-Kutta-Fehlberg method
C
```

```
      DO 30 I=1,NP
      T(I)=(I-1)*DT
C
C      Avoid the discontinuous points
C
      IF (I.EQ.9) T(I)=1.999D0
      IF (I.EQ.10) T(I-1)=2.001D0
      IF (I.EQ.13) T(I)=2.999D0
      IF (I.EQ.14) T(I-1)=3.001D0
      IF(I.EQ.1) GO TO 16

      IM=I-1
      CALL DESOLV(RHSF,NV,T(IM),T(I),YOLD,EPS,TSTART,TMIN,TMAX,
     + YNEW,FLAG)
      IF (FLAG.EQ.0.0) GO TO 80
      GO TO 16
15    CALL ROOT(RHSF,NV,0.D0,YOLD,EPSR,ALPHA,YNEW,FLAG)
      IF(FLAG.EQ.0) GO TO 60
16    CALL AUXS(T(I),YNEW)
      CALL AUXM(T(I),YNEW)
      CALL AUXSI(T(I),YNEW)
C
C      Store the intermediate results
C
      SOLN(1,I)=T(I)
      SOLN(2,I)=CM
      SOLN(3,I)=CAVM
      SOLN(4,I)=PIM
      SOLN(5,I)=PM
      SOLN(6,I)=FM
      SOLN(7,I)=VPLM
      SOLN(8,I)=RM
      SOLN(9,I)=LM
      SOLN(10,I)=QPLM
      SOLN(11,I)=QLM
      SOLN(12,I)=QDM
      SOLN(13,I)=CS
      SOLN(14,I)=CAVS
      SOLN(15,I)=PIS
      SOLN(16,I)=PS
      SOLN(17,I)=FS
      SOLN(18,I)=VPLS
      SOLN(19,I)=RS
      SOLN(20,I)=LS
      SOLN(21,I)=QPLS
      SOLN(22,I)=QLS
      SOLN(23,I)=QDS
      SOLN(24,I)=PA
      SOLN(25,I)=PV
      SOLN(26,I)=PIPL
      SOLN(27,I)=CPL
      SOLN(28,I)=CSI
      SOLN(29,I)=CAVSI
      SOLN(30,I)=PISI
      SOLN(31,I)=PSI
      SOLN(32,I)=FSI
      SOLN(33,I)=VPLSI
      SOLN(34,I)=RSI
      SOLN(35,I)=LSI
      SOLN(36,I)=QPLSI
```

```
      SOLN(37,I)=QLSI
      SOLN(38,I)=QDSI
      VPL(I)=YNEW(1)
      QPL(I)=YNEW(2)
      VS(I)=YNEW(3)
      QS(I)=YNEW(4)
      VM(I)=YNEW(5)
      QM(I)=YNEW(6)
      VSI(I)=YNEW(7)
      QSI(I)=YNEW(8)
C
C      Calculate the sum of squares of differences between the
C      simulation and experimental results
C
      IF(T(I).EQ.1.0D0) DIS(1,1)=((VPL(I)-4.17D0)/6.12D0)**2
      IF(T(I).EQ.1.0D0) DIS(1,2)=((SOLN(26,I)-13.4D0)/20.0D0)**2
      IF(T(I).EQ.1.0D0) DIS(1,3)=((SOLN(30,I)-9.25D0)/9.0D0)**2
      IF(T(I).EQ.1.0D0) DIS(1,4)=((VSI(I)-7.852D0)/6.752D0)**2
      IF(T(I).EQ.1.0D0) DIS(1,5)=((VS(I)-10.4D0)/10.128D0)**2
      IF(T(I).EQ.1.0D0) DIS(1,6)=((QSI(I)-120.37D0)/111.4D0)**2
      IF(T(I).EQ.1.999D0) DIS(2,1)=((VPL(I)-4.17D0)/6.12D0)**2
      IF(T(I).EQ.1.999D0) DIS(2,2)=((SOLN(26,I)-17.6D0)/20.0D0)**2
      IF(T(I).EQ.1.999D0) DIS(2,3)=((SOLN(30,I)-10.47D0)/9.0D0)**2
      IF(T(I).EQ.1.999D0) DIS(2,4)=((VSI(I)-7.43D0)/6.752D0)**2
      IF(T(I).EQ.1.999D0) DIS(2,5)=((VS(I)-11.35D0)/10.128D0)**2
      IF(T(I).EQ.1.999D0) DIS(2,6)=((QSI(I)-204.1D0)/111.4D0)**2
      IF(T(I).EQ.2.999D0) DIS(3,1)=((VPL(I)-4.13D0)/6.12D0)**2
      IF(T(I).EQ.2.999D0) DIS(3,2)=((SOLN(26,I)-14.2D0)/20.0D0)**2
      IF(T(I).EQ.2.999D0) DIS(3,3)=((SOLN(30,I)-8.D0)/9.0D0)**2
      IF(T(I).EQ.2.999D0) DIS(3,4)=((VSI(I)-7.93D0)/6.752D0)**2
      IF(T(I).EQ.2.999D0) DIS(3,5)=((VS(I)-11.15D0)/10.128D0)**2
      IF(T(I).EQ.2.999D0) DIS(3,6)=((QSI(I)-105.4D0)/111.4D0)**2
      DO 20 J=1,NV
      YOLD(J)=YNEW(J)
20    CONTINUE
30    CONTINUE
      DISTA=0.0D0
      DO 91 I=1,6
      DIST(I)=0.0D0
      DO 92 J=1,3
      DIST(I)=DIST(I)+DIS(J,I)
92    CONTINUE
      DISTA=DISTA+DIST(I)
91    CONTINUE
C
C      Print the output results: dependent and supplemental
C      variables for each compartment and the sum of squares
C
      WRITE(6,93)
93    FORMAT(/,8X,'1',10X,'2',8X,'3',10X,'4',9X,'5',8X,'6')
      WRITE(6,94) (DIST(I),I=1,6)
94    FORMAT(//,2X,6F10.5)
      WRITE(6,95) DISTA
95    FORMAT(/,2X,'DISTANCE=',F10.5)
      WRITE(4,40)
40    FORMAT(//1X,'Transient response for 40% burn',///,
     1 5X,'Time',6X,'VPL',8X,'VS',8X,'VM',7X,'VSI',8X,'QPL',8X,'QS',
     2 8X,'QM',8X,'QSI',/)
      WRITE(4,50) (T(I),VPL(I),VS(I),VM(I),VSI(I),QPL(I),QS(I),QM(I),
     1 QSI(I),I=1,NP)
```

```
50    FORMAT(1X,5F10.5,4F10.4)
      WRITE(4,55) VPL(NP),VS(NP),VM(NP),VSI(NP),QPL(NP),QS(NP),QM(NP)
     1 ,QSI(NP)
55    FORMAT(1X,' Infinity ',4F10.5,4F10.4)
      WRITE(4,26)
26    FORMAT(//,2X,'TIME',7X,'CM',11X,'CAVM',10X,'PIM',12X,'PM')
      WRITE(4,32)((SOLN(J,I),J=1,5),I=1,NP)
32    FORMAT(1X,F5.2,4E14.5)
      WRITE(4,17)
17    FORMAT(///,2X,'TIME',7X,'FM',12X,'VPLM',11X,'RM',12X,'LM',11X,
     1 'QPLM',10X,'QLM',11X,'QDM')
      WRITE(4,13)(SOLN(1,I),(SOLN(J,I),J=6,12),I=1,NP)
13    FORMAT(1X,F5.2,7E14.5)
      WRITE(4,19)
19    FORMAT(//,2X,'TIME',7X,'CS',11X,'CAVS',10X,'PIS',12X,'PS')
      WRITE(4,14)(SOLN(1,I),(SOLN(J,I),J=13,16),I=1,NP)
      WRITE(4,18)
18    FORMAT(///,2X,'TIME',7X,'FS',12X,'VPLS',11X,'RS',12X,'LS',11X,
     1 'QPLS',10X,'QLS',11X,'QDM')
14    FORMAT(1X,F5.2,4E14.5)
      WRITE(4,25)(SOLN(1,I),(SOLN(J,I),J=17,23),I=1,NP)
25    FORMAT(1X,F5.2,7E14.5)
      WRITE(4,63)
63    FORMAT(//,2X,'TIME',7X,'CSI',10X,'CAVSI',9X,'PISI',11X,'PSI')
      WRITE(4,64) (SOLN(1,I),(SOLN(J,I),J=28,31),I=1,NP)
64    FORMAT(1X,F5.2,4F14.5)
      WRITE(4,61)
61    FORMAT(//,2X,'TIME',7X,'FSI',11X,'VPLSI',10X,'RSI',11X,'LSI',
     1 10X,'QPLSI',9X,'QLSI',10X,'QDSI')
      WRITE(4,62)(SOLN(1,I),(SOLN(J,I),J=32,38),I=1,NP)
62    FORMAT(1X,F5.2,7E14.5)
      WRITE(4,21)
21    FORMAT(///,2X,'TIME',7X,'PA',12X,'PV',12X,'PIPL',11X,'CPL')
      WRITE(4,22)(SOLN(1,I),(SOLN(J,I),J=24,27),I=1,NP)
22    FORMAT(1X,F5.2,4E14.5)
C
C      Plot the results of six variables: volume of the intact skin,
C      protein content in the injured skin, COP in the injured skin,
C      volume of the injured skin, volume of plasma and
C      COP in plasma
C
      RK1=K1
      RK2=K2
      RK3=K3
      RK4=K4
      RK5=K5
      RK6=K6
      RK7=K7
      CALL CAP(RK1,RK2,RK3,RK4,RK5,RK6,RK7)
      CALL PVPL(T,VPL,NP)
      DO 234 I=1,51
      SOL(I)=SOLN(26,I)
234   CONTINUE
      CALL PCOPP(T,SOL,NP)
      DO 235 I=1,51
      SOL(I)=SOLN(30,I)
235   CONTINUE
      CALL PCOPII(T,SOL,NP)
      DO 236 I=1,51
      SOL(I)=SOLN(15,I)
```

```
236   CONTINUE
      CALL PTTWI(T,VSI,NP)
      CALL PTTW(T,VS,NP)
      CALL PQI(T,QSI,NP)
      CALL PLOTND
      STOP
60    WRITE(5,70)
70    FORMAT(1X,'Root-solver fails!')
80    WRITE(5,90) T(I)
90    FORMAT(1X,'ODE-solver fails at T =',F8.4)
      STOP
      END
C
C       Evaluate the rignt-hand-size functions of the eight
C       differential equations
C
      DOUBLE PRECISION FUNCTION RHSF(I,X,Y)
      IMPLICIT REAL*8(A-H,L,O-Z)
      COMMON/BLKG/FS,VPLS,RS,LS,QPLS,QDS,QLS
      COMMON/BLKH/FM,VPLM,RM,LM,QPLM,QDM,QLM
      COMMON/BLKM/FSI,VPLSI,RSI,LSI,QPLSI,QDSI,QLSI
      DIMENSION Y(8)
      GO TO (10,20,30,40,50,60,70,80),I
10    CALL AUXS(X,Y)
      CALL AUXM(X,Y)
      CALL AUXSI(X,Y)
      RHSF3=FS+VPLS-RS-LS
      RHSF5=FM+VPLM-RM-LM
      RHSF7=FSI+VPLSI-RSI-LSI
      RHSF=-RHSF3-RHSF5-RHSF7
      RETURN
20    RHSF4=QPLS+QDS-QLS
      RHSF6=QPLM+QDM-QLM
      RHSF8=QPLSI+QDSI-QLSI
      RHSF=-RHSF4-RHSF6-RHSF8
      RETURN
30    RHSF=RHSF3
      RETURN
40    RHSF=RHSF4
      RETURN
50    RHSF=RHSF5
      RETURN
60    RHSF=RHSF6
      RETURN
70    RHSF=RHSF7
      RETURN
80    RHSF=RHSF8
      RETURN
      END
C
C       Calculate the auxiliary relationships for skin
C
      SUBROUTINE AUXS(X,Y)
      IMPLICIT REAL*8(A-H,K,L,O-Z)
      COMMON/BLKA/PAO,PVO,VES,VEM,VESI
      COMMON/BLKC/APL1,APL2,APL3,AS1,AS2,AS3,AS1I,AS2I,AS3I,
     1        AM1,AM2,AM3
      COMMON/BLKM/FSI,VPLSI,RSI,LSI,QPLSI,QDSI,QLSI
      COMMON/BLKG/FS,VPLS,RS,LS,QPLS,QDS,QLS
      COMMON/BLKI/KFS,KPLS,KRS,LSO,SLS,PSO,PSS
```

```
      COMMON/BLKK/PA,PV,CPL,PIPL,CS,CAVS,PS,PIS,CM,CAVM,PM,PIM,
     1       CSI,CAVSI,PSI,PISI
      COMMON/BLKZ/DEGREE
      DIMENSION Y(8)
      COMMON/BLKS/AA,BB
      COMMON/BLKW/K1,K2,K3,K4,K5,K6,K7
      KFS=K5*0.0556150*DEXP(-AA*X)+0.055615DO
      KPLS=K3*0.01632DO*DEXP(-AA*X)+0.01632DO
      KRS=K5*0.176613DO*DEXP(-AA*X)+0.176613DO
      LSO=0.2532DO*(1.DO+0.ODO*DEXP(-AA*X))
      SLS=0.75900DO*(1.DO+0.ODO*DEXP(-AA*X))
      PA=FCOMPA(Y(1))
      PV=FCOMPV(Y(1))
      CPL=Y(2)/Y(1)
      PIPL=CPL*(APL1+CPL*(APL2+CPL*APL3))
      CS=Y(4)/Y(3)
      CAVS=Y(4)/(Y(3)-VES)
      PS=FCOMPS(Y(3)/(1.DO-DEGREE))
      PIS=CAVS*(AS1+CAVS*(AS2+CAVS*AS3))
      FS=KFS*(PA-PS-(PIPL-PIS))
      VPLS=KPLS*(PV-PS)
      RS=KRS*(PS-PV-(PIS-PIPL))
      LS=LSO+SLS*(PS-PSO)
      IF(LS.LT.LSO) LS=LSO*(PS+7.84DO)/(PSO+7.84DO)
      IF(LS.LT.O.DO) LS=0.DO
      QPLS=VPLS*CPL
      QDS=PSS*(CPL-CAVS)
      QLS=LS*CS
      RETURN
      END
C
C      Calculate the auxiliary relationships for injured skin
C
      SUBROUTINE AUXSI(X,Y)
      IMPLICIT REAL*8(A-H,K,L,O-Z)
      COMMON/BLKA/PAO,PVO,VES,VEM,VESI
      COMMON/BLKC/APL1,APL2,APL3,AS1,AS2,AS3,AS1I,AS2I,AS3I,
     1       AM1,AM2,AM3
      COMMON/BLKL/KFSI,KPLSI,KRSI,LSOI,SLSI,PSOI,PSSI
      COMMON/BLKM/FSI,VPLSI,RSI,LSI,QPLSI,QDSI,QLSI
      COMMON/BLKG/FS,VPLS,RS,LS,QPLS,QDS,QLS
      COMMON/BLKI/KFS,KPLS,KRS,LSO,SLS,PSO,PSS
      COMMON/BLKK/PA,PV,CPL,PIPL,CS,CAVS,PS,PIS,CM,CAVM,PM,PIM,
     1       CSI,CAVSI,PSI,PISI
      COMMON/BLKZ/DEGREE
      COMMON/BLKT/PSIT(10),TT(10),NPSIT
      COMMON/BLKS/AA,BB
      COMMON/BLKW/K1,K2,K3,K4,K5,K6,K7
      DIMENSION Y(8)
      KFSI=K4*0.037077DO*DEXP(-AA*X)+0.037077DO
      KPLSI=K1*0.01088DO*DEXP(-AA*X)+0.01088DO
      KRSI=K4*0.117742DO*DEXP(-AA*X)+0.117742DO
      LSOI=0.1688DO*(1.DO+K7*DEXP(-BB*X))
      SLSI=0.506040DO*(1.DO+K7*DEXP(-BB*X))
      PA=FPAI(Y(1))
      PV=FPVI(Y(1))
      CPL=Y(2)/Y(1)
      PIPL=CPL*(APL1+CPL*(APL2+CPL*APL3))
      CSI=Y(8)/Y(7)
      CAVSI=Y(8)/(Y(7)-VESI)
```

```
C
C      Determination of the tissue pressure in the first three hours
C      in the injured skin
C
      DO 10 I=2,NPSIT
      IF (TT(I).GT.X) GOTO 20
10    CONTINUE
      PSI=PSIT(NPSIT)
      GOTO 30
20    IM=I-1
      PSI=PSIT(IM)+(PSIT(I)-PSIT(IM))*(X-TT(IM))/(TT(I)-TT(IM))
30    IF (X.GE.3.DO) PSI=FCOMPS(Y(7)/DEGREE)
      PISI=CAVSI*(AS1I+CAVSI*(AS2I+CAVSI*AS3I))
      FSI=KFSI*(PA-PSI-(PIPL-PISI))
      VPLSI=KPLSI*(PV-PSI)
      RSI=KRSI*(PSI-PV-(PISI-PIPL))
      LSI=LSOI+SLSI*(PSI-PSOI)
      IF(LSI.LT.LSOI) LSI=LSOI*(PSI+7.84DO)/(PSOI+7.84DO)
      IF(LSI.LE.O.DO) LSI=O.DO
      IF(LSI.LE.K7*LSOI.AND.X.LT.3.DO) LSI=K7*LSOI
      QPLSI=VPLSI*CPL
      QDSI=PSSI*(CPL-CAVSI)
      QLSI=LSI*CSI
      RETURN
      END
C
C      Calculation of the auxiliary relationships for muscle
C
      SUBROUTINE AUXM(X,Y)
      IMPLICIT REAL*8(A-H,K,L,O-Z)
      COMMON/BLKA/PAO,PVO,VES,VEM,VESI
      COMMON/BLKC/APL1,APL2,APL3,AS1,AS2,AS3,AS1I,AS2I,AS3I,
     1      AM1,AM2,AM3
      COMMON/BLKH/FM,VPLM,RM,LM,QPLM,QDM,QLM
      COMMON/BLKJ/KFM,KPLM,KRM,LMO,SLM,PMO,PSM
      COMMON/BLKK/PA,PV,CPL,PIPL,CS,CAVS,PS,PIS,CM,CAVM,PM,PIM,
     1       CSI,CAVSI,PSI,PISI
      COMMON/BLKZ/DEGREE
      COMMON/BLKS/AA,BB
      COMMON/BLKW/K1,K2,K3,K4,K5,K6,K7
      DIMENSION Y(8)
      KFM=K5*0.063446DO*DEXP(-AA*X)+0.063446DO
      KPLM=K3*0.014545DO*DEXP(-AA*X)+0.014545DO
      KRM=K5*0.158575DO*DEXP(-AA*X)+0.158575DO
      LMO=0.26025DO*(1.DO+0.ODO*DEXP(-AA*X))
      SLM=1.2065DO*(1.DO+0.ODO*DEXP(-AA*X))
      PA=FCOMPA(Y(1))
      PV=FCOMPV(Y(1))
      CPL=Y(2)/Y(1)
      PIPL=CPL*(APL1+CPL*(APL2+CPL*APL3))
      CM=Y(6)/Y(5)
      CAVM=Y(6)/(Y(5)-VEM)
      PM=FCOMPM(Y(5))
      PIM=CAVM*(AM1+CAVM*(AM2+CAVM*AM3))
      FM=KFM*(PA-PM-(PIPL-PIM))
      VPLM=KPLM*(PV-PM)
      RM=KRM*(PM-PV-(PIM-PIPL))
      LM=LMO+SLM*(PM-PMO)
      IF(LM.LT.LMO) LM=LMO*(PM+6.78DO)/(PMO+6.78DO)
      IF(LM.LT.O.DO) LM=O.DO
```

```
      QPLM=VPLM*CPL
      QDM=PSM*(CPL-CAVM)
      QLM=LM*CM
      RETURN
      END
C
C      Estimation of the compliance relationship for skin
C
      SUBROUTINE SPLINS
      IMPLICIT REAL*8(A-H,O-Z)
      COMMON/BLKD/X(20),Y(20),A1,BN,N,NM
      COMMON/BLKO/Q(100),R(101),S(100)
      DIMENSION H(100),A(101),B(101),C(101),D(101)
      DO 10 I=1,NM
10    H(I)=X(I+1)-X(I)
      B(1)=2.DO*H(1)
      C(1)=H(1)
      D(1)=3.DO*((Y(2)-Y(1))/H(1)-A1)
      DO 20 I=2,NM
      IP=I+1
      IM=I-1
      A(I)=H(IM)
      B(I)=2.DO*(H(IM)+H(I))
      C(I)=H(I)
20    D(I)=3.DO*((Y(IP)-Y(I))/H(I)-(Y(I)-Y(IM))/H(IM))
      A(N)=H(NM)
      B(N)=2.DO*H(NM)
      D(N)=-3.DO*((Y(N)-Y(NM))/H(NM)-BN)
      CALL TDMA(A,B,C,D,R,N)
      DO 30 I=1,NM
      IP=I+1
      Q(I)=(Y(IP)-Y(I))/H(I)-H(I)*(2.DO*R(I)+R(IP))/3.DO
30    S(I)=(R(IP)-R(I))/(3.DO*H(I))
      RETURN
      END
C
C      Estimation of the compliance relationship for muscle
C
      SUBROUTINE SPLINM
      IMPLICIT REAL*8(A-H,O-Z)
      COMMON/BLKE/X(19),Y(19),A1,BN,N,NM
      COMMON/BLKP/Q(100),R(101),S(100)
      DIMENSION H(100),A(101),B(101),C(101),D(101)
      DO 10 I=1,NM
10    H(I)=X(I+1)-X(I)
      B(1)=2.DO*H(1)
      C(1)=H(1)
      D(1)=3.DO*((Y(2)-Y(1))/H(1)-A1)
      DO 20 I=2,NM
      IP=I+1
      IM=I-1
      A(I)=H(IM)
      B(I)=2.DO*(H(IM)+H(I))
      C(I)=H(I)
20    D(I)=3.DO*((Y(IP)-Y(I))/H(I)-(Y(I)-Y(IM))/H(IM))
      A(N)=H(NM)
      B(N)=2.DO*H(NM)
      D(N)=-3.DO*((Y(N)-Y(NM))/H(NM)-BN)
      CALL TDMA(A,B,C,D,R,N)
      DO 30 I=1,NM
```

```
      IP=I+1
      Q(I)=(Y(IP)-Y(I))/H(I)-H(I)*(2.DO*R(I)+R(IP))/3.DO
30    S(I)=(R(IP)-R(I))/(3.DO*H(I))
      RETURN
      END
C
C
      SUBROUTINE TDMA(A,B,C,D,X,N)
C
C      Thomas algorithm
C
      IMPLICIT REAL*8(A-H,O-Z)
      DIMENSION A(N),B(N),C(N),D(N),X(N),P(101),Q(101)
      NM=N-1
      P(1)=-C(1)/B(1)
      Q(1)=D(1)/B(1)
      DO 10 I=2,N
      IM=I-1
      DEN=A(I)*P(IM)+B(I)
      P(I)=-C(I)/DEN
10    Q(I)=(D(I)-A(I)*Q(IM))/DEN
      X(N)=Q(N)
      DO 20 II=1,NM
      I=N-II
20    X(I)=P(I)*X(I+1)+Q(I)
      RETURN
      END
C
C      Calculation of the arterial capillary pressure in the
C      normal tissues
C
      DOUBLE PRECISION FUNCTION FCOMPA(V)
      IMPLICIT REAL*8(A-H,K,O-Z)
      COMMON/BLKA/PAO,PVO,VES,VEM,VESI
      COMMON/BLKB/VPLO,QPLO,VSO,VSOI,QSO,QSOI,VMO,QMO
      COMMON/BLKW/K1,K2,K3,K4,K5,K6,K7
      FCOMPA=17.64DO
      RETURN
      END
C
C      Calculation of the arterial capillary pressure in the
C      injured skin
C
      DOUBLE PRECISION FUNCTION FPAI(V)
      IMPLICIT REAL*8(A-H,K,O-Z)
      COMMON/BLKA/PAO,PVO,VES,VEM,VESI
      COMMON/BLKB/VPLO,QPLO,VSO,VSOI,QSO,QSOI,VMO,QMO
      COMMON/BLKW/K1,K2,K3,K4,K5,K6,K7
      FPAI=K6
      RETURN
      END
C
C      Calculaton of the venous capillary pressure in the
C      normal tissues
C
      DOUBLE PRECISION FUNCTION FCOMPV(V)
      IMPLICIT REAL*8(A-H,O-Z)
      COMMON/BLKA/PAO,PVO,VES,VEM,VESI
      COMMON/BLKB/VPLO,QPLO,VSO,VSOI,QSOI,QSO,VMO,QMO
      FCOMPV=4.72DO+5.1193DO*(V-VPLO)
```

```
      IF(FCOMPV.LT.2.DO) FCOMPV=2.DO
      RETURN
      END
C
C      Calculation of the venous capillary pressure in the
C      injured skin
C
      DOUBLE PRECISION FUNCTION FPVI(V)
      IMPLICIT REAL*8(A-H,O-Z)
      COMMON/BLKA/PAO,PVO,VES,VEM,VESI
      COMMON/BLKB/VPLO,QPLO,VSO,VSOI,QSOI,QSO,VMO,QMO
      FPVI=4.72DO+5.1193DO*(V-VPLO)
      IF(FPVI.LT.2.DO) FPVI=2.DO
      RETURN
      END
C
C      Evaluation of the compliance relationship for skin:
C      the skin fluid pressure as a function of skin
C      volume
C
      DOUBLE PRECISION FUNCTION FCOMPS(V)
      IMPLICIT REAL*8(A-H,O-Z)
      IF(V.LE.16.88DO) GO TO 10
      IF(V.GE.32.58DO) GO TO 20
      FCOMPS=FS(V)
      RETURN
10    FCOMPS=-1.21DO+0.523723DO*(V-16.88DO)
      RETURN
20    FCOMPS=0.65DO+0.001621DO*(V-32.58DO)
      RETURN
      END
C
C      Evaluation of the compliance relationship for muscle:
C      the muscle fluid pressure as a function of muscle volume
C
      DOUBLE PRECISION FUNCTION FCOMPM(V)
      IMPLICIT REAL*8(A-H,O-Z)
      IF(V.LE.10.41DO) GO TO 10
      IF(V.GE.18.22DO) GO TO 20
      FCOMPM=FM(V)
      RETURN
10    FCOMPM=-0.51DO+0.802817DO*(V-10.41DO)
      RETURN
20    FCOMPM=0.50DO+0.005239DO*(V-18.22DO)
      RETURN
      END
C
C
      DOUBLE PRECISION FUNCTION FS(Z)
      IMPLICIT REAL*8(A-H,O-Z)
      COMMON/BLKD/X(20),Y(20),A1,BN,N,NM
      COMMON/BLKO/Q(100),R(101),S(100)
      I=1
      IF(Z.LT.X(1)) GO TO 30
      IF(Z.GE.X(NM)) GO TO 20
      J=NM
10    K=(I+J)/2
      IF(Z.LT.X(K)) J=K
      IF(Z.GE.X(K)) I=K
      IF(J.EQ.I+1) GO TO 30
```

```
      GO TO 10
20    I=NM
30    DX=Z-X(I)
      FS=Y(I)+DX*(Q(I)+DX*(R(I)+DX*S(I)))
      RETURN
      END
C
C
      DOUBLE PRECISION FUNCTION FM(Z)
      IMPLICIT REAL*8(A-H,O-Z)
      COMMON/BLKE/X(19),Y(19),A1,BN,N,NM
      COMMON/BLKP/Q(100),R(101),S(100)
      I=1
      IF(Z.LT.X(1)) GO TO 30
      IF(Z.GE.X(NM)) GO TO 20
      J=NM
10    K=(I+J)/2
      IF(Z.LT.X(K)) J=K
      IF(Z.GE.X(K)) I=K
      IF(J.EQ.I+1) GO TO 30
      GO TO 10
20    I=NM
30    DX=Z-X(I)
      FM=Y(I)+DX*(Q(I)+DX*(R(I)+DX*S(I)))
      RETURN
      END
C
C       This subroutine is for solving the ordinary differential
C       equations using Runge-Kutta-Fehlberg method
C
      SUBROUTINE DESOLV(F,M,A,B,YO,EPS,HSTART,HMIN,HMAX,YB,FLAG)
      IMPLICIT REAL*8(A-H,O-Z)
      DIMENSION YO(M),YA(10),YB(M)
      EXTERNAL F
      INTEGER FLAG
      BMA=B-A
      HOLD=HSTART
      X=A
      DO 10 I=1,M
10    YA(I)=YO(I)
20    CALL RKF(F,M,X,YA,HOLD,YB,YDIF)
      GAMMA=.8DO*(EPS*HOLD/(BMA*YDIF))**0.25DO
      HNEW=GAMMA*HOLD
      IF(GAMMA.GE.1.DO) GO TO 30
      IF(HNEW.LT.HOLD/10.DO) HNEW=HOLD/10.
      IF(HNEW.LT.HMIN) GO TO 50
      HOLD=HNEW
      GO TO 20
30    IF(HNEW.GT.5.DO*HOLD) HNEW=5.DO*HOLD
      IF(HNEW.GT.HMAX) HNEW=HMAX
      IF(X+HOLD.GE.B) GO TO 70
      X=X+HOLD
      HOLD=HNEW
      DO 40 I=1,M
40    YA(I)=YB(I)
      GO TO 20
50    FLAG=0
      B=X
      DO 60 I=1,M
60    YB(I)=YA(I)
```

```
      RETURN
70    FLAG=1
      HSTART=HNEW
      HOLD=B-X
      CALL RKF(F,M,X,YA,HOLD,YB,YDIF)
      RETURN
      END
C
C
C
      SUBROUTINE RKF(F,M,X,YOLD,H,YNEW,YDIFM)
      IMPLICIT REAL*8(A-H,O-Z)
      DIMENSION YOLD(M),YNEW(M),YARG1(10),YARG2(10)
      REAL*8 K1(10),K2(10),K3(10),K4(10),K5(10),K6(10)
      DATA C21,C31,C32,C33/.25DO,.375DO,.09375DO,.28125DO/
      DATA C41,C42/.9230769230769230730O,0.8793809740555302570O/
      DATA C43,C44/-3.2771961766044606100,3.3208921256258532300/
      DATA C51,C52/2.032407407407407220O,-8.DO/
      DATA C53,C54/7.173489278752436470O,-.20589668615984405DO/
      DATA C61,C62/.5DO,-.29629629629629629400/
      DATA C63,C64/2.DO,-1.38167641325536050O/
      DATA C65,C66/.452972709551656916DO,-.275DO/
      DATA C71,C72/.11851851851851850900,.51898635477582845400/
      DATA C73,C74/.506131490342016654DO,-.18DO/
      DATA C75,C81/.0363636363636363636DO,.00277777777777777780O/
      DATA C82,C83/-.029941520467836256800,-.0291998936735778838DO/
      DATA C84,C85/.02DO,.0363636363636363636DO/
      DO 10 I=1,M
      K1(I)=H*F(I,X,YOLD)
10    YARG1(I)=YOLD(I)+C21*K1(I)
      XARG=X+C21*H
      DO 20 I=1,M
      K2(I)=H*F(I,XARG,YARG1)
20    YARG2(I)=YOLD(I)+C32*K1(I)+C33*K2(I)
      XARG=X+C31*H
      DO 30 I=1,M
      K3(I)=H*F(I,XARG,YARG2)
30    YARG1(I)=YOLD(I)+C42*K1(I)+C43*K2(I)+C44*K3(I)
      XARG=X+C41*H
      DO 40 I=1,M
      K4(I)=H*F(I,XARG,YARG1)
40    YARG2(I)=YOLD(I)+C51*K1(I)+C52*K2(I)+C53*K3(I)+C54*K4(I)
      XARG=X+H
      DO 50 I=1,M
      K5(I)=H*F(I,XARG,YARG2)
50    YARG1(I)=YOLD(I)+C62*K1(I)+C63*K2(I)+C64*K3(I)+C65*K4(I)
     1 +C66*K5(I)
      XARG=X+C61*H
      DO 60 I=1,M
60    K6(I)=H*F(I,XARG,YARG1)
      YDIFM=0.DO
      DO 70 I=1,M
      YNEW(I)=YOLD(I)+C71*K1(I)+C72*K3(I)+C73*K4(I)+C74*K5(I)+
     1 C75*K6(I)
      YDIF=DABS(C81*K1(I)+C82*K3(I)+C83*K4(I)+C84*K5(I)+C85*K6(I))
70    IF(YDIF.GT.YDIFM) YDIFM=YDIF
      RETURN
      END
C
C      Plotting of plasma volume
```

```
C
      SUBROUTINE PVPL(X,Y,NP)
      IMPLICIT REAL*8(A-H,O-Z)
      REAL*4 RX(51),RY(51),XE(3),YE(3),DE1(3),BAR1,BAR2,BAR3,BAR4
      REAL*4 TX,TY,TDE1,TDE2,DE2(3)
      DIMENSION X(51),Y(51)
      DATA XE/1.0,2.0,3.0/
      DATA YE/4.17,4.17,4.13/
      DATA DE1/0.564,0.156,0.639/
      DATA DE2/0.505,0.154,0.57/
      CALL PLCTRL('METRIC',1)
      CALL PALPHA('SANSERIF.2 ',0)
      CALL FTNCMD('ASSIGN 7=-SCR;')
      CALL AXES(4.7,7.2,6.,1.0,2.0.,2.0,-1,'TIME (hour)',11,6.,
     1 0.75,2,0.0,2.0,-1,'PLASMA VOLUME (ml)',18,0.25)
      DO 10 I=1,NP
      RX(I)=X(I)
      IF (RX(I).GT.6.0) II=I-1
      IF (RX(I).GT.6.0) GOTO 11
      RY(I)=Y(I)
10    CONTINUE
11    CALL DLINE1(RX,RY,II,0.0,4.7,1.0,0.0,7.2,1.3333,0.1,0.1,
     1 0.0,0.005,-12.0,18.0,1.0,'40 PER BURN',11,0.3,100.)
      DO 20 I=1,3
      TX=XE(I)+4.7
      TY=YE(I)/1.3333+7.2
      TDE1=DE1(I)/1.3333
      TDE2=DE2(I)/1.3333
      CALL SYMBOL(TX,TY,0.1,4,1)
      BAR1=TY+TDE1
      BAR2=TY-TDE2
      BAR3=TX+0.1
      BAR4=TX-0.1
      CALL PLOT(BAR4,BAR1,3)
      CALL PLOT(BAR3,BAR1,2)
      CALL PLOT(TX,BAR1,3)
      CALL PLOT(TX,BAR2,2)
      CALL PLOT(BAR4,BAR2,3)
      CALL PLOT(BAR3,BAR2,2)
20    CONTINUE
      RETURN
      END
C
C      Plotting of COP in plasma
C
      SUBROUTINE PCOPP(X,Y,NP)
      IMPLICIT REAL*8(A-H,O-Z)
      REAL*4 RX(51),RY(51),XE(3),YE(3),DE(3),BAR1,BAR2,BAR3,BAR4
      REAL*4 TX,TY,TDE
      DATA XE/1.0,2.0,3.0/
      DATA YE/13.4,17.6,14.2/
      DATA DE/2.27,0.595,1.495/
      DIMENSION X(51),Y(51)
      CALL AXES(13.5,7.2,6.,1.0,2.0.,2.0,-1,'TIME (hour)',11,6.,
     1 0.6,2,10.0,4.0,-1,'COP IN PLASMA (ml)'
     2 ,18,0.25)
      DO 10 I=1,NP
      RX(I)=X(I)
      IF (RX(I).GT.6.0) II=I-1
      IF (RX(I).GT.6.0) GOTO 11
```

```
      RY(I)=Y(I)
10    CONTINUE
11    CALL DLINE1(RX,RY,II,0.0,13.5,1.0,10.0,7.2,3.333,0.1,0.1,
     1 0.0,0.005,-12.0,19.0,1.0,'40 PER BURN',11,0.3,100.)
      DO 20 I=1,3
      TX=XE(I)+13.5
      TY=(YE(I)-10.0)/3.333+7.2
      TDE=DE(I)/3.333
      CALL SYMBOL(TX,TY,0.1,4,1)
      BAR1=TY+TDE
      BAR2=TY-TDE
      BAR3=TX+0.1
      BAR4=TX-0.1
      CALL PLOT(BAR4,BAR1,3)
      CALL PLOT(BAR3,BAR1,2)
      CALL PLOT(TX,BAR1,3)
      CALL PLOT(TX,BAR2,2)
      CALL PLOT(BAR4,BAR2,3)
      CALL PLOT(BAR3,BAR2,2)
20    CONTINUE
      RETURN
      END
C
C       Plotting of COP in the injured skin
C
      SUBROUTINE PCOPII(X,Y,NP)
      IMPLICIT REAL*8(A-H,O-Z)
      REAL*4 RX(51),RY(51),XE(3),YE(3),DE(3)
      REAL*4 BAR1,BAR2,BAR3,BAR4,TX,TY,YDE
      DATA XE/1.0,2.0,3.0/
      DATA YE/9.248,10.47,8.0/
      DATA DE/2.064,1.653,0.917/
      DIMENSION X(51),Y(51)
      CALL XAXIS(4.7,13.5,6.0,0.01,1.0,0.15,2,2,0.0,2.0,0.0,
     1 0.0,-1,'.',1,0.0,0.0,2,6.0)
      CALL YAXIS(4.7,13.5,6.0,0.01,0.6,0.15,2,2,5.0,2.0,0.1875,
     1 0.1875,-1,'COP IN INJURED SKIN (mmhg)',26,0.25,0.1875,2,6.0)
      DO 10 I=1,NP
      RX(I)=X(I)
      IF (RX(I).GT.6.0) II=I-1
      IF (RX(I).GT.6.0) GOTO 11
      RY(I)=Y(I)
10    CONTINUE
11    CALL DLINE1(RX,RY,II,0.0,4.7,1.0,5.0,13.5,1.6667,0.1,0.1,
     1 0.0,0.005,-12.0,18.0,1.0,'40 PER BURN',11,0.3,100.)
      DO 20 I=1,3
      TX=XE(I)+4.7
      TY=(YE(I)-5.0)/1.6667+13.5
      TDE=DE(I)/1.6667
      CALL SYMBOL(TX,TY,0.1,4,1)
      BAR1=TY+TDE
      BAR2=TY-TDE
      BAR3=TX+0.1
      BAR4=TX-0.1
      CALL PLOT(BAR4,BAR1,3)
      CALL PLOT(BAR3,BAR1,2)
      CALL PLOT(TX,BAR1,3)
      CALL PLOT(TX,BAR2,2)
      CALL PLOT(BAR4,BAR2,3)
      CALL PLOT(BAR3,BAR2,2)
```

```
20    CONTINUE
      RETURN
      END
C
C      Plotting of water content in the injured tissue
C
      SUBROUTINE PTTWI(X,Y,NP)
      IMPLICIT REAL*8(A-H,O-Z)
      REAL*4 RX(51),RY(51),XE(3),YE(3),DE(3)
      REAL*4 BAR1,BAR2,BAR3,BAR4,TX,TY,TDE
      DIMENSION X(51),Y(51)
      DATA XE/1.0,2.0,3.0/
      DATA YE/7.852,7.43,7.93/
      DATA DE/0.95,0.7587,0.683/
      CALL XAXIS(13.5,13.5,6.0,0.01,1.0,0.15,2,2,0.0,2.0,0.0,
     1 0.0,-1,'.',1,0.0,0.0,2,6.0)
      CALL YAXIS(13.5,13.5,6.0,0.01,0.6,0.15,2,2,5.0,2.0,0.1875,
     1 0.1875,-1,'VOLUME OF INJURED SKIN (ml)',27,0.25,0.1875,2,6.0)
      DO 10 I=1,NP
      RX(I)=X(I)
      IF (RX(I).GT.6.0) II=I-1
      IF (RX(I).GT.6.0) GOTO 11
      RY(I)=Y(I)
10    CONTINUE
11    CALL DLINE1(RX,RY,II,0.0,13.5,1.,5.0,13.5,1.667,0.1,0.1,
     1 0.0,0.005,-12.0,18.0,1.0,'10 PER BURN',11,0.3,100.)
      DO 20 I=1,3
      TX=XE(I)+13.5
      TY=(YE(I)-5.0)/1.6667+13.5
      TDE=DE(I)/1.6667
      CALL SYMBOL(TX,TY,0.1,4,1)
      BAR1=TY+TDE
      BAR2=TY-TDE
      BAR3=TX+0.1
      BAR4=TX-0.1
      CALL PLOT(BAR4,BAR1,3)
      CALL PLOT(BAR3,BAR1,2)
      CALL PLOT(TX,BAR1,3)
      CALL PLOT(TX,BAR2,2)
      CALL PLOT(BAR4,BAR2,3)
      CALL PLOT(BAR3,BAR2,2)
20    CONTINUE
      RETURN
      END
C
C      Plotting of water content in the intact skin
C
      SUBROUTINE PTTW(X,Y,NP)
      IMPLICIT REAL*8(A-H,O-Z)
      REAL*4 RX(51),RY(51),XE(3),YE(3),DE(3)
      REAL*4 BAR1,BAR2,BAR3,TX,TY,TDE
      DATA XE/1.0,2.0,3.0/
      DATA YE/10.4,11.4,11.15/
      DATA DE/1.56,1.22,0.68/
      DIMENSION X(51),Y(51)
      CALL XAXIS(4.7,19.8,6.0,0.01,1.0,0.15,2,2,0.0,2.0,0.0,
     1 0.0,-1,'.',1,0.0,0.0,2,6.0)
      CALL YAXIS(4.7,19.8,6.0,0.01,0.6,0.15,2,2,5.0,2.0,0.1875,
     1 0.1875,-1,'VOLUME OF INTACT SKIN (ml)',26,0.25,0.1875,2,6.0)
      DO 10 I=1,NP
```

```
      RX(I)=X(I)
      IF (RX(I).GT.6.0) II=I-1
      IF (RX(I).GT.6.0) GOTO 11
      RY(I)=Y(I)
10    CONTINUE
11    CALL DLINE1(RX,RY,II,0.0,4.7,1.0,5.0,19.8,1.6666667,0.1,0.1,
     1 0.0,0.005,-12.0,18.0,1.0,'10 PER BURN',11,0.3,100.)
      DO 20 I=1,3
      TX=XE(I)+4.7
      TY=(YE(I)-5.0)/1.6667+19.8
      TDE=DE(I)/1.6667
      CALL SYMBOL(TX,TY,0.1,4,1)
      BAR1=TY+TDE
      BAR2=TY-TDE
      BAR3=TX+0.1
      BAR4=TX-0.1
      CALL PLOT(BAR4,BAR1,3)
      CALL PLOT(BAR3,BAR1,2)
      CALL PLOT(TX,BAR1,3)
      CALL PLOT(TX,BAR2,2)
      CALL PLOT(BAR4,BAR2,3)
      CALL PLOT(BAR3,BAR2,2)
20    CONTINUE
      RETURN
      END
C
C      Plotting of protein content in injured skin
C
      SUBROUTINE PQI(X,Y,NP)
      IMPLICIT REAL*8(A-H,O-Z)
      REAL*4 RX(51),RY(51),XE(3),YE(3),DE(3)
      REAL BAR1,BAR2,BAR3,BAR4,TX,TY,TDE
      DATA XE/1.0,2.0,3.0/
      DATA YE/120.37,204.1,105.4/
      DATA DE/44.86,111.4,5.98/
      DIMENSION X(51),Y(51)
      CALL XAXIS(13.5,19.8,6.0,0.01,1.0,0.15,2,2,0.0,2.0,0.0,
     1 0.0,-1,'.',1,0.0,0.0,2,6.0)
      CALL YAXIS(13.5,19.8,6.0,0.01,0.6,0.15,2,2,0.0,70.0,0.1875,
     1 0.1875,-1,'PROTEIN IN INJURED SKIN (mg)',28,0.25,0.1875,2,6.0)
      DO 10 I=1,NP
      RX(I)=X(I)
      IF (RX(I).GT.6.0) II=I-1
      IF (RX(I).GT.6.0) GOTO 11
      RY(I)=Y(I)
10    CONTINUE
11    CALL DLINE1(RX,RY,II,0.0,13.5,1.0,0.0,19.8,54.0000,0.1,0.1,
     1 0.0,0.005,-12.0,18.0,1.0,'10 PER BURN',11,0.3,100.)
      DO 20 I=1,3
      TX=XE(I)+13.5
      TY=YE(I)/54.000+19.8
      TDE=DE(I)/54.0000
      CALL SYMBOL(TX,TY,0.1,4,1)
      BAR1=TY+TDE
      BAR2=TY-TDE
      BAR3=TX+0.1
      BAR4=TX-0.1
      CALL PLOT(BAR4,BAR1,3)
      CALL PLOT(BAR3,BAR1,2)
      CALL PLOT(TX,BAR1,3)
```

```
      CALL PLOT(TX,BAR2,2)
      CALL PLOT(BAR4,BAR2,3)
      CALL PLOT(BAR3,BAR2,2)
20    CONTINUE
C      CALL PLOT(25.,0.0,-3)
      RETURN
      END
C      CALL DLINE1(RX,RY,NP,0.0,4.0,6.667,0.0,7.0,0.3333333,0.1,0.1,
C    1 0.0,0.02,12.0,18.0,1.0,'40 PER BURN',11,0.3,100.)
C
C      Plotting of the caption in the output graphs
C
      SUBROUTINE CAP(A,B,C,D,E,F,G)
      IMPLICIT REAL*4(A-H,O-Z)
      LOGICAL*1 CHAR(20)
      CALL PLCTRL('METRIC',1)
      CALL PALPHA('SANSERIF.2 ',0)
      CALL FTNCMD('ASSIGN 7=-SCR;')
      CALL PSYM(4.7,5.0,0.25,'KPLSI=',0.0,6)
      CALL CONVT(A,1,CHAR,NC)
      CALL PSYM(7.7,5.0,0.25,CHAR,0.0,NC)
      CALL PSYM(13.5,5.0,0.25,'Pif=',0.0,4)
      CALL PSYM(15.5,5.0,0.25,'top',0.0,3)
      CALL PSYM(4.7,4.2,0.25,'KPLS,KPLM=',0.0,10)
      CALL CONVT(C,1,CHAR,NC)
      CALL PSYM(7.7,4.2,0.25,CHAR,0.0,NC)
      CALL PSYM(13.5,4.2,0.25,'KFSI,KRSI=',0.0,10)
      CALL CONVT(D,2,CHAR,NC)
      CALL PSYM(15.5,4.2,0.25,CHAR,0.0,NC)
      CALL PSYM(4.7,3.4,0.25,'KFM(S),KRM(S)=',0.0,14)
      CALL CONVT(E,1,CHAR,NC)
      CALL PSYM(7.7,3.4,0.25,CHAR,0.0,NC)
      CALL PSYM(13.5,3.4,0.25,'PAI=',0.0,4)
      CALL CONVT(F,1,CHAR,NC)
      CALL PSYM(15.5,3.4,0.25,CHAR,0.0,NC)
      CALL PSYM(4.7,2.6,0.25,'LSI=',0.0,4)
      CALL CONVT(G,1,CHAR,NC)
      CALL PSYM(7.7,2.6,0.25,CHAR,0.0,NC)
      RETURN
      END
```

APPENDIX C:

SAMPLE CALCULATION For NORMALIZING EXPERIMENTAL DATA

The experimental data used to compare with the simulation predictions are from the work of Lund and Reed [45]. These experimental results with their standard deviations are tabulated in Tables C.1 and C.2 for 10% and 40% burn, respectively.

The normal values measured in the experiments of Lund and Reed [45] and the normal values assumed by Bert et al. (and also used as starting values in the present simulation) are somewhat different. Therefore it was necessary to normalize the experimental data before comparisons could be made. The calculational procedure used for this purpose is based on direct proportionality, i.e., if the normal values of the experiment and the simulation are U and V, respectively, and if the experimental value is W at any given time, then the normalized value X is:

$$X = VW/U \tag{C.1}$$

Table C.2 and C.4 list the normalized experimental data which are used as a basis of comparison with the simulation results and which are also plotted in the output response

Table C.1 Experimental Data for 10% Burn by Lund and Reed [45]

	Initial	60 min post burn	120 min post burn	180 min post burn
V_s (ml)	1.49±0.18	1.62±0.18	1.57±0.21	1.53±0.04
Q_b (mg)	14.9±3.0	42.9±21.6	41.7±15.3	40.6±12.6
Π_b (mmhg)	11.2±2.2	15.1±3.4	14.8±2.9	15.3±2.1
V_b	1.78±0.22	3.06±0.75	2.91±0.69	2.99±0.62
Hematocrit(%)	49.9±2.0	52.4±1.8	55.5±2.1	55.4±1.7
Π_p (mmhg)	16.8±2.4	12.5±3.3	14.6±3.4	13.9±3.0

Table C.2 Normalized Experimental Data for 10% Burn

	Initial	60 min post burn	120 min post burn	180 min post burn
V_s (ml)	15.19	16.52±1.84	16.00±2.14	15.60±0.41
Q_b (mg)	27.85	80.19±40.37	77.94±28.60	75.89±23.55
Π_b (mmhg)	9.00	10.79±2.45	12.69±2.49	12.87±1.77
V_b	1.69	2.90±0.71	2.76±0.65	2.84±0.59
V_p (ml)	6.12	5.41±0.40	4.87±0.43	4.73±0.34
Π_p (mmhg)	20.00	15.43±4.07	17.8±4.15	15.53±3.35

Table C.3 Experimental Data for 40% Burn by Lund and Reed [45]

	Initial Value	60 min post burn	120 min post burn	180 min post burn
V_s(ml)	1.49±0.18	1.53±0.23	1.67±0.18	1.64±0.10
Q_b(mg)	14.9±3.0	16.1±6.0	27.3±14.9	14.1±0.8
Π_b (mmhg)	10.5±2.0	11.2±2.5	11.4±1.8	9.6±1.1
V_b(ml)	1.78±0.22	2.07±0.25	1.96±0.20	2.09±0.18
Hematocrit(%)	49.6±1.8	58.5±3.1	59.0±0.9	60.0±3.5
Π_p(mmhg)	18.9±3.0	12.4±3.4	14.8±0.50	15.2±1.6

Table C.4 Normalized Experimental Data for 40% Burn

	Initial Value	60 min post burn	120 min post burn	180 min post burn
V_s(ml)	10.13	10.40±1.56	11.35±1.22	11.15±0.68
Q_b(mg)	111.4	120.4±44.9	204.1±111.4	105.4±6.0
Π_b (mmhg)	9.00	9.25±2.06	10.47±1.65	8.00±0.92
V_b(ml)	6.75	7.85±0.95	7.43±0.76	7.93±0.68
V_p	6.12	4.17+0.564	4.17+0.156	4.13+0.639
Π_p(mmhg)	20.00	13.40±2.27	17.62±0.60	14.20±1.50

graphs. These data are calculated from Equation C.1, except for the plasma volume (V_p) which is derived from the hematocrit data. A typical example calculation illustrating the use of Equation C.1 is given below. Protein content in the injured skin one hour after a 40% burn:

initial experimental value: 14.9 mg (Table C.3),

initial simulation value: 111.4 mg (Table C.4),

experimental value: 16.1 mg (Table C.3)

normalized experimental value:

$$(111.4)\cdot(16.1)/(14.9) = 120.37 \text{ (mg)}$$

The plasma volumes were calculated from the measured hematocrit. By definition, the hematocrit is the volume percentage of erythrocytes (red cells) in whole blood. Assume the red cell volume is Y and that it is constant. Assume the initial experimental hematocrit value and the value at a certain measuring time postburn are U and W, respectively, and the initial volume of plasma in the simulation is V. Therefore, if X is now the normalized plasma volume, then by definition:

$$U = Y/(Y+V) \qquad \text{C.2}$$

and

$$W = Y/(Y+X) \tag{C.3}$$

Thus, when Y is eliminated by combining Equations C.2 and C.3, the following expression for the plasma volume is obtained, namely

$$X = V\cdot(1-W)\cdot U/[W\cdot(1-U)] \tag{C.4}$$

For example, at two hours after the initiation of a 40% burn:
initial experimental value of hematocrit: 49.5% (Table C.3),
initial simulation value of plasma: 6.12 ml (Table C.4),
experimental value of hematocrit: 59% (Table C.3),
normalized experimental value:

$$6.12\cdot(1-0.59)\cdot 0.495/[0.59\cdot(1-0.495)] = 4.17 \text{ (ml)}$$

All the normalized values of plasma volume are calculated in this manner.

The normalized experimental value of the water content of the tissues cannot be derived directly from Equation C.1, since the total tissue water measured includes the intracellular water. For example, let's look at the water content in the intact tissue. After a 10% burn, assuming that there are no cells damaged in the intact skin, the normalized values for tissue water content can be calculated in two ways:

1. Assume the intracellular water can be ignored. The normalized values for tissue content in this case are calculated from Equation C.1. These values are shown in Table C.3.
2. Assume the intracellular water is 20% of the total tissue water, and there is no cellular damage after the burn.

   The normal value of interstitial fluid volume from the experiment is therefore

   $$(0.8)\cdot(1.49\text{ml}) = 1.19(\text{ml}).$$

   If it is assumed also that the change in tissue water equals the change of total tissue water (i.e., cellular water volume remains constant), then the value for the intact skin fluid volume after one hour becomes:

   $$1.19\text{ml}+(1.62-1.49)\text{ml} = 1.32\ (\text{ml})$$

   Similarly, after two hours the experimental result becomes:

   $$1.19\text{ml}+(1.57-1.49)\text{ml} = 1.27\ (\text{ml})$$

   and after three hours the experimental result becomes:

   $$1.19\text{ml}+(1.53-1.49)\text{ml} = 1.23\ (\text{ml}).$$

   The normal value of skin interstitial fluid volume used in the simulations: 15.2 (ml).

Therefore, the normalized experimental value after one hour:

$$(15.2)\cdot(1.32)/(1.19) = 16.9 \text{ (ml)},$$

after two hours:

$$(15.2)\cdot(1.27)/(1.19) = 16.2 \text{ (ml)}, \text{ and}$$

after three hours:

$$(15.2)\cdot(1.23)/(1.19) = 15.7 \text{ (ml)}$$

There is only a very small difference between the normalized experimental values in these two cases. Additionally, these differences are insignificant compared to the experimental error. Because of these insignificant differences and because the fraction of intracellular water in the tissue is not precisely known for rat skin, the normalized experimental data for intact tissue volumes used for comparison with the simulation predictions are taken from Table C.4 which is based on the assumption that the intracellular water can be ignored.

The analysis of the water content of the injured tissue could be more complicated than that for the intact skin since a fraction of the cells in the injured skin may be damaged after the burn. The normalized values of water content in the injured skin are calculated for three cases based on three different assumptions. Using the 40% burn as an example:

1. Assume the intracellular water can be ignored. The

normalized values in this case can be calculated directly from Equation C.1 and are listed in Table C.4.

2. Assume the intracellular water is 20% of the total tissue water and none of the cells are damaged after the burn.

   The normal experimental value for skin interstitial water in the experiment:

   $(0.8)\cdot(1.78\text{ml}) = 1.42$ ml.

   Assume that the change of tissue water equals the change of total tissue water, then the experimental result becomes after one hour:

   $$1.42\text{ml}+(2.07-1.78)\text{ml}=1.71 \text{ ml},$$

   after two hours:

   $$1.42\text{ml}+(1.96-1.78)\text{ml}=1.60 \text{ ml and}$$

   after three hours:

   $$1.42\text{ml}+(2.09-1.78)\text{ml}=1.73 \text{ ml}.$$

   The initial value used in the simulation is 6.75 ml for intact skin. The normalized experimental values therefore become after one hour:

   $$(6.75)\cdot(1.71)/(1.42) = 8.13 \text{ (ml)},$$

   after two hours:

   $$(6.75)\cdot(1.60)/(1.42) = 7.6 \text{ (ml) and}$$

   after three hours:

   $$(6.75)\cdot(1.73)/(1.42) = 8.22 \text{ (ml)}.$$

3. Assume that 20% of the total tissue water is cellular water, that all the cells are damaged after the burn and the cellular water disappears after the cells are

damaged (possibly through exudation and evaporation). In this case, the experimental data after the burn only reflect the interstitial tissue water content.

The normal value of skin interstitial water of the experiment:

$$(0.8)\cdot(1.78\text{ml}) = 1.42\ (\text{ml}).$$

The experimental values are 2.07 ml after one hour, 1.96 ml after two hours and 2.09 ml after three hours.

The starting value for injured skin fluid volume used in the simulation for a 40% burn injury is 6.75 ml.

The normalized experimental values therefore become after one hour:

$$(6.75)\cdot(2.07)/(1.42) = 9.84\ (\text{ml}),$$

after two hours:

$$(6.75)\cdot(1.96)/(1.42) = 9.32\ (\text{ml}) \text{ and}$$

after three hours:

$$(6.75)\cdot(2.09)/(1.42) = 9.93\ (\text{ml}).$$

The differences between the normalized values calculated in Cases 1, 2 and 3 are small and insignificant compared to the errors in the experiment. It is likely that not all the cells in the injured skin are damaged and further, the estimate of 20% intracellular water is believed to be high. Hence, Case 3 is an extreme case and it reflects the largest possible differences in injured skin fluid volume obtained through the normalization procedure. Not enough information is presently available regarding the proportion of the cells damaged and the percentage of intracellular water. Thus to simplify the problem and to eliminate questionable assumptions, the normalized values of the injured skin are calculated as shown in Case 1. These values for 10% and 40% burns are listed in Table C.2 and C.4, respectively.

APPENDIX D

Appendix D contains a complete listing of the transient responses of all variables in the burn model obtained using the most reasonable parameter changes for the 10% and 40% burns. For the 10% burn, the perturbations are: A = 35.0, P_b = Upper Curve, B=-0.5 and P_a and P_v return to normal at 9 hours postburn. For the 40% burn, the perturbations are: A = 4.0, P_b = Upper Curve, B=10.0 and C=-0.95.

Transient response for 10% burn

Time	VPL	VS	VM	VSI	QPL	QS	QM	QSI
0.0	6.12000	15.19200	10.41000	1.68800	219.7080	250.6500	134.3000	27.8500
0.25000	6.00146	15.08145	10.33068	1.99641	210.1180	250.4275	134.1690	37.7935
0.50000	5.79813	14.97750	10.25856	2.37581	199.4926	249.9929	133.9134	49.1091
0.75100	5.60125	14.86457	10.18335	2.76083	189.6315	249.3480	133.5336	59.9950
1.00000	5.49779	14.75638	10.11262	3.04320	183.2112	248.5482	133.0620	67.6866
1.25000	5.42652	14.68170	10.06297	3.23882	179.3557	247.7217	132.5748	72.8558
1.50000	5.36123	14.62802	10.02627	3.39448	176.6358	246.9063	132.0941	76.8718
1.75000	5.32722	14.58496	9.99606	3.50176	175.1717	246.1016	131.6197	79.6149
2.00000	5.33391	14.55002	9.97087	3.55520	175.0289	245.3064	131.1510	81.0217
2.25000	5.37287	14.52241	9.95028	3.56445	175.9284	244.5193	130.6873	81.3730
2.50100	5.42882	14.50048	9.93331	3.54738	177.4350	243.7425	130.2299	81.1007
2.75000	5.50187	14.48290	9.91915	3.50609	179.4992	242.9721	129.7765	80.2602
3.00100	5.57712	14.47794	9.91269	3.44225	182.0269	242.2386	129.3454	78.8971
3.25000	5.61444	14.48273	9.91199	3.40084	183.9680	241.5670	128.9513	78.0217
3.50000	5.65051	14.48739	9.91107	3.36103	185.8108	240.9368	128.5819	77.1785
3.75000	5.68481	14.49223	9.91020	3.32276	187.5586	240.3489	128.2379	76.3625
4.00000	5.71745	14.49732	9.90946	3.28577	189.2225	239.8012	127.9181	75.5662
4.25000	5.74858	14.50267	9.90890	3.24986	190.8116	239.2918	127.6213	74.7833
4.50000	5.77832	14.50826	9.90854	3.21487	192.3331	238.8191	127.3465	74.0092
4.75000	5.80682	14.51410	9.90841	3.18068	193.7937	238.3814	127.0928	73.2401
5.00000	5.83419	14.52017	9.90852	3.14712	195.1992	237.9773	126.8594	72.4721
5.25000	5.86055	14.52649	9.90889	3.11407	196.5549	237.6053	126.6454	71.7023
5.50000	5.88598	14.53306	9.90953	3.08143	197.8651	237.2644	126.4501	70.9283
5.75000	5.91055	14.53989	9.91045	3.04910	199.1337	236.9534	126.2729	70.1480
6.00100	5.93425	14.54695	9.91167	3.01713	200.3589	236.6722	126.1136	69.3632
6.25000	5.95723	14.55429	9.91319	2.98529	201.5490	236.4186	125.9710	68.5693
6.50000	5.97963	14.56193	9.91503	2.95342	202.7107	236.1909	125.8440	67.7624
6.75000	6.00138	14.56985	9.91718	2.92159	203.8410	235.9891	125.7327	66.9452
7.00000	6.02254	14.57807	9.91965	2.88974	204.9418	235.8124	125.6366	66.1171
7.25000	6.04313	14.58658	9.92245	2.85784	206.0145	235.6601	125.5552	65.2781
7.50000	6.06319	14.59539	9.92558	2.82585	207.0606	235.5313	125.4880	64.4281
7.75000	6.08273	14.60450	9.92903	2.79374	208.0810	235.4253	125.4346	63.5671
8.00000	6.10178	14.61392	9.93281	2.76149	209.0768	235.3414	125.3945	62.6953
8.25000	6.12035	14.62364	9.93692	2.72909	210.0488	235.2789	125.3672	61.8130
8.50000	6.13847	14.63367	9.94135	2.69651	210.9978	235.2371	125.3525	60.9207
8.75000	6.15615	14.64401	9.94610	2.66374	211.9242	235.2153	125.3499	60.0186
9.00100	6.17333	14.65461	9.95115	2.63091	212.8253	235.2129	125.3588	59.1110
9.25000	6.05222	14.73798	10.01296	2.60684	213.5121	235.3169	125.4300	58.2490
9.50000	6.04200	14.75848	10.03447	2.57505	214.3196	235.3761	125.4730	57.3393
9.75000	6.05277	14.76778	10.04775	2.54169	215.1330	235.4413	125.5183	56.4153
10.00000	6.06713	14.77582	10.05913	2.50792	215.9314	235.5218	125.5717	55.4831
10.25000	6.08183	14.78433	10.06986	2.47397	216.7107	235.6186	125.6341	54.5447
10.50000	6.09628	14.79357	10.08024	2.43990	217.4703	235.7314	125.7053	53.6010
10.75000	6.11037	14.80351	10.09038	2.40574	218.2100	235.8596	125.7851	52.6533
11.00000	6.12407	14.81408	10.10033	2.37152	218.9296	236.0025	125.8732	51.7026
11.25000	6.13738	14.82520	10.11016	2.33726	219.6289	236.1596	125.9694	50.7501
11.50000	6.15028	14.83682	10.11989	2.30301	220.3076	236.3302	126.0733	49.7969
11.75000	6.16278	14.84887	10.12955	2.26880	220.9656	236.5136	126.1845	48.8443
12.00000	6.17483	14.86129	10.13917	2.23471	221.6017	236.7092	126.3028	47.8943
12.25000	6.18632	14.87398	10.14874	2.20096	222.2126	236.9162	126.4278	46.9513
12.50000	6.19716	14.88682	10.15821	2.16782	222.7943	237.1340	126.5590	46.0207
12.75000	6.20729	14.89968	10.16755	2.13547	223.3439	237.3615	126.6960	45.1067
13.00000	6.21673	14.91248	10.17674	2.10405	223.8599	237.5979	126.8382	44.2121

13.25000	6.22539	14.92513	10.18575	2.07374	224.3397	237.8422	126.9850	43.3411
13.50000	6.23315	14.93750	10.19452	2.04483	224.7791	238.0936	127.1360	42.4993
13.75000	6.23990	14.94946	10.20299	2.01765	225.1734	238.3508	127.2904	41.6935
14.00000	6.24556	14.96085	10.21107	1.99252	225.5180	238.6126	127.4475	40.9299
14.25000	6.25009	14.97154	10.21870	1.96967	225.8100	238.8778	127.6066	40.2135
14.50000	6.25359	14.98145	10.22585	1.94911	226.0504	239.1452	127.7669	39.5455
14.75000	6.25621	14.99060	10.23252	1.93068	226.2428	239.4136	127.9279	38.9237
15.00000	6.25809	14.99903	10.23875	1.91413	226.3926	239.6821	128.0888	38.3445
15.25000	6.25936	15.00684	10.24461	1.89919	226.5050	239.9501	128.2493	37.8036
15.50000	6.26008	15.01410	10.25015	1.88567	226.5846	240.2167	128.4090	37.2977
15.75000	6.26031	15.02088	10.25540	1.87340	226.6351	240.4814	128.5676	36.8240
16.00000	6.26011	15.02724	10.26041	1.86224	226.6598	240.7437	128.7246	36.3799
16.25000	6.25953	15.03321	10.26519	1.85207	226.6618	241.0031	128.8798	35.9632
16.50000	6.25861	15.03883	10.26976	1.84280	226.6435	241.2593	129.0331	35.5721
16.75000	6.25740	15.04414	10.27415	1.83431	226.6075	241.5119	129.1841	35.2044
17.00000	6.25593	15.04915	10.27838	1.82654	226.5561	241.7606	129.3328	34.8585
17.25000	6.25426	15.05391	10.28245	1.81938	226.4914	242.0052	129.4789	34.5325
17.50000	6.25240	15.05844	10.28638	1.81277	226.4153	242.2455	129.6224	34.2249
17.75000	6.25040	15.06277	10.29019	1.80664	226.3295	242.4812	129.7631	33.9342
18.00000	6.24827	15.06690	10.29389	1.80093	226.2355	242.7124	129.9010	33.6591
18.25000	6.24605	15.07087	10.29748	1.79560	226.1348	242.9389	130.0360	33.3983
18.50000	6.24374	15.07468	10.30097	1.79061	226.0284	243.1606	130.1681	33.1509
18.75000	6.24137	15.07835	10.30437	1.78591	225.9174	243.3775	130.2973	32.9159
19.00000	6.23894	15.08190	10.30768	1.78149	225.8026	243.5895	130.4235	32.6924
19.25000	6.23648	15.08531	10.31090	1.77730	225.6849	243.7967	130.5467	32.4797
19.50000	6.23400	15.08862	10.31405	1.77334	225.5649	243.9990	130.6670	32.2771
19.75000	6.23149	15.09182	10.31711	1.76957	225.4433	244.1965	130.7843	32.0839
20.00000	6.22898	15.09492	10.32010	1.76600	225.3205	244.3892	130.8986	31.8997
20.25000	6.22647	15.09792	10.32302	1.76260	225.1969	244.5771	131.0101	31.7239
20.50000	6.22396	15.10083	10.32586	1.75935	225.0731	244.7603	131.1186	31.5560
20.75000	6.22146	15.10364	10.32863	1.75626	224.9493	244.9388	131.2243	31.3957
21.00000	6.21898	15.10638	10.33133	1.75331	224.8257	245.1126	131.3272	31.2425
21.25000	6.21652	15.10903	10.33396	1.75049	224.7028	245.2819	131.4272	31.0960
21.50000	6.21408	15.11160	10.33652	1.74780	224.5807	245.4467	131.5246	30.9561
21.75000	6.21167	15.11409	10.33901	1.74523	224.4595	245.6071	131.6192	30.8222
22.00000	6.20928	15.11650	10.34144	1.74277	224.3396	245.7631	131.7112	30.6942
22.25000	6.20693	15.11885	10.34380	1.74042	224.2209	245.9148	131.8005	30.5717
22.50000	6.20462	15.12112	10.34609	1.73818	224.1038	246.0624	131.8873	30.4546
22.75000	6.20233	15.12332	10.34832	1.73603	223.9882	246.2058	131.9716	30.3425
23.00000	6.20009	15.12546	10.35049	1.73397	223.8743	246.3451	132.0534	30.2352
23.25000	6.19788	15.12752	10.35259	1.73200	223.7621	246.4805	132.1328	30.1326
23.50000	6.19571	15.12953	10.35464	1.73012	223.6518	246.6120	132.2099	30.0343
23.75000	6.19359	15.13147	10.35663	1.72831	223.5434	246.7398	132.2846	29.9403
24.00000	6.19150	15.13336	10.35855	1.72659	223.4369	246.8638	132.3571	29.8503
24.25000	6.18946	15.13518	10.36042	1.72494	223.3324	246.9841	132.4273	29.7641
24.50000	6.18746	15.13695	10.36224	1.72335	223.2300	247.1010	132.4954	29.6816
24.75000	6.18550	15.13867	10.36400	1.72184	223.1296	247.2144	132.5614	29.6026
25.00000	6.18358	15.14033	10.36571	1.72039	223.0312	247.3243	132.6254	29.5270
25.25000	6.18170	15.14193	10.36736	1.71900	222.9350	247.4310	132.6873	29.4547
25.50000	6.17987	15.14349	10.36896	1.71767	222.8408	247.5345	132.7473	29.3854
25.75000	6.17808	15.14500	10.37052	1.71640	222.7487	247.6348	132.8054	29.3190
26.00000	6.17633	15.14646	10.37202	1.71518	222.6587	247.7321	132.8616	29.2555
26.25000	6.17463	15.14788	10.37348	1.71402	222.5708	247.8264	132.9161	29.1947
26.50000	6.17296	15.14925	10.37489	1.71290	222.4850	247.9178	132.9687	29.1365
26.75000	6.17134	15.15057	10.37625	1.71183	222.4012	248.0064	133.0197	29.0808
27.00000	6.16976	15.15186	10.37758	1.71081	222.3194	248.0922	133.0690	29.0274
27.25000	6.16821	15.15310	10.37886	1.70983	222.2397	248.1753	133.1167	28.9763
27.50000	6.16671	15.15431	10.38009	1.70889	222.1619	248.2559	133.1628	28.9274
27.75000	6.16525	15.15547	10.38129	1.70799	222.0862	248.3339	133.2073	28.8806
28.00000	6.16382	15.15660	10.38245	1.70713	222.0123	248.4094	133.2504	28.8358

28.25000	6.16244	15.15769	10.38356	1.70631	221.9404	248.4826	133.2921	28.7929
28.50000	6.16109	15.15875	10.38465	1.70552	221.8704	248.5534	133.3323	28.7518
28.75000	6.15977	15.15977	10.38569	1.70477	221.8023	248.6220	133.3712	28.7125
29.00000	6.15850	15.16076	10.38670	1.70404	221.7360	248.6884	133.4087	28.6749
29.25000	6.15726	15.16172	10.38768	1.70335	221.6715	248.7526	133.4450	28.6389
29.50000	6.15605	15.16264	10.38862	1.70269	221.6088	248.8148	133.4800	28.6044
29.75000	6.15488	15.16354	10.38953	1.70205	221.5478	248.8749	133.5138	28.5715
30.00000	6.15374	15.16441	10.39041	1.70145	221.4885	248.9331	133.5465	28.5399
30.25000	6.15263	15.16525	10.39125	1.70086	221.4309	248.9894	133.5780	28.5097
30.50000	6.15156	15.16606	10.39207	1.70031	221.3750	249.0439	133.6084	28.4808
30.75000	6.15052	15.16685	10.39286	1.69977	221.3206	249.0966	133.6377	28.4531
31.00000	6.14950	15.16761	10.39362	1.69926	221.2678	249.1476	133.6660	28.4266
31.25000	6.14852	15.16834	10.39436	1.69878	221.2166	249.1969	133.6933	28.4013
31.50000	6.14757	15.16905	10.39507	1.69831	221.1668	249.2445	133.7196	28.3771
31.75000	6.14664	15.16974	10.39575	1.69786	221.1185	249.2906	133.7450	28.3539
32.00000	6.14575	15.17041	10.39641	1.69743	221.0717	249.3352	133.7695	28.3317
32.25000	6.14488	15.17105	10.39705	1.69702	221.0262	249.3783	133.7931	28.3105
32.50000	6.14404	15.17167	10.39766	1.69663	220.9821	249.4199	133.8158	28.2902
32.75000	6.14322	15.17228	10.39825	1.69626	220.9394	249.4602	133.8377	28.2707
33.00000	6.14243	15.17286	10.39882	1.69590	220.8979	249.4991	133.8588	28.2522
33.25000	6.14166	15.17342	10.39936	1.69555	220.8578	249.5367	133.8791	28.2344
33.50000	6.14092	15.17397	10.39989	1.69522	220.8188	249.5731	133.8987	28.2174
33.75000	6.14020	15.17450	10.40040	1.69491	220.7811	249.6082	133.9176	28.2011
34.00000	6.13950	15.17501	10.40089	1.69461	220.7445	249.6421	133.9357	28.1856
34.25000	6.13882	15.17550	10.40136	1.69432	220.7091	249.6749	133.9532	28.1707
34.50000	6.13817	15.17598	10.40181	1.69404	220.6748	249.7066	133.9700	28.1565
34.75000	6.13754	15.17644	10.40224	1.69378	220.6416	249.7373	133.9862	28.1429
35.00000	6.13693	15.17689	10.40266	1.69353	220.6094	249.7668	134.0018	28.1299
35.25000	6.13633	15.17732	10.40306	1.69329	220.5783	249.7954	134.0168	28.1175
35.50000	6.13576	15.17773	10.40345	1.69305	220.5481	249.8230	134.0312	28.1056
35.75000	6.13520	15.17814	10.40382	1.69283	220.5190	249.8497	134.0451	28.0942
36.00000	6.13467	15.17853	10.40418	1.69262	220.4907	249.8755	134.0584	28.0834
36.25000	6.13415	15.17891	10.40453	1.69242	220.4634	249.9004	134.0712	28.0730
36.50000	6.13365	15.17927	10.40486	1.69223	220.4370	249.9244	134.0836	28.0631
36.75000	6.13316	15.17963	10.40517	1.69204	220.4114	249.9476	134.0954	28.0536
37.00000	6.13269	15.17997	10.40548	1.69186	220.3867	249.9700	134.1068	28.0445
37.25000	6.13224	15.18030	10.40577	1.69169	220.3628	249.9917	134.1177	28.0358
37.50000	6.13180	15.18062	10.40605	1.69153	220.3397	250.0126	134.1282	28.0275
37.75000	6.13137	15.18093	10.40632	1.69138	220.3173	250.0328	134.1383	28.0196
38.00000	6.13096	15.18123	10.40658	1.69123	220.2957	250.0523	134.1480	28.0120
38.25000	6.13057	15.18152	10.40683	1.69109	220.2748	250.0711	134.1573	28.0048
38.50000	6.13019	15.18180	10.40706	1.69095	220.2546	250.0893	134.1662	27.9979
38.75000	6.12982	15.18207	10.40729	1.69082	220.2351	250.1069	134.1747	27.9913
39.00000	6.12946	15.18234	10.40751	1.69070	220.2163	250.1238	134.1829	27.9849
39.25000	6.12912	15.18259	10.40772	1.69058	220.1981	250.1402	134.1908	27.9789
39.50000	6.12878	15.18284	10.40792	1.69046	220.1805	250.1560	134.1983	27.9731
39.75000	6.12846	15.18307	10.40811	1.69036	220.1635	250.1713	134.2056	27.9676
40.00000	6.12815	15.18330	10.40829	1.69025	220.1471	250.1860	134.2125	27.9624
40.25000	6.12785	15.18353	10.40847	1.69015	220.1313	250.2003	134.2192	27.9573
40.50000	6.12756	15.18374	10.40864	1.69006	220.1160	250.2140	134.2255	27.9525
40.75000	6.12728	15.18395	10.40880	1.68997	220.1012	250.2273	134.2316	27.9479
41.00000	6.12701	15.18416	10.40895	1.68988	220.0869	250.2401	134.2375	27.9435
41.25000	6.12675	15.18435	10.40910	1.68980	220.0732	250.2525	134.2430	27.9393
41.50000	6.12650	15.18454	10.40924	1.68972	220.0599	250.2644	134.2484	27.9353
41.75000	6.12626	15.18473	10.40937	1.68964	220.0471	250.2759	134.2535	27.9315
42.00000	6.12603	15.18490	10.40950	1.68957	220.0347	250.2871	134.2584	27.9278
42.25000	6.12580	15.18508	10.40962	1.68950	220.0227	250.2978	134.2631	27.9244
42.50000	6.12559	15.18524	10.40974	1.68943	220.0112	250.3082	134.2675	27.9210
42.75000	6.12538	15.18541	10.40985	1.68937	220.0001	250.3182	134.2718	27.9178
43.00000	6.12517	15.18556	10.40996	1.68931	219.9894	250.3279	134.2759	27.9148

43.25000	6.12498	15.18571	10.41005	1.68925	219.9791	250.3373	134.2798	27.9119
43.50000	6.12480	15.18587	10.41013	1.68920	219.9693	250.3463	134.2832	27.9091
43.75000	6.12464	15.18602	10.41020	1.68914	219.9601	250.3551	134.2864	27.9064
44.00000	6.12448	15.18617	10.41026	1.68910	219.9514	250.3635	134.2892	27.9039
44.25000	6.12432	15.18632	10.41031	1.68905	219.9430	250.3717	134.2918	27.9015
44.50000	6.12418	15.18647	10.41035	1.68900	219.9351	250.3796	134.2941	27.8992
44.75000	6.12404	15.18662	10.41038	1.68896	219.9275	250.3873	134.2962	27.8969
45.00000	6.12391	15.18677	10.41041	1.68892	219.9203	250.3947	134.2981	27.8948
45.25000	6.12378	15.18691	10.41043	1.68888	219.9134	250.4019	134.2999	27.8928
45.50000	6.12366	15.18705	10.41045	1.68884	219.9068	250.4089	134.3015	27.8909
45.75000	6.12354	15.18718	10.41047	1.68881	219.9005	250.4156	134.3029	27.8890
46.00000	6.12343	15.18732	10.41048	1.68877	219.8944	250.4222	134.3042	27.8872
46.25000	6.12332	15.18745	10.41049	1.68874	219.8885	250.4285	134.3054	27.8856
46.50000	6.12322	15.18757	10.41050	1.68871	219.8829	250.4347	134.3064	27.8839
46.75000	6.12312	15.18770	10.41050	1.68868	219.8775	250.4407	134.3074	27.8824
47.00000	6.12302	15.18782	10.41051	1.68865	219.8723	250.4465	134.3083	27.8809
47.25000	6.12293	15.18793	10.41051	1.68863	219.8673	250.4521	134.3091	27.8795
47.50000	6.12284	15.18805	10.41051	1.68860	219.8625	250.4575	134.3098	27.8782
47.75000	6.12275	15.18816	10.41052	1.68857	219.8579	250.4628	134.3104	27.8769
48.00000	6.12267	15.18827	10.41052	1.68855	219.8534	250.4679	134.3110	27.8756
48.25000	6.12259	15.18837	10.41051	1.68853	219.8491	250.4729	134.3115	27.8745
48.50000	6.12251	15.18847	10.41051	1.68850	219.8449	250.4778	134.3120	27.8733
48.75000	6.12244	15.18857	10.41051	1.68848	219.8409	250.4824	134.3124	27.8723
49.00000	6.12236	15.18867	10.41051	1.68846	219.8370	250.4870	134.3127	27.8712
49.25000	6.12229	15.18876	10.41050	1.68844	219.8333	250.4914	134.3130	27.8703
49.50000	6.12223	15.18885	10.41050	1.68843	219.8296	250.4957	134.3133	27.8693
49.75000	6.12216	15.18894	10.41049	1.68841	219.8261	250.4999	134.3135	27.8684
50.00000	6.12210	15.18903	10.41049	1.68839	219.8227	250.5039	134.3137	27.8676

TIME	CM	CAVM	PIM	PM
0.0	0.12901E+02	0.17196E+02	0.90000E+01	-0.51000E+00
0.25	0.12987E+02	0.17355E+02	0.91212E+01	-0.57368E+00
0.50	0.13054E+02	0.17485E+02	0.92208E+01	-0.63158E+00
0.75	0.13113E+02	0.17609E+02	0.93159E+01	-0.69196E+00
1.00	0.13158E+02	0.17712E+02	0.93957E+01	-0.74874E+00
1.25	0.13175E+02	0.17764E+02	0.94367E+01	-0.78860E+00
1.50	0.13175E+02	0.17787E+02	0.94547E+01	-0.81807E+00
1.75	0.13167E+02	0.17796E+02	0.94613E+01	-0.84232E+00
2.00	0.13153E+02	0.17793E+02	0.94592E+01	-0.86254E+00
2.25	0.13134E+02	0.17780E+02	0.94488E+01	-0.87907E+00
2.50	0.13110E+02	0.17759E+02	0.94323E+01	-0.89269E+00
2.75	0.13083E+02	0.17731E+02	0.94108E+01	-0.90407E+00
3.00	0.13048E+02	0.17688E+02	0.93771E+01	-0.90925E+00
3.25	0.13010E+02	0.17636E+02	0.93366E+01	-0.90981E+00
3.50	0.12974E+02	0.17587E+02	0.92992E+01	-0.91055E+00
3.75	0.12940E+02	0.17542E+02	0.92645E+01	-0.91125E+00
4.00	0.12909E+02	0.17500E+02	0.92322E+01	-0.91184E+00
4.25	0.12879E+02	0.17461E+02	0.92020E+01	-0.91229E+00
4.50	0.12852E+02	0.17424E+02	0.91739E+01	-0.91258E+00
4.75	0.12827E+02	0.17390E+02	0.91476E+01	-0.91269E+00
5.00	0.12803E+02	0.17358E+02	0.91230E+01	-0.91260E+00
5.25	0.12781E+02	0.17328E+02	0.91000E+01	-0.91230E+00
5.50	0.12760E+02	0.17299E+02	0.90785E+01	-0.91179E+00
5.75	0.12741E+02	0.17273E+02	0.90584E+01	-0.91104E+00
6.00	0.12724E+02	0.17248E+02	0.90397E+01	-0.91007E+00
6.25	0.12707E+02	0.17225E+02	0.90222E+01	-0.90885E+00
6.50	0.12692E+02	0.17203E+02	0.90057E+01	-0.90737E+00
6.75	0.12678E+02	0.17183E+02	0.89904E+01	-0.90564E+00
7.00	0.12665E+02	0.17164E+02	0.89761E+01	-0.90366E+00

7.25	0.12654E+02	0.17147E+02	0.89628E+01	-0.90141E+00
7.50	0.12643E+02	0.17130E+02	0.89503E+01	-0.89890E+00
7.75	0.12633E+02	0.17115E+02	0.89388E+01	-0.89613E+00
8.00	0.12624E+02	0.17100E+02	0.89280E+01	-0.89310E+00
8.25	0.12616E+02	0.17087E+02	0.89180E+01	-0.88980E+00
8.50	0.12609E+02	0.17075E+02	0.89087E+01	-0.88624E+00
8.75	0.12603E+02	0.17063E+02	0.89002E+01	-0.88243E+00
9.00	0.12597E+02	0.17053E+02	0.88923E+01	-0.87837E+00
9.25	0.12527E+02	0.16920E+02	0.87931E+01	-0.82875E+00
9.50	0.12504E+02	0.16877E+02	0.87610E+01	-0.81148E+00
9.75	0.12492E+02	0.16853E+02	0.87431E+01	-0.80082E+00
10.00	0.12483E+02	0.16835E+02	0.87294E+01	-0.79168E+00
10.25	0.12476E+02	0.16819E+02	0.87176E+01	-0.78307E+00
10.50	0.12470E+02	0.16805E+02	0.87074E+01	-0.77474E+00
10.75	0.12466E+02	0.16793E+02	0.86984E+01	-0.76660E+00
11.00	0.12462E+02	0.16782E+02	0.86906E+01	-0.75861E+00
11.25	0.12460E+02	0.16773E+02	0.86839E+01	-0.75072E+00
11.50	0.12458E+02	0.16765E+02	0.86780E+01	-0.74291E+00
11.75	0.12457E+02	0.16759E+02	0.86730E+01	-0.73515E+00
12.00	0.12457E+02	0.16753E+02	0.86688E+01	-0.72742E+00
12.25	0.12457E+02	0.16748E+02	0.86654E+01	-0.71975E+00
12.50	0.12459E+02	0.16745E+02	0.86627E+01	-0.71214E+00
12.75	0.12461E+02	0.16742E+02	0.86608E+01	-0.70464E+00
13.00	0.12464E+02	0.16740E+02	0.86597E+01	-0.69726E+00
13.25	0.12467E+02	0.16740E+02	0.86593E+01	-0.69003E+00
13.50	0.12471E+02	0.16740E+02	0.86597E+01	-0.68299E+00
13.75	0.12476E+02	0.16742E+02	0.86609E+01	-0.67619E+00
14.00	0.12481E+02	0.16745E+02	0.86630E+01	-0.66970E+00
14.25	0.12488E+02	0.16749E+02	0.86661E+01	-0.66358E+00
14.50	0.12495E+02	0.16754E+02	0.86700E+01	-0.65784E+00
14.75	0.12502E+02	0.16761E+02	0.86748E+01	-0.65249E+00
15.00	0.12510E+02	0.16768E+02	0.86802E+01	-0.64748E+00
15.25	0.12519E+02	0.16776E+02	0.86863E+01	-0.64278E+00
15.50	0.12528E+02	0.16785E+02	0.86927E+01	-0.63833E+00
15.75	0.12537E+02	0.16794E+02	0.86995E+01	-0.63411E+00
16.00	0.12546E+02	0.16804E+02	0.87066E+01	-0.63010E+00
16.25	0.12555E+02	0.16814E+02	0.87138E+01	-0.62626E+00
16.50	0.12564E+02	0.16824E+02	0.87212E+01	-0.62259E+00
16.75	0.12574E+02	0.16834E+02	0.87286E+01	-0.61906E+00
17.00	0.12583E+02	0.16844E+02	0.87361E+01	-0.61567E+00
17.25	0.12592E+02	0.16854E+02	0.87436E+01	-0.61240E+00
17.50	0.12601E+02	0.16864E+02	0.87511E+01	-0.60924E+00
17.75	0.12610E+02	0.16874E+02	0.87585E+01	-0.60618E+00
18.00	0.12619E+02	0.16884E+02	0.87658E+01	-0.60322E+00
18.25	0.12628E+02	0.16893E+02	0.87730E+01	-0.60034E+00
18.50	0.12636E+02	0.16903E+02	0.87800E+01	-0.59753E+00
18.75	0.12645E+02	0.16912E+02	0.87870E+01	-0.59480E+00
19.00	0.12653E+02	0.16921E+02	0.87938E+01	-0.59215E+00
19.25	0.12661E+02	0.16930E+02	0.88004E+01	-0.58956E+00
19.50	0.12669E+02	0.16939E+02	0.88069E+01	-0.58703E+00
19.75	0.12676E+02	0.16947E+02	0.88132E+01	-0.58457E+00
20.00	0.12684E+02	0.16956E+02	0.88194E+01	-0.58217E+00
20.25	0.12691E+02	0.16964E+02	0.88254E+01	-0.57983E+00
20.50	0.12698E+02	0.16971E+02	0.88312E+01	-0.57755E+00
20.75	0.12705E+02	0.16979E+02	0.88369E+01	-0.57532E+00
21.00	0.12712E+02	0.16986E+02	0.88424E+01	-0.57316E+00
21.25	0.12718E+02	0.16994E+02	0.88477E+01	-0.57105E+00
21.50	0.12724E+02	0.17000E+02	0.88530E+01	-0.56899E+00
21.75	0.12730E+02	0.17007E+02	0.88580E+01	-0.56699E+00
22.00	0.12736E+02	0.17014E+02	0.88629E+01	-0.56504E+00

22.25	0.12742E+02	0.17020E+02	0.88677E+01	-0.56315E+00
22.50	0.12748E+02	0.17026E+02	0.88723E+01	-0.56131E+00
22.75	0.12753E+02	0.17032E+02	0.88768E+01	-0.55952E+00
23.00	0.12758E+02	0.17038E+02	0.88811E+01	-0.55778E+00
23.25	0.12763E+02	0.17044E+02	0.88853E+01	-0.55609E+00
23.50	0.12768E+02	0.17049E+02	0.88894E+01	-0.55444E+00
23.75	0.12773E+02	0.17054E+02	0.88934E+01	-0.55285E+00
24.00	0.12778E+02	0.17060E+02	0.88972E+01	-0.55130E+00
24.25	0.12782E+02	0.17064E+02	0.89009E+01	-0.54980E+00
24.50	0.12786E+02	0.17069E+02	0.89045E+01	-0.54834E+00
24.75	0.12791E+02	0.17074E+02	0.89080E+01	-0.54693E+00
25.00	0.12795E+02	0.17078E+02	0.89114E+01	-0.54556E+00
25.25	0.12799E+02	0.17083E+02	0.89146E+01	-0.54423E+00
25.50	0.12802E+02	0.17087E+02	0.89178E+01	-0.54295E+00
25.75	0.12806E+02	0.17091E+02	0.89208E+01	-0.54170E+00
26.00	0.12810E+02	0.17095E+02	0.89238E+01	-0.54049E+00
26.25	0.12813E+02	0.17099E+02	0.89266E+01	-0.53932E+00
26.50	0.12816E+02	0.17102E+02	0.89294E+01	-0.53819E+00
26.75	0.12820E+02	0.17106E+02	0.89321E+01	-0.53709E+00
27.00	0.12823E+02	0.17109E+02	0.89347E+01	-0.53603E+00
27.25	0.12826E+02	0.17113E+02	0.89371E+01	-0.53500E+00
27.50	0.12829E+02	0.17116E+02	0.89396E+01	-0.53401E+00
27.75	0.12831E+02	0.17119E+02	0.89419E+01	-0.53305E+00
28.00	0.12834E+02	0.17122E+02	0.89441E+01	-0.53212E+00
28.25	0.12837E+02	0.17125E+02	0.89463E+01	-0.53122E+00
28.50	0.12839E+02	0.17128E+02	0.89484E+01	-0.53035E+00
28.75	0.12842E+02	0.17130E+02	0.89505E+01	-0.52952E+00
29.00	0.12844E+02	0.17133E+02	0.89524E+01	-0.52871E+00
29.25	0.12846E+02	0.17135E+02	0.89543E+01	-0.52792E+00
29.50	0.12849E+02	0.17138E+02	0.89561E+01	-0.52717E+00
29.75	0.12851E+02	0.17140E+02	0.89579E+01	-0.52644E+00
30.00	0.12853E+02	0.17142E+02	0.89596E+01	-0.52573E+00
30.25	0.12855E+02	0.17145E+02	0.89612E+01	-0.52505E+00
30.50	0.12857E+02	0.17147E+02	0.89628E+01	-0.52439E+00
30.75	0.12859E+02	0.17149E+02	0.89644E+01	-0.52376E+00
31.00	0.12860E+02	0.17151E+02	0.89658E+01	-0.52315E+00
31.25	0.12862E+02	0.17153E+02	0.89673E+01	-0.52256E+00
31.50	0.12864E+02	0.17154E+02	0.89686E+01	-0.52199E+00
31.75	0.12865E+02	0.17156E+02	0.89700E+01	-0.52144E+00
32.00	0.12867E+02	0.17158E+02	0.89712E+01	-0.52091E+00
32.25	0.12868E+02	0.17159E+02	0.89725E+01	-0.52040E+00
32.50	0.12870E+02	0.17161E+02	0.89736E+01	-0.51991E+00
32.75	0.12871E+02	0.17163E+02	0.89748E+01	-0.51944E+00
33.00	0.12873E+02	0.17164E+02	0.89759E+01	-0.51898E+00
33.25	0.12874E+02	0.17165E+02	0.89769E+01	-0.51854E+00
33.50	0.12875E+02	0.17167E+02	0.89780E+01	-0.51812E+00
33.75	0.12876E+02	0.17168E+02	0.89789E+01	-0.51771E+00
34.00	0.12877E+02	0.17169E+02	0.89799E+01	-0.51732E+00
34.25	0.12878E+02	0.17171E+02	0.89808E+01	-0.51694E+00
34.50	0.12879E+02	0.17172E+02	0.89817E+01	-0.51658E+00
34.75	0.12881E+02	0.17173E+02	0.89825E+01	-0.51623E+00
35.00	0.12881E+02	0.17174E+02	0.89833E+01	-0.51589E+00
35.25	0.12882E+02	0.17175E+02	0.89841E+01	-0.51557E+00
35.50	0.12883E+02	0.17176E+02	0.89849E+01	-0.51526E+00
35.75	0.12884E+02	0.17177E+02	0.89856E+01	-0.51496E+00
36.00	0.12885E+02	0.17178E+02	0.89863E+01	-0.51467E+00
36.25	0.12886E+02	0.17179E+02	0.89870E+01	-0.51440E+00
36.50	0.12887E+02	0.17180E+02	0.89876E+01	-0.51413E+00
36.75	0.12887E+02	0.17180E+02	0.89882E+01	-0.51388E+00
37.00	0.12888E+02	0.17181E+02	0.89888E+01	-0.51363E+00

37.25	0.12889E+02	0.17182E+02	0.89894E+01	-0.51340E+00
37.50	0.12889E+02	0.17183E+02	0.89899E+01	-0.51317E+00
37.75	0.12890E+02	0.17183E+02	0.89905E+01	-0.51296E+00
38.00	0.12891E+02	0.17184E+02	0.89910E+01	-0.51275E+00
38.25	0.12891E+02	0.17185E+02	0.89915E+01	-0.51255E+00
38.50	0.12892E+02	0.17185E+02	0.89919E+01	-0.51236E+00
38.75	0.12892E+02	0.17186E+02	0.89924E+01	-0.51218E+00
39.00	0.12893E+02	0.17186E+02	0.89928E+01	-0.51200E+00
39.25	0.12893E+02	0.17187E+02	0.89932E+01	-0.51183E+00
39.50	0.12894E+02	0.17187E+02	0.89936E+01	-0.51167E+00
39.75	0.12894E+02	0.17188E+02	0.89940E+01	-0.51152E+00
40.00	0.12895E+02	0.17188E+02	0.89944E+01	-0.51137E+00
40.25	0.12895E+02	0.17189E+02	0.89947E+01	-0.51123E+00
40.50	0.12896E+02	0.17189E+02	0.89951E+01	-0.51109E+00
40.75	0.12896E+02	0.17190E+02	0.89954E+01	-0.51097E+00
41.00	0.12896E+02	0.17190E+02	0.89957E+01	-0.51084E+00
41.25	0.12897E+02	0.17191E+02	0.89960E+01	-0.51072E+00
41.50	0.12897E+02	0.17191E+02	0.89963E+01	-0.51061E+00
41.75	0.12897E+02	0.17191E+02	0.89965E+01	-0.51050E+00
42.00	0.12898E+02	0.17192E+02	0.89968E+01	-0.51040E+00
42.25	0.12898E+02	0.17192E+02	0.89971E+01	-0.51030E+00
42.50	0.12898E+02	0.17192E+02	0.89973E+01	-0.51021E+00
42.75	0.12899E+02	0.17193E+02	0.89975E+01	-0.51012E+00
43.00	0.12899E+02	0.17193E+02	0.89977E+01	-0.51004E+00
43.25	0.12899E+02	0.17193E+02	0.89980E+01	-0.50996E+00
43.50	0.12899E+02	0.17193E+02	0.89982E+01	-0.50991E+00
43.75	0.12899E+02	0.17194E+02	0.89983E+01	-0.50986E+00
44.00	0.12900E+02	0.17194E+02	0.89985E+01	-0.50982E+00
44.25	0.12900E+02	0.17194E+02	0.89987E+01	-0.50979E+00
44.50	0.12900E+02	0.17194E+02	0.89989E+01	-0.50977E+00
44.75	0.12900E+02	0.17195E+02	0.89990E+01	-0.50974E+00
45.00	0.12900E+02	0.17195E+02	0.89991E+01	-0.50972E+00
45.25	0.12901E+02	0.17195E+02	0.89993E+01	-0.50971E+00
45.50	0.12901E+02	0.17195E+02	0.89994E+01	-0.50969E+00
45.75	0.12901E+02	0.17195E+02	0.89995E+01	-0.50968E+00
46.00	0.12901E+02	0.17195E+02	0.89996E+01	-0.50967E+00
46.25	0.12901E+02	0.17196E+02	0.89997E+01	-0.50967E+00
46.50	0.12901E+02	0.17196E+02	0.89998E+01	-0.50966E+00
46.75	0.12901E+02	0.17196E+02	0.89999E+01	-0.50966E+00
47.00	0.12901E+02	0.17196E+02	0.90000E+01	-0.50965E+00
47.25	0.12901E+02	0.17196E+02	0.90000E+01	-0.50965E+00
47.50	0.12901E+02	0.17196E+02	0.90001E+01	-0.50965E+00
47.75	0.12901E+02	0.17196E+02	0.90002E+01	-0.50965E+00
48.00	0.12901E+02	0.17196E+02	0.90002E+01	-0.50965E+00
48.25	0.12902E+02	0.17196E+02	0.90003E+01	-0.50965E+00
48.50	0.12902E+02	0.17196E+02	0.90003E+01	-0.50965E+00
48.75	0.12902E+02	0.17196E+02	0.90004E+01	-0.50965E+00
49.00	0.12902E+02	0.17196E+02	0.90004E+01	-0.50966E+00
49.25	0.12902E+02	0.17196E+02	0.90004E+01	-0.50966E+00
49.50	0.12902E+02	0.17197E+02	0.90005E+01	-0.50966E+00
49.75	0.12902E+02	0.17197E+02	0.90005E+01	-0.50967E+00
50.00	0.12902E+02	0.17197E+02	0.90005E+01	-0.50967E+00

TIME	FM	VPLM	RM	LM	QPLM	QLM	QDM
0.0	0.59956E+00	0.81888E-01	0.85155E+00	0.26025E+00	0.29398E+01	0.33575E+01	0.25957E-15
0.25	0.67000E+00	0.73988E-01	0.77173E+00	0.25761E+00	0.25904E+01	0.33457E+01	0.24502E-15
0.50	0.71863E+00	0.59690E-01	0.81526E+00	0.25520E+00	0.20537E+01	0.33314E+01	0.23483E-15
0.75	0.76279E+00	0.45909E-01	0.86471E+00	0.25270E+00	0.15543E+01	0.33136E+01	0.22546E-15

1.00	0.80368E+00	0.39980E-01	0.83615E+00	0.25034E+00	0.13323E+01	0.32940E+01	0.21667E-15
1.25	0.82506E+00	0.40560E-01	0.78270E+00	0.24869E+00	0.13406E+01	0.32763E+01	0.21215E-15
1.50	0.83427E+00	0.40989E-01	0.75969E+00	0.24746E+00	0.13505E+01	0.32603E+01	0.21038E-15
1.75	0.84003E+00	0.41342E-01	0.74530E+00	0.24646E+00	0.13594E+01	0.32451E+01	0.20937E-15
2.00	0.84516E+00	0.41636E-01	0.73246E+00	0.24562E+00	0.13662E+01	0.32307E+01	0.20846E-15
2.25	0.84968E+00	0.41876E-01	0.72117E+00	0.24493E+00	0.13712E+01	0.32169E+01	0.20767E-15
2.50	0.85299E+00	0.42074E-01	0.71289E+00	0.24437E+00	0.13751E+01	0.32037E+01	0.20713E-15
2.75	0.85577E+00	0.42240E-01	0.70596E+00	0.24389E+00	0.13781E+01	0.31910E+01	0.20670E-15
3.00	0.85320E+00	0.47272E-01	0.65832E+00	0.24368E+00	0.15429E+01	0.31796E+01	0.20748E-15
3.25	0.84316E+00	0.50060E-01	0.65311E+00	0.24365E+00	0.16403E+01	0.31699E+01	0.20999E-15
3.50	0.83398E+00	0.52756E-01	0.64678E+00	0.24362E+00	0.17348E+01	0.31607E+01	0.21228E-15
3.75	0.82540E+00	0.55320E-01	0.64039E+00	0.24360E+00	0.18252E+01	0.31521E+01	0.21442E-15
4.00	0.81731E+00	0.57759E-01	0.63412E+00	0.24357E+00	0.19116E+01	0.31442E+01	0.21643E-15
4.25	0.80964E+00	0.60084E-01	0.62801E+00	0.24355E+00	0.19943E+01	0.31368E+01	0.21832E-15
4.50	0.80234E+00	0.62303E-01	0.62210E+00	0.24354E+00	0.20738E+01	0.31300E+01	0.22011E-15
4.75	0.79539E+00	0.64426E-01	0.61634E+00	0.24354E+00	0.21501E+01	0.31238E+01	0.22182E-15
5.00	0.78875E+00	0.66463E-01	0.61073E+00	0.24354E+00	0.22237E+01	0.31180E+01	0.22343E-15
5.25	0.78238E+00	0.68421E-01	0.60524E+00	0.24355E+00	0.22948E+01	0.31128E+01	0.22497E-15
5.50	0.77627E+00	0.70307E-01	0.59988E+00	0.24357E+00	0.23635E+01	0.31081E+01	0.22644E-15
5.75	0.77039E+00	0.72126E-01	0.59462E+00	0.24360E+00	0.24300E+01	0.31038E+01	0.22785E-15
6.00	0.76475E+00	0.73876E-01	0.58949E+00	0.24364E+00	0.24943E+01	0.31001E+01	0.22919E-15
6.25	0.75930E+00	0.75570E-01	0.58445E+00	0.24369E+00	0.25567E+01	0.30967E+01	0.23048E-15
6.50	0.75401E+00	0.77216E-01	0.57949E+00	0.24376E+00	0.26176E+01	0.30938E+01	0.23171E-15
6.75	0.74889E+00	0.78811E-01	0.57462E+00	0.24383E+00	0.26769E+01	0.30913E+01	0.23290E-15
7.00	0.74393E+00	0.80357E-01	0.56983E+00	0.24391E+00	0.27345E+01	0.30892E+01	0.23405E-15
7.25	0.73913E+00	0.81858E-01	0.56513E+00	0.24400E+00	0.27906E+01	0.30875E+01	0.23515E-15
7.50	0.73446E+00	0.83315E-01	0.56051E+00	0.24411E+00	0.28452E+01	0.30862E+01	0.23620E-15
7.75	0.72993E+00	0.84729E-01	0.55597E+00	0.24422E+00	0.28985E+01	0.30853E+01	0.23722E-15
8.00	0.72553E+00	0.86104E-01	0.55151E+00	0.24435E+00	0.29503E+01	0.30847E+01	0.23820E-15
8.25	0.72125E+00	0.87439E-01	0.54713E+00	0.24449E+00	0.30009E+01	0.30845E+01	0.23915E-15
8.50	0.71709E+00	0.88736E-01	0.54282E+00	0.24463E+00	0.30501E+01	0.30846E+01	0.24006E-15
8.75	0.71304E+00	0.89997E-01	0.53859E+00	0.24479E+00	0.30981E+01	0.30851E+01	0.24094E-15
9.00	0.70911E+00	0.91217E-01	0.53445E+00	0.24496E+00	0.31447E+01	0.30859E+01	0.24178E-15
9.25	0.93982E+00	0.93114E-01	0.65872E+00	0.24702E+00	0.32849E+01	0.30944E+01	0.25477E-15
9.50	0.92397E+00	0.92102E-01	0.70665E+00	0.24774E+00	0.32670E+01	0.30977E+01	0.25805E-15
9.75	0.91744E+00	0.92749E-01	0.71422E+00	0.24818E+00	0.32966E+01	0.31003E+01	0.25937E-15
10.00	0.91284E+00	0.93685E-01	0.71407E+00	0.24856E+00	0.33343E+01	0.31028E+01	0.26029E-15
10.25	0.90874E+00	0.94654E-01	0.71236E+00	0.24892E+00	0.33728E+01	0.31055E+01	0.26109E-15
10.50	0.90489E+00	0.95609E-01	0.71026E+00	0.24926E+00	0.34106E+01	0.31084E+01	0.26184E-15
10.75	0.90122E+00	0.96540E-01	0.70801E+00	0.24960E+00	0.34476E+01	0.31115E+01	0.26255E-15
11.00	0.89770E+00	0.97444E-01	0.70568E+00	0.24993E+00	0.34835E+01	0.31147E+01	0.26322E-15
11.25	0.89433E+00	0.98319E-01	0.70330E+00	0.25026E+00	0.35184E+01	0.31181E+01	0.26385E-15
11.50	0.89110E+00	0.99167E-01	0.70090E+00	0.25058E+00	0.35522E+01	0.31218E+01	0.26445E-15
11.75	0.88800E+00	0.99984E-01	0.69851E+00	0.25090E+00	0.35849E+01	0.31255E+01	0.26501E-15
12.00	0.88502E+00	0.10077E+00	0.69618E+00	0.25123E+00	0.36164E+01	0.31295E+01	0.26555E-15
12.25	0.88215E+00	0.10151E+00	0.69401E+00	0.25154E+00	0.36464E+01	0.31336E+01	0.26606E-15
12.50	0.87940E+00	0.10221E+00	0.69209E+00	0.25186E+00	0.36745E+01	0.31379E+01	0.26654E-15
12.75	0.87679E+00	0.10286E+00	0.69039E+00	0.25217E+00	0.37008E+01	0.31423E+01	0.26699E-15
13.00	0.87432E+00	0.10345E+00	0.68888E+00	0.25248E+00	0.37252E+01	0.31468E+01	0.26741E-15
13.25	0.87201E+00	0.10399E+00	0.68763E+00	0.25278E+00	0.37474E+01	0.31514E+01	0.26779E-15
13.50	0.86986E+00	0.10447E+00	0.68672E+00	0.25307E+00	0.37672E+01	0.31560E+01	0.26814E-15
13.75	0.86786E+00	0.10487E+00	0.68622E+00	0.25335E+00	0.37843E+01	0.31608E+01	0.26845E-15
14.00	0.86605E+00	0.10520E+00	0.68615E+00	0.25362E+00	0.37985E+01	0.31655E+01	0.26872E-15
14.25	0.86446E+00	0.10544E+00	0.68646E+00	0.25388E+00	0.38096E+01	0.31703E+01	0.26895E-15
14.50	0.86310E+00	0.10562E+00	0.68701E+00	0.25411E+00	0.38179E+01	0.31750E+01	0.26913E-15
14.75	0.86200E+00	0.10574E+00	0.68763E+00	0.25434E+00	0.38238E+01	0.31797E+01	0.26926E-15
15.00	0.86114E+00	0.10581E+00	0.68825E+00	0.25454E+00	0.38277E+01	0.31844E+01	0.26934E-15
15.25	0.86050E+00	0.10583E+00	0.68883E+00	0.25474E+00	0.38297E+01	0.31890E+01	0.26937E-15
15.50	0.86004E+00	0.10582E+00	0.68938E+00	0.25492E+00	0.38302E+01	0.31936E+01	0.26937E-15
15.75	0.85975E+00	0.10578E+00	0.68993E+00	0.25510E+00	0.38293E+01	0.31981E+01	0.26933E-15

16.00	0.85959E+00	0.10570E+00	0.69048E+00	0.25527E+00	0.38272E+01	0.32025E+01	0.26927E-15
16.25	0.85956E+00	0.10560E+00	0.69104E+00	0.25542E+00	0.38240E+01	0.32069E+01	0.26919E-15
16.50	0.85963E+00	0.10548E+00	0.69161E+00	0.25558E+00	0.38199E+01	0.32112E+01	0.26908E-15
16.75	0.85979E+00	0.10534E+00	0.69219E+00	0.25572E+00	0.38149E+01	0.32154E+01	0.26896E-15
17.00	0.86003E+00	0.10518E+00	0.69277E+00	0.25586E+00	0.38092E+01	0.32195E+01	0.26882E-15
17.25	0.86035E+00	0.10501E+00	0.69335E+00	0.25600E+00	0.38029E+01	0.32236E+01	0.26868E-15
17.50	0.86072E+00	0.10483E+00	0.69393E+00	0.25613E+00	0.37960E+01	0.32276E+01	0.26852E-15
17.75	0.86114E+00	0.10463E+00	0.69451E+00	0.25626E+00	0.37888E+01	0.32315E+01	0.26835E-15
18.00	0.86160E+00	0.10443E+00	0.69508E+00	0.25638E+00	0.37812E+01	0.32353E+01	0.26817E-15
18.25	0.86209E+00	0.10422E+00	0.69566E+00	0.25650E+00	0.37734E+01	0.32391E+01	0.26800E-15
18.50	0.86261E+00	0.10401E+00	0.69623E+00	0.25662E+00	0.37653E+01	0.32427E+01	0.26781E-15
18.75	0.86315E+00	0.10379E+00	0.69680E+00	0.25673E+00	0.37570E+01	0.32463E+01	0.26763E-15
19.00	0.86371E+00	0.10358E+00	0.69738E+00	0.25684E+00	0.37487E+01	0.32498E+01	0.26744E-15
19.25	0.86428E+00	0.10335E+00	0.69795E+00	0.25695E+00	0.37402E+01	0.32532E+01	0.26725E-15
19.50	0.86486E+00	0.10313E+00	0.69852E+00	0.25705E+00	0.37317E+01	0.32566E+01	0.26707E-15
19.75	0.86545E+00	0.10291E+00	0.69909E+00	0.25715E+00	0.37231E+01	0.32598E+01	0.26688E-15
20.00	0.86603E+00	0.10269E+00	0.69966E+00	0.25725E+00	0.37146E+01	0.32630E+01	0.26669E-15
20.25	0.86662E+00	0.10247E+00	0.70023E+00	0.25735E+00	0.37060E+01	0.32661E+01	0.26651E-15
20.50	0.86721E+00	0.10225E+00	0.70079E+00	0.25745E+00	0.36975E+01	0.32691E+01	0.26633E-15
20.75	0.86780E+00	0.10203E+00	0.70135E+00	0.25754E+00	0.36891E+01	0.32720E+01	0.26615E-15
21.00	0.86838E+00	0.10181E+00	0.70191E+00	0.25763E+00	0.36807E+01	0.32749E+01	0.26597E-15
21.25	0.86896E+00	0.10160E+00	0.70246E+00	0.25772E+00	0.36724E+01	0.32776E+01	0.26579E-15
21.50	0.86953E+00	0.10139E+00	0.70301E+00	0.25780E+00	0.36642E+01	0.32803E+01	0.26562E-15
21.75	0.87010E+00	0.10118E+00	0.70356E+00	0.25788E+00	0.36561E+01	0.32830E+01	0.26545E-15
22.00	0.87066E+00	0.10097E+00	0.70410E+00	0.25797E+00	0.36481E+01	0.32855E+01	0.26529E-15
22.25	0.87121E+00	0.10077E+00	0.70463E+00	0.25804E+00	0.36403E+01	0.32880E+01	0.26512E-15
22.50	0.87175E+00	0.10057E+00	0.70515E+00	0.25812E+00	0.36325E+01	0.32904E+01	0.26496E-15
22.75	0.87228E+00	0.10038E+00	0.70567E+00	0.25819E+00	0.36249E+01	0.32927E+01	0.26481E-15
23.00	0.87281E+00	0.10018E+00	0.70618E+00	0.25827E+00	0.36174E+01	0.32950E+01	0.26465E-15
23.25	0.87333E+00	0.99994E-01	0.70668E+00	0.25834E+00	0.36101E+01	0.32972E+01	0.26450E-15
23.50	0.87383E+00	0.99808E-01	0.70717E+00	0.25841E+00	0.36029E+01	0.32994E+01	0.26435E-15
23.75	0.87433E+00	0.99627E-01	0.70766E+00	0.25847E+00	0.35958E+01	0.33014E+01	0.26421E-15
24.00	0.87482E+00	0.99449E-01	0.70813E+00	0.25854E+00	0.35889E+01	0.33035E+01	0.26407E-15
24.25	0.87529E+00	0.99275E-01	0.70860E+00	0.25860E+00	0.35821E+01	0.33054E+01	0.26393E-15
24.50	0.87576E+00	0.99105E-01	0.70906E+00	0.25866E+00	0.35755E+01	0.33073E+01	0.26380E-15
24.75	0.87622E+00	0.98938E-01	0.70951E+00	0.25872E+00	0.35690E+01	0.33091E+01	0.26367E-15
25.00	0.87666E+00	0.98776E-01	0.70995E+00	0.25877E+00	0.35627E+01	0.33109E+01	0.26354E-15
25.25	0.87710E+00	0.98617E-01	0.71037E+00	0.25883E+00	0.35565E+01	0.33126E+01	0.26341E-15
25.50	0.87753E+00	0.98461E-01	0.71080E+00	0.25888E+00	0.35504E+01	0.33143E+01	0.26329E-15
25.75	0.87795E+00	0.98310E-01	0.71121E+00	0.25893E+00	0.35445E+01	0.33159E+01	0.26317E-15
26.00	0.87835E+00	0.98162E-01	0.71161E+00	0.25898E+00	0.35388E+01	0.33175E+01	0.26306E-15
26.25	0.87875E+00	0.98018E-01	0.71200E+00	0.25903E+00	0.35332E+01	0.33190E+01	0.26295E-15
26.50	0.87914E+00	0.97878E-01	0.71238E+00	0.25908E+00	0.35277E+01	0.33205E+01	0.26284E-15
26.75	0.87952E+00	0.97741E-01	0.71276E+00	0.25913E+00	0.35224E+01	0.33219E+01	0.26273E-15
27.00	0.87988E+00	0.97608E-01	0.71312E+00	0.25917E+00	0.35172E+01	0.33233E+01	0.26263E-15
27.25	0.88024E+00	0.97478E-01	0.71348E+00	0.25921E+00	0.35121E+01	0.33246E+01	0.26253E-15
27.50	0.88059E+00	0.97352E-01	0.71382E+00	0.25925E+00	0.35072E+01	0.33259E+01	0.26243E-15
27.75	0.88093E+00	0.97229E-01	0.71416E+00	0.25929E+00	0.35024E+01	0.33271E+01	0.26234E-15
28.00	0.88126E+00	0.97109E-01	0.71449E+00	0.25933E+00	0.34977E+01	0.33283E+01	0.26224E-15
28.25	0.88159E+00	0.96993E-01	0.71481E+00	0.25937E+00	0.34932E+01	0.33295E+01	0.26215E-15
28.50	0.88190E+00	0.96880E-01	0.71512E+00	0.25941E+00	0.34888E+01	0.33306E+01	0.26207E-15
28.75	0.88220E+00	0.96770E-01	0.71543E+00	0.25944E+00	0.34845E+01	0.33317E+01	0.26198E-15
29.00	0.88250E+00	0.96663E-01	0.71572E+00	0.25947E+00	0.34803E+01	0.33327E+01	0.26190E-15
29.25	0.88279E+00	0.96559E-01	0.71601E+00	0.25951E+00	0.34763E+01	0.33337E+01	0.26182E-15
29.50	0.88307E+00	0.96458E-01	0.71629E+00	0.25954E+00	0.34724E+01	0.33347E+01	0.26174E-15
29.75	0.88334E+00	0.96360E-01	0.71656E+00	0.25957E+00	0.34685E+01	0.33357E+01	0.26167E-15
30.00	0.88361E+00	0.96265E-01	0.71682E+00	0.25960E+00	0.34648E+01	0.33366E+01	0.26160E-15
30.25	0.88386E+00	0.96173E-01	0.71708E+00	0.25963E+00	0.34612E+01	0.33374E+01	0.26153E-15
30.50	0.88411E+00	0.96084E-01	0.71733E+00	0.25965E+00	0.34577E+01	0.33383E+01	0.26146E-15
30.75	0.88435E+00	0.95997E-01	0.71757E+00	0.25968E+00	0.34544E+01	0.33391E+01	0.26139E-15

31.00	0.88459E+00	0.95912E-01	0.71780E+00	0.25970E+00	0.34511E+01	0.33399E+01	0.26133E-15
31.25	0.88482E+00	0.95831E-01	0.71803E+00	0.25973E+00	0.34479E+01	0.33407E+01	0.26127E-15
31.50	0.88504E+00	0.95752E-01	0.71825E+00	0.25975E+00	0.34448E+01	0.33414E+01	0.26121E-15
31.75	0.88525E+00	0.95675E-01	0.71847E+00	0.25978E+00	0.34418E+01	0.33421E+01	0.26115E-15
32.00	0.88546E+00	0.95600E-01	0.71867E+00	0.25980E+00	0.34389E+01	0.33428E+01	0.26109E-15
32.25	0.88566E+00	0.95528E-01	0.71888E+00	0.25982E+00	0.34361E+01	0.33434E+01	0.26104E-15
32.50	0.88586E+00	0.95458E-01	0.71907E+00	0.25984E+00	0.34333E+01	0.33441E+01	0.26098E-15
32.75	0.88605E+00	0.95390E-01	0.71926E+00	0.25986E+00	0.34307E+01	0.33447E+01	0.26093E-15
33.00	0.88623E+00	0.95325E-01	0.71945E+00	0.25988E+00	0.34281E+01	0.33453E+01	0.26088E-15
33.25	0.88641E+00	0.95261E-01	0.71962E+00	0.25990E+00	0.34257E+01	0.33458E+01	0.26084E-15
33.50	0.88658E+00	0.95200E-01	0.71980E+00	0.25991E+00	0.34233E+01	0.33464E+01	0.26079E-15
33.75	0.88675E+00	0.95140E-01	0.71996E+00	0.25993E+00	0.34209E+01	0.33469E+01	0.26074E-15
34.00	0.88691E+00	0.95083E-01	0.72013E+00	0.25995E+00	0.34187E+01	0.33474E+01	0.26070E-15
34.25	0.88706E+00	0.95027E-01	0.72028E+00	0.25996E+00	0.34165E+01	0.33479E+01	0.26066E-15
34.50	0.88722E+00	0.94973E-01	0.72044E+00	0.25998E+00	0.34144E+01	0.33484E+01	0.26062E-15
34.75	0.88736E+00	0.94921E-01	0.72058E+00	0.25999E+00	0.34124E+01	0.33488E+01	0.26058E-15
35.00	0.88750E+00	0.94870E-01	0.72073E+00	0.26001E+00	0.34104E+01	0.33493E+01	0.26054E-15
35.25	0.88764E+00	0.94821E-01	0.72086E+00	0.26002E+00	0.34085E+01	0.33497E+01	0.26051E-15
35.50	0.88777E+00	0.94774E-01	0.72100E+00	0.26003E+00	0.34066E+01	0.33501E+01	0.26047E-15
35.75	0.88790E+00	0.94729E-01	0.72113E+00	0.26004E+00	0.34048E+01	0.33505E+01	0.26044E-15
36.00	0.88803E+00	0.94684E-01	0.72125E+00	0.26006E+00	0.34031E+01	0.33508E+01	0.26040E-15
36.25	0.88815E+00	0.94642E-01	0.72137E+00	0.26007E+00	0.34015E+01	0.33512E+01	0.26037E-15
36.50	0.88826E+00	0.94601E-01	0.72149E+00	0.26008E+00	0.33998E+01	0.33515E+01	0.26034E-15
36.75	0.88838E+00	0.94561E-01	0.72160E+00	0.26009E+00	0.33983E+01	0.33519E+01	0.26031E-15
37.00	0.88848E+00	0.94522E-01	0.72171E+00	0.26010E+00	0.33968E+01	0.33522E+01	0.26028E-15
37.25	0.88859E+00	0.94485E-01	0.72182E+00	0.26011E+00	0.33953E+01	0.33525E+01	0.26025E-15
37.50	0.88869E+00	0.94449E-01	0.72192E+00	0.26012E+00	0.33939E+01	0.33528E+01	0.26023E-15
37.75	0.88879E+00	0.94414E-01	0.72202E+00	0.26013E+00	0.33926E+01	0.33531E+01	0.26020E-15
38.00	0.88888E+00	0.94381E-01	0.72212E+00	0.26014E+00	0.33913E+01	0.33533E+01	0.26018E-15
38.25	0.88898E+00	0.94348E-01	0.72221E+00	0.26014E+00	0.33900E+01	0.33536E+01	0.26015E-15
38.50	0.88906E+00	0.94317E-01	0.72230E+00	0.26015E+00	0.33888E+01	0.33538E+01	0.26013E-15
38.75	0.88915E+00	0.94287E-01	0.72238E+00	0.26016E+00	0.33876E+01	0.33541E+01	0.26011E-15
39.00	0.88923E+00	0.94258E-01	0.72247E+00	0.26017E+00	0.33865E+01	0.33543E+01	0.26009E-15
39.25	0.88931E+00	0.94230E-01	0.72255E+00	0.26017E+00	0.33854E+01	0.33545E+01	0.26006E-15
39.50	0.88939E+00	0.94203E-01	0.72263E+00	0.26018E+00	0.33843E+01	0.33547E+01	0.26004E-15
39.75	0.88946E+00	0.94176E-01	0.72270E+00	0.26019E+00	0.33833E+01	0.33549E+01	0.26003E-15
40.00	0.88953E+00	0.94151E-01	0.72277E+00	0.26019E+00	0.33823E+01	0.33551E+01	0.26001E-15
40.25	0.88960E+00	0.94127E-01	0.72284E+00	0.26020E+00	0.33813E+01	0.33553E+01	0.25999E-15
40.50	0.88967E+00	0.94103E-01	0.72291E+00	0.26020E+00	0.33804E+01	0.33555E+01	0.25997E-15
40.75	0.88974E+00	0.94081E-01	0.72298E+00	0.26021E+00	0.33795E+01	0.33557E+01	0.25995E-15
41.00	0.88980E+00	0.94059E-01	0.72304E+00	0.26022E+00	0.33787E+01	0.33558E+01	0.25994E-15
41.25	0.88986E+00	0.94038E-01	0.72310E+00	0.26022E+00	0.33778E+01	0.33560E+01	0.25992E-15
41.50	0.88992E+00	0.94017E-01	0.72316E+00	0.26022E+00	0.33770E+01	0.33561E+01	0.25991E-15
41.75	0.88997E+00	0.93998E-01	0.72322E+00	0.26023E+00	0.33763E+01	0.33563E+01	0.25989E-15
42.00	0.89003E+00	0.93979E-01	0.72327E+00	0.26023E+00	0.33755E+01	0.33564E+01	0.25988E-15
42.25	0.89008E+00	0.93961E-01	0.72332E+00	0.26024E+00	0.33748E+01	0.33565E+01	0.25987E-15
42.50	0.89013E+00	0.93943E-01	0.72338E+00	0.26024E+00	0.33741E+01	0.33567E+01	0.25985E-15
42.75	0.89018E+00	0.93926E-01	0.72342E+00	0.26024E+00	0.33735E+01	0.33568E+01	0.25984E-15
43.00	0.89022E+00	0.93910E-01	0.72347E+00	0.26025E+00	0.33728E+01	0.33569E+01	0.25983E-15
43.25	0.89027E+00	0.93895E-01	0.72351E+00	0.26029E+00	0.33722E+01	0.33575E+01	0.25982E-15
43.50	0.89032E+00	0.93881E-01	0.72354E+00	0.26036E+00	0.33717E+01	0.33585E+01	0.25981E-15
43.75	0.89036E+00	0.93868E-01	0.72357E+00	0.26042E+00	0.33712E+01	0.33592E+01	0.25980E-15
44.00	0.89040E+00	0.93855E-01	0.72359E+00	0.26046E+00	0.33707E+01	0.33599E+01	0.25979E-15
44.25	0.89044E+00	0.93843E-01	0.72361E+00	0.26050E+00	0.33702E+01	0.33604E+01	0.25978E-15
44.50	0.89048E+00	0.93832E-01	0.72363E+00	0.26053E+00	0.33698E+01	0.33609E+01	0.25977E-15
44.75	0.89052E+00	0.93821E-01	0.72366E+00	0.26056E+00	0.33693E+01	0.33613E+01	0.25976E-15
45.00	0.89055E+00	0.93811E-01	0.72368E+00	0.26058E+00	0.33689E+01	0.33616E+01	0.25975E-15
45.25	0.89058E+00	0.93802E-01	0.72370E+00	0.26060E+00	0.33685E+01	0.33619E+01	0.25974E-15
45.50	0.89062E+00	0.93792E-01	0.72372E+00	0.26062E+00	0.33682E+01	0.33622E+01	0.25974E-15
45.75	0.89065E+00	0.93783E-01	0.72374E+00	0.26063E+00	0.33678E+01	0.33624E+01	0.25973E-15

46.00	0.89067E+00	0.93775E-01	0.72376E+00	0.26064E+00	0.33675E+01	0.33625E+01	0.25972E-15
46.25	0.89070E+00	0.93767E-01	0.72378E+00	0.26065E+00	0.33672E+01	0.33627E+01	0.25972E-15
46.50	0.89073E+00	0.93759E-01	0.72380E+00	0.26066E+00	0.33669E+01	0.33628E+01	0.25971E-15
46.75	0.89075E+00	0.93751E-01	0.72382E+00	0.26066E+00	0.33666E+01	0.33629E+01	0.25970E-15
47.00	0.89078E+00	0.93744E-01	0.72384E+00	0.26067E+00	0.33663E+01	0.33629E+01	0.25970E-15
47.25	0.89080E+00	0.93737E-01	0.72385E+00	0.26067E+00	0.33660E+01	0.33630E+01	0.25969E-15
47.50	0.89082E+00	0.93731E-01	0.72387E+00	0.26067E+00	0.33657E+01	0.33630E+01	0.25969E-15
47.75	0.89084E+00	0.93724E-01	0.72389E+00	0.26067E+00	0.33655E+01	0.33631E+01	0.25968E-15
48.00	0.89086E+00	0.93718E-01	0.72391E+00	0.26067E+00	0.33652E+01	0.33631E+01	0.25968E-15
48.25	0.89088E+00	0.93712E-01	0.72393E+00	0.26067E+00	0.33650E+01	0.33631E+01	0.25968E-15
48.50	0.89090E+00	0.93706E-01	0.72394E+00	0.26067E+00	0.33648E+01	0.33631E+01	0.25967E-15
48.75	0.89092E+00	0.93701E-01	0.72396E+00	0.26067E+00	0.33645E+01	0.33630E+01	0.25967E-15
49.00	0.89093E+00	0.93695E-01	0.72398E+00	0.26067E+00	0.33643E+01	0.33630E+01	0.25966E-15
49.25	0.89095E+00	0.93690E-01	0.72399E+00	0.26066E+00	0.33641E+01	0.33630E+01	0.25966E-15
49.50	0.89096E+00	0.93685E-01	0.72401E+00	0.26066E+00	0.33639E+01	0.33629E+01	0.25966E-15
49.75	0.89098E+00	0.93680E-01	0.72403E+00	0.26065E+00	0.33637E+01	0.33629E+01	0.25965E-15
50.00	0.89099E+00	0.93676E-01	0.72404E+00	0.26065E+00	0.33636E+01	0.33628E+01	0.25965E-15

TIME	CS	CAVS	PIS	PS
0.0	0.16499E+02	0.21998E+02	0.90000E+01	-0.12100E+01
0.25	0.16605E+02	0.22194E+02	0.91130E+01	-0.12743E+01
0.50	0.16691E+02	0.22362E+02	0.92106E+01	-0.13348E+01
0.75	0.16775E+02	0.22532E+02	0.93106E+01	-0.14005E+01
1.00	0.16843E+02	0.22681E+02	0.93993E+01	-0.14635E+01
1.25	0.16873E+02	0.22761E+02	0.94469E+01	-0.15070E+01
1.50	0.16879E+02	0.22798E+02	0.94694E+01	-0.15382E+01
1.75	0.16874E+02	0.22815E+02	0.94793E+01	-0.15632E+01
2.00	0.16860E+02	0.22815E+02	0.94794E+01	-0.15836E+01
2.25	0.16837E+02	0.22800E+02	0.94706E+01	-0.15996E+01
2.50	0.16809E+02	0.22774E+02	0.94551E+01	-0.16124E+01
2.75	0.16776E+02	0.22740E+02	0.94343E+01	-0.16226E+01
3.00	0.16732E+02	0.22682E+02	0.93996E+01	-0.16255E+01
3.25	0.16680E+02	0.22609E+02	0.93562E+01	-0.16227E+01
3.50	0.16631E+02	0.22540E+02	0.93154E+01	-0.16200E+01
3.75	0.16585E+02	0.22475E+02	0.92769E+01	-0.16172E+01
4.00	0.16541E+02	0.22413E+02	0.92405E+01	-0.16142E+01
4.25	0.16500E+02	0.22354E+02	0.92061E+01	-0.16111E+01
4.50	0.16461E+02	0.22298E+02	0.91735E+01	-0.16079E+01
4.75	0.16424E+02	0.22245E+02	0.91426E+01	-0.16045E+01
5.00	0.16389E+02	0.22195E+02	0.91134E+01	-0.16009E+01
5.25	0.16357E+02	0.22147E+02	0.90857E+01	-0.15973E+01
5.50	0.16326E+02	0.22102E+02	0.90595E+01	-0.15934E+01
5.75	0.16297E+02	0.22059E+02	0.90347E+01	-0.15895E+01
6.00	0.16270E+02	0.22018E+02	0.90113E+01	-0.15854E+01
6.25	0.16244E+02	0.21980E+02	0.89892E+01	-0.15811E+01
6.50	0.16220E+02	0.21943E+02	0.89681E+01	-0.15766E+01
6.75	0.16197E+02	0.21908E+02	0.89482E+01	-0.15720E+01
7.00	0.16176E+02	0.21875E+02	0.89293E+01	-0.15673E+01
7.25	0.16156E+02	0.21843E+02	0.89115E+01	-0.15623E+01
7.50	0.16137E+02	0.21814E+02	0.88946E+01	-0.15572E+01
7.75	0.16120E+02	0.21786E+02	0.88785E+01	-0.15519E+01
8.00	0.16104E+02	0.21759E+02	0.88634E+01	-0.15464E+01
8.25	0.16089E+02	0.21733E+02	0.88491E+01	-0.15407E+01
8.50	0.16075E+02	0.21710E+02	0.88355E+01	-0.15349E+01
8.75	0.16062E+02	0.21687E+02	0.88227E+01	-0.15289E+01
9.00	0.16050E+02	0.21665E+02	0.88106E+01	-0.15227E+01
9.25	0.15967E+02	0.21510E+02	0.87233E+01	-0.14742E+01
9.50	0.15949E+02	0.21475E+02	0.87039E+01	-0.14623E+01
9.75	0.15943E+02	0.21463E+02	0.86971E+01	-0.14569E+01

10.00	0.15940E+02	0.21454E+02	0.86924E+01	-0.14522E+01
10.25	0.15937E+02	0.21447E+02	0.86880E+01	-0.14472E+01
10.50	0.15935E+02	0.21439E+02	0.86837E+01	-0.14419E+01
10.75	0.15933E+02	0.21431E+02	0.86794E+01	-0.14361E+01
11.00	0.15931E+02	0.21423E+02	0.86752E+01	-0.14299E+01
11.25	0.15930E+02	0.21416E+02	0.86711E+01	-0.14234E+01
11.50	0.15929E+02	0.21409E+02	0.86672E+01	-0.14167E+01
11.75	0.15928E+02	0.21402E+02	0.86634E+01	-0.14097E+01
12.00	0.15928E+02	0.21396E+02	0.86599E+01	-0.14024E+01
12.25	0.15928E+02	0.21390E+02	0.86567E+01	-0.13951E+01
12.50	0.15929E+02	0.21385E+02	0.86538E+01	-0.13876E+01
12.75	0.15931E+02	0.21381E+02	0.86515E+01	-0.13801E+01
13.00	0.15933E+02	0.21377E+02	0.86496E+01	-0.13727E+01
13.25	0.15936E+02	0.21375E+02	0.86483E+01	-0.13653E+01
13.50	0.15939E+02	0.21374E+02	0.86477E+01	-0.13581E+01
13.75	0.15944E+02	0.21374E+02	0.86477E+01	-0.13511E+01
14.00	0.15949E+02	0.21376E+02	0.86486E+01	-0.13445E+01
14.25	0.15955E+02	0.21379E+02	0.86505E+01	-0.13383E+01
14.50	0.15963E+02	0.21384E+02	0.86532E+01	-0.13325E+01
14.75	0.15971E+02	0.21390E+02	0.86568E+01	-0.13272E+01
15.00	0.15980E+02	0.21398E+02	0.86612E+01	-0.13223E+01
15.25	0.15989E+02	0.21407E+02	0.86662E+01	-0.13177E+01
15.50	0.15999E+02	0.21417E+02	0.86717E+01	-0.13135E+01
15.75	0.16010E+02	0.21428E+02	0.86776E+01	-0.13096E+01
16.00	0.16020E+02	0.21439E+02	0.86839E+01	-0.13059E+01
16.25	0.16031E+02	0.21451E+02	0.86904E+01	-0.13024E+01
16.50	0.16042E+02	0.21463E+02	0.86971E+01	-0.12991E+01
16.75	0.16054E+02	0.21475E+02	0.87040E+01	-0.12960E+01
17.00	0.16065E+02	0.21488E+02	0.87110E+01	-0.12931E+01
17.25	0.16076E+02	0.21500E+02	0.87180E+01	-0.12904E+01
17.50	0.16087E+02	0.21513E+02	0.87251E+01	-0.12877E+01
17.75	0.16098E+02	0.21526E+02	0.87322E+01	-0.12852E+01
18.00	0.16109E+02	0.21538E+02	0.87392E+01	-0.12828E+01
18.25	0.16120E+02	0.21551E+02	0.87462E+01	-0.12805E+01
18.50	0.16130E+02	0.21563E+02	0.87532E+01	-0.12783E+01
18.75	0.16141E+02	0.21575E+02	0.87600E+01	-0.12761E+01
19.00	0.16151E+02	0.21587E+02	0.87668E+01	-0.12741E+01
19.25	0.16161E+02	0.21599E+02	0.87734E+01	-0.12721E+01
19.50	0.16171E+02	0.21611E+02	0.87799E+01	-0.12702E+01
19.75	0.16181E+02	0.21622E+02	0.87863E+01	-0.12683E+01
20.00	0.16190E+02	0.21633E+02	0.87925E+01	-0.12665E+01
20.25	0.16199E+02	0.21644E+02	0.87987E+01	-0.12647E+01
20.50	0.16208E+02	0.21655E+02	0.88047E+01	-0.12631E+01
20.75	0.16217E+02	0.21665E+02	0.88105E+01	-0.12614E+01
21.00	0.16226E+02	0.21675E+02	0.88162E+01	-0.12598E+01
21.25	0.16234E+02	0.21685E+02	0.88218E+01	-0.12583E+01
21.50	0.16242E+02	0.21695E+02	0.88272E+01	-0.12568E+01
21.75	0.16250E+02	0.21704E+02	0.88325E+01	-0.12553E+01
22.00	0.16258E+02	0.21713E+02	0.88377E+01	-0.12539E+01
22.25	0.16265E+02	0.21722E+02	0.88427E+01	-0.12526E+01
22.50	0.16273E+02	0.21731E+02	0.88476E+01	-0.12512E+01
22.75	0.16280E+02	0.21739E+02	0.88524E+01	-0.12500E+01
23.00	0.16287E+02	0.21748E+02	0.88571E+01	-0.12487E+01
23.25	0.16294E+02	0.21756E+02	0.88616E+01	-0.12475E+01
23.50	0.16300E+02	0.21763E+02	0.88660E+01	-0.12464E+01
23.75	0.16306E+02	0.21771E+02	0.88702E+01	-0.12452E+01
24.00	0.16313E+02	0.21778E+02	0.88744E+01	-0.12441E+01
24.25	0.16319E+02	0.21785E+02	0.88784E+01	-0.12431E+01
24.50	0.16324E+02	0.21792E+02	0.88823E+01	-0.12420E+01
24.75	0.16330E+02	0.21799E+02	0.88861E+01	-0.12410E+01

25.00	0.16335E+02	0.21805E+02	0.88898E+01	-0.12401E+01
25.25	0.16341E+02	0.21812E+02	0.88934E+01	-0.12391E+01
25.50	0.16346E+02	0.21818E+02	0.88969E+01	-0.12382E+01
25.75	0.16351E+02	0.21824E+02	0.89003E+01	-0.12373E+01
26.00	0.16356E+02	0.21830E+02	0.89036E+01	-0.12365E+01
26.25	0.16360E+02	0.21835E+02	0.89067E+01	-0.12357E+01
26.50	0.16365E+02	0.21841E+02	0.89098E+01	-0.12349E+01
26.75	0.16369E+02	0.21846E+02	0.89128E+01	-0.12341E+01
27.00	0.16374E+02	0.21851E+02	0.89157E+01	-0.12334E+01
27.25	0.16378E+02	0.21856E+02	0.89185E+01	-0.12326E+01
27.50	0.16382E+02	0.21861E+02	0.89212E+01	-0.12319E+01
27.75	0.16386E+02	0.21865E+02	0.89239E+01	-0.12313E+01
28.00	0.16390E+02	0.21870E+02	0.89264E+01	-0.12306E+01
28.25	0.16393E+02	0.21874E+02	0.89289E+01	-0.12300E+01
28.50	0.16397E+02	0.21878E+02	0.89313E+01	-0.12294E+01
28.75	0.16400E+02	0.21882E+02	0.89336E+01	-0.12288E+01
29.00	0.16403E+02	0.21886E+02	0.89358E+01	-0.12282E+01
29.25	0.16407E+02	0.21890E+02	0.89380E+01	-0.12276E+01
29.50	0.16410E+02	0.21894E+02	0.89401E+01	-0.12271E+01
29.75	0.16413E+02	0.21897E+02	0.89421E+01	-0.12266E+01
30.00	0.16416E+02	0.21901E+02	0.89441E+01	-0.12261E+01
30.25	0.16418E+02	0.21904E+02	0.89460E+01	-0.12256E+01
30.50	0.16421E+02	0.21907E+02	0.89479E+01	-0.12251E+01
30.75	0.16424E+02	0.21910E+02	0.89496E+01	-0.12246E+01
31.00	0.16426E+02	0.21913E+02	0.89514E+01	-0.12242E+01
31.25	0.16429E+02	0.21916E+02	0.89530E+01	-0.12238E+01
31.50	0.16431E+02	0.21919E+02	0.89546E+01	-0.12234E+01
31.75	0.16433E+02	0.21922E+02	0.89562E+01	-0.12230E+01
32.00	0.16436E+02	0.21925E+02	0.89577E+01	-0.12226E+01
32.25	0.16438E+02	0.21927E+02	0.89592E+01	-0.12222E+01
32.50	0.16440E+02	0.21930E+02	0.89606E+01	-0.12218E+01
32.75	0.16442E+02	0.21932E+02	0.89619E+01	-0.12215E+01
33.00	0.16444E+02	0.21934E+02	0.89632E+01	-0.12211E+01
33.25	0.16446E+02	0.21936E+02	0.89645E+01	-0.12208E+01
33.50	0.16447E+02	0.21939E+02	0.89657E+01	-0.12205E+01
33.75	0.16449E+02	0.21941E+02	0.89669E+01	-0.12202E+01
34.00	0.16451E+02	0.21943E+02	0.89681E+01	-0.12199E+01
34.25	0.16453E+02	0.21945E+02	0.89692E+01	-0.12196E+01
34.50	0.16454E+02	0.21946E+02	0.89702E+01	-0.12193E+01
34.75	0.16456E+02	0.21948E+02	0.89713E+01	-0.12191E+01
35.00	0.16457E+02	0.21950E+02	0.89723E+01	-0.12188E+01
35.25	0.16458E+02	0.21952E+02	0.89732E+01	-0.12185E+01
35.50	0.16460E+02	0.21953E+02	0.89742E+01	-0.12183E+01
35.75	0.16461E+02	0.21955E+02	0.89751E+01	-0.12181E+01
36.00	0.16462E+02	0.21956E+02	0.89759E+01	-0.12178E+01
36.25	0.16464E+02	0.21958E+02	0.89767E+01	-0.12176E+01
36.50	0.16465E+02	0.21959E+02	0.89776E+01	-0.12174E+01
36.75	0.16466E+02	0.21961E+02	0.89783E+01	-0.12172E+01
37.00	0.16467E+02	0.21962E+02	0.89791E+01	-0.12170E+01
37.25	0.16468E+02	0.21963E+02	0.89798E+01	-0.12168E+01
37.50	0.16469E+02	0.21964E+02	0.89805E+01	-0.12166E+01
37.75	0.16470E+02	0.21966E+02	0.89812E+01	-0.12164E+01
38.00	0.16471E+02	0.21967E+02	0.89818E+01	-0.12163E+01
38.25	0.16472E+02	0.21968E+02	0.89825E+01	-0.12161E+01
38.50	0.16473E+02	0.21969E+02	0.89831E+01	-0.12159E+01
38.75	0.16474E+02	0.21970E+02	0.89836E+01	-0.12158E+01
39.00	0.16475E+02	0.21971E+02	0.89842E+01	-0.12156E+01
39.25	0.16475E+02	0.21972E+02	0.89847E+01	-0.12155E+01
39.50	0.16476E+02	0.21973E+02	0.89853E+01	-0.12153E+01
39.75	0.16477E+02	0.21974E+02	0.89858E+01	-0.12152E+01

40.00	0.16478E+02	0.21974E+02	0.89863E+01	-0.12151E+01
40.25	0.16478E+02	0.21975E+02	0.89867E+01	-0.12149E+01
40.50	0.16479E+02	0.21976E+02	0.89872E+01	-0.12148E+01
40.75	0.16480E+02	0.21977E+02	0.89876E+01	-0.12147E+01
41.00	0.16480E+02	0.21978E+02	0.89880E+01	-0.12146E+01
41.25	0.16481E+02	0.21978E+02	0.89885E+01	-0.12145E+01
41.50	0.16482E+02	0.21979E+02	0.89888E+01	-0.12143E+01
41.75	0.16482E+02	0.21980E+02	0.89892E+01	-0.12142E+01
42.00	0.16483E+02	0.21980E+02	0.89896E+01	-0.12141E+01
42.25	0.16483E+02	0.21981E+02	0.89899E+01	-0.12140E+01
42.50	0.16484E+02	0.21981E+02	0.89903E+01	-0.12139E+01
42.75	0.16484E+02	0.21982E+02	0.89906E+01	-0.12138E+01
43.00	0.16485E+02	0.21983E+02	0.89909E+01	-0.12137E+01
43.25	0.16485E+02	0.21983E+02	0.89912E+01	-0.12137E+01
43.50	0.16485E+02	0.21984E+02	0.89915E+01	-0.12136E+01
43.75	0.16486E+02	0.21984E+02	0.89918E+01	-0.12135E+01
44.00	0.16486E+02	0.21985E+02	0.89920E+01	-0.12134E+01
44.25	0.16487E+02	0.21985E+02	0.89923E+01	-0.12133E+01
44.50	0.16487E+02	0.21985E+02	0.89925E+01	-0.12132E+01
44.75	0.16487E+02	0.21986E+02	0.89927E+01	-0.12131E+01
45.00	0.16488E+02	0.21986E+02	0.89929E+01	-0.12130E+01
45.25	0.16488E+02	0.21986E+02	0.89931E+01	-0.12130E+01
45.50	0.16488E+02	0.21987E+02	0.89933E+01	-0.12129E+01
45.75	0.16489E+02	0.21987E+02	0.89935E+01	-0.12128E+01
46.00	0.16489E+02	0.21987E+02	0.89937E+01	-0.12127E+01
46.25	0.16489E+02	0.21988E+02	0.89939E+01	-0.12126E+01
46.50	0.16489E+02	0.21988E+02	0.89941E+01	-0.12126E+01
46.75	0.16490E+02	0.21988E+02	0.89942E+01	-0.12125E+01
47.00	0.16490E+02	0.21989E+02	0.89944E+01	-0.12124E+01
47.25	0.16490E+02	0.21989E+02	0.89945E+01	-0.12124E+01
47.50	0.16490E+02	0.21989E+02	0.89947E+01	-0.12123E+01
47.75	0.16491E+02	0.21989E+02	0.89948E+01	-0.12122E+01
48.00	0.16491E+02	0.21990E+02	0.89950E+01	-0.12122E+01
48.25	0.16491E+02	0.21990E+02	0.89951E+01	-0.12121E+01
48.50	0.16491E+02	0.21990E+02	0.89952E+01	-0.12121E+01
48.75	0.16492E+02	0.21990E+02	0.89954E+01	-0.12120E+01
49.00	0.16492E+02	0.21991E+02	0.89955E+01	-0.12119E+01
49.25	0.16492E+02	0.21991E+02	0.89956E+01	-0.12119E+01
49.50	0.16492E+02	0.21991E+02	0.89957E+01	-0.12118E+01
49.75	0.16492E+02	0.21991E+02	0.89958E+01	-0.12118E+01
50.00	0.16492E+02	0.21991E+02	0.89959E+01	-0.12117E+01

TIME	FS	VPLS	RS	LS	OPLS	OLS	ODM
0.0	0.84681E+00	0.15496E+00	0.12369E+01	0.37980E+00	0.55630E+01	0.62662E+01	0.38585E-15
0.25	0.93881E+00	0.14168E+00	0.11056E+01	0.37611E+00	0.49603E+01	0.62454E+01	0.35574E-15
0.50	0.10028E+01	0.11768E+00	0.11782E+01	0.37265E+00	0.40488E+01	0.62200E+01	0.33431E-15
0.75	0.10617E+01	0.94613E-01	0.12581E+01	0.36889E+00	0.32031E+01	0.61879E+01	0.31429E-15
1.00	0.11167E+01	0.84786E-01	0.12064E+01	0.36528E+00	0.28255E+01	0.61525E+01	0.29541E-15
1.25	0.11457E+01	0.85850E-01	0.11144E+01	0.36279E+00	0.28375E+01	0.61213E+01	0.28563E-15
1.50	0.11584E+01	0.86615E-01	0.10743E+01	0.36100E+00	0.28537E+01	0.60933E+01	0.28168E-15
1.75	0.11663E+01	0.87228E-01	0.10492E+01	0.35956E+00	0.28683E+01	0.60672E+01	0.27943E-15
2.00	0.11732E+01	0.87726E-01	0.10271E+01	0.35840E+00	0.28787E+01	0.60424E+01	0.27754E-15
2.25	0.11792E+01	0.88119E-01	0.10080E+01	0.35748E+00	0.28854E+01	0.60190E+01	0.27599E-15
2.50	0.11836E+01	0.88432E-01	0.99409E+00	0.35675E+00	0.28903E+01	0.59967E+01	0.27504E-15
2.75	0.11872E+01	0.88682E-01	0.98261E+00	0.35616E+00	0.28933E+01	0.59751E+01	0.27437E-15
3.00	0.11836E+01	0.97096E-01	0.90391E+00	0.35600E+00	0.31690E+01	0.59564E+01	0.27635E-15
3.25	0.11699E+01	0.10171E+00	0.89688E+00	0.35616E+00	0.33326E+01	0.59406E+01	0.28195E-15
3.50	0.11572E+01	0.10616E+00	0.88813E+00	0.35631E+00	0.34909E+01	0.59257E+01	0.28711E-15

3.75	0.11453E+01	0.11039E+00	0.87937E+00	0.35647E+00	0.36421E+01	0.59120E+01	0.29194E-15
4.00	0.11340E+01	0.11441E+00	0.87093E+00	0.35664E+00	0.37864E+01	0.58993E+01	0.29651E-15
4.25	0.11233E+01	0.11823E+00	0.86281E+00	0.35682E+00	0.39244E+01	0.58875E+01	0.30084E-15
4.50	0.11130E+01	0.12188E+00	0.85504E+00	0.35701E+00	0.40568E+01	0.58767E+01	0.30495E-15
4.75	0.11032E+01	0.12537E+00	0.84757E+00	0.35720E+00	0.41839E+01	0.58667E+01	0.30887E-15
5.00	0.10938E+01	0.12871E+00	0.84033E+00	0.35740E+00	0.43064E+01	0.58577E+01	0.31261E-15
5.25	0.10848E+01	0.13192E+00	0.83330E+00	0.35762E+00	0.44246E+01	0.58494E+01	0.31618E-15
5.50	0.10761E+01	0.13502E+00	0.82646E+00	0.35783E+00	0.45388E+01	0.58419E+01	0.31959E-15
5.75	0.10677E+01	0.13800E+00	0.81978E+00	0.35806E+00	0.46494E+01	0.58353E+01	0.32286E-15
6.00	0.10596E+01	0.14087E+00	0.81327E+00	0.35830E+00	0.47562E+01	0.58293E+01	0.32599E-15
6.25	0.10518E+01	0.14364E+00	0.80689E+00	0.35854E+00	0.48599E+01	0.58241E+01	0.32899E-15
6.50	0.10442E+01	0.14634E+00	0.80062E+00	0.35880E+00	0.49610E+01	0.58196E+01	0.33188E-15
6.75	0.10368E+01	0.14896E+00	0.79447E+00	0.35906E+00	0.50594E+01	0.58157E+01	0.33467E-15
7.00	0.10297E+01	0.15149E+00	0.78842E+00	0.35933E+00	0.51551E+01	0.58125E+01	0.33735E-15
7.25	0.10228E+01	0.15395E+00	0.78248E+00	0.35962E+00	0.52483E+01	0.58100E+01	0.33993E-15
7.50	0.10161E+01	0.15634E+00	0.77665E+00	0.35991E+00	0.53390E+01	0.58080E+01	0.34241E-15
7.75	0.10095E+01	0.15866E+00	0.77091E+00	0.36022E+00	0.54274E+01	0.58067E+01	0.34481E-15
8.00	0.10032E+01	0.16091E+00	0.76526E+00	0.36053E+00	0.55136E+01	0.58059E+01	0.34711E-15
8.25	0.99698E+00	0.16310E+00	0.75972E+00	0.36085E+00	0.55975E+01	0.58058E+01	0.34934E-15
8.50	0.99096E+00	0.16523E+00	0.75426E+00	0.36119E+00	0.56793E+01	0.58061E+01	0.35148E-15
8.75	0.98510E+00	0.16729E+00	0.74890E+00	0.36153E+00	0.57591E+01	0.58070E+01	0.35355E-15
9.00	0.97942E+00	0.16930E+00	0.74366E+00	0.36189E+00	0.58365E+01	0.58084E+01	0.35554E-15
9.25	0.12839E+01	0.17252E+00	0.94779E+00	0.36467E+00	0.60861E+01	0.58225E+01	0.38215E-15
9.50	0.12645E+01	0.17094E+00	0.10231E+01	0.36535E+00	0.60636E+01	0.58268E+01	0.38848E-15
9.75	0.12573E+01	0.17216E+00	0.10314E+01	0.36566E+00	0.61191E+01	0.58297E+01	0.39080E-15
10.00	0.12524E+01	0.17385E+00	0.10276E+01	0.36593E+00	0.61872E+01	0.58328E+01	0.39235E-15
10.25	0.12479E+01	0.17557E+00	0.10218E+01	0.36621E+00	0.62559E+01	0.58363E+01	0.39374E-15
10.50	0.12436E+01	0.17725E+00	0.10159E+01	0.36652E+00	0.63228E+01	0.58404E+01	0.39507E-15
10.75	0.12393E+01	0.17887E+00	0.10103E+01	0.36685E+00	0.63877E+01	0.58449E+01	0.39636E-15
11.00	0.12352E+01	0.18044E+00	0.10050E+01	0.36720E+00	0.64504E+01	0.58499E+01	0.39761E-15
11.25	0.12311E+01	0.18195E+00	0.99993E+00	0.36757E+00	0.65110E+01	0.58553E+01	0.39883E-15
11.50	0.12271E+01	0.18340E+00	0.99514E+00	0.36796E+00	0.65694E+01	0.58611E+01	0.40001E-15
11.75	0.12232E+01	0.18479E+00	0.99061E+00	0.36836E+00	0.66257E+01	0.58673E+01	0.40114E-15
12.00	0.12193E+01	0.18612E+00	0.98640E+00	0.36878E+00	0.66796E+01	0.58738E+01	0.40223E-15
12.25	0.12156E+01	0.18738E+00	0.98265E+00	0.36920E+00	0.67308E+01	0.58807E+01	0.40329E-15
12.50	0.12120E+01	0.18856E+00	0.97945E+00	0.36963E+00	0.67789E+01	0.58878E+01	0.40429E-15
12.75	0.12085E+01	0.18965E+00	0.97674E+00	0.37006E+00	0.68236E+01	0.58952E+01	0.40524E-15
13.00	0.12052E+01	0.19065E+00	0.97443E+00	0.37048E+00	0.68650E+01	0.59028E+01	0.40612E-15
13.25	0.12021E+01	0.19155E+00	0.97261E+00	0.37090E+00	0.69028E+01	0.59106E+01	0.40693E-15
13.50	0.11992E+01	0.19235E+00	0.97142E+00	0.37132E+00	0.69364E+01	0.59185E+01	0.40768E-15
13.75	0.11964E+01	0.19302E+00	0.97093E+00	0.37171E+00	0.69655E+01	0.59265E+01	0.40834E-15
14.00	0.11939E+01	0.19357E+00	0.97117E+00	0.37209E+00	0.69895E+01	0.59346E+01	0.40892E-15
14.25	0.11917E+01	0.19399E+00	0.97203E+00	0.37245E+00	0.70085E+01	0.59426E+01	0.40940E-15
14.50	0.11898E+01	0.19428E+00	0.97326E+00	0.37278E+00	0.70228E+01	0.59506E+01	0.40977E-15
14.75	0.11883E+01	0.19448E+00	0.97460E+00	0.37309E+00	0.70330E+01	0.59585E+01	0.41002E-15
15.00	0.11871E+01	0.19460E+00	0.97590E+00	0.37337E+00	0.70397E+01	0.59664E+01	0.41016E-15
15.25	0.11862E+01	0.19464E+00	0.97710E+00	0.37363E+00	0.70435E+01	0.59741E+01	0.41021E-15
15.50	0.11855E+01	0.19463E+00	0.97822E+00	0.37387E+00	0.70447E+01	0.59817E+01	0.41017E-15
15.75	0.11851E+01	0.19456E+00	0.97930E+00	0.37410E+00	0.70436E+01	0.59892E+01	0.41006E-15
16.00	0.11848E+01	0.19445E+00	0.98034E+00	0.37431E+00	0.70404E+01	0.59966E+01	0.40989E-15
16.25	0.11848E+01	0.19429E+00	0.98138E+00	0.37451E+00	0.70354E+01	0.60039E+01	0.40967E-15
16.50	0.11848E+01	0.19410E+00	0.98240E+00	0.37469E+00	0.70288E+01	0.60110E+01	0.40940E-15
16.75	0.11850E+01	0.19387E+00	0.98340E+00	0.37487E+00	0.70208E+01	0.60180E+01	0.40910E-15
17.00	0.11853E+01	0.19361E+00	0.98438E+00	0.37504E+00	0.70116E+01	0.60249E+01	0.40876E-15
17.25	0.11858E+01	0.19333E+00	0.98533E+00	0.37520E+00	0.70014E+01	0.60316E+01	0.40839E-15
17.50	0.11863E+01	0.19304E+00	0.98626E+00	0.37535E+00	0.69904E+01	0.60382E+01	0.40799E-15
17.75	0.11868E+01	0.19273E+00	0.98716E+00	0.37549E+00	0.69787E+01	0.60447E+01	0.40758E-15
18.00	0.11875E+01	0.19240E+00	0.98804E+00	0.37563E+00	0.69664E+01	0.60510E+01	0.40716E-15
18.25	0.11881E+01	0.19206E+00	0.98890E+00	0.37576E+00	0.69536E+01	0.60572E+01	0.40672E-15
18.50	0.11889E+01	0.19172E+00	0.98974E+00	0.37589E+00	0.69404E+01	0.60632E+01	0.40628E-15

18.75	0.11896E+01	0.19137E+00	0.99056E+00	0.37601E+00	0.69270E+01	0.60691E+01	0.40583E-15
19.00	0.11904E+01	0.19102E+00	0.99137E+00	0.37613E+00	0.69134E+01	0.60749E+01	0.40537E-15
19.25	0.11912E+01	0.19066E+00	0.99217E+00	0.37624E+00	0.68996E+01	0.60805E+01	0.40492E-15
19.50	0.11920E+01	0.19030E+00	0.99295E+00	0.37635E+00	0.68857E+01	0.60860E+01	0.40446E-15
19.75	0.11928E+01	0.18994E+00	0.99373E+00	0.37646E+00	0.68717E+01	0.60914E+01	0.40401E-15
20.00	0.11937E+01	0.18958E+00	0.99450E+00	0.37656E+00	0.68578E+01	0.60966E+01	0.40356E-15
20.25	0.11945E+01	0.18923E+00	0.99525E+00	0.37666E+00	0.68438E+01	0.61017E+01	0.40311E-15
20.50	0.11953E+01	0.18887E+00	0.99600E+00	0.37676E+00	0.68300E+01	0.61067E+01	0.40267E-15
20.75	0.11962E+01	0.18852E+00	0.99673E+00	0.37685E+00	0.68162E+01	0.61115E+01	0.40223E-15
21.00	0.11970E+01	0.18817E+00	0.99746E+00	0.37695E+00	0.68025E+01	0.61162E+01	0.40180E-15
21.25	0.11978E+01	0.18782E+00	0.99818E+00	0.37703E+00	0.67890E+01	0.61208E+01	0.40137E-15
21.50	0.11987E+01	0.18748E+00	0.99889E+00	0.37712E+00	0.67756E+01	0.61253E+01	0.40095E-15
21.75	0.11995E+01	0.18714E+00	0.99958E+00	0.37720E+00	0.67623E+01	0.61296E+01	0.40054E-15
22.00	0.12003E+01	0.18681E+00	0.10003E+01	0.37728E+00	0.67493E+01	0.61338E+01	0.40013E-15
22.25	0.12011E+01	0.18648E+00	0.10009E+01	0.37736E+00	0.67364E+01	0.61380E+01	0.39973E-15
22.50	0.12018E+01	0.18616E+00	0.10016E+01	0.37744E+00	0.67238E+01	0.61419E+01	0.39934E-15
22.75	0.12026E+01	0.18584E+00	0.10023E+01	0.37751E+00	0.67113E+01	0.61458E+01	0.39896E-15
23.00	0.12034E+01	0.18553E+00	0.10029E+01	0.37758E+00	0.66991E+01	0.61496E+01	0.39859E-15
23.25	0.12041E+01	0.18522E+00	0.10035E+01	0.37765E+00	0.66870E+01	0.61533E+01	0.39822E-15
23.50	0.12048E+01	0.18492E+00	0.10041E+01	0.37772E+00	0.66752E+01	0.61568E+01	0.39786E-15
23.75	0.12056E+01	0.18463E+00	0.10047E+01	0.37778E+00	0.66637E+01	0.61603E+01	0.39751E-15
24.00	0.12063E+01	0.18434E+00	0.10053E+01	0.37785E+00	0.66523E+01	0.61636E+01	0.39717E-15
24.25	0.12070E+01	0.18406E+00	0.10059E+01	0.37791E+00	0.66412E+01	0.61669E+01	0.39683E-15
24.50	0.12076E+01	0.18378E+00	0.10065E+01	0.37796E+00	0.66304E+01	0.61700E+01	0.39651E-15
24.75	0.12083E+01	0.18351E+00	0.10070E+01	0.37802E+00	0.66198E+01	0.61731E+01	0.39619E-15
25.00	0.12089E+01	0.18325E+00	0.10076E+01	0.37808E+00	0.66094E+01	0.61761E+01	0.39587E-15
25.25	0.12096E+01	0.18299E+00	0.10081E+01	0.37813E+00	0.65992E+01	0.61790E+01	0.39557E-15
25.50	0.12102E+01	0.18274E+00	0.10086E+01	0.37818E+00	0.65893E+01	0.61818E+01	0.39527E-15
25.75	0.12108E+01	0.18249E+00	0.10091E+01	0.37823E+00	0.65796E+01	0.61845E+01	0.39499E-15
26.00	0.12114E+01	0.18225E+00	0.10096E+01	0.37828E+00	0.65702E+01	0.61871E+01	0.39470E-15
26.25	0.12120E+01	0.18202E+00	0.10101E+01	0.37833E+00	0.65610E+01	0.61896E+01	0.39443E-15
26.50	0.12125E+01	0.18179E+00	0.10106E+01	0.37837E+00	0.65520E+01	0.61921E+01	0.39416E-15
26.75	0.12131E+01	0.18157E+00	0.10110E+01	0.37842E+00	0.65432E+01	0.61945E+01	0.39390E-15
27.00	0.12136E+01	0.18135E+00	0.10115E+01	0.37846E+00	0.65347E+01	0.61968E+01	0.39365E-15
27.25	0.12141E+01	0.18114E+00	0.10119E+01	0.37850E+00	0.65264E+01	0.61991E+01	0.39341E-15
27.50	0.12147E+01	0.18093E+00	0.10123E+01	0.37854E+00	0.65183E+01	0.62013E+01	0.39317E-15
27.75	0.12152E+01	0.18073E+00	0.10127E+01	0.37858E+00	0.65104E+01	0.62034E+01	0.39294E-15
28.00	0.12156E+01	0.18054E+00	0.10131E+01	0.37862E+00	0.65027E+01	0.62054E+01	0.39271E-15
28.25	0.12161E+01	0.18035E+00	0.10135E+01	0.37866E+00	0.64953E+01	0.62074E+01	0.39249E-15
28.50	0.12166E+01	0.18017E+00	0.10139E+01	0.37869E+00	0.64880E+01	0.62093E+01	0.39228E-15
28.75	0.12170E+01	0.17999E+00	0.10142E+01	0.37873E+00	0.64810E+01	0.62111E+01	0.39207E-15
29.00	0.12174E+01	0.17981E+00	0.10146E+01	0.37876E+00	0.64741E+01	0.62129E+01	0.39187E-15
29.25	0.12179E+01	0.17964E+00	0.10149E+01	0.37879E+00	0.64674E+01	0.62147E+01	0.39168E-15
29.50	0.12183E+01	0.17948E+00	0.10153E+01	0.37882E+00	0.64610E+01	0.62164E+01	0.39149E-15
29.75	0.12187E+01	0.17932E+00	0.10156E+01	0.37885E+00	0.64547E+01	0.62180E+01	0.39130E-15
30.00	0.12191E+01	0.17916E+00	0.10159E+01	0.37888E+00	0.64485E+01	0.62196E+01	0.39112E-15
30.25	0.12194E+01	0.17901E+00	0.10162E+01	0.37891E+00	0.64426E+01	0.62211E+01	0.39095E-15
30.50	0.12198E+01	0.17887E+00	0.10165E+01	0.37894E+00	0.64368E+01	0.62225E+01	0.39078E-15
30.75	0.12201E+01	0.17873E+00	0.10168E+01	0.37896E+00	0.64313E+01	0.62240E+01	0.39062E-15
31.00	0.12205E+01	0.17859E+00	0.10171E+01	0.37899E+00	0.64258E+01	0.62253E+01	0.39046E-15
31.25	0.12208E+01	0.17845E+00	0.10174E+01	0.37901E+00	0.64206E+01	0.62267E+01	0.39031E-15
31.50	0.12212E+01	0.17832E+00	0.10176E+01	0.37904E+00	0.64154E+01	0.62280E+01	0.39016E-15
31.75	0.12215E+01	0.17820E+00	0.10179E+01	0.37906E+00	0.64105E+01	0.62292E+01	0.39002E-15
32.00	0.12218E+01	0.17808E+00	0.10181E+01	0.37908E+00	0.64057E+01	0.62304E+01	0.38988E-15
32.25	0.12221E+01	0.17796E+00	0.10184E+01	0.37910E+00	0.64010E+01	0.62316E+01	0.38975E-15
32.50	0.12224E+01	0.17784E+00	0.10186E+01	0.37912E+00	0.63965E+01	0.62327E+01	0.38961E-15
32.75	0.12226E+01	0.17773E+00	0.10188E+01	0.37914E+00	0.63921E+01	0.62338E+01	0.38949E-15
33.00	0.12229E+01	0.17763E+00	0.10191E+01	0.37916E+00	0.63879E+01	0.62349E+01	0.38937E-15
33.25	0.12232E+01	0.17752E+00	0.10193E+01	0.37918E+00	0.63838E+01	0.62359E+01	0.38925E-15
33.50	0.12234E+01	0.17742E+00	0.10195E+01	0.37920E+00	0.63798E+01	0.62369E+01	0.38913E-15

33.75	0.12237E+01	0.17732E+00	0.10197E+01	0.37922E+00	0.63759E+01	0.62378E+01	0.38902E-15
34.00	0.12239E+01	0.17723E+00	0.10199E+01	0.37923E+00	0.63722E+01	0.62387E+01	0.38891E-15
34.25	0.12241E+01	0.17714E+00	0.10201E+01	0.37925E+00	0.63686E+01	0.62396E+01	0.38881E-15
34.50	0.12243E+01	0.17705E+00	0.10202E+01	0.37927E+00	0.63651E+01	0.62405E+01	0.38871E-15
34.75	0.12246E+01	0.17696E+00	0.10204E+01	0.37928E+00	0.63617E+01	0.62413E+01	0.38861E-15
35.00	0.12248E+01	0.17688E+00	0.10206E+01	0.37930E+00	0.63584E+01	0.62421E+01	0.38852E-15
35.25	0.12250E+01	0.17680E+00	0.10208E+01	0.37931E+00	0.63552E+01	0.62429E+01	0.38843E-15
35.50	0.12252E+01	0.17672E+00	0.10209E+01	0.37932E+00	0.63522E+01	0.62436E+01	0.38834E-15
35.75	0.12254E+01	0.17665E+00	0.10211E+01	0.37934E+00	0.63492E+01	0.62443E+01	0.38825E-15
36.00	0.12255E+01	0.17657E+00	0.10212E+01	0.37935E+00	0.63463E+01	0.62450E+01	0.38817E-15
36.25	0.12257E+01	0.17650E+00	0.10214E+01	0.37936E+00	0.63435E+01	0.62457E+01	0.38809E-15
36.50	0.12259E+01	0.17643E+00	0.10215E+01	0.37938E+00	0.63409E+01	0.62464E+01	0.38801E-15
36.75	0.12260E+01	0.17637E+00	0.10216E+01	0.37939E+00	0.63382E+01	0.62470E+01	0.38794E-15
37.00	0.12262E+01	0.17630E+00	0.10218E+01	0.37940E+00	0.63357E+01	0.62476E+01	0.38787E-15
37.25	0.12264E+01	0.17624E+00	0.10219E+01	0.37941E+00	0.63333E+01	0.62482E+01	0.38780E-15
37.50	0.12265E+01	0.17618E+00	0.10220E+01	0.37942E+00	0.63310E+01	0.62488E+01	0.38773E-15
37.75	0.12267E+01	0.17613E+00	0.10221E+01	0.37943E+00	0.63287E+01	0.62493E+01	0.38767E-15
38.00	0.12268E+01	0.17607E+00	0.10222E+01	0.37944E+00	0.63265E+01	0.62498E+01	0.38760E-15
38.25	0.12269E+01	0.17602E+00	0.10224E+01	0.37945E+00	0.63244E+01	0.62503E+01	0.38754E-15
38.50	0.12271E+01	0.17596E+00	0.10225E+01	0.37946E+00	0.63223E+01	0.62508E+01	0.38749E-15
38.75	0.12272E+01	0.17591E+00	0.10226E+01	0.37947E+00	0.63203E+01	0.62513E+01	0.38743E-15
39.00	0.12273E+01	0.17587E+00	0.10227E+01	0.37948E+00	0.63184E+01	0.62518E+01	0.38737E-15
39.25	0.12274E+01	0.17582E+00	0.10228E+01	0.37949E+00	0.63166E+01	0.62522E+01	0.38732E-15
39.50	0.12275E+01	0.17577E+00	0.10228E+01	0.37949E+00	0.63148E+01	0.62526E+01	0.38727E-15
39.75	0.12276E+01	0.17573E+00	0.10229E+01	0.37950E+00	0.63131E+01	0.62531E+01	0.38722E-15
40.00	0.12277E+01	0.17569E+00	0.10230E+01	0.37951E+00	0.63114E+01	0.62535E+01	0.38717E-15
40.25	0.12279E+01	0.17565E+00	0.10231E+01	0.37952E+00	0.63098E+01	0.62538E+01	0.38713E-15
40.50	0.12279E+01	0.17561E+00	0.10232E+01	0.37952E+00	0.63082E+01	0.62542E+01	0.38708E-15
40.75	0.12280E+01	0.17557E+00	0.10233E+01	0.37953E+00	0.63067E+01	0.62546E+01	0.38704E-15
41.00	0.12281E+01	0.17553E+00	0.10233E+01	0.37954E+00	0.63053E+01	0.62549E+01	0.38700E-15
41.25	0.12282E+01	0.17550E+00	0.10234E+01	0.37955E+00	0.63039E+01	0.62553E+01	0.38696E-15
41.50	0.12283E+01	0.17546E+00	0.10235E+01	0.37955E+00	0.63025E+01	0.62556E+01	0.38692E-15
41.75	0.12284E+01	0.17543E+00	0.10235E+01	0.37956E+00	0.63012E+01	0.62559E+01	0.38689E-15
42.00	0.12285E+01	0.17540E+00	0.10236E+01	0.37956E+00	0.63000E+01	0.62562E+01	0.38685E-15
42.25	0.12285E+01	0.17537E+00	0.10237E+01	0.37957E+00	0.62988E+01	0.62565E+01	0.38682E-15
42.50	0.12286E+01	0.17534E+00	0.10237E+01	0.37957E+00	0.62976E+01	0.62568E+01	0.38678E-15
42.75	0.12287E+01	0.17531E+00	0.10238E+01	0.37958E+00	0.62965E+01	0.62570E+01	0.38675E-15
43.00	0.12288E+01	0.17528E+00	0.10238E+01	0.37959E+00	0.62954E+01	0.62573E+01	0.38672E-15
43.25	0.12288E+01	0.17526E+00	0.10239E+01	0.37959E+00	0.62943E+01	0.62576E+01	0.38669E-15
43.50	0.12289E+01	0.17523E+00	0.10239E+01	0.37960E+00	0.62934E+01	0.62578E+01	0.38666E-15
43.75	0.12290E+01	0.17521E+00	0.10240E+01	0.37960E+00	0.62924E+01	0.62581E+01	0.38663E-15
44.00	0.12290E+01	0.17519E+00	0.10240E+01	0.37961E+00	0.62916E+01	0.62583E+01	0.38661E-15
44.25	0.12291E+01	0.17517E+00	0.10240E+01	0.37961E+00	0.62907E+01	0.62585E+01	0.38658E-15
44.50	0.12291E+01	0.17514E+00	0.10241E+01	0.37962E+00	0.62899E+01	0.62587E+01	0.38656E-15
44.75	0.12292E+01	0.17513E+00	0.10241E+01	0.37962E+00	0.62891E+01	0.62589E+01	0.38654E-15
45.00	0.12292E+01	0.17511E+00	0.10241E+01	0.37963E+00	0.62884E+01	0.62591E+01	0.38651E-15
45.25	0.12293E+01	0.17509E+00	0.10242E+01	0.37963E+00	0.62877E+01	0.62593E+01	0.38649E-15
45.50	0.12293E+01	0.17507E+00	0.10242E+01	0.37963E+00	0.62870E+01	0.62595E+01	0.38647E-15
45.75	0.12293E+01	0.17505E+00	0.10242E+01	0.37964E+00	0.62863E+01	0.62597E+01	0.38646E-15
46.00	0.12294E+01	0.17504E+00	0.10242E+01	0.37964E+00	0.62857E+01	0.62599E+01	0.38644E-15
46.25	0.12294E+01	0.17502E+00	0.10243E+01	0.37965E+00	0.62851E+01	0.62601E+01	0.38642E-15
46.50	0.12295E+01	0.17501E+00	0.10243E+01	0.37965E+00	0.62845E+01	0.62603E+01	0.38640E-15
46.75	0.12295E+01	0.17499E+00	0.10243E+01	0.37966E+00	0.62839E+01	0.62604E+01	0.38639E-15
47.00	0.12295E+01	0.17498E+00	0.10244E+01	0.37966E+00	0.62834E+01	0.62606E+01	0.38637E-15
47.25	0.12295E+01	0.17497E+00	0.10244E+01	0.37966E+00	0.62829E+01	0.62607E+01	0.38636E-15
47.50	0.12296E+01	0.17495E+00	0.10244E+01	0.37967E+00	0.62824E+01	0.62609E+01	0.38634E-15
47.75	0.12296E+01	0.17494E+00	0.10244E+01	0.37967E+00	0.62819E+01	0.62610E+01	0.38633E-15
48.00	0.12296E+01	0.17493E+00	0.10245E+01	0.37968E+00	0.62814E+01	0.62612E+01	0.38631E-15
48.25	0.12297E+01	0.17492E+00	0.10245E+01	0.37968E+00	0.62809E+01	0.62613E+01	0.38630E-15
48.50	0.12297E+01	0.17491E+00	0.10245E+01	0.37968E+00	0.62805E+01	0.62615E+01	0.38629E-15

48.75	0.12297E+01	0.17490E+00	0.10245E+01	0.37969E+00	0.62801E+01	0.62616E+01	0.38628E-15
49.00	0.12297E+01	0.17489E+00	0.10246E+01	0.37969E+00	0.62797E+01	0.62617E+01	0.38627E-15
49.25	0.12298E+01	0.17488E+00	0.10246E+01	0.37969E+00	0.62793E+01	0.62618E+01	0.38625E-15
49.50	0.12298E+01	0.17487E+00	0.10246E+01	0.37970E+00	0.62789E+01	0.62620E+01	0.38624E-15
49.75	0.12298E+01	0.17486E+00	0.10246E+01	0.37970E+00	0.62785E+01	0.62621E+01	0.38623E-15
50.00	0.12298E+01	0.17485E+00	0.10246E+01	0.37970E+00	0.62782E+01	0.62622E+01	0.38622E-15

TIME	CSI	CAVSI	PISI	PSI
0.0	16.49882	21.99842	9.00000	-1.21000
0.25	18.93071	24.00483	10.21845	-10.00000
0.50	20.67047	25.13505	10.96807	-11.00000
0.75	21.73079	25.65173	11.32712	-11.52252
1.00	22.24190	25.82273	11.44829	-7.00000
1.25	22.49458	25.86459	11.47814	-6.00000
1.50	22.64609	25.86113	11.47567	-5.00000
1.75	22.73568	25.85100	11.46844	-3.00000
2.00	22.78962	25.85907	11.47420	-1.00000
2.25	22.82908	25.89480	11.49972	-0.42500
2.50	22.86211	25.94904	11.53856	0.14770
2.75	22.89168	26.02398	11.59243	0.72500
3.00	22.92022	26.12272	11.66374	1.29770
3.25	22.94190	26.19198	11.71402	0.65232
3.50	22.96272	26.25981	11.76344	0.65167
3.75	22.98166	26.32502	11.81112	0.65105
4.00	22.99803	26.38697	11.85660	0.65045
4.25	23.01125	26.44521	11.89949	0.64955
4.50	23.02089	26.49931	11.93947	0.64755
4.75	23.02658	26.54901	11.97629	0.64552
5.00	23.02810	26.59413	12.00982	0.64344
5.25	23.02526	26.63462	12.03998	0.64130
5.50	23.01795	26.67044	12.06673	0.63909
5.75	23.00612	26.70166	12.09007	0.63680
6.00	22.98983	26.72826	12.11000	0.63444
6.25	22.96902	26.75046	12.12665	0.63197
6.50	22.94369	26.76851	12.14021	0.62937
6.75	22.91398	26.78250	12.15073	0.62666
7.00	22.87999	26.79262	12.15834	0.62382
7.25	22.84182	26.79908	12.16320	0.62084
7.50	22.79958	26.80209	12.16547	0.61772
7.75	22.75340	26.80188	12.16531	0.61446
8.00	22.70340	26.79866	12.16289	0.61105
8.25	22.64971	26.79267	12.15837	0.60748
8.50	22.59243	26.78411	12.15194	0.60375
8.75	22.53169	26.77320	12.14374	0.59985
9.00	22.46787	26.76022	12.13398	0.59578
9.25	22.34468	26.66054	12.05932	0.59266
9.50	22.26725	26.63165	12.03777	0.58831
9.75	22.19598	26.61489	12.02528	0.58342
10.00	22.12316	26.59887	12.01335	0.57805
10.25	22.04740	26.58157	12.00048	0.57215
10.50	21.96851	26.56274	11.98649	0.56566
10.75	21.88652	26.54242	11.97141	0.55851
11.00	21.80149	26.52072	11.95532	0.55061
11.25	21.71348	26.49772	11.93829	0.54191
11.50	21.62254	26.47351	11.92039	0.53236
11.75	21.52873	26.44813	11.90164	0.52168
12.00	21.43201	26.42139	11.88193	0.50748
12.25	21.33219	26.39255	11.86070	0.48675
12.50	21.22905	26.36055	11.83719	0.45962

12.75	21.12258	26.32472	11.81090	0.42845
13.00	21.01287	26.28468	11.78160	0.39320
13.25	20.89997	26.23967	11.74874	0.35115
13.50	20.78381	26.18842	11.71143	0.30037
13.75	20.66437	26.12946	11.66863	0.24002
14.00	20.54177	26.06136	11.61938	0.17079
14.25	20.41638	25.98328	11.56314	0.09630
14.50	20.28898	25.89561	11.50030	0.02223
14.75	20.16062	25.79984	11.43201	-0.04792
15.00	20.03235	25.69786	11.35969	-0.11266
15.25	19.90509	25.59152	11.28473	-0.17238
15.50	19.77953	25.48228	11.20820	-0.22798
15.75	19.65622	25.37133	11.13095	-0.28004
16.00	19.53555	25.25959	11.05365	-0.32897
16.25	19.41783	25.14784	10.97683	-0.37505
16.50	19.30331	25.03671	10.90092	-0.41844
16.75	19.19215	24.92677	10.82629	-0.45916
17.00	19.08448	24.81852	10.75325	-0.49726
17.25	18.98039	24.71236	10.68207	-0.53286
17.50	18.87992	24.60864	10.61294	-0.56614
17.75	18.78305	24.50761	10.54599	-0.59728
18.00	18.68978	24.40948	10.48133	-0.62646
18.25	18.60004	24.31436	10.41899	-0.65385
18.50	18.51375	24.22232	10.35899	-0.67961
18.75	18.43084	24.13341	10.30133	-0.70388
19.00	18.35120	24.04762	10.24597	-0.72679
19.25	18.27473	23.96493	10.19286	-0.74844
19.50	18.20132	23.88529	10.14195	-0.76895
19.75	18.13087	23.80865	10.09316	-0.78839
20.00	18.06327	23.73492	10.04643	-0.80687
20.25	17.99839	23.66402	10.00168	-0.82445
20.50	17.93615	23.59587	9.95883	-0.84119
20.75	17.87642	23.53038	9.91780	-0.85715
21.00	17.81912	23.46744	9.87853	-0.87238
21.25	17.76415	23.40698	9.84092	-0.88692
21.50	17.71141	23.34890	9.80492	-0.90080
21.75	17.66080	23.29311	9.77045	-0.91407
22.00	17.61225	23.23954	9.73745	-0.92675
22.25	17.56568	23.18808	9.70585	-0.93888
22.50	17.52099	23.13868	9.67559	-0.95048
22.75	17.47813	23.09123	9.64661	-0.96157
23.00	17.43700	23.04568	9.61886	-0.97219
23.25	17.39755	23.00195	9.59229	-0.98235
23.50	17.35971	22.95997	9.56684	-0.99207
23.75	17.32341	22.91968	9.54247	-1.00138
24.00	17.28859	22.88100	9.51913	-1.01029
24.25	17.25519	22.84388	9.49677	-1.01882
24.50	17.22316	22.80825	9.47537	-1.02698
24.75	17.19245	22.77406	9.45486	-1.03480
25.00	17.16299	22.74126	9.43522	-1.04229
25.25	17.13474	22.70979	9.41642	-1.04946
25.50	17.10765	22.67960	9.39840	-1.05632
25.75	17.08168	22.65063	9.38115	-1.06289
26.00	17.05678	22.62285	9.36463	-1.06919
26.25	17.03291	22.59621	9.34882	-1.07521
26.50	17.01002	22.57065	9.33367	-1.08099
26.75	16.98809	22.54615	9.31916	-1.08651
27.00	16.96706	22.52266	9.30527	-1.09181
27.25	16.94692	22.50013	9.29197	-1.09688
27.50	16.92761	22.47854	9.27924	-1.10173

27.75	16.90910	22.45784	9.26704	-1.10638
28.00	16.89137	22.43801	9.25537	-1.11083
28.25	16.87438	22.41899	9.24420	-1.11509
28.50	16.85811	22.40078	9.23350	-1.11917
28.75	16.84252	22.38332	9.22326	-1.12308
29.00	16.82759	22.36659	9.21346	-1.12682
29.25	16.81328	22.35057	9.20408	-1.13041
29.50	16.79959	22.33523	9.19510	-1.13384
29.75	16.78647	22.32053	9.18651	-1.13712
30.00	16.77390	22.30645	9.17829	-1.14027
30.25	16.76188	22.29296	9.17042	-1.14328
30.50	16.75036	22.28005	9.16289	-1.14616
30.75	16.73933	22.26769	9.15569	-1.14892
31.00	16.72878	22.25586	9.14880	-1.15156
31.25	16.71868	22.24453	9.14221	-1.15409
31.50	16.70901	22.23369	9.13590	-1.15652
31.75	16.69975	22.22331	9.12987	-1.15883
32.00	16.69090	22.21338	9.12410	-1.16105
32.25	16.68242	22.20387	9.11858	-1.16318
32.50	16.67431	22.19477	9.11330	-1.16521
32.75	16.66655	22.18607	9.10825	-1.16716
33.00	16.65913	22.17775	9.10342	-1.16902
33.25	16.65203	22.16978	9.09881	-1.17080
33.50	16.64523	22.16216	9.09440	-1.17251
33.75	16.63873	22.15487	9.09018	-1.17414
34.00	16.63252	22.14790	9.08614	-1.17570
34.25	16.62657	22.14124	9.08228	-1.17720
34.50	16.62089	22.13486	9.07860	-1.17863
34.75	16.61545	22.12876	9.07507	-1.18000
35.00	16.61025	22.12294	9.07170	-1.18131
35.25	16.60528	22.11736	9.06848	-1.18256
35.50	16.60053	22.11203	9.06541	-1.18376
35.75	16.59599	22.10694	9.06247	-1.18491
36.00	16.59164	22.10207	9.05966	-1.18601
36.25	16.58749	22.09742	9.05697	-1.18706
36.50	16.58352	22.09297	9.05440	-1.18806
36.75	16.57973	22.08872	9.05195	-1.18903
37.00	16.57610	22.08466	9.04961	-1.18995
37.25	16.57263	22.08078	9.04737	-1.19083
37.50	16.56932	22.07707	9.04523	-1.19167
37.75	16.56616	22.07352	9.04319	-1.19247
38.00	16.56313	22.07013	9.04124	-1.19324
38.25	16.56024	22.06690	9.03937	-1.19398
38.50	16.55748	22.06381	9.03759	-1.19468
38.75	16.55484	22.06085	9.03589	-1.19536
39.00	16.55232	22.05803	9.03427	-1.19600
39.25	16.54991	22.05534	9.03272	-1.19662
39.50	16.54761	22.05276	9.03123	-1.19721
39.75	16.54541	22.05031	9.02982	-1.19777
40.00	16.54331	22.04796	9.02847	-1.19831
40.25	16.54130	22.04571	9.02718	-1.19882
40.50	16.53939	22.04357	9.02595	-1.19932
40.75	16.53756	22.04153	9.02477	-1.19979
41.00	16.53581	22.03957	9.02364	-1.20024
41.25	16.53414	22.03771	9.02257	-1.20067
41.50	16.53255	22.03593	9.02155	-1.20108
41.75	16.53102	22.03423	9.02057	-1.20148
42.00	16.52957	22.03260	9.01964	-1.20185
42.25	16.52818	22.03105	9.01875	-1.20221
42.50	16.52685	22.02957	9.01789	-1.20256

42.75	16.52559	22.02816	9.01708	-1.20289
43.00	16.52438	22.02681	9.01631	-1.20320
43.25	16.52322	22.02552	9.01557	-1.20350
43.50	16.52211	22.02429	9.01485	-1.20379
43.75	16.52105	22.02310	9.01417	-1.20406
44.00	16.52003	22.02195	9.01351	-1.20431
44.25	16.51906	22.02085	9.01288	-1.20456
44.50	16.51812	22.01980	9.01228	-1.20479
44.75	16.51723	22.01879	9.01170	-1.20501
45.00	16.51637	22.01783	9.01114	-1.20522
45.25	16.51555	22.01691	9.01061	-1.20542
45.50	16.51477	22.01602	9.01011	-1.20562
45.75	16.51402	22.01518	9.00962	-1.20580
46.00	16.51331	22.01438	9.00916	-1.20598
46.25	16.51262	22.01361	9.00872	-1.20615
46.50	16.51197	22.01287	9.00830	-1.20631
46.75	16.51135	22.01217	9.00789	-1.20646
47.00	16.51075	22.01150	9.00751	-1.20661
47.25	16.51018	22.01086	9.00714	-1.20675
47.50	16.50964	22.01025	9.00679	-1.20689
47.75	16.50912	22.00967	9.00646	-1.20702
48.00	16.50863	22.00911	9.00614	-1.20714
48.25	16.50815	22.00858	9.00583	-1.20726
48.50	16.50770	22.00808	9.00554	-1.20738
48.75	16.50727	22.00759	9.00527	-1.20749
49.00	16.50686	22.00713	9.00500	-1.20759
49.25	16.50647	22.00669	9.00475	-1.20769
49.50	16.50610	22.00628	9.00451	-1.20779
49.75	16.50574	22.00588	9.00428	-1.20788
50.00	16.50540	22.00550	9.00406	-1.20797

TIME	FSI	VPLSI	RSI	LSI	QPLSI	QLSI	QDSI
0.0	0.47045E-01	0.61983E+00	0.68719E-01	0.42200E-01	0.22252E+02	0.69625E+00	0.12058E-16
0.25	0.10321E+00	0.13436E+01	-0.87914E-01	0.0	0.47040E+02	0.0	0.95465E-17
0.50	0.12051E+00	0.12668E+01	-0.11383E+00	0.0	0.43586E+02	0.0	0.80416E-17
0.75	0.13356E+00	0.11580E+01	-0.12600E+00	0.0	0.39205E+02	0.0	0.71154E-17
1.00	0.11725E+00	0.69942E+00	-0.52642E-01	0.53466E-02	0.23308E+02	0.11892E+00	0.65067E-17
1.25	0.11744E+00	0.56047E+00	-0.34730E-01	0.11712E-01	0.18525E+02	0.26345E+00	0.62338E-17
1.50	0.11597E+00	0.43673E+00	-0.12324E-01	0.18077E-01	0.14389E+02	0.40936E+00	0.61459E-17
1.75	0.10750E+00	0.26911E+00	0.28897E-01	0.30807E-01	0.88491E+01	0.70041E+00	0.60987E-17
2.00	0.98258E-01	0.13139E+00	0.67955E-01	0.68767E-01	0.43115E+01	0.15672E+01	0.60328E-17
2.25	0.97638E-01	0.10206E+00	0.75602E-01	0.14151E+00	0.33417E+01	0.32306E+01	0.59406E-17
2.50	0.96755E-01	0.80535E-01	0.81461E-01	0.21396E+00	0.26322E+01	0.48916E+01	0.58415E-17
2.75	0.95682E-01	0.65408E-01	0.85322E-01	0.28700E+00	0.21339E+01	0.65698E+01	0.57256E-17
3.00	0.94041E-01	0.52503E-01	0.89866E-01	0.35945E+00	0.17136E+01	0.82387E+01	0.56512E-17
3.25	0.99897E-01	0.89562E-01	0.74276E-01	0.27780E+00	0.29347E+01	0.63733E+01	0.57028E-17
3.50	0.10121E+00	0.93183E-01	0.72668E-01	0.27772E+00	0.30642E+01	0.63772E+01	0.57455E-17
3.75	0.10245E+00	0.95802E-01	0.70986E-01	0.27764E+00	0.31608E+01	0.63807E+01	0.57835E-17
4.00	0.10361E+00	0.97559E-01	0.69278E-01	0.27757E+00	0.32288E+01	0.63835E+01	0.58188E-17
4.25	0.10469E+00	0.98602E-01	0.67562E-01	0.27745E+00	0.32729E+01	0.63845E+01	0.58526E-17
4.50	0.10570E+00	0.99073E-01	0.65839E-01	0.27720E+00	0.32977E+01	0.63814E+01	0.58859E-17
4.75	0.10663E+00	0.99030E-01	0.64148E-01	0.27694E+00	0.33050E+01	0.63770E+01	0.59193E-17
5.00	0.10749E+00	0.98562E-01	0.62496E-01	0.27668E+00	0.32977E+01	0.63714E+01	0.59533E-17
5.25	0.10826E+00	0.97742E-01	0.60893E-01	0.27641E+00	0.32781E+01	0.63644E+01	0.59883E-17
5.50	0.10896E+00	0.96634E-01	0.59344E-01	0.27613E+00	0.32485E+01	0.63559E+01	0.60246E-17
5.75	0.10959E+00	0.95291E-01	0.57854E-01	0.27584E+00	0.32105E+01	0.63460E+01	0.60625E-17
6.00	0.11014E+00	0.93763E-01	0.56434E-01	0.27554E+00	0.31657E+01	0.63346E+01	0.61018E-17
6.25	0.11063E+00	0.92047E-01	0.55081E-01	0.27523E+00	0.31142E+01	0.63217E+01	0.61428E-17
6.50	0.11106E+00	0.90244E-01	0.53786E-01	0.27490E+00	0.30593E+01	0.63072E+01	0.61858E-17

6.75	0.11142E+00	0.88349E-01	0.52558E-01	0.27456E+00	0.30008E+01	0.62912E+01	0.62304E-17
7.00	0.11173E+00	0.86386E-01	0.51395E-01	0.27420E+00	0.29396E+01	0.62736E+01	0.62767E-17
7.25	0.11198E+00	0.84376E-01	0.50297E-01	0.27382E+00	0.28764E+01	0.62545E+01	0.63245E-17
7.50	0.11218E+00	0.82335E-01	0.49262E-01	0.27343E+00	0.28118E+01	0.62340E+01	0.63737E-17
7.75	0.11233E+00	0.80279E-01	0.48287E-01	0.27301E+00	0.27462E+01	0.62120E+01	0.64242E-17
8.00	0.11244E+00	0.78220E-01	0.47370E-01	0.27258E+00	0.26802E+01	0.61885E+01	0.64759E-17
8.25	0.11251E+00	0.76169E-01	0.46508E-01	0.27213E+00	0.26141E+01	0.61637E+01	0.65287E-17
8.50	0.11253E+00	0.74134E-01	0.45697E-01	0.27166E+00	0.25482E+01	0.61374E+01	0.65823E-17
8.75	0.11253E+00	0.72124E-01	0.44935E-01	0.27116E+00	0.24829E+01	0.61098E+01	0.66367E-17
9.00	0.11249E+00	0.70153E-01	0.44221E-01	0.27065E+00	0.24185E+01	0.60809E+01	0.66915E-17
9.25	0.14531E+00	0.69491E-01	0.63950E-01	0.27025E+00	0.24515E+01	0.60387E+01	0.74747E-17
9.50	0.14391E+00	0.65712E-01	0.71680E-01	0.26970E+00	0.23309E+01	0.60056E+01	0.76674E-17
9.75	0.14367E+00	0.63541E-01	0.72665E-01	0.26909E+00	0.22584E+01	0.59726E+01	0.77438E-17
10.00	0.14362E+00	0.61697E-01	0.72409E-01	0.26841E+00	0.21958E+01	0.59380E+01	0.77989E-17
10.25	0.14359E+00	0.59953E-01	0.71943E-01	0.26766E+00	0.21363E+01	0.59012E+01	0.78504E-17
10.50	0.14355E+00	0.58271E-01	0.71457E-01	0.26684E+00	0.20787E+01	0.58621E+01	0.79015E-17
10.75	0.14349E+00	0.56644E-01	0.70984E-01	0.26593E+00	0.20229E+01	0.58204E+01	0.79528E-17
11.00	0.14341E+00	0.55074E-01	0.70527E-01	0.26494E+00	0.19688E+01	0.57760E+01	0.80043E-17
11.25	0.14332E+00	0.53558E-01	0.70085E-01	0.26383E+00	0.19166E+01	0.57288E+01	0.80558E-17
11.50	0.14322E+00	0.52097E-01	0.69657E-01	0.26263E+00	0.18662E+01	0.56786E+01	0.81074E-17
11.75	0.14312E+00	0.50693E-01	0.69236E-01	0.26127E+00	0.18176E+01	0.56249E+01	0.81590E-17
12.00	0.14303E+00	0.49364E-01	0.68767E-01	0.25948E+00	0.17716E+01	0.55612E+01	0.82109E-17
12.25	0.14298E+00	0.48126E-01	0.68198E-01	0.25686E+00	0.17287E+01	0.54793E+01	0.82637E-17
12.50	0.14296E+00	0.46968E-01	0.67571E-01	0.25342E+00	0.16886E+01	0.53800E+01	0.83184E-17
12.75	0.14295E+00	0.45868E-01	0.66962E-01	0.24948E+00	0.16504E+01	0.52697E+01	0.83754E-17
13.00	0.14294E+00	0.44822E-01	0.66376E-01	0.24502E+00	0.16140E+01	0.51486E+01	0.84347E-17
13.25	0.14297E+00	0.43846E-01	0.65761E-01	0.23970E+00	0.15800E+01	0.50098E+01	0.84972E-17
13.50	0.14303E+00	0.42945E-01	0.65106E-01	0.23328E+00	0.15487E+01	0.48484E+01	0.85639E-17
13.75	0.14314E+00	0.42116E-01	0.64431E-01	0.22564E+00	0.15198E+01	0.46628E+01	0.86359E-17
14.00	0.14327E+00	0.41348E-01	0.63793E-01	0.21688E+00	0.14930E+01	0.44552E+01	0.87145E-17
14.25	0.14340E+00	0.40614E-01	0.63305E-01	0.20746E+00	0.14674E+01	0.42356E+01	0.88001E-17
14.50	0.14348E+00	0.39883E-01	0.63094E-01	0.19809E+00	0.14417E+01	0.40190E+01	0.88919E-17
14.75	0.14349E+00	0.39140E-01	0.63201E-01	0.18921E+00	0.14154E+01	0.38147E+01	0.89886E-17
15.00	0.14342E+00	0.38385E-01	0.63606E-01	0.18102E+00	0.13886E+01	0.36264E+01	0.90883E-17
15.25	0.14331E+00	0.37625E-01	0.64249E-01	0.17347E+00	0.13615E+01	0.34529E+01	0.91898E-17
15.50	0.14315E+00	0.36871E-01	0.65071E-01	0.16644E+00	0.13345E+01	0.32920E+01	0.92919E-17
15.75	0.14297E+00	0.36128E-01	0.66029E-01	0.15985E+00	0.13079E+01	0.31420E+01	0.93940E-17
16.00	0.14277E+00	0.35400E-01	0.67092E-01	0.15366E+00	0.12817E+01	0.30018E+01	0.94954E-17
16.25	0.14255E+00	0.34690E-01	0.68235E-01	0.14783E+00	0.12561E+01	0.28705E+01	0.95955E-17
16.50	0.14232E+00	0.33999E-01	0.69439E-01	0.14234E+00	0.12312E+01	0.27476E+01	0.96939E-17
16.75	0.14209E+00	0.33330E-01	0.70691E-01	0.13719E+00	0.12070E+01	0.26329E+01	0.97904E-17
17.00	0.14185E+00	0.32681E-01	0.71977E-01	0.13237E+00	0.11835E+01	0.25262E+01	0.98845E-17
17.25	0.14161E+00	0.32054E-01	0.73285E-01	0.12786E+00	0.11608E+01	0.24269E+01	0.99760E-17
17.50	0.14137E+00	0.31449E-01	0.74601E-01	0.12365E+00	0.11389E+01	0.23346E+01	0.10065E-16
17.75	0.14113E+00	0.30868E-01	0.75916E-01	0.11971E+00	0.11177E+01	0.22486E+01	0.10151E-16
18.00	0.14090E+00	0.30309E-01	0.77220E-01	0.11602E+00	0.10974E+01	0.21685E+01	0.10233E-16
18.25	0.14067E+00	0.29773E-01	0.78507E-01	0.11256E+00	0.10779E+01	0.20936E+01	0.10313E-16
18.50	0.14045E+00	0.29261E-01	0.79771E-01	0.10930E+00	0.10593E+01	0.20235E+01	0.10390E-16
18.75	0.14024E+00	0.28771E-01	0.81007E-01	0.10623E+00	0.10414E+01	0.19579E+01	0.10463E-16
19.00	0.14003E+00	0.28303E-01	0.82213E-01	0.10333E+00	0.10244E+01	0.18962E+01	0.10534E-16
19.25	0.13984E+00	0.27857E-01	0.83386E-01	0.10059E+00	0.10081E+01	0.18383E+01	0.10602E-16
19.50	0.13965E+00	0.27432E-01	0.84524E-01	0.97998E-01	0.99257E+00	0.17837E+01	0.10667E-16
19.75	0.13947E+00	0.27027E-01	0.85628E-01	0.95538E-01	0.97779E+00	0.17322E+01	0.10729E-16
20.00	0.13930E+00	0.26642E-01	0.86696E-01	0.93200E-01	0.96372E+00	0.16835E+01	0.10788E-16
20.25	0.13914E+00	0.26276E-01	0.87727E-01	0.90976E-01	0.95034E+00	0.16374E+01	0.10845E-16
20.50	0.13899E+00	0.25928E-01	0.88724E-01	0.88858E-01	0.93761E+00	0.15938E+01	0.10900E-16
20.75	0.13885E+00	0.25597E-01	0.89685E-01	0.86839E-01	0.92552E+00	0.15524E+01	0.10952E-16
21.00	0.13871E+00	0.25283E-01	0.90613E-01	0.84912E-01	0.91403E+00	0.15131E+01	0.11002E-16
21.25	0.13858E+00	0.24985E-01	0.91507E-01	0.83073E-01	0.90312E+00	0.14757E+01	0.11049E-16
21.50	0.13846E+00	0.24702E-01	0.92368E-01	0.81317E-01	0.89275E+00	0.14402E+01	0.11095E-16

21.75	0.13835E+00	0.24434E-01	0.93199E-01	0.79638E-01	0.88291E+00	0.14065E+01	0.11139E-16
22.00	0.13824E+00	0.24179E-01	0.93998E-01	0.78034E-01	0.87357E+00	0.13743E+01	0.11180E-16
22.25	0.13814E+00	0.23937E-01	0.94769E-01	0.76499E-01	0.86471E+00	0.13438E+01	0.11220E-16
22.50	0.13804E+00	0.23708E-01	0.95511E-01	0.75032E-01	0.85630E+00	0.13146E+01	0.11259E-16
22.75	0.13795E+00	0.23490E-01	0.96225E-01	0.73628E-01	0.84832E+00	0.12869E+01	0.11295E-16
23.00	0.13787E+00	0.23284E-01	0.96913E-01	0.72285E-01	0.84074E+00	0.12604E+01	0.11330E-16
23.25	0.13778E+00	0.23088E-01	0.97575E-01	0.71000E-01	0.83356E+00	0.12352E+01	0.11363E-16
23.50	0.13771E+00	0.22903E-01	0.98213E-01	0.69770E-01	0.82674E+00	0.12112E+01	0.11395E-16
23.75	0.13764E+00	0.22727E-01	0.98826E-01	0.68592E-01	0.82027E+00	0.11883E+01	0.11426E-16
24.00	0.13757E+00	0.22560E-01	0.99417E-01	0.67465E-01	0.81414E+00	0.11664E+01	0.11455E-16
24.25	0.13751E+00	0.22402E-01	0.99985E-01	0.66386E-01	0.80831E+00	0.11455E+01	0.11483E-16
24.50	0.13745E+00	0.22252E-01	0.10053E+00	0.65353E-01	0.80279E+00	0.11256E+01	0.11510E-16
24.75	0.13739E+00	0.22109E-01	0.10106E+00	0.64364E-01	0.79755E+00	0.11066E+01	0.11535E-16
25.00	0.13734E+00	0.21974E-01	0.10157E+00	0.63417E-01	0.79257E+00	0.10884E+01	0.11559E-16
25.25	0.13729E+00	0.21846E-01	0.10205E+00	0.62510E-01	0.78785E+00	0.10711E+01	0.11583E-16
25.50	0.13724E+00	0.21725E-01	0.10252E+00	0.61642E-01	0.78338E+00	0.10545E+01	0.11605E-16
25.75	0.13720E+00	0.21610E-01	0.10297E+00	0.60810E-01	0.77913E+00	0.10387E+01	0.11626E-16
26.00	0.13715E+00	0.21500E-01	0.10341E+00	0.60014E-01	0.77509E+00	0.10236E+01	0.11646E-16
26.25	0.13711E+00	0.21397E-01	0.10382E+00	0.59252E-01	0.77126E+00	0.10092E+01	0.11666E-16
26.50	0.13708E+00	0.21298E-01	0.10422E+00	0.58522E-01	0.76763E+00	0.99545E+00	0.11684E-16
26.75	0.13704E+00	0.21205E-01	0.10461E+00	0.57822E-01	0.76418E+00	0.98229E+00	0.11702E-16
27.00	0.13701E+00	0.21116E-01	0.10498E+00	0.57153E-01	0.76090E+00	0.96971E+00	0.11719E-16
27.25	0.13698E+00	0.21032E-01	0.10534E+00	0.56511E-01	0.75779E+00	0.95769E+00	0.11735E-16
27.50	0.13695E+00	0.20953E-01	0.10568E+00	0.55897E-01	0.75484E+00	0.94621E+00	0.11751E-16
27.75	0.13693E+00	0.20877E-01	0.10601E+00	0.55309E-01	0.75203E+00	0.93523E+00	0.11765E-16
28.00	0.13690E+00	0.20805E-01	0.10633E+00	0.54746E-01	0.74937E+00	0.92474E+00	0.11779E-16
28.25	0.13688E+00	0.20737E-01	0.10663E+00	0.54207E-01	0.74684E+00	0.91471E+00	0.11793E-16
28.50	0.13686E+00	0.20672E-01	0.10693E+00	0.53691E-01	0.74443E+00	0.90512E+00	0.11805E-16
28.75	0.13684E+00	0.20611E-01	0.10721E+00	0.53196E-01	0.74215E+00	0.89596E+00	0.11818E-16
29.00	0.13682E+00	0.20552E-01	0.10748E+00	0.52723E-01	0.73998E+00	0.88720E+00	0.11829E-16
29.25	0.13680E+00	0.20497E-01	0.10774E+00	0.52269E-01	0.73791E+00	0.87882E+00	0.11840E-16
29.50	0.13679E+00	0.20444E-01	0.10799E+00	0.51835E-01	0.73595E+00	0.87081E+00	0.11851E-16
29.75	0.13677E+00	0.20394E-01	0.10823E+00	0.51420E-01	0.73409E+00	0.86316E+00	0.11861E-16
30.00	0.13676E+00	0.20346E-01	0.10846E+00	0.51022E-01	0.73232E+00	0.85584E+00	0.11871E-16
30.25	0.13675E+00	0.20301E-01	0.10868E+00	0.50641E-01	0.73063E+00	0.84884E+00	0.11880E-16
30.50	0.13673E+00	0.20258E-01	0.10890E+00	0.50276E-01	0.72903E+00	0.84214E+00	0.11889E-16
30.75	0.13672E+00	0.20217E-01	0.10910E+00	0.49927E-01	0.72750E+00	0.83575E+00	0.11897E-16
31.00	0.13671E+00	0.20179E-01	0.10930E+00	0.49593E-01	0.72605E+00	0.82963E+00	0.11905E-16
31.25	0.13671E+00	0.20142E-01	0.10948E+00	0.49273E-01	0.72467E+00	0.82377E+00	0.11913E-16
31.50	0.13670E+00	0.20107E-01	0.10967E+00	0.48966E-01	0.72336E+00	0.81818E+00	0.11920E-16
31.75	0.13669E+00	0.20073E-01	0.10984E+00	0.48673E-01	0.72211E+00	0.81283E+00	0.11927E-16
32.00	0.13668E+00	0.20042E-01	0.11001E+00	0.48392E-01	0.72092E+00	0.80771E+00	0.11933E-16
32.25	0.13668E+00	0.20011E-01	0.11017E+00	0.48124E-01	0.71979E+00	0.80282E+00	0.11939E-16
32.50	0.13667E+00	0.19983E-01	0.11032E+00	0.47866E-01	0.71872E+00	0.79814E+00	0.11945E-16
32.75	0.13667E+00	0.19955E-01	0.11047E+00	0.47620E-01	0.71769E+00	0.79366E+00	0.11951E-16
33.00	0.13666E+00	0.19929E-01	0.11061E+00	0.47384E-01	0.71671E+00	0.78938E+00	0.11956E-16
33.25	0.13666E+00	0.19905E-01	0.11075E+00	0.47159E-01	0.71578E+00	0.78529E+00	0.11962E-16
33.50	0.13665E+00	0.19881E-01	0.11088E+00	0.46943E-01	0.71490E+00	0.78138E+00	0.11967E-16
33.75	0.13665E+00	0.19859E-01	0.11100E+00	0.46737E-01	0.71405E+00	0.77764E+00	0.11971E-16
34.00	0.13665E+00	0.19837E-01	0.11112E+00	0.46539E-01	0.71325E+00	0.77406E+00	0.11976E-16
34.25	0.13664E+00	0.19817E-01	0.11124E+00	0.46350E-01	0.71248E+00	0.77064E+00	0.11980E-16
34.50	0.13664E+00	0.19798E-01	0.11135E+00	0.46169E-01	0.71175E+00	0.76736E+00	0.11984E-16
34.75	0.13664E+00	0.19779E-01	0.11146E+00	0.45995E-01	0.71106E+00	0.76423E+00	0.11988E-16
35.00	0.13664E+00	0.19762E-01	0.11156E+00	0.45830E-01	0.71039E+00	0.76124E+00	0.11991E-16
35.25	0.13664E+00	0.19745E-01	0.11166E+00	0.45671E-01	0.70976E+00	0.75838E+00	0.11995E-16
35.50	0.13664E+00	0.19729E-01	0.11175E+00	0.45519E-01	0.70916E+00	0.75564E+00	0.11998E-16
35.75	0.13664E+00	0.19714E-01	0.11184E+00	0.45374E-01	0.70858E+00	0.75303E+00	0.12001E-16
36.00	0.13663E+00	0.19700E-01	0.11193E+00	0.45235E-01	0.70804E+00	0.75053E+00	0.12004E-16
36.25	0.13663E+00	0.19686E-01	0.11201E+00	0.45102E-01	0.70751E+00	0.74813E+00	0.12007E-16
36.50	0.13663E+00	0.19673E-01	0.11209E+00	0.44975E-01	0.70701E+00	0.74585E+00	0.12009E-16

36.75	0.13663E+00	0.19660E-01	0.11217E+00	0.44853E-01	0.70654E+00	0.74366E+00	0.12012E-16
37.00	0.13663E+00	0.19648E-01	0.11224E+00	0.44737E-01	0.70608E+00	0.74157E+00	0.12014E-16
37.25	0.13664E+00	0.19637E-01	0.11231E+00	0.44626E-01	0.70565E+00	0.73957E+00	0.12017E-16
37.50	0.13664E+00	0.19626E-01	0.11238E+00	0.44519E-01	0.70524E+00	0.73766E+00	0.12019E-16
37.75	0.13664E+00	0.19616E-01	0.11244E+00	0.44418E-01	0.70484E+00	0.73583E+00	0.12021E-16
38.00	0.13664E+00	0.19606E-01	0.11250E+00	0.44320E-01	0.70447E+00	0.73408E+00	0.12023E-16
38.25	0.13664E+00	0.19596E-01	0.11256E+00	0.44227E-01	0.70411E+00	0.73241E+00	0.12025E-16
38.50	0.13664E+00	0.19587E-01	0.11262E+00	0.44138E-01	0.70376E+00	0.73081E+00	0.12027E-16
38.75	0.13664E+00	0.19579E-01	0.11267E+00	0.44053E-01	0.70343E+00	0.72928E+00	0.12028E-16
39.00	0.13664E+00	0.19571E-01	0.11273E+00	0.43971E-01	0.70312E+00	0.72782E+00	0.12030E-16
39.25	0.13664E+00	0.19563E-01	0.11278E+00	0.43893E-01	0.70282E+00	0.72643E+00	0.12031E-16
39.50	0.13664E+00	0.19555E-01	0.11282E+00	0.43819E-01	0.70254E+00	0.72509E+00	0.12033E-16
39.75	0.13664E+00	0.19548E-01	0.11287E+00	0.43747E-01	0.70226E+00	0.72382E+00	0.12034E-16
40.00	0.13665E+00	0.19541E-01	0.11291E+00	0.43679E-01	0.70200E+00	0.72260E+00	0.12035E-16
40.25	0.13665E+00	0.19535E-01	0.11296E+00	0.43614E-01	0.70175E+00	0.72143E+00	0.12037E-16
40.50	0.13665E+00	0.19529E-01	0.11300E+00	0.43551E-01	0.70151E+00	0.72031E+00	0.12038E-16
40.75	0.13665E+00	0.19523E-01	0.11304E+00	0.43492E-01	0.70129E+00	0.71925E+00	0.12039E-16
41.00	0.13665E+00	0.19517E-01	0.11307E+00	0.43435E-01	0.70107E+00	0.71823E+00	0.12040E-16
41.25	0.13665E+00	0.19512E-01	0.11311E+00	0.43380E-01	0.70086E+00	0.71726E+00	0.12041E-16
41.50	0.13665E+00	0.19507E-01	0.11314E+00	0.43328E-01	0.70066E+00	0.71633E+00	0.12042E-16
41.75	0.13666E+00	0.19502E-01	0.11318E+00	0.43278E-01	0.70047E+00	0.71544E+00	0.12043E-16
42.00	0.13666E+00	0.19497E-01	0.11321E+00	0.43231E-01	0.70029E+00	0.71459E+00	0.12044E-16
42.25	0.13666E+00	0.19492E-01	0.11324E+00	0.43185E-01	0.70012E+00	0.71377E+00	0.12044E-16
42.50	0.13666E+00	0.19488E-01	0.11327E+00	0.43142E-01	0.69995E+00	0.71300E+00	0.12045E-16
42.75	0.13666E+00	0.19484E-01	0.11329E+00	0.43100E-01	0.69979E+00	0.71225E+00	0.12046E-16
43.00	0.13666E+00	0.19480E-01	0.11332E+00	0.43060E-01	0.69964E+00	0.71154E+00	0.12047E-16
43.25	0.13667E+00	0.19476E-01	0.11335E+00	0.43022E-01	0.69950E+00	0.71086E+00	0.12047E-16
43.50	0.13667E+00	0.19473E-01	0.11337E+00	0.42986E-01	0.69936E+00	0.71022E+00	0.12048E-16
43.75	0.13667E+00	0.19470E-01	0.11339E+00	0.42952E-01	0.69924E+00	0.70961E+00	0.12048E-16
44.00	0.13667E+00	0.19467E-01	0.11341E+00	0.42919E-01	0.69911E+00	0.70903E+00	0.12049E-16
44.25	0.13667E+00	0.19464E-01	0.11343E+00	0.42889E-01	0.69900E+00	0.70848E+00	0.12050E-16
44.50	0.13667E+00	0.19461E-01	0.11345E+00	0.42859E-01	0.69889E+00	0.70796E+00	0.12050E-16
44.75	0.13667E+00	0.19458E-01	0.11347E+00	0.42831E-01	0.69879E+00	0.70745E+00	0.12051E-16
45.00	0.13667E+00	0.19456E-01	0.11348E+00	0.42805E-01	0.69869E+00	0.70698E+00	0.12051E-16
45.25	0.13667E+00	0.19453E-01	0.11350E+00	0.42779E-01	0.69860E+00	0.70652E+00	0.12052E-16
45.50	0.13668E+00	0.19451E-01	0.11352E+00	0.42755E-01	0.69851E+00	0.70608E+00	0.12052E-16
45.75	0.13668E+00	0.19449E-01	0.11353E+00	0.42731E-01	0.69842E+00	0.70566E+00	0.12052E-16
46.00	0.13668E+00	0.19447E-01	0.11355E+00	0.42709E-01	0.69834E+00	0.70526E+00	0.12053E-16
46.25	0.13668E+00	0.19445E-01	0.11356E+00	0.42687E-01	0.69827E+00	0.70488E+00	0.12053E-16
46.50	0.13668E+00	0.19443E-01	0.11358E+00	0.42667E-01	0.69819E+00	0.70452E+00	0.12054E-16
46.75	0.13668E+00	0.19441E-01	0.11359E+00	0.42647E-01	0.69812E+00	0.70417E+00	0.12054E-16
47.00	0.13668E+00	0.19440E-01	0.11360E+00	0.42629E-01	0.69806E+00	0.70383E+00	0.12054E-16
47.25	0.13668E+00	0.19438E-01	0.11361E+00	0.42611E-01	0.69799E+00	0.70351E+00	0.12055E-16
47.50	0.13668E+00	0.19436E-01	0.11363E+00	0.42593E-01	0.69793E+00	0.70320E+00	0.12055E-16
47.75	0.13668E+00	0.19435E-01	0.11364E+00	0.42577E-01	0.69787E+00	0.70291E+00	0.12055E-16
48.00	0.13668E+00	0.19433E-01	0.11365E+00	0.42561E-01	0.69782E+00	0.70263E+00	0.12055E-16
48.25	0.13668E+00	0.19432E-01	0.11366E+00	0.42546E-01	0.69776E+00	0.70236E+00	0.12056E-16
48.50	0.13668E+00	0.19431E-01	0.11367E+00	0.42532E-01	0.69771E+00	0.70210E+00	0.12056E-16
48.75	0.13668E+00	0.19429E-01	0.11368E+00	0.42518E-01	0.69766E+00	0.70186E+00	0.12056E-16
49.00	0.13668E+00	0.19428E-01	0.11369E+00	0.42505E-01	0.69761E+00	0.70162E+00	0.12056E-16
49.25	0.13669E+00	0.19427E-01	0.11370E+00	0.42492E-01	0.69757E+00	0.70140E+00	0.12057E-16
49.50	0.13669E+00	0.19426E-01	0.11370E+00	0.42480E-01	0.69752E+00	0.70118E+00	0.12057E-16
49.75	0.13669E+00	0.19425E-01	0.11371E+00	0.42468E-01	0.69748E+00	0.70097E+00	0.12057E-16
50.00	0.13669E+00	0.19424E-01	0.11372E+00	0.42457E-01	0.69744E+00	0.70078E+00	0.12057E-16

TIME	PA	PV	PIPL	CPL
0.0	0.19940E+02	0.51200E+01	0.20000E+02	0.35900E+02
0.25	0.19940E+02	0.45131E+01	0.19075E+02	0.35011E+02

0.50	0.19940E+02	0.34722E+01	0.18466E+02	0.34406E+02
0.75	0.19940E+02	0.24644E+01	0.17925E+02	0.33855E+02
1.00	0.19940E+02	0.19347E+01	0.17417E+02	0.33324E+02
1.25	0.19940E+02	0.15698E+01	0.17161E+02	0.33052E+02
1.50	0.19940E+02	0.12356E+01	0.17063E+02	0.32947E+02
1.75	0.19940E+02	0.10615E+01	0.17004E+02	0.32882E+02
2.00	0.19940E+02	0.10957E+01	0.16941E+02	0.32814E+02
2.25	0.19940E+02	0.12952E+01	0.16876E+02	0.32744E+02
2.50	0.19940E+02	0.15817E+01	0.16821E+02	0.32684E+02
2.75	0.19940E+02	0.19556E+01	0.16767E+02	0.32625E+02
3.00	0.19940E+02	0.23408E+01	0.16779E+02	0.32638E+02
3.25	0.19940E+02	0.25319E+01	0.16897E+02	0.32767E+02
3.50	0.19940E+02	0.27165E+01	0.17005E+02	0.32884E+02
3.75	0.19940E+02	0.28921E+01	0.17106E+02	0.32993E+02
4.00	0.19940E+02	0.30592E+01	0.17202E+02	0.33096E+02
4.25	0.19940E+02	0.32186E+01	0.17293E+02	0.33193E+02
4.50	0.19940E+02	0.33709E+01	0.17380E+02	0.33285E+02
4.75	0.19940E+02	0.35167E+01	0.17464E+02	0.33373E+02
5.00	0.19940E+02	0.36569E+01	0.17544E+02	0.33458E+02
5.25	0.19940E+02	0.37918E+01	0.17621E+02	0.33539E+02
5.50	0.19940E+02	0.39220E+01	0.17695E+02	0.33616E+02
5.75	0.19940E+02	0.40478E+01	0.17767E+02	0.33691E+02
6.00	0.19940E+02	0.41691E+01	0.17836E+02	0.33763E+02
6.25	0.19940E+02	0.42867E+01	0.17903E+02	0.33833E+02
6.50	0.19940E+02	0.44014E+01	0.17969E+02	0.33900E+02
6.75	0.19940E+02	0.45128E+01	0.18032E+02	0.33966E+02
7.00	0.19940E+02	0.46211E+01	0.18094E+02	0.34029E+02
7.25	0.19940E+02	0.47265E+01	0.18154E+02	0.34091E+02
7.50	0.19940E+02	0.48292E+01	0.18213E+02	0.34150E+02
7.75	0.19940E+02	0.49292E+01	0.18270E+02	0.34208E+02
8.00	0.19940E+02	0.50267E+01	0.18326E+02	0.34265E+02
8.25	0.19940E+02	0.51218E+01	0.18380E+02	0.34320E+02
8.50	0.19940E+02	0.52146E+01	0.18433E+02	0.34373E+02
8.75	0.19940E+02	0.53051E+01	0.18484E+02	0.34425E+02
9.00	0.19940E+02	0.53930E+01	0.18534E+02	0.34475E+02
9.25	0.24540E+02	0.55730E+01	0.19349E+02	0.35278E+02
9.50	0.24540E+02	0.55207E+01	0.19549E+02	0.35472E+02
9.75	0.24540E+02	0.55758E+01	0.19624E+02	0.35543E+02
10.00	0.24540E+02	0.56493E+01	0.19673E+02	0.35590E+02
10.25	0.24540E+02	0.57246E+01	0.19718E+02	0.35632E+02
10.50	0.24540E+02	0.57986E+01	0.19760E+02	0.35673E+02
10.75	0.24540E+02	0.58707E+01	0.19801E+02	0.35711E+02
11.00	0.24540E+02	0.59408E+01	0.19840E+02	0.35749E+02
11.25	0.24540E+02	0.60090E+01	0.19879E+02	0.35785E+02
11.50	0.24540E+02	0.60750E+01	0.19916E+02	0.35821E+02
11.75	0.24540E+02	0.61390E+01	0.19952E+02	0.35855E+02
12.00	0.24540E+02	0.62007E+01	0.19987E+02	0.35888E+02
12.25	0.24540E+02	0.62595E+01	0.20021E+02	0.35920E+02
12.50	0.24540E+02	0.63150E+01	0.20054E+02	0.35951E+02
12.75	0.24540E+02	0.63669E+01	0.20086E+02	0.35981E+02
13.00	0.24540E+02	0.64152E+01	0.20116E+02	0.36009E+02
13.25	0.24540E+02	0.64595E+01	0.20145E+02	0.36036E+02
13.50	0.24540E+02	0.64993E+01	0.20173E+02	0.36062E+02
13.75	0.24540E+02	0.65338E+01	0.20198E+02	0.36086E+02
14.00	0.24540E+02	0.65628E+01	0.20222E+02	0.36109E+02
14.25	0.24540E+02	0.65860E+01	0.20245E+02	0.36129E+02
14.50	0.24540E+02	0.66039E+01	0.20264E+02	0.36147E+02
14.75	0.24540E+02	0.66173E+01	0.20281E+02	0.36163E+02
15.00	0.24540E+02	0.66269E+01	0.20295E+02	0.36176E+02
15.25	0.24540E+02	0.66334E+01	0.20306E+02	0.36187E+02

15.50	0.24540E+02	0.66371E+01	0.20316E+02	0.36195E+02
15.75	0.24540E+02	0.66383E+01	0.20323E+02	0.36202E+02
16.00	0.24540E+02	0.66373E+01	0.20328E+02	0.36207E+02
16.25	0.24540E+02	0.66343E+01	0.20332E+02	0.36211E+02
16.50	0.24540E+02	0.66296E+01	0.20335E+02	0.36213E+02
16.75	0.24540E+02	0.66234E+01	0.20336E+02	0.36214E+02
17.00	0.24540E+02	0.66159E+01	0.20336E+02	0.36215E+02
17.25	0.24540E+02	0.66073E+01	0.20336E+02	0.36214E+02
17.50	0.24540E+02	0.65978E+01	0.20334E+02	0.36213E+02
17.75	0.24540E+02	0.65876E+01	0.20332E+02	0.36210E+02
18.00	0.24540E+02	0.65767E+01	0.20329E+02	0.36208E+02
18.25	0.24540E+02	0.65653E+01	0.20326E+02	0.36204E+02
18.50	0.24540E+02	0.65535E+01	0.20322E+02	0.36201E+02
18.75	0.24540E+02	0.65413E+01	0.20317E+02	0.36197E+02
19.00	0.24540E+02	0.65289E+01	0.20313E+02	0.36192E+02
19.25	0.24540E+02	0.65163E+01	0.20308E+02	0.36188E+02
19.50	0.24540E+02	0.65036E+01	0.20302E+02	0.36183E+02
19.75	0.24540E+02	0.64908E+01	0.20297E+02	0.36178E+02
20.00	0.24540E+02	0.64779E+01	0.20292E+02	0.36173E+02
20.25	0.24540E+02	0.64650E+01	0.20286E+02	0.36168E+02
20.50	0.24540E+02	0.64522E+01	0.20280E+02	0.36162E+02
20.75	0.24540E+02	0.64394E+01	0.20274E+02	0.36157E+02
21.00	0.24540E+02	0.64267E+01	0.20269E+02	0.36152E+02
21.25	0.24540E+02	0.64141E+01	0.20263E+02	0.36146E+02
21.50	0.24540E+02	0.64016E+01	0.20257E+02	0.36141E+02
21.75	0.24540E+02	0.63893E+01	0.20251E+02	0.36135E+02
22.00	0.24540E+02	0.63771E+01	0.20245E+02	0.36130E+02
22.25	0.24540E+02	0.63650E+01	0.20239E+02	0.36124E+02
22.50	0.24540E+02	0.63532E+01	0.20234E+02	0.36119E+02
22.75	0.24540E+02	0.63415E+01	0.20228E+02	0.36114E+02
23.00	0.24540E+02	0.63300E+01	0.20222E+02	0.36108E+02
23.25	0.24540E+02	0.63187E+01	0.20217E+02	0.36103E+02
23.50	0.24540E+02	0.63076E+01	0.20211E+02	0.36098E+02
23.75	0.24540E+02	0.62967E+01	0.20206E+02	0.36093E+02
24.00	0.24540E+02	0.62860E+01	0.20200E+02	0.36088E+02
24.25	0.24540E+02	0.62756E+01	0.20195E+02	0.36083E+02
24.50	0.24540E+02	0.62653E+01	0.20190E+02	0.36078E+02
24.75	0.24540E+02	0.62553E+01	0.20184E+02	0.36073E+02
25.00	0.24540E+02	0.62455E+01	0.20179E+02	0.36068E+02
25.25	0.24540E+02	0.62359E+01	0.20174E+02	0.36064E+02
25.50	0.24540E+02	0.62265E+01	0.20170E+02	0.36059E+02
25.75	0.24540E+02	0.62173E+01	0.20165E+02	0.36055E+02
26.00	0.24540E+02	0.62084E+01	0.20160E+02	0.36050E+02
26.25	0.24540E+02	0.61996E+01	0.20156E+02	0.36046E+02
26.50	0.24540E+02	0.61911E+01	0.20151E+02	0.36042E+02
26.75	0.24540E+02	0.61828E+01	0.20147E+02	0.36038E+02
27.00	0.24540E+02	0.61747E+01	0.20142E+02	0.36034E+02
27.25	0.24540E+02	0.61668E+01	0.20138E+02	0.36030E+02
27.50	0.24540E+02	0.61591E+01	0.20134E+02	0.36026E+02
27.75	0.24540E+02	0.61516E+01	0.20130E+02	0.36022E+02
28.00	0.24540E+02	0.61443E+01	0.20126E+02	0.36019E+02
28.25	0.24540E+02	0.61372E+01	0.20122E+02	0.36015E+02
28.50	0.24540E+02	0.61303E+01	0.20119E+02	0.36012E+02
28.75	0.24540E+02	0.61236E+01	0.20115E+02	0.36008E+02
29.00	0.24540E+02	0.61171E+01	0.20112E+02	0.36005E+02
29.25	0.24540E+02	0.61107E+01	0.20108E+02	0.36002E+02
29.50	0.24540E+02	0.61046E+01	0.20105E+02	0.35999E+02
29.75	0.24540E+02	0.60985E+01	0.20102E+02	0.35995E+02
30.00	0.24540E+02	0.60927E+01	0.20098E+02	0.35993E+02
30.25	0.24540E+02	0.60871E+01	0.20095E+02	0.35990E+02

30.50	0.24540E+02	0.60816E+01	0.20092E+02	0.35987E+02
30.75	0.24540E+02	0.60762E+01	0.20089E+02	0.35984E+02
31.00	0.24540E+02	0.60710E+01	0.20087E+02	0.35981E+02
31.25	0.24540E+02	0.60660E+01	0.20084E+02	0.35979E+02
31.50	0.24540E+02	0.60611E+01	0.20081E+02	0.35976E+02
31.75	0.24540E+02	0.60564E+01	0.20079E+02	0.35974E+02
32.00	0.24540E+02	0.60518E+01	0.20076E+02	0.35971E+02
32.25	0.24540E+02	0.60474E+01	0.20074E+02	0.35969E+02
32.50	0.24540E+02	0.60430E+01	0.20071E+02	0.35967E+02
32.75	0.24540E+02	0.60389E+01	0.20069E+02	0.35965E+02
33.00	0.24540E+02	0.60348E+01	0.20067E+02	0.35963E+02
33.25	0.24540E+02	0.60309E+01	0.20064E+02	0.35961E+02
33.50	0.24540E+02	0.60271E+01	0.20062E+02	0.35959E+02
33.75	0.24540E+02	0.60234E+01	0.20060E+02	0.35957E+02
34.00	0.24540E+02	0.60198E+01	0.20058E+02	0.35955E+02
34.25	0.24540E+02	0.60164E+01	0.20056E+02	0.35953E+02
34.50	0.24540E+02	0.60130E+01	0.20054E+02	0.35951E+02
34.75	0.24540E+02	0.60098E+01	0.20053E+02	0.35950E+02
35.00	0.24540E+02	0.60066E+01	0.20051E+02	0.35948E+02
35.25	0.24540E+02	0.60036E+01	0.20049E+02	0.35946E+02
35.50	0.24540E+02	0.60007E+01	0.20048E+02	0.35945E+02
35.75	0.24540E+02	0.59978E+01	0.20046E+02	0.35943E+02
36.00	0.24540E+02	0.59951E+01	0.20044E+02	0.35942E+02
36.25	0.24540E+02	0.59924E+01	0.20043E+02	0.35940E+02
36.50	0.24540E+02	0.59899E+01	0.20041E+02	0.35939E+02
36.75	0.24540E+02	0.59874E+01	0.20040E+02	0.35938E+02
37.00	0.24540E+02	0.59850E+01	0.20039E+02	0.35936E+02
37.25	0.24540E+02	0.59826E+01	0.20037E+02	0.35935E+02
37.50	0.24540E+02	0.59804E+01	0.20036E+02	0.35934E+02
37.75	0.24540E+02	0.59782E+01	0.20035E+02	0.35933E+02
38.00	0.24540E+02	0.59761E+01	0.20034E+02	0.35932E+02
38.25	0.24540E+02	0.59741E+01	0.20032E+02	0.35931E+02
38.50	0.24540E+02	0.59721E+01	0.20031E+02	0.35930E+02
38.75	0.24540E+02	0.59703E+01	0.20030E+02	0.35929E+02
39.00	0.24540E+02	0.59684E+01	0.20029E+02	0.35928E+02
39.25	0.24540E+02	0.59667E+01	0.20028E+02	0.35927E+02
39.50	0.24540E+02	0.59650E+01	0.20027E+02	0.35926E+02
39.75	0.24540E+02	0.59633E+01	0.20026E+02	0.35925E+02
40.00	0.24540E+02	0.59617E+01	0.20025E+02	0.35924E+02
40.25	0.24540E+02	0.59602E+01	0.20025E+02	0.35923E+02
40.50	0.24540E+02	0.59587E+01	0.20024E+02	0.35922E+02
40.75	0.24540E+02	0.59573E+01	0.20023E+02	0.35921E+02
41.00	0.24540E+02	0.59559E+01	0.20022E+02	0.35921E+02
41.25	0.24540E+02	0.59546E+01	0.20021E+02	0.35920E+02
41.50	0.24540E+02	0.59533E+01	0.20021E+02	0.35919E+02
41.75	0.24540E+02	0.59521E+01	0.20020E+02	0.35919E+02
42.00	0.24540E+02	0.59509E+01	0.20019E+02	0.35918E+02
42.25	0.24540E+02	0.59497E+01	0.20018E+02	0.35917E+02
42.50	0.24540E+02	0.59486E+01	0.20018E+02	0.35917E+02
42.75	0.24540E+02	0.59475E+01	0.20017E+02	0.35916E+02
43.00	0.24540E+02	0.59465E+01	0.20017E+02	0.35916E+02
43.25	0.24540E+02	0.59455E+01	0.20016E+02	0.35915E+02
43.50	0.24540E+02	0.59446E+01	0.20015E+02	0.35915E+02
43.75	0.24540E+02	0.59437E+01	0.20015E+02	0.35914E+02
44.00	0.24540E+02	0.59429E+01	0.20014E+02	0.35913E+02
44.25	0.24540E+02	0.59421E+01	0.20014E+02	0.35913E+02
44.50	0.24540E+02	0.59414E+01	0.20013E+02	0.35913E+02
44.75	0.24540E+02	0.59407E+01	0.20013E+02	0.35912E+02
45.00	0.24540E+02	0.59400E+01	0.20012E+02	0.35912E+02
45.25	0.24540E+02	0.59394E+01	0.20012E+02	0.35911E+02

45.50	0.24540E+02	0.59387E+01	0.20012E+02	0.35911E+02
45.75	0.24540E+02	0.59381E+01	0.20011E+02	0.35911E+02
46.00	0.24540E+02	0.59376E+01	0.20011E+02	0.35910E+02
46.25	0.24540E+02	0.59370E+01	0.20011E+02	0.35910E+02
46.50	0.24540E+02	0.59365E+01	0.20010E+02	0.35910E+02
46.75	0.24540E+02	0.59360E+01	0.20010E+02	0.35909E+02
47.00	0.24540E+02	0.59355E+01	0.20010E+02	0.35909E+02
47.25	0.24540E+02	0.59350E+01	0.20009E+02	0.35909E+02
47.50	0.24540E+02	0.59345E+01	0.20009E+02	0.35909E+02
47.75	0.24540E+02	0.59341E+01	0.20009E+02	0.35908E+02
48.00	0.24540E+02	0.59337E+01	0.20009E+02	0.35908E+02
48.25	0.24540E+02	0.59332E+01	0.20008E+02	0.35908E+02
48.50	0.24540E+02	0.59329E+01	0.20008E+02	0.35908E+02
48.75	0.24540E+02	0.59325E+01	0.20008E+02	0.35907E+02
49.00	0.24540E+02	0.59321E+01	0.20008E+02	0.35907E+02
49.25	0.24540E+02	0.59317E+01	0.20007E+02	0.35907E+02
49.50	0.24540E+02	0.59314E+01	0.20007E+02	0.35907E+02
49.75	0.24540E+02	0.59311E+01	0.20007E+02	0.35907E+02
50.00	0.24540E+02	0.59307E+01	0.20007E+02	0.35906E+02

Transient response for 40% burn

Time	VPL	VS	VM	VSI	QPL	QS	QM	QSI
0.0	6.12000	10.12800	10.41000	6.75200	219.7080	167.1000	134.3000	111.4000
0.25000	5.76732	10.18468	10.42232	7.03569	199.2503	173.7529	139.4516	120.0532
0.50000	5.45823	10.17064	10.38660	7.39452	183.6520	177.3437	142.0454	129.4669
0.75000	5.15146	10.18020	10.37834	7.70001	171.4574	180.2769	144.1270	136.6467
1.00000	4.90870	10.20438	10.39019	7.90672	162.3339	182.8800	146.0220	141.2721
1.25000	4.70789	10.23423	10.41421	8.05367	155.1550	185.1430	147.7341	144.4759
1.50000	4.50719	10.26038	10.43791	8.20452	148.6377	187.0951	149.2390	147.5361
1.75000	4.35641	10.28163	10.45796	8.31400	143.3910	188.7751	150.5382	149.8036
2.00100	4.28610	10.30604	10.48173	8.33612	140.0367	190.1792	151.6264	150.6657
2.25000	4.29316	10.33832	10.51346	8.26506	138.7819	191.2923	152.4877	149.9461
2.50000	4.35964	10.37659	10.55114	8.12264	139.4092	192.1051	153.1112	147.8825
2.75000	4.48956	10.41826	10.59225	7.90993	141.9202	192.6121	153.4911	144.4846
3.00100	4.68367	10.46167	10.63519	7.62947	146.2741	192.8194	153.6321	139.7825
3.25000	4.75820	10.49554	10.66919	7.48707	148.9090	192.7680	153.5664	137.2646
3.50000	4.83901	10.51469	10.68926	7.36704	151.5439	192.5315	153.3535	135.0791
3.75000	4.91841	10.52370	10.69968	7.26820	154.1127	192.1587	153.0332	133.2034
4.00000	4.99426	10.52520	10.70288	7.18767	156.5933	191.6860	152.6347	131.5939
4.25000	5.06635	10.52099	10.70050	7.12217	158.9820	191.1417	152.1806	130.2038
4.50000	5.13499	10.51244	10.69386	7.06871	161.2817	190.5474	151.6883	128.9905
4.75000	5.20054	10.50066	10.68401	7.02479	163.4973	189.9198	151.1717	127.9192
5.00000	5.26328	10.48652	10.67180	6.98840	165.6325	189.2718	150.6413	126.9624
5.25000	5.32343	10.47071	10.65792	6.95794	167.6910	188.6131	150.1053	126.0987
5.50000	5.38117	10.45376	10.64292	6.93214	169.6756	187.9511	149.5699	125.3113
5.75000	5.43663	10.43610	10.62724	6.91003	171.5890	187.2915	149.0401	124.5874
6.00000	5.48994	10.41805	10.61120	6.89081	173.4335	186.6385	148.5193	123.9167
6.25000	5.54119	10.39985	10.59507	6.87389	175.2114	185.9950	148.0101	123.2915
6.50000	5.59046	10.38171	10.57904	6.85880	176.9244	185.3636	147.5144	122.7056
6.75000	5.62661	10.36846	10.56743	6.84751	178.4853	184.7849	147.0687	122.1691
7.00000	5.65302	10.35886	10.55902	6.83910	179.8927	184.2615	146.6758	121.6780
7.25000	5.67622	10.35028	10.55149	6.83202	181.1943	183.7737	146.3187	121.2213
7.50000	5.69768	10.34215	10.54437	6.82579	182.4107	183.3137	145.9903	120.7933
7.75000	5.71785	10.33434	10.53760	6.82021	183.5554	182.8765	145.6858	120.3902
8.00000	5.73696	10.32680	10.53112	6.81512	184.6386	182.4585	145.4016	120.0093
8.25000	5.75515	10.31948	10.52494	6.81043	185.6683	182.0568	145.1347	119.6482
8.50000	5.77253	10.31236	10.51903	6.80607	186.6513	181.6691	144.8828	119.3049
8.75000	5.78920	10.30544	10.51337	6.80199	187.5928	181.2935	144.6436	118.9781
9.00000	5.80522	10.29870	10.50794	6.79814	188.4974	180.9287	144.4156	118.6663
9.25000	5.82066	10.29212	10.50273	6.79448	189.3687	180.5734	144.1973	118.3686
9.50000	5.83556	10.28571	10.49772	6.79100	190.2095	180.2268	143.9875	118.0841
9.75000	5.84998	10.27944	10.49290	6.78768	191.0225	179.8882	143.7854	117.8120
10.00000	5.86394	10.27331	10.48825	6.78451	191.8095	179.5569	143.5900	117.5515
10.25000	5.87746	10.26733	10.48375	6.78146	192.5724	179.2325	143.4008	117.3022
10.50000	5.89058	10.26148	10.47940	6.77854	193.3124	178.9148	143.2173	117.0635
10.75000	5.90332	10.25576	10.47520	6.77573	194.0307	178.6034	143.0390	116.8349
11.00000	5.91568	10.25017	10.47112	6.77303	194.7283	178.2982	142.8655	116.6160
11.25000	5.92769	10.24470	10.46716	6.77044	195.4060	177.9989	142.6967	116.4064
11.50000	5.93935	10.23937	10.46333	6.76796	196.0646	177.7056	142.5322	116.2056
11.75000	5.95068	10.23415	10.45960	6.76557	196.7045	177.4182	142.3719	116.0135
12.00000	5.96168	10.22906	10.45599	6.76328	197.3263	177.1365	142.2156	115.8295
12.25000	5.97236	10.22409	10.45248	6.76107	197.9305	176.8606	142.0633	115.6535
12.50000	5.98274	10.21923	10.44907	6.75896	198.5175	176.5905	141.9149	115.4851

TIME	CM	CAVM	PIM	PM
0.0	0.12901E+02	0.17196E+02	0.90000E+01	-0.51000E+00
0.25	0.13380E+02	0.17827E+02	0.94860E+01	-0.50163E+00
0.50	0.13676E+02	0.18242E+02	0.98144E+01	-0.52878E+00
0.75	0.13887E+02	0.18529E+02	0.10046E+02	-0.53542E+00
1.00	0.14054E+02	0.18744E+02	0.10222E+02	-0.52590E+00
1.25	0.14186E+02	0.18906E+02	0.10355E+02	-0.50714E+00
1.50	0.14298E+02	0.19041E+02	0.10468E+02	-0.49107E+00
1.75	0.14395E+02	0.19157E+02	0.10566E+02	-0.47756E+00
2.00	0.14466E+02	0.19238E+02	0.10633E+02	-0.46164E+00
2.25	0.14504E+02	0.19269E+02	0.10660E+02	-0.44059E+00
2.50	0.14511E+02	0.19257E+02	0.10649E+02	-0.41587E+00
2.75	0.14491E+02	0.19205E+02	0.10606E+02	-0.38931E+00
3.00	0.14446E+02	0.19120E+02	0.10534E+02	-0.36207E+00
3.25	0.14393E+02	0.19031E+02	0.10460E+02	-0.34089E+00
3.50	0.14347E+02	0.18958E+02	0.10398E+02	-0.32855E+00
3.75	0.14303E+02	0.18894E+02	0.10345E+02	-0.32220E+00
4.00	0.14261E+02	0.18837E+02	0.10298E+02	-0.32026E+00
4.25	0.14222E+02	0.18787E+02	0.10257E+02	-0.32171E+00
4.50	0.14185E+02	0.18741E+02	0.10219E+02	-0.32575E+00
4.75	0.14149E+02	0.18700E+02	0.10186E+02	-0.33177E+00
5.00	0.14116E+02	0.18663E+02	0.10155E+02	-0.33928E+00
5.25	0.14084E+02	0.18628E+02	0.10127E+02	-0.34787E+00
5.50	0.14053E+02	0.18596E+02	0.10101E+02	-0.35722E+00
5.75	0.14024E+02	0.18567E+02	0.10076E+02	-0.36707E+00
6.00	0.13996E+02	0.18539E+02	0.10054E+02	-0.37722E+00
6.25	0.13970E+02	0.18513E+02	0.10032E+02	-0.38751E+00
6.50	0.13944E+02	0.18488E+02	0.10012E+02	-0.39780E+00
6.75	0.13917E+02	0.18459E+02	0.99887E+01	-0.40530E+00
7.00	0.13891E+02	0.18429E+02	0.99645E+01	-0.41075E+00
7.25	0.13867E+02	0.18401E+02	0.99424E+01	-0.41565E+00
7.50	0.13845E+02	0.18377E+02	0.99223E+01	-0.42028E+00
7.75	0.13825E+02	0.18354E+02	0.99040E+01	-0.42472E+00
8.00	0.13807E+02	0.18333E+02	0.98872E+01	-0.42896E+00
8.25	0.13790E+02	0.18314E+02	0.98717E+01	-0.43302E+00
8.50	0.13773E+02	0.18296E+02	0.98571E+01	-0.43691E+00
8.75	0.13758E+02	0.18278E+02	0.98433E+01	-0.44065E+00
9.00	0.13743E+02	0.18262E+02	0.98303E+01	-0.44423E+00
9.25	0.13729E+02	0.18247E+02	0.98178E+01	-0.44768E+00
9.50	0.13716E+02	0.18232E+02	0.98058E+01	-0.45100E+00
9.75	0.13703E+02	0.18217E+02	0.97942E+01	-0.45421E+00
10.00	0.13691E+02	0.18203E+02	0.97830E+01	-0.45730E+00
10.25	0.13678E+02	0.18189E+02	0.97721E+01	-0.46030E+00
10.50	0.13667E+02	0.18176E+02	0.97616E+01	-0.46320E+00
10.75	0.13655E+02	0.18163E+02	0.97512E+01	-0.46601E+00
11.00	0.13644E+02	0.18151E+02	0.97412E+01	-0.46874E+00
11.25	0.13633E+02	0.18138E+02	0.97314E+01	-0.47139E+00
11.50	0.13622E+02	0.18126E+02	0.97217E+01	-0.47396E+00
11.75	0.13612E+02	0.18114E+02	0.97124E+01	-0.47646E+00
12.00	0.13601E+02	0.18103E+02	0.97032E+01	-0.47889E+00
12.25	0.13591E+02	0.18092E+02	0.96942E+01	-0.48125E+00

TIME	FM	VPLM	RM	LM	QPLM	QLM	QDM
0.0	0.45364E+00	0.83677E+00	0.91498E+00	0.26025E+00	0.30040E+02	0.33575E+01	0.25957E-15
0.25	0.57232E+00	0.51868E+00	0.90466E+00	0.27035E+00	0.17919E+02	0.36173E+01	0.23205E-15
0.50	0.65088E+00	0.36447E+00	0.85332E+00	0.25947E+00	0.12263E+02	0.35485E+01	0.21378E-15
0.75	0.68794E+00	0.34698E+00	0.76069E+00	0.25919E+00	0.11549E+02	0.35995E+01	0.20475E-15
1.00	0.71117E+00	0.32834E+00	0.70265E+00	0.25959E+00	0.10858E+02	0.36482E+01	0.19882E-15

1.25	0.72520E+00	0.30966E+00	0.66758E+00	0.26370E+00	0.10205E+02	0.37409E+01	0.19499E-15
1.50	0.73003E+00	0.29244E+00	0.65550E+00	0.28309E+00	0.96441E+01	0.40475E+01	0.19342E-15
1.75	0.73910E+00	0.27655E+00	0.63283E+00	0.29938E+00	0.91027E+01	0.43095E+01	0.19092E-15
2.00	0.75659E+00	0.26142E+00	0.58912E+00	0.31859E+00	0.85410E+01	0.46087E+01	0.18644E-15
2.25	0.77694E+00	0.24658E+00	0.53826E+00	0.34400E+00	0.79709E+01	0.49894E+01	0.18120E-15
2.50	0.79451E+00	0.23235E+00	0.49433E+00	0.37382E+00	0.74300E+01	0.54246E+01	0.17654E-15
2.75	0.81053E+00	0.21885E+00	0.45429E+00	0.40586E+00	0.69182E+01	0.58812E+01	0.17217E-15
3.00	0.82517E+00	0.20618E+00	0.41771E+00	0.43873E+00	0.64392E+01	0.63377E+01	0.16807E-15
3.25	0.81559E+00	0.19474E+00	0.44166E+00	0.46429E+00	0.60944E+01	0.66827E+01	0.17020E-15
3.50	0.80972E+00	0.18474E+00	0.45633E+00	0.47917E+00	0.57856E+01	0.68744E+01	0.17152E-15
3.75	0.80503E+00	0.17579E+00	0.46805E+00	0.48683E+00	0.55083E+01	0.69629E+01	0.17264E-15
4.00	0.80079E+00	0.16768E+00	0.47864E+00	0.48917E+00	0.52576E+01	0.69760E+01	0.17372E-15
4.25	0.79685E+00	0.16027E+00	0.48850E+00	0.48743E+00	0.50291E+01	0.69321E+01	0.17477E-15
4.50	0.79317E+00	0.15343E+00	0.49768E+00	0.48255E+00	0.48191E+01	0.68448E+01	0.17579E-15
4.75	0.78976E+00	0.14710E+00	0.50621E+00	0.47528E+00	0.46246E+01	0.67250E+01	0.17678E-15
5.00	0.78659E+00	0.14120E+00	0.51414E+00	0.46623E+00	0.44435E+01	0.65812E+01	0.17773E-15
5.25	0.78363E+00	0.13568E+00	0.52152E+00	0.45586E+00	0.42741E+01	0.64203E+01	0.17864E-15
5.50	0.78088E+00	0.13050E+00	0.52841E+00	0.44458E+00	0.41149E+01	0.62479E+01	0.17951E-15
5.75	0.77829E+00	0.12562E+00	0.53487E+00	0.43269E+00	0.39649E+01	0.60682E+01	0.18034E-15
6.00	0.77587E+00	0.12102E+00	0.54094E+00	0.42044E+00	0.38233E+01	0.58847E+01	0.18114E-15
6.25	0.77358E+00	0.11667E+00	0.54666E+00	0.40803E+00	0.36892E+01	0.57001E+01	0.18190E-15
6.50	0.77140E+00	0.11299E+00	0.55065E+00	0.39562E+00	0.35757E+01	0.55166E+01	0.18263E-15
6.75	0.76627E+00	0.11730E+00	0.53413E+00	0.38658E+00	0.37209E+01	0.53800E+01	0.18406E-15
7.00	0.75945E+00	0.11894E+00	0.52972E+00	0.38000E+00	0.37851E+01	0.52786E+01	0.18587E-15
7.25	0.75279E+00	0.11967E+00	0.52755E+00	0.37409E+00	0.38201E+01	0.51875E+01	0.18763E-15
7.50	0.74655E+00	0.11990E+00	0.52572E+00	0.36849E+00	0.38387E+01	0.51019E+01	0.18927E-15
7.75	0.74074E+00	0.11979E+00	0.52387E+00	0.36315E+00	0.38454E+01	0.50206E+01	0.19080E-15
8.00	0.73529E+00	0.11941E+00	0.52197E+00	0.35803E+00	0.38429E+01	0.49432E+01	0.19222E-15
8.25	0.73016E+00	0.11882E+00	0.52003E+00	0.35313E+00	0.38333E+01	0.48695E+01	0.19356E-15
8.50	0.72530E+00	0.11808E+00	0.51808E+00	0.34843E+00	0.38181E+01	0.47991E+01	0.19483E-15
8.75	0.72067E+00	0.11722E+00	0.51612E+00	0.34393E+00	0.37984E+01	0.47318E+01	0.19603E-15
9.00	0.71624E+00	0.11627E+00	0.51417E+00	0.33960E+00	0.37755E+01	0.46673E+01	0.19718E-15
9.25	0.71200E+00	0.11526E+00	0.51225E+00	0.33544E+00	0.37500E+01	0.46054E+01	0.19828E-15
9.50	0.70791E+00	0.11421E+00	0.51035E+00	0.33143E+00	0.37227E+01	0.45459E+01	0.19933E-15
9.75	0.70398E+00	0.11313E+00	0.50849E+00	0.32756E+00	0.36941E+01	0.44886E+01	0.20035E-15
10.00	0.70017E+00	0.11204E+00	0.50667E+00	0.32383E+00	0.36647E+01	0.44334E+01	0.20133E-15
10.25	0.69649E+00	0.11094E+00	0.50489E+00	0.32021E+00	0.36349E+01	0.43800E+01	0.20227E-15
10.50	0.69292E+00	0.10985E+00	0.50316E+00	0.31672E+00	0.36049E+01	0.43284E+01	0.20319E-15
10.75	0.68946E+00	0.10877E+00	0.50148E+00	0.31332E+00	0.35751E+01	0.42784E+01	0.20407E-15
11.00	0.68610E+00	0.10771E+00	0.49984E+00	0.31003E+00	0.35455E+01	0.42300E+01	0.20493E-15
11.25	0.68284E+00	0.10667E+00	0.49825E+00	0.30684E+00	0.35165E+01	0.41830E+01	0.20576E-15
11.50	0.67966E+00	0.10566E+00	0.49671E+00	0.30373E+00	0.34880E+01	0.41375E+01	0.20657E-15
11.75	0.67658E+00	0.10468E+00	0.49522E+00	0.30072E+00	0.34602E+01	0.40932E+01	0.20735E-15
12.00	0.67358E+00	0.10373E+00	0.49378E+00	0.29779E+00	0.34333E+01	0.40503E+01	0.20812E-15
12.25	0.67067E+00	0.10281E+00	0.49238E+00	0.29494E+00	0.34071E+01	0.40086E+01	0.20885E-15

TIME	CS	CAVS	PIS	PS
0.0	0.16499E+02	0.21998E+02	0.90000E+01	-0.12100E+01
0.25	0.17060E+02	0.22705E+02	0.94135E+01	-0.11610E+01
0.50	0.17437E+02	0.23217E+02	0.97234E+01	-0.11731E+01
0.75	0.17709E+02	0.23571E+02	0.99433E+01	-0.11649E+01
1.00	0.17922E+02	0.23836E+02	0.10111E+02	-0.11440E+01
1.25	0.18091E+02	0.24038E+02	0.10240E+02	-0.11182E+01
1.50	0.18235E+02	0.24209E+02	0.10350E+02	-0.10957E+01
1.75	0.18360E+02	0.24359E+02	0.10448E+02	-0.10774E+01
2.00	0.18453E+02	0.24463E+02	0.10517E+02	-0.10563E+01
2.25	0.18503E+02	0.24505E+02	0.10544E+02	-0.10285E+01
2.50	0.18513E+02	0.24489E+02	0.10534E+02	-0.99561E+00
2.75	0.18488E+02	0.24424E+02	0.10491E+02	-0.95977E+00

3.00	0.18431E+02	0.24316E+02	0.10420E+02	-0.92243E+00
3.25	0.18367E+02	0.24206E+02	0.10349E+02	-0.89330E+00
3.50	0.18311E+02	0.24119E+02	0.10292E+02	-0.87684E+00
3.75	0.18260E+02	0.24045E+02	0.10244E+02	-0.86908E+00
4.00	0.18212E+02	0.23981E+02	0.10203E+02	-0.86779E+00
4.25	0.18168E+02	0.23926E+02	0.10168E+02	-0.87142E+00
4.50	0.18126E+02	0.23877E+02	0.10137E+02	-0.87877E+00
4.75	0.18086E+02	0.23833E+02	0.10109E+02	-0.88890E+00
5.00	0.18049E+02	0.23794E+02	0.10084E+02	-0.90106E+00
5.25	0.18013E+02	0.23759E+02	0.10061E+02	-0.91466E+00
5.50	0.17979E+02	0.23726E+02	0.10041E+02	-0.92923E+00
5.75	0.17946E+02	0.23695E+02	0.10022E+02	-0.94442E+00
6.00	0.17915E+02	0.23667E+02	0.10003E+02	-0.95994E+00
6.25	0.17884E+02	0.23640E+02	0.99865E+01	-0.97560E+00
6.50	0.17855E+02	0.23614E+02	0.99703E+01	-0.99121E+00
6.75	0.17822E+02	0.23580E+02	0.99490E+01	-0.10026E+01
7.00	0.17788E+02	0.23542E+02	0.99252E+01	-0.10109E+01
7.25	0.17755E+02	0.23506E+02	0.99024E+01	-0.10182E+01
7.50	0.17725E+02	0.23471E+02	0.98809E+01	-0.10252E+01
7.75	0.17696E+02	0.23439E+02	0.98606E+01	-0.10320E+01
8.00	0.17668E+02	0.23408E+02	0.98414E+01	-0.10385E+01
8.25	0.17642E+02	0.23378E+02	0.98230E+01	-0.10448E+01
8.50	0.17617E+02	0.23350E+02	0.98054E+01	-0.10509E+01
8.75	0.17592E+02	0.23322E+02	0.97884E+01	-0.10568E+01
9.00	0.17568E+02	0.23295E+02	0.97719E+01	-0.10626E+01
9.25	0.17545E+02	0.23269E+02	0.97558E+01	-0.10683E+01
9.50	0.17522E+02	0.23244E+02	0.97402E+01	-0.10738E+01
9.75	0.17500E+02	0.23219E+02	0.97249E+01	-0.10792E+01
10.00	0.17478E+02	0.23195E+02	0.97099E+01	-0.10845E+01
10.25	0.17457E+02	0.23171E+02	0.96952E+01	-0.10897E+01
10.50	0.17436E+02	0.23147E+02	0.96807E+01	-0.10947E+01
10.75	0.17415E+02	0.23124E+02	0.96666E+01	-0.10997E+01
11.00	0.17395E+02	0.23101E+02	0.96526E+01	-0.11045E+01
11.25	0.17375E+02	0.23079E+02	0.96389E+01	-0.11092E+01
11.50	0.17355E+02	0.23057E+02	0.96255E+01	-0.11138E+01
11.75	0.17336E+02	0.23035E+02	0.96123E+01	-0.11183E+01
12.00	0.17317E+02	0.23014E+02	0.95993E+01	-0.11227E+01
12.25	0.17298E+02	0.22993E+02	0.95866E+01	-0.11270E+01

TIME	FS	VPLS	RS	LS	QPLS	QLS	QDM
0.0	0.43658E+00	0.10646E+01	0.89543E+00	0.25320E+00	0.38217E+02	0.41775E+01	0.19292E-15
0.25	0.53432E+00	0.69430E+00	0.90392E+00	0.29040E+00	0.23987E+02	0.49543E+01	0.16436E-15
0.50	0.60132E+00	0.51314E+00	0.85266E+00	0.28119E+00	0.17266E+02	0.49031E+01	0.14475E-15
0.75	0.63233E+00	0.48598E+00	0.75418E+00	0.28746E+00	0.16175E+02	0.50905E+01	0.13478E-15
1.00	0.65158E+00	0.45856E+00	0.69306E+00	0.30331E+00	0.15165E+02	0.54359E+01	0.12815E-15
1.25	0.66323E+00	0.43213E+00	0.65604E+00	0.32286E+00	0.14242E+02	0.58407E+01	0.12377E-15
1.50	0.66702E+00	0.40777E+00	0.64401E+00	0.33998E+00	0.13447E+02	0.61994E+01	0.12170E-15
1.75	0.67471E+00	0.38542E+00	0.61958E+00	0.35388E+00	0.12686E+02	0.64973E+01	0.11873E-15
2.00	0.68980E+00	0.36418E+00	0.57166E+00	0.36984E+00	0.11898E+02	0.68247E+01	0.11392E-15
2.25	0.70729E+00	0.34332E+00	0.51612E+00	0.39093E+00	0.11098E+02	0.72335E+01	0.10855E-15
2.50	0.72227E+00	0.32327E+00	0.46857E+00	0.41592E+00	0.10337E+02	0.77001E+01	0.10392E-15
2.75	0.73583E+00	0.30419E+00	0.42551E+00	0.44313E+00	0.96157E+01	0.81925E+01	0.99745E-16
3.00	0.74816E+00	0.28623E+00	0.38636E+00	0.47147E+00	0.89390E+01	0.86896E+01	0.95957E-16
3.25	0.73946E+00	0.27007E+00	0.41396E+00	0.49357E+00	0.84518E+01	0.90653E+01	0.98379E-16
3.50	0.73434E+00	0.25609E+00	0.43023E+00	0.50607E+00	0.80202E+01	0.92665E+01	0.99899E-16
3.75	0.73046E+00	0.24370E+00	0.44256E+00	0.51196E+00	0.76360E+01	0.93481E+01	0.10116E-15
4.00	0.72711E+00	0.23254E+00	0.45318E+00	0.51294E+00	0.72914E+01	0.93416E+01	0.10233E-15
4.25	0.72412E+00	0.22240E+00	0.46268E+00	0.51018E+00	0.69789E+01	0.92689E+01	0.10345E-15

4.50	0.72143E+00	0.21309E+00	0.47123E+00	0.50460E+00	0.66929E+01	0.91464E+01	0.10452E-15
4.75	0.71900E+00	0.20449E+00	0.47893E+00	0.49691E+00	0.64288E+01	0.89874E+01	0.10554E-15
5.00	0.71681E+00	0.19648E+00	0.48591E+00	0.48768E+00	0.61831E+01	0.88022E+01	0.10651E-15
5.25	0.71481E+00	0.18899E+00	0.49226E+00	0.47736E+00	0.59534E+01	0.85989E+01	0.10744E-15
5.50	0.71297E+00	0.18196E+00	0.49808E+00	0.46630E+00	0.57375E+01	0.83838E+01	0.10832E-15
5.75	0.71128E+00	0.17534E+00	0.50346E+00	0.45478E+00	0.55339E+01	0.81616E+01	0.10916E-15
6.00	0.70971E+00	0.16908E+00	0.50844E+00	0.44299E+00	0.53414E+01	0.79362E+01	0.10997E-15
6.25	0.70824E+00	0.16316E+00	0.51310E+00	0.43111E+00	0.51590E+01	0.77102E+01	0.11074E-15
6.50	0.70686E+00	0.15803E+00	0.51589E+00	0.41927E+00	0.50012E+01	0.74859E+01	0.11149E-15
6.75	0.70270E+00	0.16186E+00	0.49642E+00	0.41061E+00	0.51343E+01	0.73179E+01	0.11299E-15
7.00	0.69690E+00	0.16269E+00	0.49094E+00	0.40434E+00	0.51771E+01	0.71924E+01	0.11491E-15
7.25	0.69116E+00	0.16253E+00	0.48820E+00	0.39674E+00	0.51882E+01	0.70798E+01	0.11680E-15
7.50	0.68575E+00	0.16186E+00	0.48599E+00	0.39343E+00	0.51820E+01	0.69736E+01	0.11857E-15
7.75	0.68067E+00	0.16085E+00	0.48388E+00	0.38833E+00	0.51637E+01	0.68719E+01	0.12023E-15
8.00	0.67588E+00	0.15959E+00	0.48179E+00	0.38340E+00	0.51363E+01	0.67741E+01	0.12180E-15
8.25	0.67135E+00	0.15815E+00	0.47973E+00	0.37862E+00	0.51020E+01	0.66796E+01	0.12328E-15
8.50	0.66705E+00	0.15657E+00	0.47770E+00	0.37397E+00	0.50626E+01	0.65881E+01	0.12469E-15
8.75	0.66293E+00	0.15490E+00	0.47570E+00	0.36945E+00	0.50194E+01	0.64993E+01	0.12603E-15
9.00	0.65898E+00	0.15317E+00	0.47375E+00	0.36504E+00	0.49736E+01	0.64131E+01	0.12733E-15
9.25	0.65519E+00	0.15141E+00	0.47184E+00	0.36074E+00	0.49260E+01	0.63291E+01	0.12857E-15
9.50	0.65153E+00	0.14963E+00	0.46999E+00	0.35654E+00	0.48773E+01	0.62474E+01	0.12977E-15
9.75	0.64799E+00	0.14786E+00	0.46819E+00	0.35244E+00	0.48282E+01	0.61677E+01	0.13093E-15
10.00	0.64457E+00	0.14610E+00	0.46645E+00	0.34844E+00	0.47790E+01	0.60900E+01	0.13205E-15
10.25	0.64125E+00	0.14437E+00	0.46476E+00	0.34452E+00	0.47302E+01	0.60142E+01	0.13314E-15
10.50	0.63802E+00	0.14267E+00	0.46314E+00	0.34070E+00	0.46821E+01	0.59402E+01	0.13420E-15
10.75	0.63489E+00	0.14101E+00	0.46157E+00	0.33695E+00	0.46348E+01	0.58680E+01	0.13523E-15
11.00	0.63185E+00	0.13940E+00	0.46006E+00	0.33330E+00	0.45887E+01	0.57976E+01	0.13623E-15
11.25	0.62889E+00	0.13784E+00	0.45860E+00	0.32972E+00	0.45438E+01	0.57288E+01	0.13720E-15
11.50	0.62601E+00	0.13632E+00	0.45721E+00	0.32623E+00	0.45002E+01	0.56617E+01	0.13815E-15
11.75	0.62320E+00	0.13486E+00	0.45587E+00	0.32281E+00	0.44581E+01	0.55962E+01	0.13907E-15
12.00	0.62047E+00	0.13346E+00	0.45458E+00	0.31948E+00	0.44174E+01	0.55324E+01	0.13997E-15
12.25	0.61782E+00	0.13211E+00	0.45336E+00	0.31622E+00	0.43782E+01	0.54701E+01	0.14084E-15

TIME	CSI	CAVSI	PISI	PSI
0.0	16.49882	21.99842	9.00000	-1.21000
0.25	17.06347	22.44956	9.26217	-21.00000
0.50	17.50848	22.68752	9.40313	-18.00000
0.75	17.74631	22.72896	9.42787	-13.00060
1.00	17.86734	22.71722	9.42085	-7.00000
1.25	17.93913	22.69609	9.40824	-7.00000
1.50	17.98230	22.64032	9.37502	-7.00000
1.75	18.01823	22.60844	9.35608	-4.05000
2.00	18.07383	22.66289	9.38845	-1.11180
2.25	18.14215	22.79833	9.46941	-0.60000
2.50	18.20622	22.98226	9.58034	-0.10000
2.75	18.26623	23.22183	9.72656	0.40000
3.00	18.32140	23.52660	9.91544	0.89800
3.25	18.33355	23.67010	10.00551	-0.28711
3.50	18.33561	23.78557	10.07851	-0.42337
3.75	18.32687	23.87071	10.13265	-0.54454
4.00	18.30830	23.92763	10.16898	-0.64710
4.25	18.28148	23.96021	10.18984	-0.73168
4.50	18.24809	23.97276	10.19788	-0.80078
4.75	18.20968	23.96930	10.19566	-0.85748
5.00	18.16759	23.95336	10.18545	-0.90443
5.25	18.12300	23.92793	10.16917	-0.94373
5.50	18.07685	23.89548	10.14844	-0.97700
5.75	18.02994	23.85804	10.12458	-1.00554
6.00	17.98289	23.81725	10.09863	-1.03035

6.25	17.93620	23.77440	10.07143	-1.05220
6.50	17.89024	23.73049	10.04363	-1.07170
6.75	17.84141	23.67846	10.01077	-1.08629
7.00	17.79153	23.62176	9.97509	-1.09716
7.25	17.74311	23.56547	9.93977	-1.10631
7.50	17.69658	23.51072	9.90552	-1.11437
7.75	17.65199	23.45779	9.87252	-1.12160
8.00	17.60928	23.40678	9.84080	-1.12818
8.25	17.56837	23.35769	9.81036	-1.13425
8.50	17.52918	23.31051	9.78119	-1.13989
8.75	17.49166	23.26522	9.75325	-1.14518
9.00	17.45571	23.22175	9.72651	-1.15017
9.25	17.42129	23.18007	9.70093	-1.15490
9.50	17.38831	23.14011	9.67647	-1.15941
9.75	17.35673	23.10182	9.65307	-1.16371
10.00	17.32647	23.06512	9.63070	-1.16783
10.25	17.29749	23.02997	9.60931	-1.17178
10.50	17.26973	22.99630	9.58886	-1.17557
10.75	17.24315	22.96406	9.56931	-1.17921
11.00	17.21769	22.93318	9.55063	-1.18270
11.25	17.19331	22.90362	9.53277	-1.18606
11.50	17.16997	22.87532	9.51571	-1.18929
11.75	17.14763	22.84823	9.49940	-1.19239
12.00	17.12625	22.82231	9.48381	-1.19536
12.25	17.10578	22.79751	9.46892	-1.19822

TIME	FSI	VPLSI	RSI	LSI	QPLSI	QLSI	QDSI
0.0	0.14553E-01	0.32259E+00	0.29848E-01	0.16880E+00	0.11581E+02	0.27850E+01	0.19292E-15
0.25	0.11222E+00	0.12425E+01	-0.17724E+00	0.0	0.42927E+02	0.0	0.16790E-15
0.50	0.15562E+00	0.99304E+00	-0.21127E+00	0.0	0.33413E+02	0.0	0.15209E-15
0.75	0.16922E+00	0.71217E+00	-0.16697E+00	0.0	0.23703E+02	0.0	0.14647E-15
1.00	0.15397E+00	0.40880E+00	-0.35973E-01	0.21386E-01	0.13519E+02	0.38212E+00	0.14368E-15
1.25	0.18146E+00	0.39135E+00	-0.45348E-01	0.21386E-01	0.12898E+02	0.38365E+00	0.14239E-15
1.50	0.20595E+00	0.37488E+00	-0.49572E-01	0.21386E-01	0.12363E+02	0.38458E+00	0.14346E-15
1.75	0.19012E+00	0.24156E+00	0.70135E-01	0.96494E-01	0.79508E+01	0.17386E+01	0.14303E-15
2.00	0.16862E+00	0.11919E+00	0.20368E+00	0.21849E+00	0.38942E+01	0.39490E+01	0.13891E-15
2.25	0.18092E+00	0.95570E-01	0.22673E+00	0.47748E+00	0.30894E+01	0.86626E+01	0.13223E-15
2.50	0.19278E+00	0.74141E-01	0.24745E+00	0.73050E+00	0.23708E+01	0.13300E+02	0.12483E-15
2.75	0.20456E+00	0.54295E-01	0.26513E+00	0.98352E+00	0.17163E+01	0.17965E+02	0.11642E-15
3.00	0.21655E+00	0.35975E-01	0.27889E+00	0.12355E+01	0.11235E+01	0.22637E+02	0.10691E-15
3.25	0.25254E+00	0.71859E-01	0.21390E+00	0.63582E+00	0.22489E+01	0.11657E+02	0.10582E-15
3.50	0.26813E+00	0.73347E-01	0.21072E+00	0.56687E+00	0.22970E+01	0.10394E+02	0.10452E-15
3.75	0.28275E+00	0.74246E-01	0.20802E+00	0.50555E+00	0.23264E+01	0.92651E+01	0.10357E-15
4.00	0.29610E+00	0.74520E-01	0.20692E+00	0.45365E+00	0.23365E+01	0.83056E+01	0.10307E-15
4.25	0.30815E+00	0.74253E-01	0.20761E+00	0.41085E+00	0.23301E+01	0.75110E+01	0.10297E-15
4.50	0.31900E+00	0.73569E-01	0.20993E+00	0.37588E+00	0.23107E+01	0.68591E+01	0.10319E-15
4.75	0.32877E+00	0.72590E-01	0.21361E+00	0.34719E+00	0.22821E+01	0.63222E+01	0.10366E-15
5.00	0.33760E+00	0.71416E-01	0.21835E+00	0.32343E+00	0.22474E+01	0.58759E+01	0.10431E-15
5.25	0.34558E+00	0.70117E-01	0.22392E+00	0.30354E+00	0.22087E+01	0.55011E+01	0.10509E-15
5.50	0.35283E+00	0.68748E-01	0.23010E+00	0.28670E+00	0.21677E+01	0.51827E+01	0.10597E-15
5.75	0.35942E+00	0.67347E-01	0.23671E+00	0.27226E+00	0.21256E+01	0.49089E+01	0.10691E-15
6.00	0.36545E+00	0.65942E-01	0.24359E+00	0.25971E+00	0.20832E+01	0.46704E+01	0.10788E-15
6.25	0.37096E+00	0.64554E-01	0.25063E+00	0.24865E+00	0.20412E+01	0.44599E+01	0.10888E-15
6.50	0.37603E+00	0.63383E-01	0.25687E+00	0.23879E+00	0.20059E+01	0.42720E+01	0.10987E-15
6.75	0.37922E+00	0.65706E-01	0.25114E+00	0.23140E+00	0.20843E+01	0.41285E+01	0.11162E-15
7.00	0.38112E+00	0.66873E-01	0.25258E+00	0.22590E+00	0.21281E+01	0.40191E+01	0.11381E-15
7.25	0.38261E+00	0.67646E-01	0.25541E+00	0.22127E+00	0.21594E+01	0.39260E+01	0.11597E-15
7.50	0.38390E+00	0.68210E-01	0.25843E+00	0.21719E+00	0.21837E+01	0.38436E+01	0.11802E-15
7.75	0.38502E+00	0.68629E-01	0.26139E+00	0.21354E+00	0.22031E+01	0.37693E+01	0.11996E-15

8.00	0.38598E+00	0.68939E-01	0.26421E+00	0.21020E+00	0.22187E+01	0.37015E+01	0.12181E-15
8.25	0.38681E+00	0.69165E-01	0.26689E+00	0.20713E+00	0.22313E+01	0.36390E+01	0.12356E-15
8.50	0.38750E+00	0.69324E-01	0.26940E+00	0.20428E+00	0.22416E+01	0.35808E+01	0.12523E-15
8.75	0.38807E+00	0.69434E-01	0.27176E+00	0.20160E+00	0.22499E+01	0.35264E+01	0.12683E-15
9.00	0.38853E+00	0.69504E-01	0.27395E+00	0.19908E+00	0.22568E+01	0.34750E+01	0.12835E-15
9.25	0.38888E+00	0.69545E-01	0.27599E+00	0.19668E+00	0.22626E+01	0.34264E+01	0.12981E-15
9.50	0.38912E+00	0.69565E-01	0.27787E+00	0.19440E+00	0.22675E+01	0.33803E+01	0.13121E-15
9.75	0.38928E+00	0.69569E-01	0.27961E+00	0.19222E+00	0.22717E+01	0.33364E+01	0.13256E-15
10.00	0.38935E+00	0.69561E-01	0.28121E+00	0.19014E+00	0.22754E+01	0.32944E+01	0.13385E-15
10.25	0.38934E+00	0.69547E-01	0.28268E+00	0.18814E+00	0.22787E+01	0.32544E+01	0.13509E-15
10.50	0.38926E+00	0.69528E-01	0.28402E+00	0.18622E+00	0.22817E+01	0.32160E+01	0.13629E-15
10.75	0.38911E+00	0.69507E-01	0.28524E+00	0.18438E+00	0.22846E+01	0.31793E+01	0.13745E-15
11.00	0.38890E+00	0.69487E-01	0.28635E+00	0.18261E+00	0.22873E+01	0.31442E+01	0.13856E-15
11.25	0.38864E+00	0.69468E-01	0.28735E+00	0.18091E+00	0.22900E+01	0.31105E+01	0.13963E-15
11.50	0.38834E+00	0.69451E-01	0.28826E+00	0.17928E+00	0.22927E+01	0.30782E+01	0.14066E-15
11.75	0.38799E+00	0.69437E-01	0.28907E+00	0.17771E+00	0.22953E+01	0.30473E+01	0.14166E-15
12.00	0.38760E+00	0.69428E-01	0.28980E+00	0.17621E+00	0.22980E+01	0.30178E+01	0.14262E-15
12.25	0.38717E+00	0.69422E-01	0.29046E+00	0.17476E+00	0.23007E+01	0.29894E+01	0.14355E-15

TIME	PA	PV	PIPL	CPL
0.0	0.17640E+02	0.47200E+01	0.20000E+02	0.35900E+02
0.25	0.17640E+02	0.29145E+01	0.18607E+02	0.34548E+02
0.50	0.17640E+02	0.20000E+01	0.17724E+02	0.33647E+02
0.75	0.17640E+02	0.20000E+01	0.17378E+02	0.33283E+02
1.00	0.17640E+02	0.20000E+01	0.17179E+02	0.33071E+02
1.25	0.17640E+02	0.20000E+01	0.17072E+02	0.32956E+02
1.50	0.17640E+02	0.20000E+01	0.17092E+02	0.32978E+02
1.75	0.17640E+02	0.20000E+01	0.17034E+02	0.32915E+02
2.00	0.17640E+02	0.20000E+01	0.16810E+02	0.32672E+02
2.25	0.17640E+02	0.20000E+01	0.16495E+02	0.32326E+02
2.50	0.17640E+02	0.20000E+01	0.16182E+02	0.31977E+02
2.75	0.17640E+02	0.20000E+01	0.15860E+02	0.31611E+02
3.00	0.17640E+02	0.20000E+01	0.15530E+02	0.31231E+02
3.25	0.17640E+02	0.20000E+01	0.15586E+02	0.31295E+02
3.50	0.17640E+02	0.20000E+01	0.15605E+02	0.31317E+02
3.75	0.17640E+02	0.20000E+01	0.15619E+02	0.31334E+02
4.00	0.17640E+02	0.20000E+01	0.15637E+02	0.31355E+02
4.25	0.17640E+02	0.20000E+01	0.15659E+02	0.31380E+02
4.50	0.17640E+02	0.20000E+01	0.15683E+02	0.31408E+02
4.75	0.17640E+02	0.20000E+01	0.15710E+02	0.31439E+02
5.00	0.17640E+02	0.20000E+01	0.15736E+02	0.31469E+02
5.25	0.17640E+02	0.20000E+01	0.15763E+02	0.31501E+02
5.50	0.17640E+02	0.20000E+01	0.15790E+02	0.31531E+02
5.75	0.17640E+02	0.20000E+01	0.15817E+02	0.31562E+02
6.00	0.17640E+02	0.20000E+01	0.15842E+02	0.31591E+02
6.25	0.17640E+02	0.20000E+01	0.15867E+02	0.31620E+02
6.50	0.17640E+02	0.20091E+01	0.15892E+02	0.31648E+02
6.75	-0.17640E+02	0.21942E+01	0.15957E+02	0.31722E+02
7.00	0.17640E+02	0.23294E+01	0.16045E+02	0.31822E+02
7.25	0.17640E+02	0.24481E+01	0.16133E+02	0.31922E+02
7.50	0.17640E+02	0.25580E+01	0.16216E+02	0.32015E+02
7.75	0.17640E+02	0.26613E+01	0.16294E+02	0.32102E+02
8.00	0.17640E+02	0.27591E+01	0.16367E+02	0.32184E+02
8.25	0.17640E+02	0.28522E+01	0.16436E+02	0.32261E+02
8.50	0.17640E+02	0.29412E+01	0.16502E+02	0.32334E+02
8.75	0.17640E+02	0.30265E+01	0.16565E+02	0.32404E+02
9.00	0.17640E+02	0.31085E+01	0.16625E+02	0.32470E+02
9.25	0.17640E+02	0.31876E+01	0.16683E+02	0.32534E+02

9.50	0.17640E+02	0.32639E+01	0.16739E+02	0.32595E+02
9.75	0.17640E+02	0.33377E+01	0.16793E+02	0.32654E+02
10.00	0.17640E+02	0.34091E+01	0.16845E+02	0.32710E+02
10.25	0.17640E+02	0.34784E+01	0.16895E+02	0.32765E+02
10.50	0.17640E+02	0.35456E+01	0.16943E+02	0.32817E+02
10.75	0.17640E+02	0.36107E+01	0.16990E+02	0.32868E+02
11.00	0.17640E+02	0.36740E+01	0.17036E+02	0.32917E+02
11.25	0.17640E+02	0.37355E+01	0.17080E+02	0.32965E+02
11.50	0.17640E+02	0.37952E+01	0.17123E+02	0.33011E+02
11.75	0.17640E+02	0.38532E+01	0.17165E+02	0.33056E+02
12.00	0.17640E+02	0.39095E+01	0.17205E+02	0.33099E+02
12.25	0.17640E+02	0.39642E+01	0.17245E+02	0.33141E+02